BERICHTE
aus dem Fachbereich Geowissenschaften
der Universität Bremen

Nr. 68

D. Hebbeln, G. Wefer, M. Baltazar, D. Beese, J. Bendtsen, M. Butzin, G. Daneri, V. Dellarossa, V. Diekamp, N. Dittert, B. Donner, M. Giese, R. Glud, J. Gundersen, R. Haese, C. Hensen, R. Hoek, O. Holby, J. Holck, S. Hormazabal, I. Hornum, M. Huhn, H. Hundahl, B. Irwin, B. Karwath, H. Kinkel, E. Kusnetsova, F. Lamy, M. Marchant, G. Meinecke, B. Meyer-Schack, C. Mikkelsen, H. Petermann, R. Prado, O. Romero, U. Rosiak, G. Ruhland, T. Schwenk, M. Segl, P.-I. Sehlstedt, G. Shaffer, S. Skoglund, R. Torres, O. Ulloa

CRUISE REPORT OF R/V SONNE CRUISE 102
VALPARAISO - VALPARAISO, 9.5. - 28.6.95

FAHRTBERICHT ZUR FS SONNE FAHRT SO-102
VALPARAISO - VALPARAISO, 9.5. - 28.6.95

Berichte, Fachbereich Geowissenschaften, Universität Bremen, No. 68
126 S., 112 Abb., 3 Tab., Bremen 1995
ISSN 0931-0800

The "Berichte aus dem Fachbereich Geowissenschaften" are produced at irregular intervals by the Department of Geosciences, Bremen University.

They serve for the publication of experimental works, Ph.D.-theses and scientific contributions made by members of the department.

Reports can be ordered from:

Gisela Eggerichs

Sonderforschungsbereich 261

Universität Bremen

Postfach 330 440

D 28334 BREMEN

Phone: (49) 421 218-4124

Fax: (49) 421 218-3116

Citation:
D. Hebbeln, G. Wefer et al.
Cruise Report of R/V SONNE Cruise 102, Valparaiso - Valparaiso, 9.5. - 28.6.95
Berichte, Fachbereich Geowissenschaften, Universität Bremen, No. 68, 126 pp., 112 figs., 3 tables, Bremen 1995.

ISSN 0931-0800

Content

1. Participants

Participants SO-102 Leg 1

Name	Discipline	Institution
Mario Baltazar	Biology	UCCE
Detlef Beese	Geology	GeoB
Martin Butzin	Oceanography	UBTO
Volker Diekamp	Geology	GeoB
Nicolas Dittert	Geology	GeoB
Ronnie Glud, Dr.	Biogeochemistry	MPIB
Jens Gundersen, Dr.	Biogeochemistry	UniA
Ralf Haese	Geochemistry	GeoB
Dierk Hebbeln, Dr.	Geology	GeoB
Christian Hensen	Geochemistry	GeoB
Ola Holby, Dr.	Biogeochemistry	MPIB
Inger Hornum	Chemistry	DFMR
Brian Irwin, Dr.	Biology	BIOD
Hanno Kinkel	Geology	GeoB
Elena Kusnetsova	Chemistry	UCV
Margarita Marchant	Geology	GeoB
Harald Petermann, Dr.	Geophysics	GeoB
Roberto Prado, Dr.	Oceanography	UV SHOA
Uwe Rosiak	Geology	GeoB
Tilmann Schwenk	Geophysics	GeoB
Monika Segl, Dr.	Geology	GeoB
Per-Ingvar Sehlstedt	Oceanography	UGOI
Gary Shaffer, Dr.	Oceanography	UCDG
Osvaldo Ulloa, Dr.	Biology	UCDG
Gerold Wefer, Dr. (chief scientist)	Geology	GeoB

Participants SO-102 Leg 2

Name	Discipline	Institution
Detlef Beese	Geology	GeoB
Jørgen Bendtsen	Oceanography	UCDG
Giovanni Daneri, Dr.	Biology	UMBP
Victor Dellarossa, Dr.	Biology	UCDB
Barbara Donner, Dr.	Geology	GeoB
Martina Giese, Dr.	Geology	GeoB
Dierk Hebbeln, Dr. (chief scientist)	Geology	GeoB
Ramses Hoek	Geology	GeoB
Jørgen Holck	Oceanography	UCDG
Samuel Hormazabal	Oceanography	UCV SHOA
Michael Huhn	Oceanography	UBTO
Henning Hundahl	Oceanography	UCDG
Brian Irwin, Dr.	Biology	BIOD
Britta Karwath	Geology	GeoB
Frank Lamy	Geology	GeoB
Margarita Marchant	Geology	GeoB
Gerrit Meinecke, Dr.	Geology	GeoB
Birgit Meyer-Schack	Geology	GeoB
Camilla Mikkelsen	Chemistry	DFMR
Oscar Romero	Geology	GeoB
Götz Ruhland	Geology	GeoB
Tilmann Schwenk	Geophysics	GeoB
Sverker Skoglund	Oceanography	UCDG
Rodrigo Torres	Chemistry	UGMC
Osvaldo Ulloa, Dr.	Biology	UCDG

Institutions

GeoB

Geowissenschaften
Universität Bremen
Klagenfurter Straße
D-28359 Bremen
Germany

BIOD

Biological Oceanography Devision
Bedford Institute of Oceanography
P.O. Box 1006
Dartmouth, Nova Scotia
Canada

UCCE

Centro EULA
Universidad de Concepcíon
Casilla 156-C
Concepcíon
Chile

DFMR

Danish Institute for Fisheries
and Marine Research
Charlottenlund Castle
DK-2920 Charlottenlund
Denmark

MPIB

Max Planck Institute for
Marine Microbiology
Fahrenheitstraße
D-28359 Bremen
Germany

UniA

Dept. of Microbial Ecology
University of Aarhus
Ny Munkegade
DK-8000 Aarhus C
Denmark

UV

Instituto Montemar
Universidad de Valparaiso

Vina del Mar
Chile

UCDG

Department of Geophysics
University of Copenhagen
Haraldsgade 6
DK-2200 Copenhagen N
Denmark

UGOI

Oceanographic Institute
University of Gothemburg
Box 4038
S-40040 Gothemburg
Sweden

UBTO

Tracer-Ozeanographie
Universität Bremen

D-28359 Bremen
Germany

UCV

Escuela de Ciencas del Mar
Universidad Catolica de Valparaiso
Casilla 1020
Valparaiso
Chile

UGMC

Department of Analytical
and Marine Chemistry
University of Gothemburg
S-41296 Gothemburg
Sweden

UMBP

Departamento de Oceanografia
y Biologia Pesquera
Universidad del Mar
Valparaiso
Chile

UCDB

Departamento de Botanica
Universidad de Concepcíon
Casilla 2407
Concepcíon
Chile

SHOA

Servicio Hidrografico
y Oceanografico
de la Armada de Chile
Valparaiso
Chile

2. Research Program

The near coastal upwelling region off Chile and Peru is one of the most productive regions of the world ocean. In cooperation between the University of Bremen and institutes in Chile, Denmark and Sweden the carbon cycle in this, on a globa scale, important area will be studied. The aim of this studies is the investigation of the present day cycling of carbon and the reconstruction of paleoenvironmental conditions, focusing on paleoproductivity, through the late Quaternary climatic cycles. Only very little is known so far about the southern part of the Peru/Chile current and about its youngest geological history. Because this is one of the most important high productivity regions of the world ocean, a detailed knowledge about the paleoproductivity is necessary to assess the role of this system throughout the late Quaternary climatic variations. A detailed study of the oceanographic and biologic conditions about the entire width of the Peru/Chile current in combination with surface sediment data will help to understand the present-day sedimentation processes within this region. In addition, this expedition provided the excellent opportunity to repeat the oceanographic measurements done during the SCORPIO cruise 28 years ago. By this repetition, variations in water mass structure and composition and changes as e.g. global warming can be detected.

Another aim of the cruise will be the improvement of the knowledge about the relationship between climate and erosion onshore, which can be studied by the analysis of the clastic portion of the sediments, which is by far the biggest portion along the continental slope. Sedimentation can be tightly coupled to ENSO (El Nino/Southern Oscillation) events, which consequences have been found almost all around the world. Rainfalls in the arid and semiarid regions of Chile associated to the El Nino events might result in strong erosion events. From the equatorial East Pacific some data exist about paleo-El Ninos, but there are no informations from the southern part of the Peru/Chile current. In the ocean off Chile the El Nino events are marked by a distinct warming of the surface ocean resulting in a drastic decrease in biological productivity. Both effects, increased terrigenous sediment supply by onshore erosion and decreased productivity by surface ocean warming, should be able to detect in the sediments as long as the sedimentation rate is high enough to allow a sufficient temporal resolution.

3. Narrative of the Cruise

R/V SONNE left Valparaiso on May 9 at 13^{00}h for the first leg of the SO-102 cruise with three hours delay, due to the closing of the harbour because of strong fog. On board were 25 scientists from 6 countries. The first two days of steaming were used by all the groups to prepare their equipment and to get used to living on a ship. On may 11 the first geological station began at 41°S and 74°20´W and within the next 3 days the first continental slope transect has been completed. In total on 7 stations (GeoB 3312 - GeoB 3318) sediment samples have been collected with the multicorer and the gravity corer between 41° and 42°S and between 74°20´ and 75°20´W down the continental slope from 600 m to 3200 m. Recovered core lengths from the gravity corer ranged between 195 to 874 cm. The sediments consisted mainly of olive to black silty clay with some dark sand layers. On two stations the benthic lander systems Profilur and Elinor have been deployed and later on recovered.

On May 16 the station work on the first hydrographic transect along 43°13´S began. Along this line 14 CTD/rosette stations have been done between 74°45´W and 86°W (GeoB 3319 - GeoB 3331). Close to the coast the distance between the stations was 15´, which increased to 30´, 1° and 2° on the way west. The temperature, salinity and fluorometer data from the CTD and the data obtained from the water samples from the rosette will be the base for the comparison to the 28 year old SCORPIO data. On some stations two CTD/rosette casts were run in order to reach a higher resolution within the water column and a multiple closing plankton net (multinet) was used to collect plankton samples with 63µm nets from the depth intervals 500 m - 300 m, 300m - 200 m, 200 m - 100 m, 100 m - 50 m, and 50 m - 0 m. In addition on three stations sediment samples have been recovered by multicorer and gravity corer. Away from the continental slope the colour of the sediments changed to white and brown, reflecting the transition from a hemipelagic to a true pelagic realm. Three more deployments of the lander systems Profilur and Elinor ended succesful, but the new developed lander S4 has not been recovered from its very first deployment. On May 20 wether S4´s flashlight nor its radiosignal could have been received and after a 4 hour search the lander has been given up.

After finishing the transect on 43°13´S on May 21 R/V SONNE headed north for two days towards the second hydrographic transect on 35°15´S. On the way north two shallow CTD/rosette stations were done each day to supply the primary production group with water

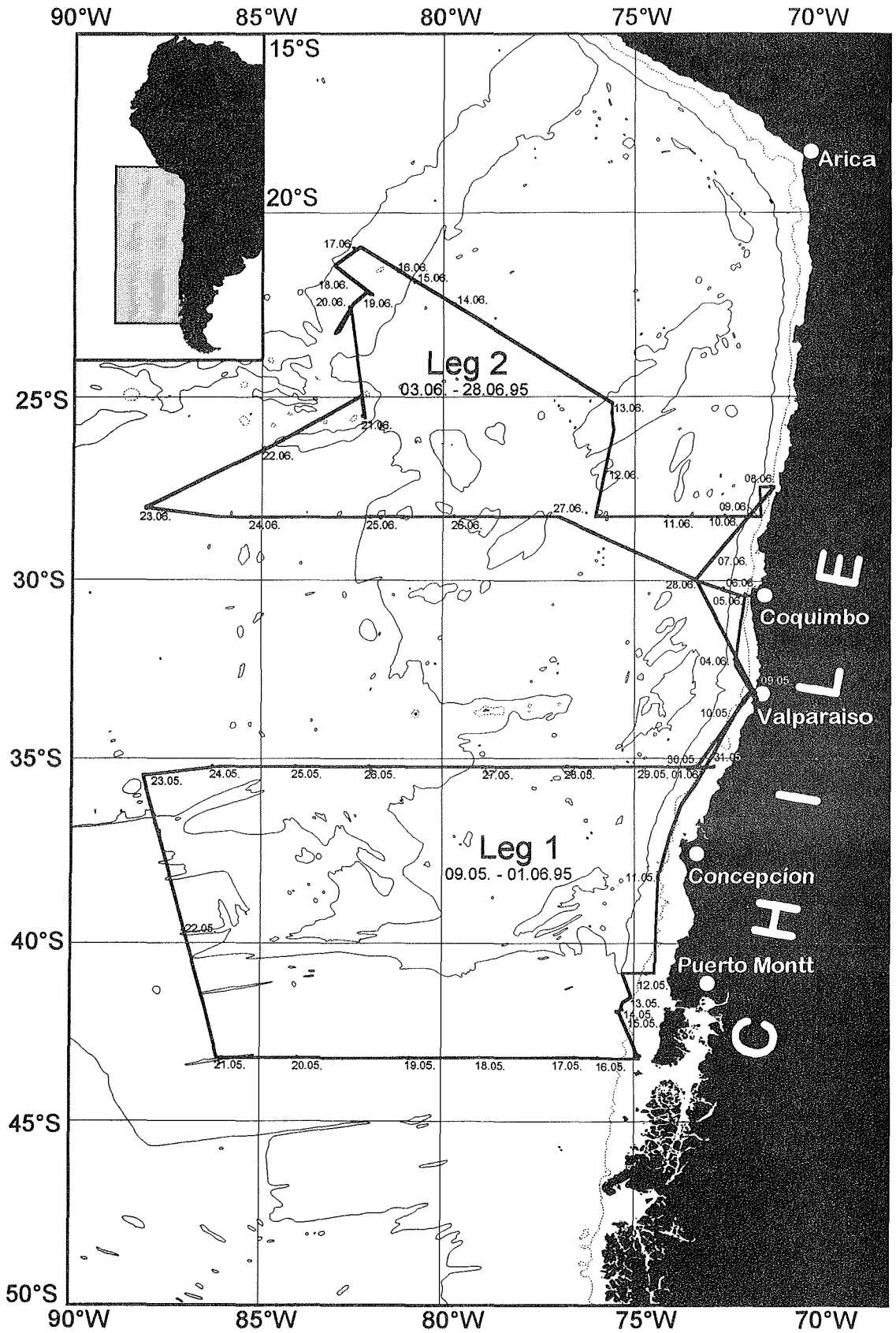

Fig. 1: Cruise track of the SONNE cruise SO-102, Leg 1 and Leg 2

for their incubation experiments. On May 23 a WOCE station on 35°30´S and 88°W has been repeated in order to calibrate the data from this cruise to the WOCE data from the same region. At the same site a 540 cm long gravity core was taken, consisting almost entirely of red deep sea clay, indicating very effective carbonate dissolution as shallow as 4032 m in this low production open ocean area.

Along the transect on 35°15´S from 86°W towards the continental slope most stations (GeoB 3337 - GeoB 3348) were CTD/rosette and multinet stations, again in decreasing distances towards the coast as on the first transect. On this part of the transect the program has only been extended by one lander deployment and by 3 geological stations. Reaching the continental slope on May 29 the focus of the station work shifted back to geology and biogeochemistry. A second geological continental slope transect has been sampled until May 31 between 35°13´S, 73°25´W and 35°17´S, 72°45´S with 9 stations from water depths between 800 m and 3800 m, with a maximum core recovery of 623 cm. Also there the sediments consisted almost entirely of olive to black silty clays with some dark sand layers. In addition, along this transect the landers Profilur and Elinor have been deployed and recovered three times.

The scientific station work of leg 1 finished on May 31 after running the last four CTD/rosette stations of the hydrographic transect. On June 1 around noon R/V SONNE reached Valparaiso. During the first leg the weather conditions were surprisingly good. No one of the storms expected and typical for the region during this time of the year hit the ship (windspeed seldom reached and never exceeded bft. 8) and sometimes the nautic and scientific crews even caugth some sunshine .

During the stay of R/V SONNE in Valparaiso a partial exchange of the scientific crew took place and only 6 of 25 scientists stayed for the second leg of the cruise. Also for this leg 25 scientists embarked, which were of 7 nationalities working in 4 countries. Leg 2 started on June 3 at 10^{00}h and 4 ½ hours later the first geological station, a continuation of a transect carried out during SO-101, began. The next morning the work on the JGOFS transect, as part of the international JGOFS Eastern Boundary Current Study started. On station GeoB 3367 an oceanographic mooring (COSMOS) equipped with three current meters could have been recovered and was deployed again for a new six months period the same day. Close to the mooring site on the continental slope sediments were sampled on two geology stations. Right after sunrise on June 5 the big JGOFS sediment trap mooring (OCEMOS) has been set free from the

bottom weight by an acoustic releaser. This 4000 m long mooring consisted of three sediment traps and five current meters. All the sediment traps, deployed in ~1000 m, ~2000 m and ~3500 m, respectively, collected the particle flux between January and June 1995 in 20 six day periods. Next morning the mooring was deployed for another six month period, to be recovered in January 1996 by the chilean R/V ABATE MOLINA. The mooring site was also sampled by CTD/rosette, multinet and multicorer to get as many data as possible from this longterm station.

On 27°30´S another continental slope transect has been sampled by multicorer and gravity corer. From 1300 m to 3600 m water depth sediment cores have been recovered from six stations (GeoB 3373 - GeoB 3378). As typical for the continental slope cores, they consisted mainly of olive to black silty clays with dark sand layers. On station GeoB 3378 the new developed TRAMP system was put into the water for a first test run. Unfortunately, the rope, on which TRAMP was mounted for the test run, broke and the whole system was lost.

The third hydrographic transect to repeat the SCORPIO cruise from 1967 on 28°15´S has been reached on June 8. R/V SONNE worked on seven stations (GeoB 3379 - GeoB 3385) on the eastern part of the transect up to 76°W, on which CTD/rosette and the multinet have been used. From 28°15´S, 76°W the ship headed north towards the Iquique Ridge, where water depths as shallow as 1100 m were found, which are not mentioned in any of the sea charts. The attempt to get a sediment core from the shallowest part failed, and multicorer and gravity corer only retrieved sediments from two sites in 2600 m and 3500 m, respectively.

After two days of steaming the Nazca Ridge was reached on the evening of June 13. During the next six days two geological transects have been completed on this ridge. The nights were spent with looking out suitable coring sites by PARASOUND and HYDROSWEEP surveys, while during the day the sampling took place. In total 9 stations on the first and 11 stations on the second transect crossing the Nazca Ridge from water depths between 4460 m to 820 m have been sampled (GeoB 3389 - GeoB 3408). However, specially on the shallow sites coring was partly problematical and some core tubes have been bent. From the shallowest sites no sediments could have been retrieved. Besides on the site in 4460 m water depth, where mostly red deep sea clay was found, the sediments consisted generally of white to brownish foraminifera and nannofossil oozes. On the shallower sites (< 2000 m) the sediments were composed partly of foraminifera sand, resulting in sampling problems with the multicorer. Due to the

coarse material the multicorer tubes have been spilled out by the water while they have been pulled upward through the water column. The work on the Nazca Ridge has been finished on June 19.

The next day sampling started on a seamount 150 nm south of the Nazca Ridge. After an extensive PARASOUND and HYDROSWEEP survey, three locations were chosen for gravity and multicorer (GeoB 3409 - GeoB 3411). Although this seamount reached up to 270 m below the sea surface, the shallowest site chosen was in 1160 m and, as on the most shallow sites, it was not possible to retrieve sediments from this water depth. However, the two other sites have been sampled succesfully.

After another 1 ½ days of steaming we reached the westernmost position of this cruise at the western end of the hydrographic transect at 28°`S and 88°W (GeoB 3414). At this WOCE site a deep CTD was run to allow the intercomparison of the data obtained during this cruise with the WOCE data. Here also the last geological sampling of the cruise took place, before R/V SONNE headed eastward to complete the hydrographic section on 28°15´S in 2° steps.

Six hydrographic stations later, consisting of two CTD/rosette casts and a multinet cast, station work endet on June 26 with the last station (GeoB 3420) of the hydrographic transect at 28°15´S and 77°W. From there R/V SONNE headed back to Valparaiso. On the way a short HYDROSWEEP survey was done, when the ship passes the sediment trap mooring site. After a total 110 stations the cruise SO-102 ended on June 28 in the harbour of Valparaiso. Also during the second leg the weather conditions were almost perfect.

4. Preliminary Results

4.1. Underway Measurements

4.1.1. Temperature and Salinity

Continuous temperature and salinity measurements from a depth of about 3 m were obtained from the thermosalinograph of RV "SONNE" during much of Leg 1 and all Leg 2. While it was functioning well, temperatures from this instrument were found to agree with surface layer

temperatures from the CTD to within about 0.02°C. Visual inspection of the thermosalinograph results showed a filament structure in the frontal region encountered at about 74°30´ W along the 35°15' S line.

4.1.2. Fluorescence

(G. Shaffer, O. Ulloa and B. Irwin)

Continuous measurements of in-situ fluorescence - a measure of phytoplankton chlorophyll-a concentration - from a depth of about 6 m were obtained throughout about the last 20 days of Leg 1 and all Leg 2 with a Turner Design field fluorometer (model 10-AU-005) used in the flow through mode. Data was logged at 30-second intervals on a PC. Water samples were taken for chlorophyll-a determinations, which together with those made on the surface layer Rosette samples will be used to calibrate the fluorometer output. Preliminary results indicate low to moderate chlorophyll-a concentrations along the 43°15'S line, the 86-88°W track, the seaward part of the 35°15'S line and line 28°15'. High concentrations were encountered within and shoreward of the frontal region at about 74°30´ W along the 35°15' S line.

4.1.3. Atmosphere and Ocean Surface Layer CO_2 Concentrations

(R. Prado and G. Shaffer)

Measurements of partial pressure of carbon dioxide in surface seawater and in marine air were carried out underway between 41°S, 74°25´W and 35°25´S, 86°W following the ship's track. The determinations were done by means of a semiautomatic carbon dioxide analysis system including a non-dispersive infrared gas analyzer (Li-Cor LI-6262) for detection. Both marine air and surface seawater were continuously sampled on top of the bridge (intake placed 2 m before it) and at the bow (6 m below sea level), respectively. Partial pressure of CO_2 was measured, in an alternating fashion, of marine air, of air from the head-space of an acrylic tube equilibrator through which seawater flowed as well as of several known standards. Temperatures of seawater in the equilibrator and at the seawater inlet were continuously measured using platinum resistance thermometers, as was geographical position with the system's GPS receiver. Data was logged on an internal PC at about six minute intervals. The temperature data, complimented with temperature data from the CTD and the thermosalinograph, as well as air pressure recorded on the ship will all be used in the final corrections of surface layer CO_2 concentrations.

Results obtained represent the first direct mesurements of pCO_2 at sea off Chile and show a net inflow of carbon dioxide to the ocean in almost all of the study area with the exception of a narrow zone of CO_2 outgassing between 75°15´W and 75°30´W close to Chiloe near 43°S. After a rough, preliminary correction for the warming between the sea water intake and the equilibrator, we found seawater pCO_2 to be between 340 and 360 ppmv with the exception of the mentioned outgassing area, in which pCO_2 of up to 450 ppmv were measured. The partial pressure of CO_2 in air is characterized by values around 365 ppmv.

4.2. Water Column Measurements and Sampling

4.2.1. CTD/Rosette

(P.-I. Sehlstedt, J. Bendtsen, S. Hormazabal and G. Shaffer)

On Leg 1, the CTD/Rosette work was concentrated on the 43°15'S line (line 1;13 stations with a total of 19 CTD casts; 8 of the stations were full water sampling stations) and on the 35°15' S line (line 2;15 stations with a total of 22 CTD casts; 9 of the stations were full water sampling stations). On Leg 2 the work was concentrated on the 28°15'S line (line 3;13 stations with a total of 23 casts; 10 of the stations were full sampling stations). These sections were designed to repeat the Eastern Boundary Current portions of the transpacific hydrographic sections made during the SCORPIO cruises 28 years ago. In addition, some shallow test stations (4 CTD casts to 100 m) were made before the transect work in Leg 1 was started and additional shallow casts in both legs (18 CTD casts in all to 100-200 m) were made before dawn and around noon to collect water for the on deck, primary production incubations. Finally, one CTD/Rosette cast was made at 35°30´S, 88°W and one at 28°S, 88°W for comparison with data from two WOCE hydrographic stations (stations 293 and 308, line P19) occupied at this position in March, 1993. On the deep stations with a full water sampling program, water was collected at about 34 depths from one deep and one shallow CTD/Rosette cast. Typical vertical resolution was 20-25 meters down to 200 m, 50 meters between 200 and 400 m, 100 meters from 400 m to 1200 m, 200 meters from 1200 m to about 4000 m and 500 m below 4000 m

During Leg 1 and 2 some preliminary comparisons were made between our CTD temperature and salinity data/lab salinometer data and corresponding data from the SCORPIO and WOCE

cruises. Good agreement among these different data sets was found below about 1500 m. Some interesting differences in temperature were found in the depth range of 300 to 1500 meters between our data and that from the SCORPIO cruises. However, careful post-calibration of our CTD, as well as an in depth analysis of our WOCE repeat station, is needed before definitive results of this comparison can be presented .

4.2.2. Laboratory Salinity Determinations

(P.-I. Sehlstedt, J. Bendtsen, H. Hundahl and G. Shaffer)

Salinity determinations of water samples from the Rosette were also carried out with a Guildline Model 8410 Portasal laboratory salinometer placed in a temperature-regulated room on board. Approximately 4 to 8 samples for salinity were taken on each CTD cast on the three main lines. Sampling was done when possible in vertical zones of quasi-homogeneous salinity values as identified on the CTD downcast. These results will be used to correct salinity values from the CTD. Comparisons in the deep water at the WOCE repeat station at 88°S, 35°30'W revealed agreement to within 0.001 between our lab salinometer salinity values and those reported for the WOCE station (this data was kindly made available to us by Dr. Lynn Talley, Scripps Institute of Oceanography).

4.2.3. Helium, Tritium and CFC's

(M. Butzin and M. Huhn)

Tracers like chlorofluorocarbons (CFC's), helium isotopes, and tritium provide a powerful tool to study oceanic transport phenomena, like for instance processes of ocean ventilation or the spreading of deep water. Water samples taken during the cruise will be analysed at the IUP Tracer Oceanography Laboratory, University of Bremen with regard to their contents of CFC-11, CFC-12, CFC-113, CCl_4, ^3He, ^4He, and tritium. The analysing method for CFC's and CCl_4 is gas chromatography. Helium isotopes are measured with a specially designed noble gas mass spectrometer. Tritium decays radioactively to ^3He and is also detected by mass spectrometry.

On Leg 1 water was collected at 6 stations at each line. At line 1 (43°15'S), the station longitudes were 75°15', 76°, 78°, 80°, 82°, and 86°W. At line 2 (35°15'S), water sampling took place at 73°15', 74°, 76°, 79°, 82°, and 86°W. For intercomparison and calibration purposes, water samples were additionally collected at the position of WOCE-Leg P19C station # 293

(coordinates 35°30'S, 88°W). On the second leg of the cruise (28°15'S) sampling took place at 11 stations (longitudes: 71°45', 72°30', 74°, 76°, 77°, 78°, 80°, 82°, 84°, 86° and 88°W). There was also intercalibration sampling at 88°W (position of WOCE-P19C station # 308).

At each station water samples for CFC and helium measurement were collected from about 20 depths. CFC sampling concentrated on the upper 2000-2500 m. Water below this depth should be free of CFC's. The region of main interest for helium measurements was the depth range of 1000-3000 m where a maximum of terrigenic helium originating from sources in the East Pacific Rise is expected. Tritium samples were collected from 12 depths focusing on the upper 1000-1500 m of the water column, being the typical penetration depth of bomb tritium into the oceans of the southern hemisphere.

4.2.4. Water Sampling for Stable Isotopes

(M. Segl)

Samples for the measurement of stable oxygen and carbon isotopes were taken from the same bottles as the ^{14}C samples. The samples were taken immediatly after opening the niskin bottle and after sampling oxygen and ^{14}C. 100 ml of water was carefully filled into a brown glass bottle avoiding air-bubbles in the water. The samples were poisoned with 1 ml saturated $HgCl_2$ solution and closed airtight with melted paraffin. They were returned to the laboratory at the University of Bremen in a 4°C container . The oxygen isotopes of the water will be measured using a commercial equilibration devise coupled to a Finnigan MAT 252 mass-spectrometer. The samples for measurement of ^{13}C of the ΣCO_2 will be prepared manually and measured also by means of the Finnigan MAT 252.

As reported by Kroopnick (1985) and later by several other authors, nutrients and ^{13}C are highly correlated to each other, as both tracers are bound in the biological cycling. Broecker and Meier-Reimer (1992) pointed out, that this tie is not perfect, as ^{13}C is influenced by air-sea exchange, which is not the case for nutrients. Comparing the ^{13}C and nutrient measurements of the samples, we want to have a closer look to coupling and decoupling mechanisms between the two tracers in the upwelling region off Chile.

4.2.5. Carbon-14

(R. Prado, G. Shaffer, R.Torres)

Water samples for determination of AMS carbon-14 (^{14}C)were collected at selected stations with the high sampling resolution in the vertical described above (at 75°15', 76°, 78°, 80°, 82°, and 86°W at 43°15´S, at 72°45', 73°15', 76° and 82°W at 35°15´S, and at 71°30', 72°30' 74° and 80°W at 28°15´S) as well as at the two WOCE repeat stations. These samples were transferred to 500 ml bottles by drawing the same as for O_2 and poisoned with 100 µl of a saturated mercuric chloride solution. The sealed samples were sent to the Ocean Tracers Laboratory of Princeton University, USA (R. Key's group) for further processing. These measurements should complement those of the other tracers and help in the estimation of ventilation rates.

4.2.6. Dissolved Inorganic Carbon and Alkalinity

(R. Prado, G. Shaffer, R. Torres)

Samples for dissolved inorganic carbon and alkalinity were collected at the same stations and depths as for carbon-14 above plus the station at 28°15´S, 77°W. All samples were poisoned with a shot of a 50% saturated mercuric chloride (0.2 ml for 250 ml sample), sealed in Pyrex grounded neck bottles and sent to the Lamont-Doherty Geological Observatory of Columbia University, USA (T. Takahashi's group) for determination. These total inorganic carbon and alkalinity measurements are sufficient to fully characterize the carbon dioxide system off Southern Chile during late fall conditions as well as to estimate values of sea surface pCO_2 where direct pCO_2 measurement were not made.

4.2.7. Dissolved Oxygen

(E. Kuznetsova, M. Baltazar; G. Daneri, V. Dellarossa)

Leg 1

Duplicate water samples for dissolved oxygen were taken from the CTD/Rosette at all depths on the full water sampling stations, on the WOCE repeat station, and on several of the trial stations at the beginning of Leg 1. The samples were analysed on board using an automatic titrator. Preliminary results indicate that the desired accuracy was not always obtained. The origin of this problem is still being investigated. In accordance with expectations based on SCORPIO cruise data, a subsurface oxygen minimum near the coast was detected along both lines.

Leg 2

The dissolved oxygen concentration was measured in all the main stations in the transect along the 28°15' S line (plus station at 77°W) and the WOCE repeat station using the Winkler technique. Oxygen measurements were done in triplicate. The precision of the analysis was good and well within the standards set by WOCE. Primary production and respiration experiments using the light and dark oxygen technique were performed daily, with surface water samples taken with a bucket. The high precision obtained in the measurement of dissolved oxygen concentration allowed us to measure productivity in oligotrophic waters.

4.2.8. Nutrients

(I. Hornum, O. Ulloa, M. Baltazar, C. Mikkelsen, V. Dellarossa)

Samples for nutrient analyses (silicate, phosphate, nitrite and nitrate) were collected from the Niskin bottles in the Rosette and analysed on board with an autoanalyser. On the full sampling stations, duplicate determinations were made at all depths. On the other stations of the sections as well as on the additional, shallow CTD casts mentioned above, single determinations were carried out. Due to problems with the nitrite and nitrate channels of the autoanalyser during part of Leg 1, some samples were also stored frozen for later analysis of nitrite and nitrate. A total of about 1800 samples were collected during Leg 1. Throughout Leg 1, the duplicate determinations agreed to within the detection level of the autoanalyzer, but an offset of about +0.05 µmol/kg for phosphate and -10% for silicate were found when compared with WOCE deep water values at the WOCE repeat station. On Leg 2 the nitrate channel got fixed and all the samples of the cruise were run. A total of about 1200 samples were collected during Leg 2.

4.2.9. Chlorophyll-a and Phaeopigments

(O. Ulloa, B. Irwin, M. Baltazar, V. Dellarossa)

Water samples were collected from the CTD/Rosette during 65 hydrographic shallow casts (down to 500 m) from up to 12 depths (38 in Leg 1 and 27 in Leg 2). Chlorophyll-a and phaeopigments were measured fluorometrically on board after extraction into ice-cold 90% acetone for 24 hours. Chl-a values along the southern transect were typically less than 1 mg/m^3 and were typically uniform throughout the surface mixed layer. As mentioned above, phytoplankton bloom conditions were encountered within and shoreward of a pronounced front near 74°30'W, 35°15'S. The organisms blooming were dinoflagellates (as verified under the micro-

scope) and maximum observed Chl-a values in this bloom reached remarkable values of up to 37.4 mg/m^3 at the surface.

4.2.10. Sampling for Dinoflagellates

(R. Hoek and B. Karwath)

Sea water samples were collected from the water column at different waterdepths ranging from surface water to 200 m and analysed on the content of living dinoflagellates. Of special interest was the appearance of calcareous and organic walled dinoflagellate resting cysts in the surveyed area, though little is known on their lateral and vertical distribution in middle to high latitudes of the Pacific. Preliminary results are presented here. Further examination on biomineralization, life cycle and systematics will be done at the University of Bremen.

Samples from different depths were collected using a combined CTD/Rosette device (10 l Niskin bottles). At every depth 5 to 10 litres of sea water have been collected. The sea water obtained was sieved using a 250 µm "Prüfsieb" (DIN 4188). After sieving the water was filtered and the suspended matter was concentrated using either a 0.2 µm or a 1.2 µm pore size celluloseacetate filter. The filtered residue was scanned for dinocyst content. Individual cysts were isolated and rinsed in polyterene Cell Wells™ with filtered sea water as a culture medium. An attempt was made to culture the cysts under "on board" conditions, i.e. the normal day night cycle and temperatures between 15^0-20^0 C.

Motile dinoflagellates were encountered in almost every sample, but were less abundant in deeper samples. Gonyaulax, Ceratium and Gymnodinium were the predominant genera. Calcareous cysts were rarely found and were more abundant in the northern profiles. Representatives of the species *`Sphaerodinella' albatrosiana*, *`Sphaerodinella' tuberosa*, *Thoracosphaera heimii* and *?`Orthopithonella' granifera* were present. Organic cysts were more abundant in the southern profiles and were found up to depths of 150 meter. The identified cysts are mainly representatives of the family Protoperidinium. Specimens of the motile stage and both calcareous - and organic cysts have been isolated in order to culture them. After one week the isolated cells were scanned. No motile stage survived after this period, while no excystment of the cysts has been identified.

4.2.11. Calcareous Nannoplankton Sampling

(H. Kinkel)

Coccolithophores are a mayor group in the marine phytoplankton and one of the most important calcium carbonate producers in the oceans. There is little known about the structure of living coccolithophore communities in the water column and their relationship to the accumulated coccolith assemblages in the underlying sediments. A detailed study of the living coccolithophore communities will lead to a better understanding and interpretation of fossil coccolith assemblages as a paleoceanographic tool.

Along the three oceanographic transects at 43°15´S, 35°15´S and at 28°15´S water samples from different depths of the upper 200 m were sampled (0m, 20m, 50m, 75m, 100m, 150m and 200m). The water samples were collected with 10l Niskin bottles on a rosette during the measurements with the shallow CTD. Depending on the productivity and the content of plankton and other organisms in the watercolumn, one to two liter of sea water were filtered by a membrane pump over a filtration unit. The filters used were of cellulose nitrate with a pore size of 0.45 µm. The filters were dried at 50°C in a drying oven and stored after that with silica gel in a air thight bag, to avoid precipitation of salt.

The filters will be prepared on an aluminium stub for scanning electron microscopy (SEM). One aspect of the SEM studies will be to determine the total ammount of coccolithophores (usually in cells x 10^6 per liter) as well as the species composition and their abundance in relation to oceanographic and biological parameters (temperature, salinity, nutrients and primary productivity) investigated by other working groups during the cruise.

4.2.12 Plankton Sampling with the Multiple Closing Net

(D. Hebbeln and H. Kinkel)

In order to investigate the assemblages of planktic foraminifera in the surface waters of the SE-Pacific the Multiple Closing Net or multinet has been used on 14 stations during SO-102/1 and 9 stations on SO-102/2. Besides the sediment trap station multinet casts have only been carried out at oceanographical stations to provide as many accompanying water column data as possible. The multinet consist of five different 63 µm nets, which allow the sampling of different levels within the water column. The levels sampled during this cruise are:

net 1: 500 m to 300 m
net 2: 300 m to 200 m
net 3: 200 m to 100 m
net 4: 100 m to 50 m
net 5: 50 m to 0 m

The multinet was lowered to 500 m water depth with 0.5 m/sec and pulled up with 0.3 m/sec. The samples have been poisened with 1 ml saturated $HgCl_2$ solution and stored at 4°C.

4.2.13. TRAMP - the Multicycling Profiler

(S. Skoglund, H. Hundahl and J. Holck)

TRAMP - a short description - TRAMP is a multicycling profiler designed for marine research and monitoring. The instrument profiles upwards and downwards along a guiding rope in the water column by regulating its volume using a closed hydraulic pump system. TRAMP operates independently and has enough battery capacity to take up to 800 profiles down to its maximum operating depth (600 m). The instrument is also suitable for single cast operation and might run in brake mode (measurements only at discrete depths) as an integrated brake and release system is available. TRAMP is built in titanium and plastic for best strength to weight ratio and non corroding operation.

Measurements are taken during upward profiling and TRAMP can be equipped with a broad variety of sensors according to operators choice. There are sensor interfaces for voltage, current, frequency and RS485/RS232 signals. Most commercial sensors measuring parameters such as pressure, temperature, conductivity, current velocity, various optical sensors, etc. can be connected.

Data is stored on a non-volatile hard drive (up to 525 Mbytes) and is dumped directly to a PC (via RS232) at recovery of the instrument. TRAMP communication runs from a PC-program via a RS232 connection. The program contains software for instrument communication and testing, set-up control, data processing and graphic presentation. TRAMP is flexible and can operate in many different ways to be chosen by its set-up control system. Operator choose cycle time, profiling and sinking velocity, deployment mode, measuring mode, sampling rate, etc.

Activity on board - After having spent a couple of days on testing and assembling the instrument in the laboratory on lower deck we decided to bring it up to main deck for field operation. We fit TRAMP into the elevator and secured it with a rope but we didn't notice the small horizontal bars located midway between the floors inside the elevator tube and sticking out a few cm. When elevating, TRAMP got stuck on the bar and the security rope cut. The rear parts of the instrument were heavily damaged and the conductivity sensor was broken at the neck.

We spent several days in the lab repairing the sensor and the rear end. Tests (dry and wet) showed that the conductivity sensor was operating properly again and we decided to go on measuring.

On Thursday 8 June 1995 we were at station 27°30,28´S and 71°29,96´W. We noted calm weather conditions, brought TRAMP up on the main deck and started to balance TRAMP. This has been done by lowering the instrument a couple of meters down into the water a repeated number of times adding/removing small weights until TRAMP was neither floating nor sinking. Finally we let TRAMP pump out about 1 l of oil (level +5) to the external bladder - thus giving the instrument a positive buoyancy of about 1 kg in sea water.

Immediately afterwards we decided to make a test profile from the ship side. This has been done by attaching the small releaser weight (5 kg) to TRAMP thereby giving the instrument a negative buoyancy and we then lowered the anchor to approximately 300 m depth. TRAMP is designed to release from the releaser weight automatically after it has detected a fixed depth (+/- 6 m) for about 3 minutes. However this operation didn't function since the brake (which operates the release mechanism) was set in a wrong start position. Starting in this faulty position the brake might close so hard that it might fail to open. Since proper operation includes both closing the brake (thereby releasing the anchor weight) and opening the brake (thereby going free from the guiding rope) - TRAMP probably didn't go free from the rope but stayed in its bottom position. It should be noted that the plastic brake clutches used to keep TRAMP tight to the rope when brake is closed, were identical to the devices used on sailing boats preventing reverse running of ropes, i.e. they are designed for exactly this kind of operation.

When we realized that TRAMP wasn't coming up by its own as intended, we decided to winch up the system. Suddenly when TRAMP and anchor were a few meters up in the air the rope

cut and TRAMP was disappearing down into the sea. The time was 15:38h Chile time and TRAMP has not been seen since. It is probably resting at 3285 m depth. According to several witnesses the rope broke 1 or 2 meters above TRAMP's highest point

We do not yet have any explanation for the accident. We used a brand new rope - one of the best ropes available on the market (named "Dyneema", 8 mm diameter, netted in 3 layers and specified for more than 4000 kg load) and our system had a total weight of about 350 kg (TRAMP and anchor included). Light wind and calm waves indicated we couldn't even be close to max. allowed load. However - based on the observation that the rope cut 1-2 m above TRAMP's highest part - there must have been something wrong with the rope (material error, accidental cutting ?).

4.2.14. Primary Production (^{14}C Method)

(O. Ulloa, B. Irwin)

On 33 stations (14 in Leg 1 and and 19 in Leg 2), water was collected in the morning (before sunrise when possible) from 6-8 depths, which were selected based on light levels available in the deck incubation system (from 90% to 1% of surface irradiance). The incubation system had also blue filters to simulate light quality. Water samples were placed in polycarbonate bottles with ^{14}C sodium bicarbonate and incubated for about 12 hours, after which they were filtered onto glass-fibre filters. The filters were dried in an oven at 50 degrees and they will be analysed by scintillation spectrometry at the University of Concepcion, Chile, after completion of the cruise.

4.2.15. New Production (^{15}N Method)

(O. Ulloa, B. Irwin)

Water samples from 6-8 depths (the same as for the ^{14}C experiments) were incubated in the deck incubation system for 3-4 hours after addition of ^{15}N potassium nitrate and ^{13}C sodium bicarbonate. Samples for ^{15}N and ^{13}C analysis were collected by filtration onto pre-combusted glass-fibre filters and immediately dried in the oven at 50 degrees for later isotopic analysis. The samples will be analysed at Bedford Institute of Oceanography, Canada.

4.2.16. Phothosynthesis-Irradiance (P-I) Experiments

(B. Irwin, O. Ulloa)

Water was collected twice per day from two depths; by bucket from the surface and from the CTD/Rosette from the chlorophyll maximum or bottom of the mixed layer (30-110 m, according to the information provided by the CTD/Rosette equipped with an in vivo fluorescence sensor). In the ship's lab, ^{14}C sodium bicarbonate was added to the samples and the samples incubated for about three hours in artificial-light-gradient incubators (P-I boxes) connected to temperature-controlled water baths. At the end of the incubation period the samples were filtered through glass-fibre filters and the filters dried in the oven; they will be analysed by scintillation spectrometry on land. A total of 148 (74 on each Leg) P-I experiments were carried out, 80 for surface waters and 68 for 30-110-m waters. In addition, 148 samples were taken for HPLC analysis, particle absorption spectra, CHN, and nutrients (silicate, phosphate, nitrite and nitrate).

4.3. Biogeochemistry - Benthic Lander Systems

(R. Glud, J. Gundersen and O. Holby)

Background - Oxygen is the energetically best electron acceptor available and is the first oxidator to be depleted in a sediment profile. The O_2 is consumed partly by heterotrophic processes mediated by microorganisms or by the higher fauna, and partly by reoxidation of upward diffusing solutes active in diagenetic processes deeper down in the sediment. For these reason O_2 uptake of sediments has often been used as a measure for the total benthic mineralisation. The total O_2 uptake of the sediment can be expressed by two processes:

Total O_2 uptake = Benthos mediated O_2 uptake + diffusive O_2 uptake

The total O_2 uptake (TOU) refers to the total O_2 consumption of the sediment. The benthos mediated O_2 uptake (BOU) equals the uptake that is related to the activity of animals living in or at the sediment e.g. the pumping of oxygenated water into the sediment by tube living polychaetes. The diffusive O_2 uptake (DOU) is the amount of oxygen transported to the sediment by molecular diffusion. From measurements of TOU and DOU it is thereby possible to quantify the effect of benthos on the benthic O_2 uptake .

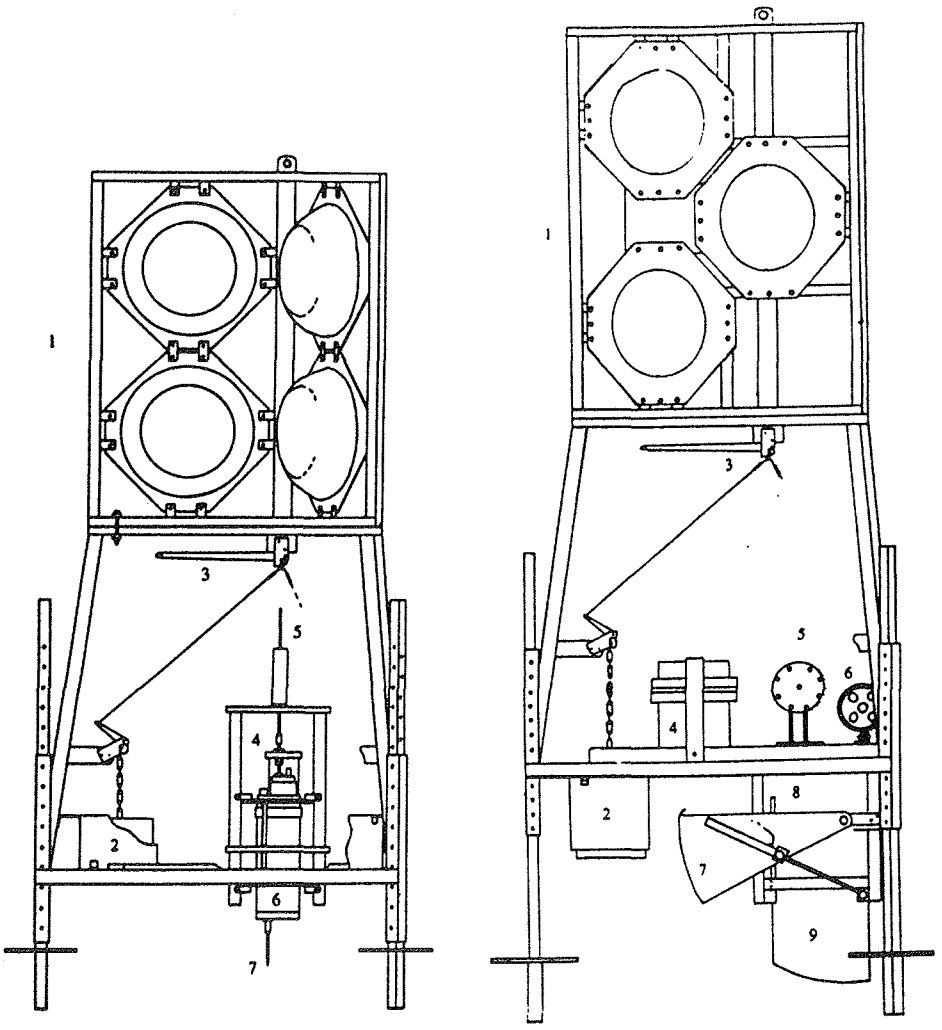

Fig. 2: The two benthic landers Profilur and Elinor. 1) flotation unit, 2) Ballast, 3) central ballast release. Profilur: 4) motor, 5) spindle, 6) electronic cylinder, 7) microsensors. Elinor: 4) Battery, 5) hydraulic unit, 6) electronic cylinder, 7) scoop, 8) lid, 9) respiration chamber (water sampling unit is not shown).

In an open water phase turbulence results in an equal distribution of solutes. However, near the sediment water interface viscous forces and adhesion result in a thin film of water where diffusion is the most important way of transporting solutes. This thin film of water (200- 1000 µm) called the diffusive boundary layer (DBL), can be very important in regulating the benthic solute exchange. By O_2 microelectrode measurements it is possible to resolve the DBL and from measurements of the near linear O_2 gradient through the DBL the diffusive O_2 uptake can be calculated by Ficks first law of diffusion.

The thickness of the oxic zone in the sediment regulates the exchange of other solutes and the rate of mineralisation by other diagenetic processes. For instance is the supply of NO_3^- from the overlying water (through the oxic zone) and from the oxic nitrification very important in regulating the denitrification rate in deeper sediment layers. Further the oxic zone regulates the efflux of reduced compounds like NH_4^+ and Mn^{2+}, since these compounds are oxidised within this layer.

The dynamics of the benthic carbonate system is of importance for the understanding of the global carbon cycle. Calcite dissolution is affected by mainly two processes, dissolution by pressure and by pH-lowering caused by benthic mineralisation. These processes can be studied from artefact free pH profiles which ony can be obtained by in situ measurements.

By use of different techniques we have studied the above mentioned dynamics along two transects off the Chilean coast from water depths between 400 m and 4000 m.

Materials and Methods - Oxygen and pH microprofiles and total benthic exchange rates, were measured both in situ by use of the two benthic landers Profilur and Elinor (Fig. 2) and in the laboratory on recovered sediment from the multicorer (MUC).

The two benthic landers work as independent vehicles. After being released from the ship they sink down to the seafloor due to a load of 150 kg ballast. Reaching the seafloor both of them perform a pre-programmed measuring routine whereafter the ballast is released and the landers return to the surface. The release of ballast can be triggered from the ship by an acoustic signal or by the lander itself through a pre-programmed subroutine. At the surface the landers are relocated by means of a flash light (at darkness), a radio transmitter or potentially an Argos satellite tracking system. As a safety routine the ballast release is also equiped with a magnesium bolt, which due to corrosion eventually will release the ballast after some days. Both landers measures the depth, temperature and O_2 concentration as they sink and rise through the water column.

Profilur is designed to measure microprofiles of chemical and physical parameters across the sediment water interface. Microgradients of O_2 and pH were studied during this cruise. Standing at the seafloor the array of microsensors is stepwise (50-100 µm) moved downwards and after each step the output of each sensor is recorded. After profiling, but before releasing the

ballast a 5 l water sample of the bottom water is taken for calibration of the sensors etc. From the obtained O_2 microprofiles the thickness of the DBL, the DOU and the O_2 penetration depth can be determined. The pH profiles are together with the O_2 profiles used for modelling and quantifying the dissolution of calcite in the upper oxic part of the sediment.

Elinor is designed to measure total benthic exchange rates of different solutes. Landing at the seafloor Elinor encloses 900 cm^2 of sediment. The closure of a lid isolates the sediment with an overlying water phase of approximately 12-14 cm (depending on chamber penetration). During incubation the O_2 concentration is continuously recorded inside the chamber by two specially designed O_2 minisensors, while the water is stirred by an impeller creating a DBL thickness of approximately 600 µm (for O_2). Further ten water samples are recovered from the enclosed water volume at a pre-programmed time intervals. The samples are later analysed for concentrations of Mn^{2+}, DIC , NO_3^-, NH_4^+ and urea. The obtained results allow the total exchange rate across the sediment water interface of these solutes to be calculated. At shallow water depths (<1000 m) $^{15}NO_3^-$ is injected into the chamber in order to measure benthic denitrifica

Table 1

Station	water depth (m)	Actions*
3312	597	EPL
3317	3012	EPL
3323	3670	EPL
3327	3530	EPL
3331	3820	PL
3337	4073	PL
3349	2470	EPL
3355	1445	EPL
3356	580	EPL

*) E= Elinor was deployed; P = Profilur was deployed; L = laboratory incubations were performed.

tion by the isotope pairing technique. Before ballast release a scoop closes beneath the chamber cathcing the incubated sediment for quantification of benthos, organic carbon and porosity. Due to the relative small benthic exchange rates in the deep sea Elinor requires incubation times of at least 20 h when the water depth reaches app. 3000 m, while 12 h. is sufficient at water depths around 500 - 1000 m.

Laboratory measurements. Microprofiles and the total exchange rates of O_2 and DIC (Mn^{2+}, nutrient and denitrification at depth < 1500 m) were also measured in the laboratory on sediment cores recovered by the "multicorer". The cores were incubated at in situ temperature, pH and O_2 concentration and the overlying water was stirred in order to obtain a DBL thickness comparable to the in situ conditions. The laboratory data are compared to the in situ data in order to study and quantify artefacts affecting chemical porewater profiles during retrieval.

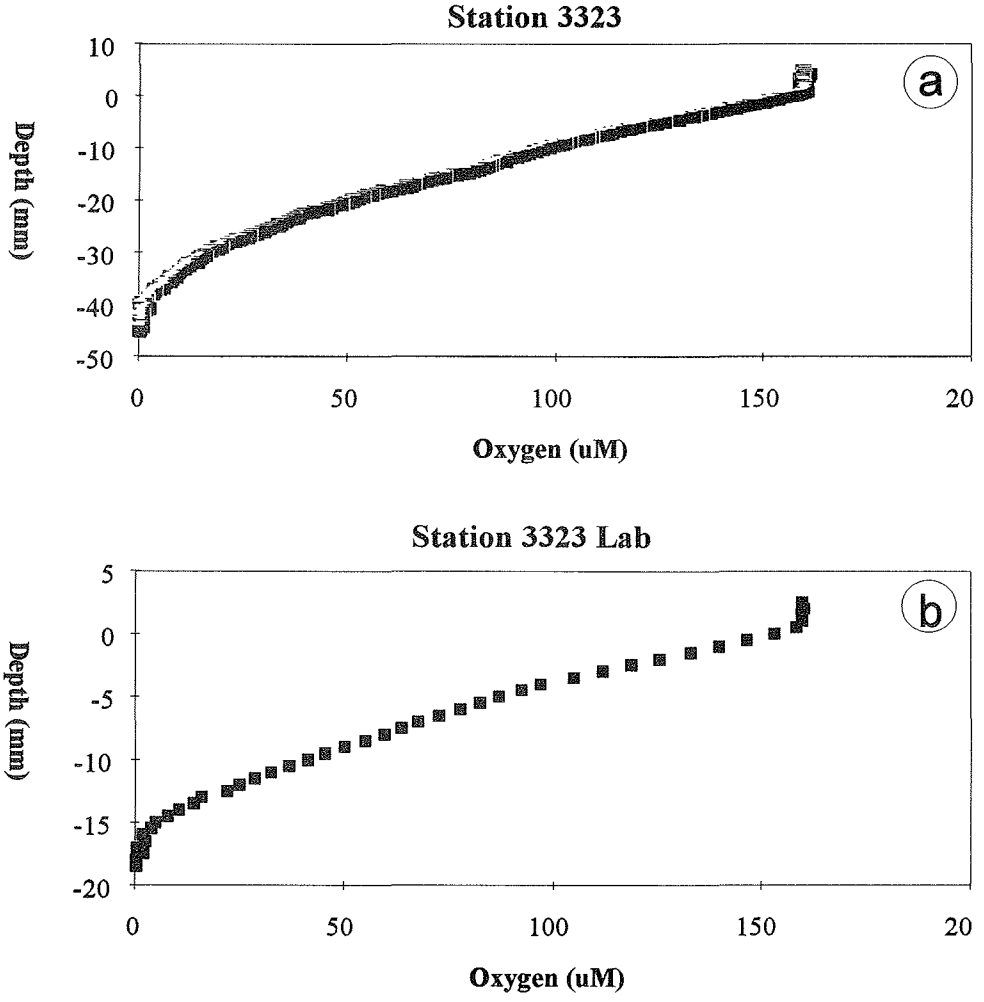

Fig. 3: a) Oxygen microprofile measured in situ at station 3323, b) Oxygen profile measured in the laboratory in a recovered core from the same station. "0" indicates sediment surface.

First results & discussion - As an example the pH and the O_2 data obtained at station 3323 are presented and briefly discussed below, analysis of nutrients etc. will be performed later back in Bremen.

Fig. 3 shows two O_2 profiles obtained in situ and in the laboratory, respectively. The O_2 penetration in situ is 40 mm and the DOU was calculated to be 5.7 mmol m^{-2} d^{-1}. The corresponding profile measured in the laboratory under semi in situ conditions only had a penetration depth of 17 mm and the DOU is 12.8 mmol m^{-2} d^{-1}. The qualitative difference between the two types of profiles was confirmed on several stations and is ascribed to artefacts introduced by the recovery of the sediment cores. The difference could be caused by a temporal heating, the cores are heated from the in situ temperature of 1.5 C to around 6.0 C during recovery, before

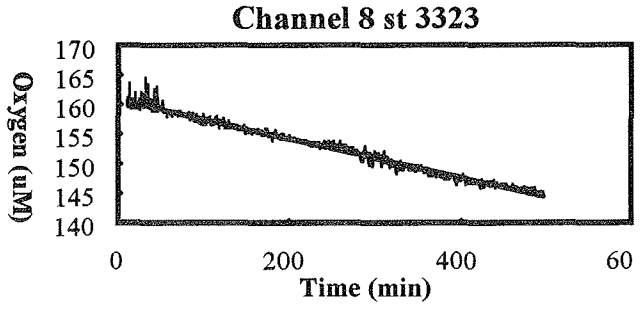

Fig. 4. Oxygen minielectrode recording of Elinor after settling of the lander at station GeoB 3323.

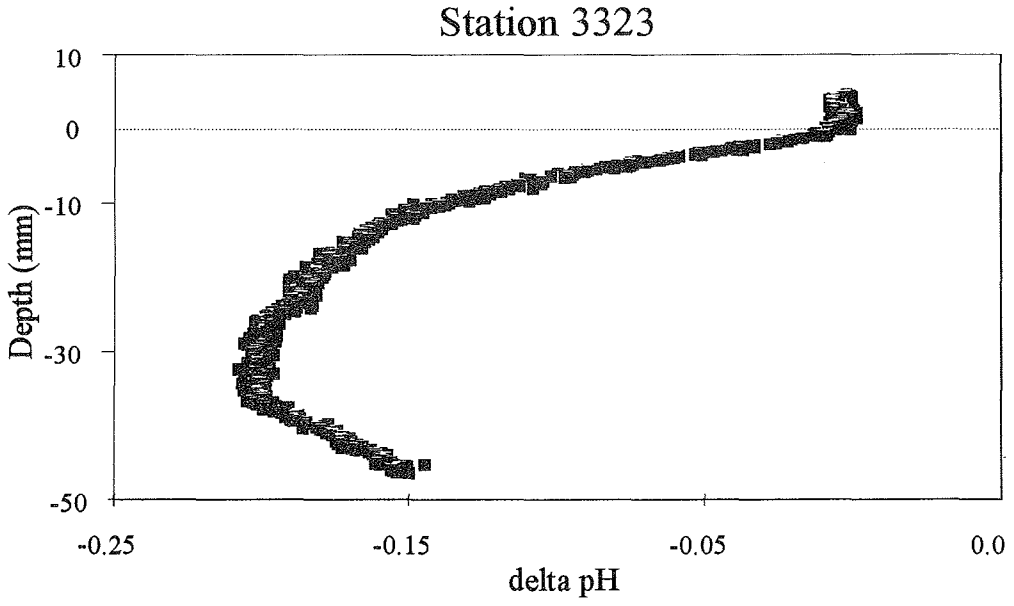

Fig. 5: pH profile measured in situ at station 3323."0" indicates sediment surface.

it is cooled down again in the incubator. This heating could stimulate the microbial activity and thereby the O_2 demand. The artefact could be further enhanced by lysis of psycophilic and/or barophilic bacteria during recovery, which would release highly labile organic components into the porewater. Water is compressed by approximately 2% at 4000 m depth and the release of the pressure during recovery could potentially also move the porewater profiles, further analysis of our data are needed in order to elucidate the problem. The total O_2 uptake rate measured at the station was 7.3 mmol m^{-2} d^{-1} (Fig. 4), this means that an O_2 uptake of 1.5 mmol m^{-2} d^{-1} is caused by non diffusional processes like benthos mediated transport. The total O_2 uptake measured in the laboratory was 9.8 mmol m^{-2} d^{-1}, the increased uptake as compared to the in situ data is ascribed to the artefact mentioned above. The total uptake measured in the laboratory is, however, also smaller than the diffusive uptake measured in the laboratory. This is probably due to the fact that the microprofile was measured relatively shortly after core

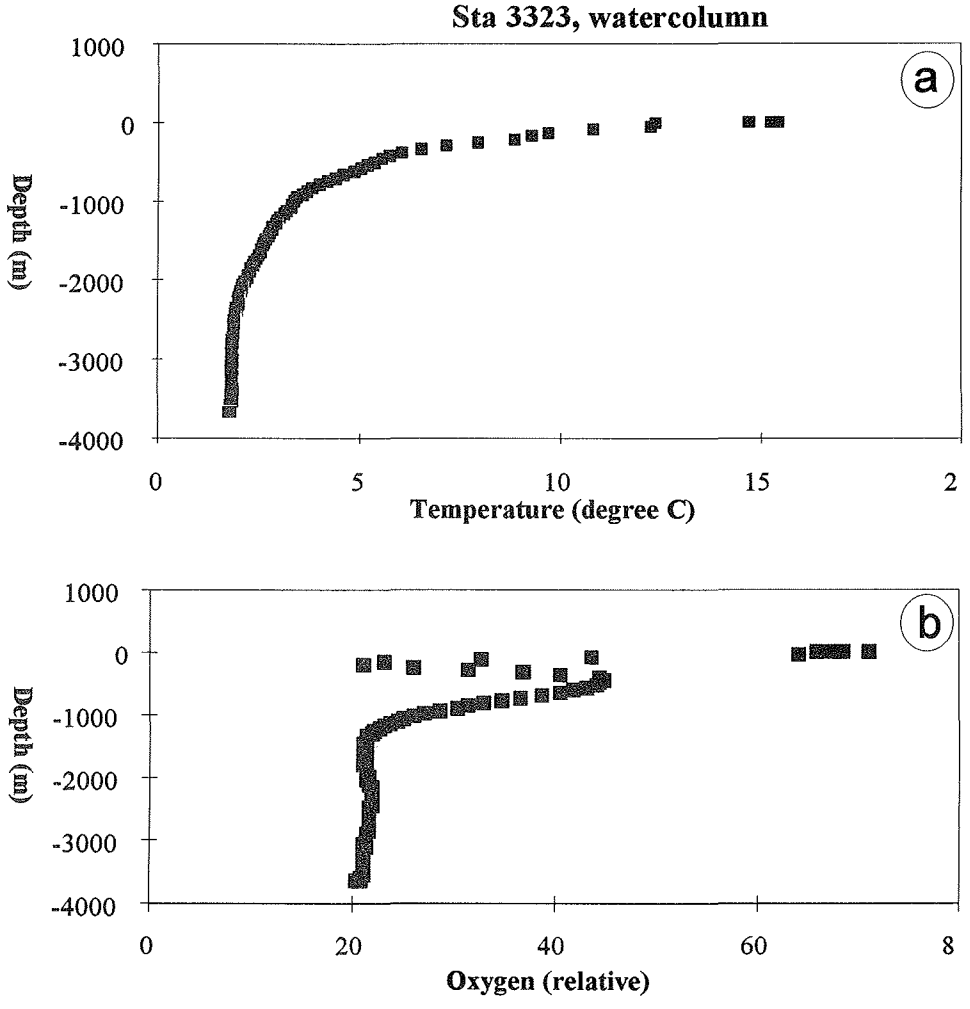

Fig. 6: a) Temperature and b) oxygen profiles measured in the water column during descend of the landers. The O_2 profile is not yet corrected for effects of pressure and temperature on the O_2 electrode response.

recovery, while the total uptake was measured after the core had equilibrated for 12 h in the incubation chamber. When the sediment core is placed in the incubation chamber at semi in situ conditions the in situ O_2 profile will slowly re-establish, which means that the O_2 uptake slowly will decrease. Profiles measured at different time intervals after core retrieval has confirmed this (data not shown).

The O_2 uptake measured at station 3323 is extremely high taking the water depth of 3670 m into account, and is approximately a factor of 5 higher than O_2 uptake rates measured at comparable depth in the upwelling region off the Namibian coast. This reflects the high load of organic carbon to the sediments off the Chilean coast.

Fig. 5 shows the in situ pH profile measured at station 3323, the profile show a distinct minimum at the oxic-anoxic interface.

Temperature and O_2 profiles in the water column as measured by the landers during descend is shown in Fig. 6, and are comparable to the obtained rosette/CTD profiles.

4.4. Underway Geophysics

4.4.1. HYDROSWEEP

(T. Schwenk and Shipboard Scientific Party)

To record continuous bathymetric profiles, the multibeam echosounder HYDROSWEEP on R/V SONNE was routinely used during leg SO-102 and managed on a 24-hour schedule by the ship´s system operator and the PARASOUND operator on the watch. The HYDROSWEEP System worked without technical problems. For better comparability with the depth generated by the PARASOUND system, the sound velocity used for the computation of the water depth was manually set constant to 1500 m/s. The multibeam sounder provided a complete coverage of the seafloor topography with a swath width of twice the water depth. The data were stored on tape and are thus available for later postprocessing. The weather conditions were most of the time good so that high quality data could be recorded during the whole cruise.

In combination with the sediment echosounder PARASOUND the HYDROSWEEP system proved to be a very efficient aid for the selection of suitable coring stations. The early and precise knowledge of the local topography around coring sites is essential to select suitables sites and to evaluate the impact of morphology, slope angles and sediment instabilities on the continuity of sedimentation.

4.4.2. PARASOUND

(T. Schwenk and Shipboard Scientific Party)

To record continuous high-resolution sediment echosounding profiles and to use as a tool for the selection of coring positions, the sediment echosounder PARASOUND was routinely used during leg SO-102 and operated on a 24 hour watch by the scientific crew. The observed penetration depth varied between only a few meters on the shelf and 100-150 m in the deep sea. The digital recording parameters were chosen and adapted accordingly.

The sediment echosounding data were routinely registered as analogue paper recordings with the DESO 25 device and in parallel digitally by means of the PARADIGMA system. The data were stored directly on 6250 bpi, 1/2" magnetic tapes using the standard, industry-compatible SEGY-format. The seismograms were sampled at a frequency of 40 kHz, with a registration-duration of 266 ms or 133 ms corresponding to a depth window of 200 / 100 m for a sound velocity of 1500 m/s. A sinusoidal wavelet with one period and a frequency of 4 kHz was standardly used as the shortest possible source signal to provide optimum resolution of reflectors and avoid interference phenomena.

An instantaneous preprocessing of the data was carried out onboard. Coloured online plots with a vertical scale of several hundred meters were produced for all profiles. Most of the changes in window depth could thereby be eliminated. From these plots a first impression could be gained of variations in sea floor morphology, sediment coverage and sedimentation patterns along the ships track. To improve the signal-to-noise ratio, the echogram sections were filtered with a bandpass filter (1.5 - 6.5 kHz). In addition the data were normalized to a constant value much smaller than the maximum average amplitude, to amplify in particular deeper and often weaker reflections.

To study the influence of frequency and length of the source signal on the reflection pattern, these parameters were systematically varied at sites, where gravity cores were recovered ('source signal test'). The frequency of the source signal was increased in steps of 0.5 kHz over the available frequency range from 2.5 to 5.5 kHz, while the pulse length was set to 1, 4, and 8 sinus periods. The setting was kept for a time span of 2 minutes to enable later signal stacking and an evaluation of the variability of seismograms from the same location. In order to quantify interference phenomena, seismograms recorded with different frequencies will be studied in more detailed, shorebased analyses.

The PARASOUND system as well as the software package PARADIGMA were working without greater problems. As minor problems could be quickly resolved, no greater losses of data can be reported, about 99.8% of data are stored on tape.

Preliminary Shipboard Results - To illustrate the different sedimentary environments, which were studied during R/V Sonne Cruise SO-102 at the South American continental margin, 6 examples of digital PARASOUND sections are presented in Fig. 8 to 13.

Fig. 8 shows a sediment basin on the continental slope of South America at a latitude of ~41° S. The basin sediments in a water depth of ~850 m allow a signal penetration of up to 80 m. Due to special circumstances the bottom echo and internal reflectors were duplicated by the 18 kHz NBS signal, which precedes the 4 kHz parametric signal by ~11 ms. The reflection pattern is charaterized by a strong sub-bottom reflector in 15 m, and parallel reflectors down to 80 m below the seafloor. The laterally varying layer thickness indicates differential subsidence or a through fill predominantly by turbidites, which are usually characterized by strong base reflectors and transparent intervals above.

The second example (Fig. 9) was recorded along a transect of oceanographic stations at 43°14´S latitude between ~74°23.2´W and ~74°51.7´W in a water depth of ~3550 m. The maximum penetration ranges from 20 to 70 m. Between 5 and 8 km and at 28 km distance diapiric structures can be observed. From the record it is difficult to decide, whether the diapirs are caused by basement structures or postdepositional tectonics. Sedimentation successively levels the morphology, which may be related to moderate current activity or turbidite deposition. Between the diapirs distinct parallel reflectors are resolved down to 70 m sub-bottom depth, which could in general be interpreted as a turbidit or pelagic sequence.

In Fig. 10 a digital Parasound section is shown along an oceanographic profil at 35°15´S between ~79°18´W and ~79°02´W. In a water depth of ~4000 m the seafloor is charaterized by a rough basement topography. A sedimentary sequence of up to 30 m thickness, with two to three distinct stronger internal reflectors, lies on top of a strong prolonged reflector. These reflectors are probably of pelagic origin and were deposited on a rough, young volcanic basement, which is indicated by several hyperbolic echoes with no internal structures.

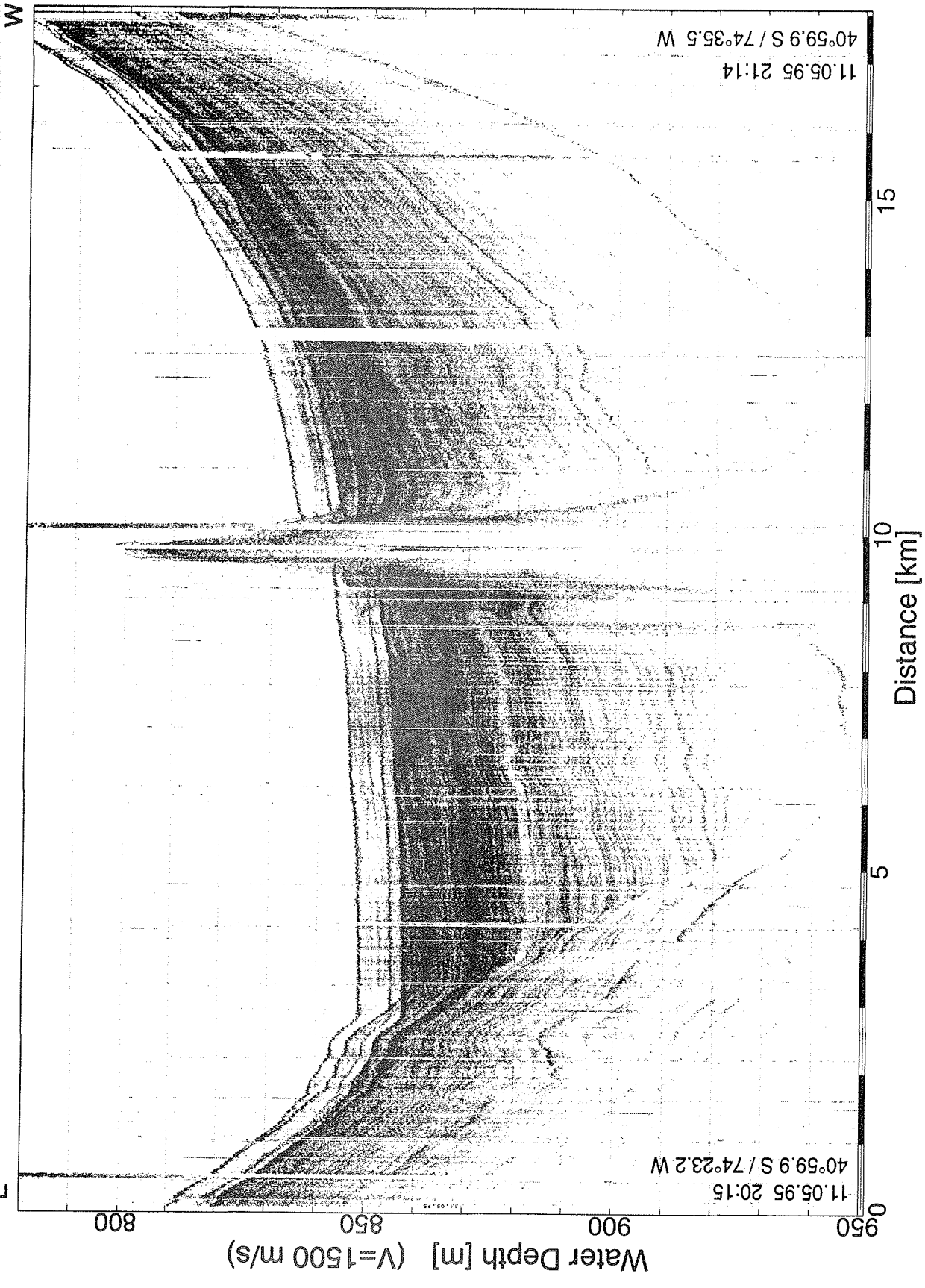

Fig. 8: Digital PARASOUND section acquired on the continental slope of South America. Vertical axis in meters, horizontal axis in km. Geographic coordinates, date and time were annotated along the horizontal axis. Horizontal bars represent distances of 1 km.

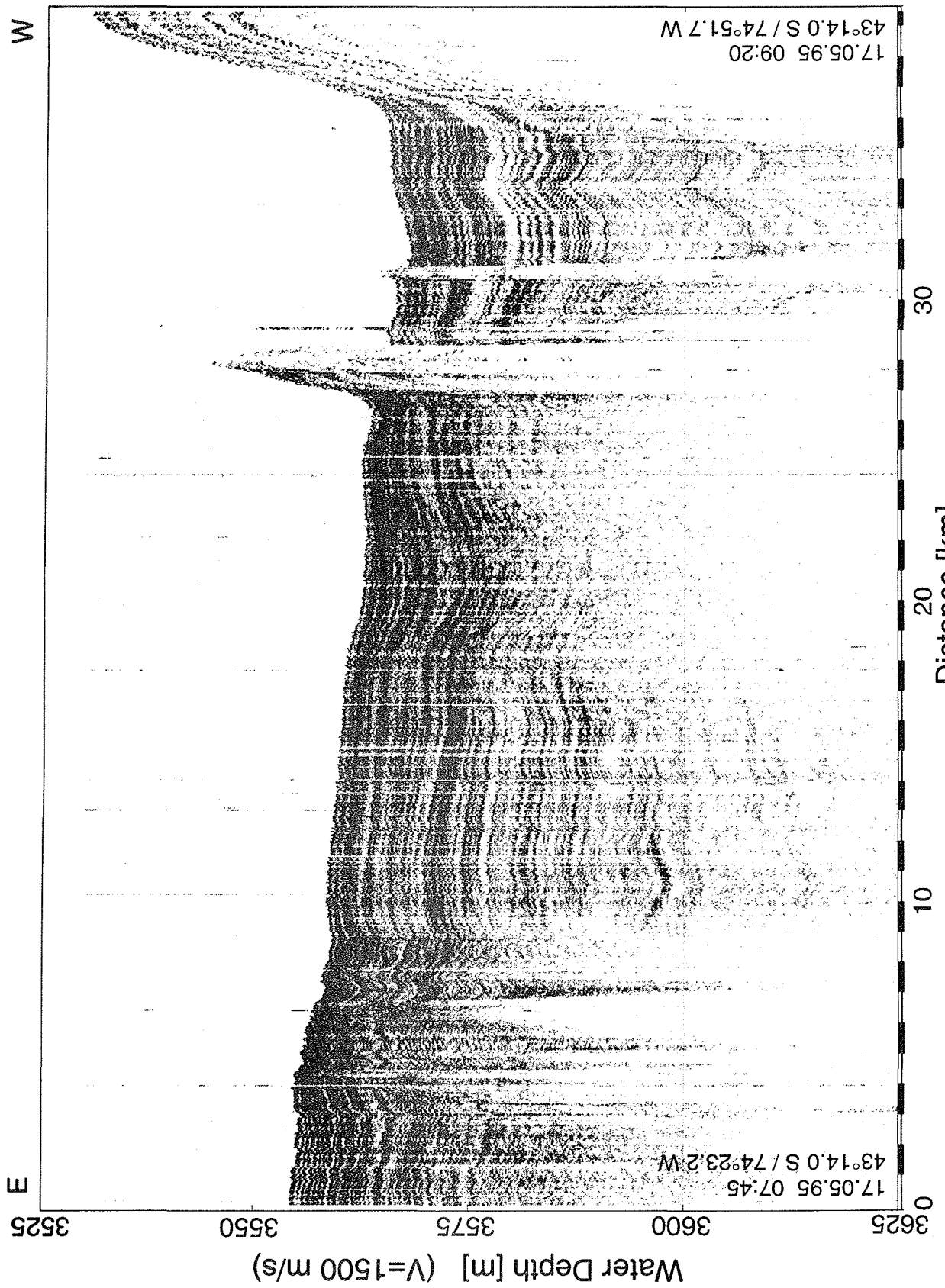

Fig. 9: Digital PARASOUND section acquired on the oceanographic profile at 43°14'S. See Fig. 8 for further explanation.

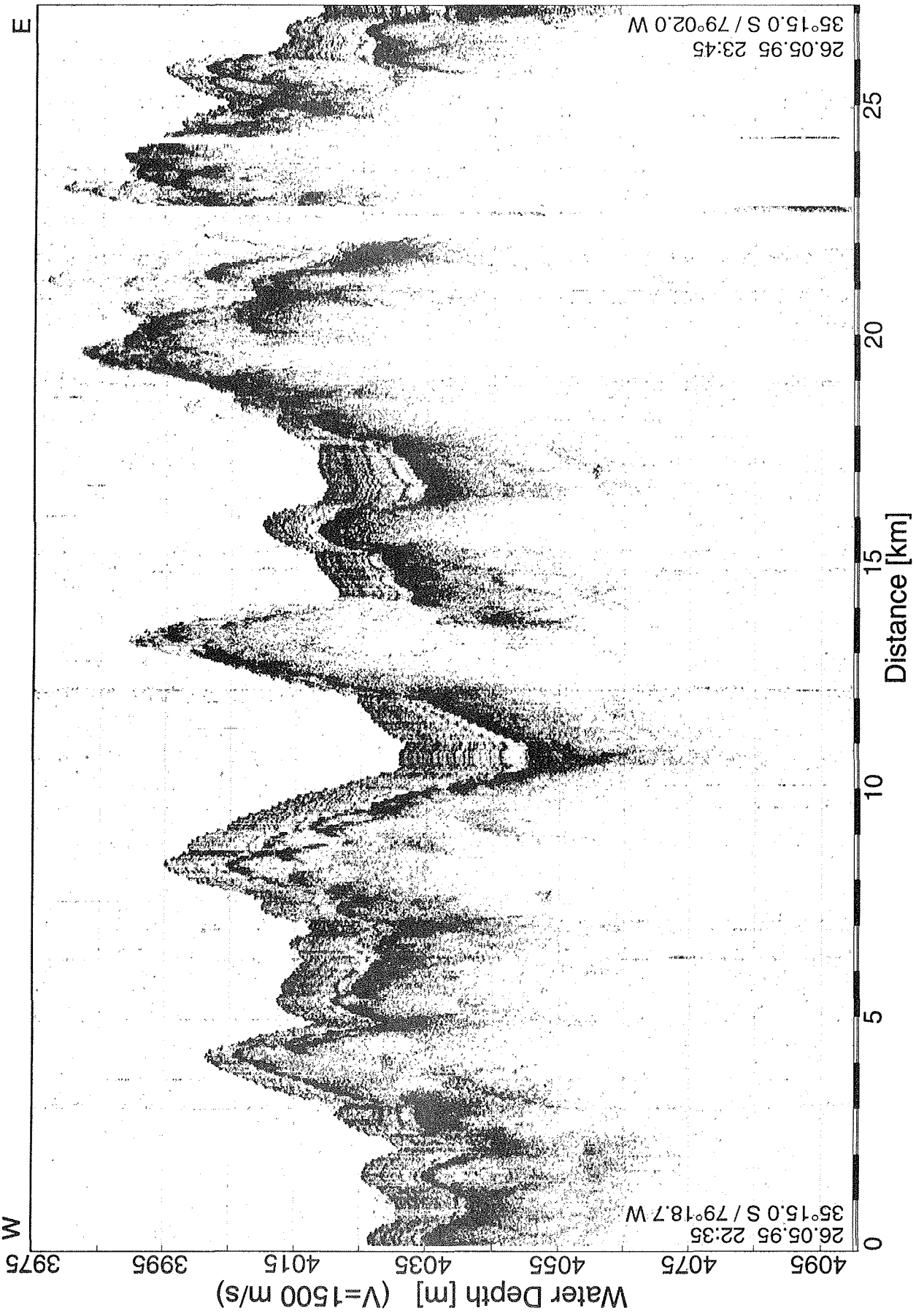

Fig. 10: Digital PARASOUND section acquired on the oceanographic profile at 35°15´S. See Fig. 8 for further explanation.

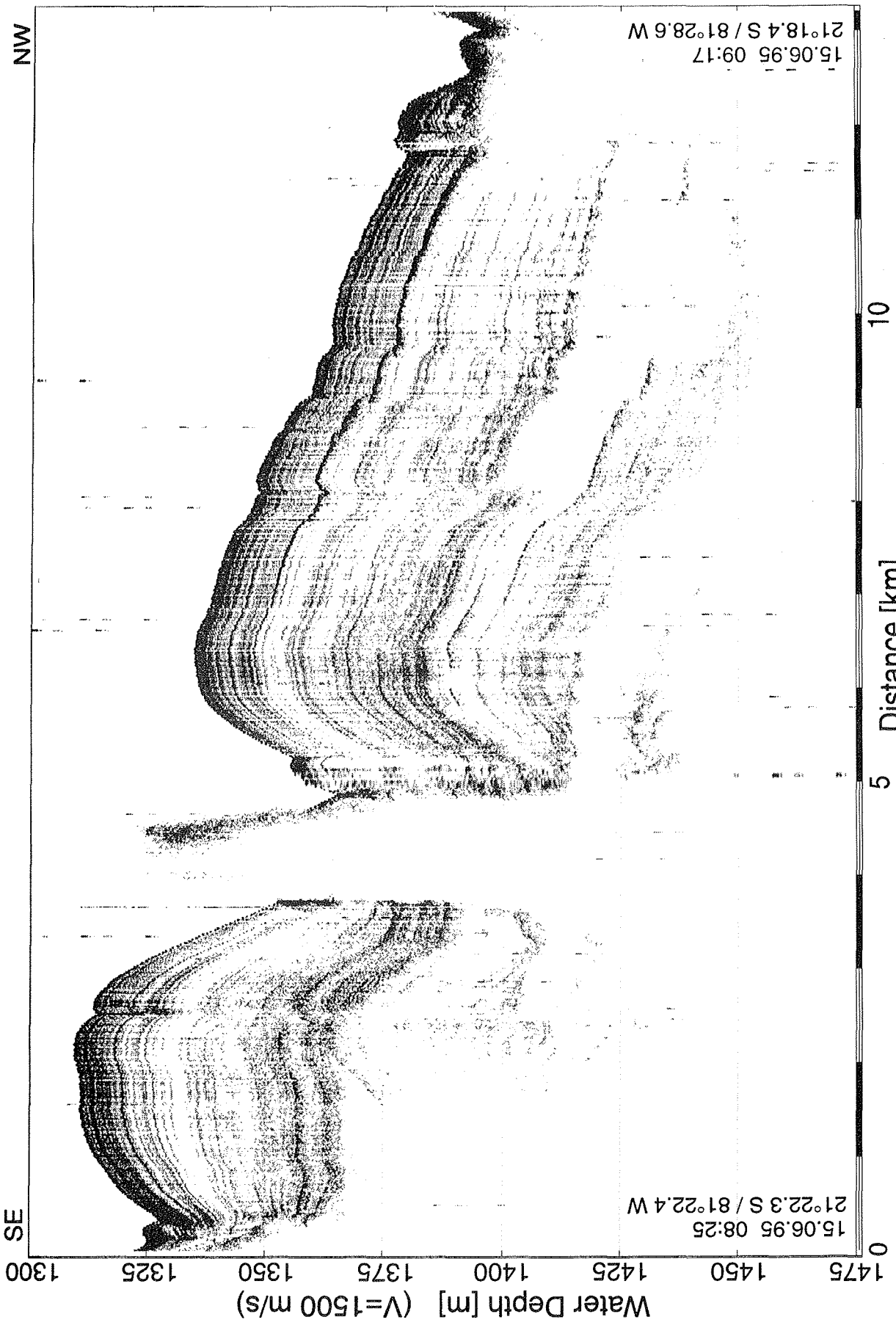

Fig. 11: Digital PARASOUND section from Nazca Ridge. See Fig. 8 for further explanation.

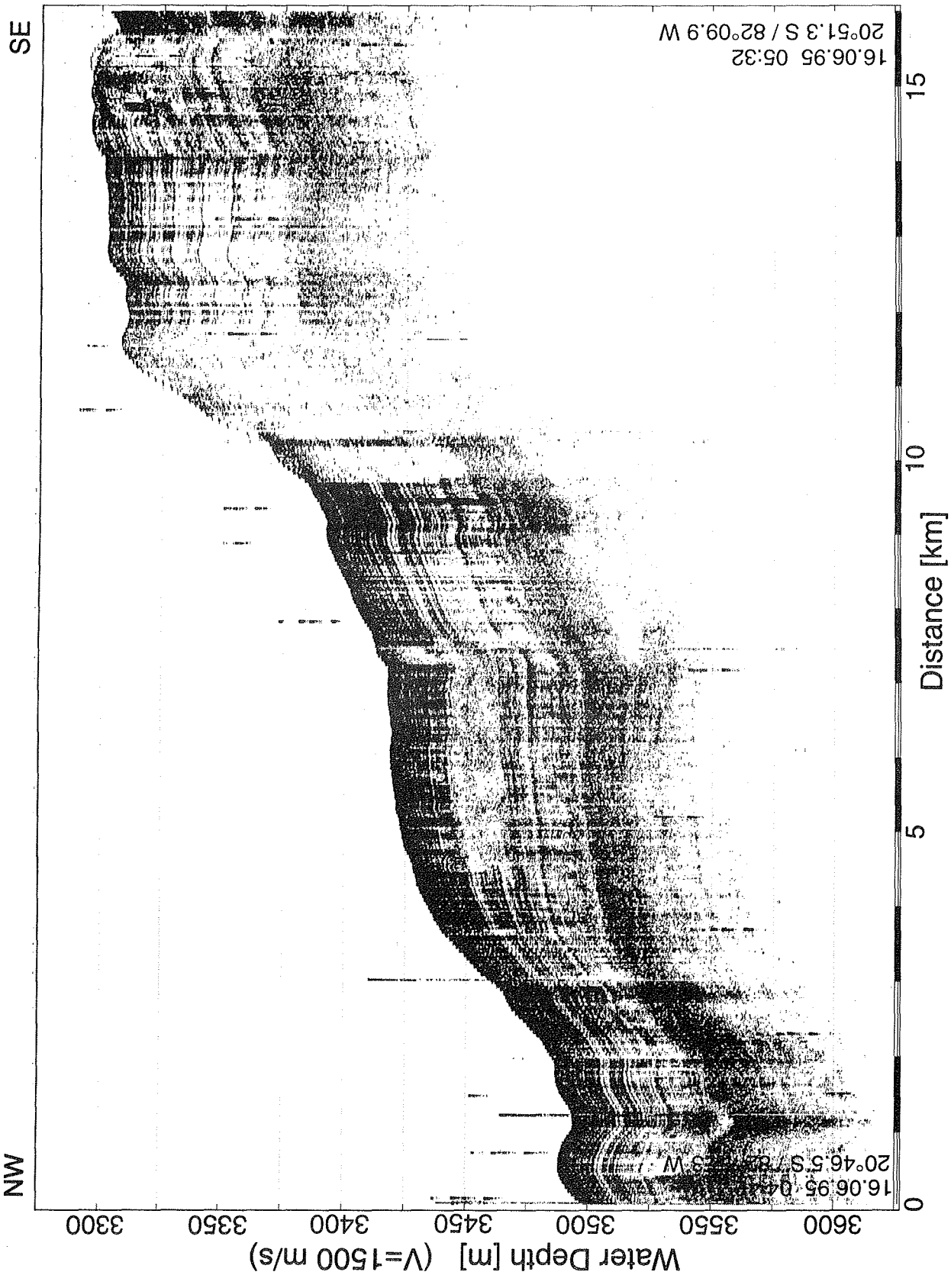

Fig. 12: Digital PARASOUND section from Nazca Ridge. See Fig. 8 for further explanation.

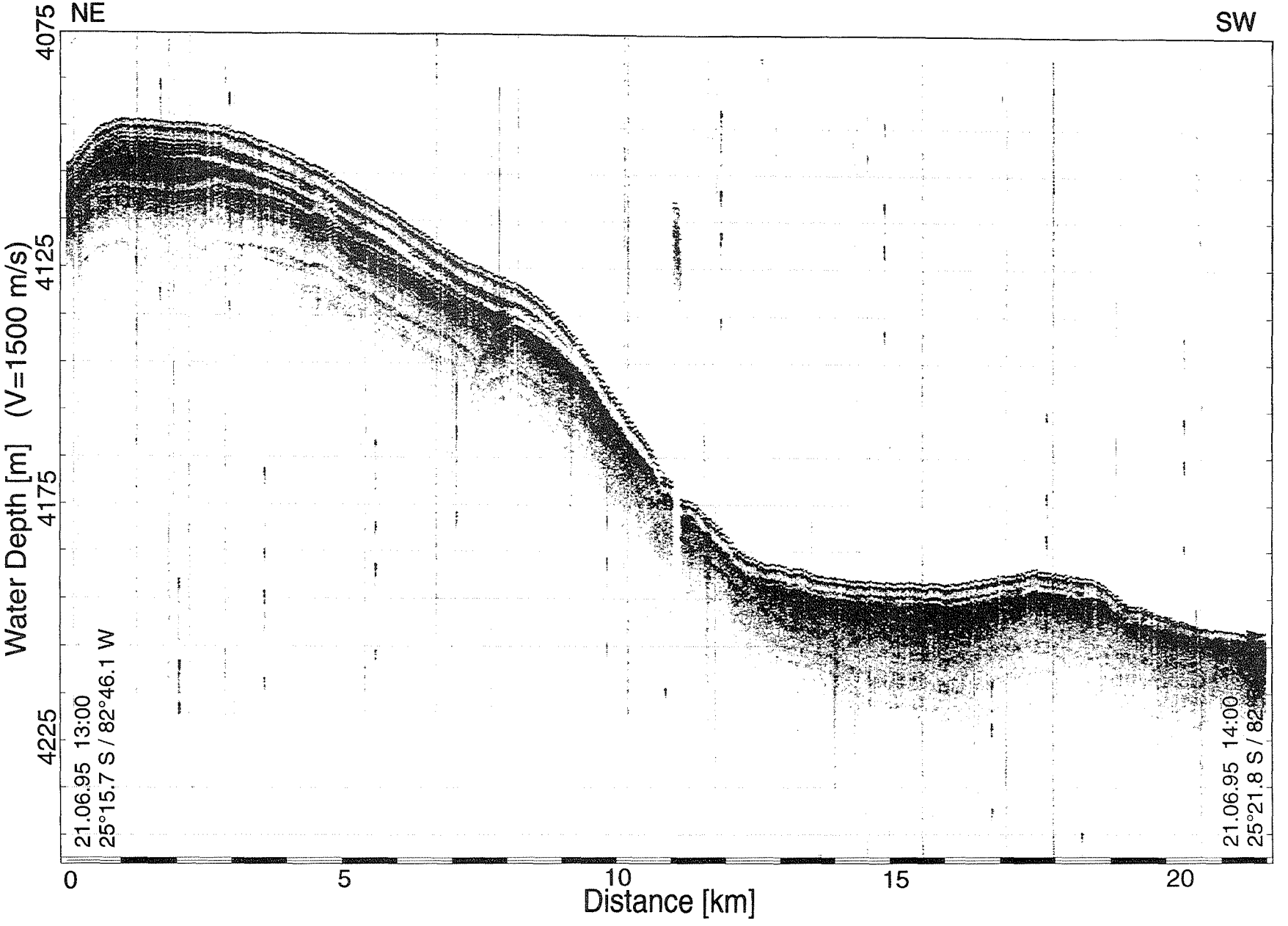

Fig. 13: Digital PARASOUND section acquired on the transect between the Nazca Ridge to the oceanographic profil at 28°15´S. See Fig. 8 for further explanation.

The following two sections in Fig. 11 and 12 were recorded on the northern part of the Nazca Ridge. The first example (Fig. 11) in a water depth between 1300 m and 1400 m lies on a SE-NW oriented profile from ~21°22´S/81°22´W to ~21°18´S/81°29´W. Down to 100 m below sea-floor, numerous distinct parallel reflectors can be found, interrupted by a basement outcrop in the interval between 4 and 5 km. Between 8 and 12 km a pronounced transparent zone is observed in ~50 m sub-bottom depth. Reflectors are interrupted, but above and below stuctures appear to be continuous. This feature can be interpreted as a slump, where a mobilization of a sediment slab is associated with minor lateral movement and vertical faults (e.g. 8 km, 9 km, 9.8 km). Similar structures have been observed e.g. in the Polar Front of the Atlantic sector of the Southern Ocean, where predominantly biosiliceous sediments were accumulated at high rates. The variation of layer thickness and depth in particular close to the basement outcrops further reveals variable current activity, which generated moats.

The second example from Nazca Ridge (Fig. 12) was recorded on a profile in southeastern direction from ~20°47´S/82°17´W to ~20°51´S/82°10´W in a water depth ranging between 3300 and 3500 m. Sedimentation appears to be similar to Fig. 11. Pelagic sediments with distinct parallel reflectors are interrupted in some places by transparent zones (5.5 to 7.5 km), which could originate from gas charging or local debris flows. Steeper parts at 10 to 12 km are transparent due to the higher inclination angle of the slope, which reduces reflected energy.

The digital PARASOUND example in Fig. 13 was measured along the transect from the Nazca-Ridge to the oceanographic profile at 28°15´S latitude. Between ~25°16´S/82°46´W and ~25°22´S/82°57´W the water depth changes from 4100 to 4200 m. Along the profile the penetration depth is small (20 m), but the accumulation rates decrease towards greater water depths. In the southwestern part of this section two or three distinct parallel reflectors are found resting on a strong prolonged reflector, but in the northeastern part at shallower water depth numerous distinct reflectors appear. This difference could be explained by different bottom current activity or by increased carbonate dissolution and CCD fluctuations.

4.5. Sediment Sampling

(D. Beese, V. Diekamp, N. Dittert, B. Donner, M. Giese, D. Hebbeln, R. Hoek, H. Kinkel, F. Lamy, G. Meinecke, B. Meyer-Schack, G. Ruhland, U. Rosiak, M. Segl and G. Wefer)

Sediment sampling - In total 67 stations have been sampled for sediments during SO-102. In addition to the data from SO-102, the sediment sampling during leg 3 of SO-101 (11 stations) will be also reported here. While multicorer and gravity corer have been used on the geological stations (11 on SO-101/3, 25 on SO-102/1 and 35 on SO-102/2), the minicorer has been attached to the CTD/Rosette on 7 of the oceanographic stations (5 on SO-102/1 and 2 on SO102/2). The sediment sampling positions are shown in Fig. 14.

Minicorer - The minicorer is a specially designed instrument, to allow sediment sampling on CTD/Rosette stations by only one deep cast. The minicorer, equipped with 4 tubes of 6 cm diameter, hangs ca. 30 m below the CTD/Rosette, which is lowered to 15 m to 20 m above seafloor to assure penetration of the minicorer into the sediment. Depth control has been provided by a 12 kHz pinger.

Depending on sediment composition and recovered number of samples the minicorer tubes have been sampled for planktic and benthic foraminifera and for organic matter.

Multicorer - The multicorer is the main tool for sampling of complete and undisturbed sediment surfaces together with the overlying bottom weater. It is equipped with 8 tubes of 10 cm diameter and 4 tubes of 6 cm diameter. Sediment recoveries with the multicorer ranged between 0 cm and 42 cm. On some stations it was not possible to retrieve any sediments with the multicorer, what is most probably due to the sediment composition. Specially sandy sediments can very easily spilled out of the tubes, while the multicorer is pulled upward through the water column. In addition, even a careful PARASOUND survey cannot always assure, that the sediments at a chosen site are really well suited, e.g. a single turbidite can sometimes hamper any penetration of the multicorer into the sediment at all.

Due to some technical problems with the multicorer the number of filled tubes was highly variable, ranging from only 4 up to 12 tubes. Thus, the sampling scheme had to be variable as well. Pricipally, the multicorers have to be sampled for the following investigations:

- planktic and benthic foraminifera assemblages: the tubes have been cut in 1 cm slices, which were stored in ethanol with bengal rose at 4°C;

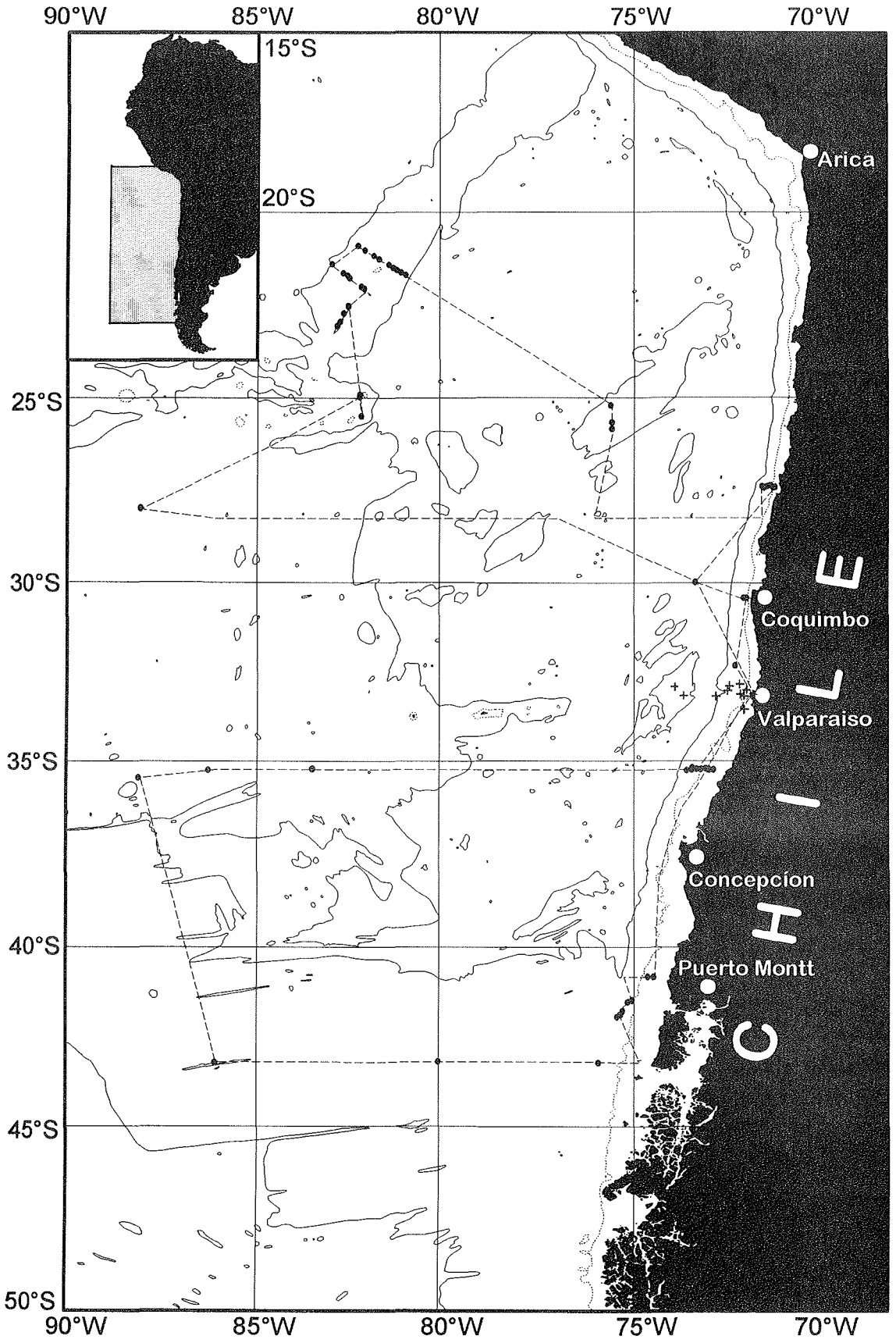

Fig. 14: Sediment sampling sites of SO-102 (dots) and of SO-101/3 (crosses)

Tab. 2: Multicorer and Minicorer (MIC) Sampling

GeoB No.	Water depth	large tubes (10cm diameter)								small tubes (6cm diameter)			
		1	2	3	4	5	6	7	8	1	2	3	4
SO-	**101/3**												
3301-1	969	-	-	-	-	-	-	-	-	-	-	-	-
3301-2	970	PP	Bio	Dino	For	For	For	Fau	Arc	-	Sed	-	Arc
3302-2	1502	PP	Bio	Dino	For	For	-	Fau	Arc	-	Sed	-	Arc
3303-1	1983	PP	Bio	Dino	For	For	For	Fau	Arc	Rad	Sed	Sur	Arc
3304-3	2413	-	Bio	-	For	-	-	Fau	Arc	For./ Rad	Sed	For	Arc
3305-2	3029	-	Bio	Dino	For	-	-	-	Arc	Fau	Sed	For.	Arc
3306-2	4076	-	-	-	-	-	-	-	-	-	-	For.	Arc
3306-3	4075	-	-	-	-	-	-	-	-	-	-	-	-
3308-3	3620	-	-	-	For./ Be	-	-	-	-	Fau	Sed/ Be	Bio	Arc
3308-4	3631	Sur	-	-	-	-	-	-	-	-	-	-	-
3311-2	471	-	-	-	-	-	-	-	-	Bio	For.	Dino	Arc
SO-	**102/1**												
3312-2	583	Mag	-	-	For	For	-	Che	-	Che	Bio	-	-
3312-7	582	-	-	-	-	-	-	-	-	-	-	-	-
3312-8	581	MPI	MPI	MPI	MPI	-	-	-	-	MPI	MPI	-	-
3313-3	851	Mag	-	-	For	For	-	Che	-	-	Bio	-	Arc
3314-2	1652	Mag	-	-	For	For	-	-	Arc	Org	DD	DD	Bio
3315-2	2001	-	-	-	-	-	-	-	-	-	-	-	-
3315-3	2001	-	-	-	-	-	-	-	-	-	-	-	-
3316-1	2574	Sur	Sur	-	-	-	-	-	-	Bio	For.	For.	For.
3316-3	2575	Mag	-	DD	-	-	-	Che	-	Che	-	-	Arc
3317-6	2923	Mag	-	-	For	-	-	Che	-	Bio	DD	For	Arc
3317-7	2919	MPI	MPI	MPI	MPI	MPI	-	-	Arc	Org	MPI	MPI	Che
3318-2	3207	Mag	Bio.	DD	For	For	-	-	Arc	Org	-	Arc	Arc
3319-2	143	-	-	-	-	-	-	-	-	-	-	-	-
3319-3	143	-	-	-	-	-	-	-	-	-	-	-	-
3321-2	593	-	-	-	-	-	-	-	-	-	-	-	-
3323-4	3697	-	-	-	-	-	-	Che	-	Che	Bio	DD	Arc
3323-5	3702	Mag	MPI	MPI	-	-	-	-	-	MPI	MPI	-	-
3323-6	3700	MPI	-	-	-	-	-	-	-	MPI	For.	For.	-
3324-1 MIC	3548									-	-	-	-
3326-1 MIC	3635									For.	Bio	-	-
3327-6	3535	-	-	-	-	-	-	-	-	For.	Bio	MPI	Mag
3328-1 MIC	3693									For.	Bio	-	Arc
3331-4	3763	-	-	-	-	-	-	-	-	-	-	-	-
3331-5	3741	Mag	Bio	DD	For	MPI	MPI	Che	Che	MPI	MPI	Arc	Arc
3336-3	3995	Mag	-	DD	For	-	-	-	-	For.	DD	Bio	Arc
3337-5	4073	Mag	MPI	MPI	Sur	-	-	-	-	MPI	MPI	Bio	Arc
3339-2	3792	Mag	Bio	DD	For	-	-	-	-	Arc	-	-	-

GeoB No.	Water depth	large tubes (10cm diameter)								small tubes (6cm diameter)			
		1	2	3	4	5	6	7	8	1	2	3	4
3345-1	4023									-	-	-	-
MIC													
3347-1	4182									For.	For.	Bio	Arc
MIC													
3349-4	2471	Mag	MPI	DD	For	Che	Che	MPI	MPI	Che	Bio	For	Arc
3350-1	3732	-	-	-	-	-	-	-	-	-	-	-	-
3352-1	2098	Mag	Bio	DD	For	For	For	Arc	Arc	Org	Arc	Arc	Arc
3353-1	3747	Mag	-	DD	For	-	-	-	-	Org	Bio	For	Arc
3354-1	3234	-	-	DD	For	-	-	-	-	Org	Bio	For	Arc
3355-4	1503	Mag	Bio	DD	For	MPI	MPI	MPI	Che	Org	For	Che	Arc
3357-1	2097	Mag	Bio	DD	For	For	-	-	Arc-	Org	For	Arc	Arc
3359-1	680	Mag	Bio	DD	For	-	-	-	-	Org	-	Arc	Arc
3360-1	583	-	-	-	-	-	-	-	-	-	-	-	-
SO-	102/2												
3365-1	2450		Bio	Dino	For	For	-	-	-	Org	Diat	For	Arc
3368-4	3240	Mag	Bio	Dino	For	For	For	-	-	Org	Diat	Arc	Arc
3371-1	3458	Mag	Bio	Dino	For	For	For	Arc	-	Org	Diat	Arc	Arc
3372-4	4409	Mag	Bio	Dino	For	For	For	-	-	Org	Diat	Arc	Arc
3373-1	1580	Mag	Bio	Dino	-	-	-	-	-	For	Diat	For	Arc
3374-1	1352	Mag	Bio	Dino	For	For	For	-	Arc	Org	Diat	-	Arc
3375-2	1948	Mag	Bio	Dino	For	-	-	-	-	Org	Diat	For	Arc
3376-2	2437	Mag	Bio	Dino	For	For	For	-	-	Org	Diat	Arc	Arc
3377-1	3576	Mag	Bio	Dino	For	For	-	-	-	Org	Diat	Arc	Arc
3378-2	3286	Mag	Bio	Dino	For	For	For	-	Arc	Org	Diat	Arc	-
3381-1	5256									Sur	Sur	Sur	-
MIC													
3383-1	4207									Bio	For	For	Arc
MIC													
3387-3	2629	-	Bio	Dino	For	For	-	-	-	Org	Diat	For	Arc
3388-2	3557	Mag	Bio	Dino	For	For	For	-	-	Org	Diat	Arc	Arc
3389-3	4482	Mag	Bio	Dino	For	For	For	-	Arc	Org	Diat	-	Arc
3390-2	3243	Mag	Bio	Dino	For	For	For	-	Arc	Org	Diat	-	Arc
3391-2	2296	-	-	-	-	-	-	-	-	-	-	-	
3391-3	2296	-	-	-	-	-	-	-	-	-	-	-	-
3392-1	1723	Mag	Bio	Dino	For	For	For	-	Arc	Org	Diat	-	Arc
3393-3	1371	-	-	-	-	-	-	-	-	-	-	-	-
3393-4	1360	Mag	Bio	Dino	For	-	-	-	-	Org	Diat	For	Arc
3394-1	1982	?	?	?	?	?	?	?	?	?	?	?	?
3395-3	2413	-	Bio	Dino	For	-	-	-	-	For	Diat	For	Arc
3396-1	3092	-	Bio	Dino	For	For	-	-	-	Org	Diat	For	Arc
3397-2	3452	Mag	Bio	Dino	For	-	-	-	-	Org	For	For	Arc
3398-1	3191	-	Bio	Dino	For	For	-	-	-	Org	Diat	For	Arc
3399-2	2890	-	Bio	Dino	For	-	-	-	-	For	Diat	For	Arc
3400-1	2541	Mag	Bio	Dino	For	-	-	-	-	Diat	For	-	Arc
3401-3	2459	Mag	Bio	Dino	For	For	-	-	-	Org	Diat	For	Arc
3402-1	2887	Mag	Bio	Dino	For	For	For	-	Arc	Org	Diat	For	Arc
3403-1	3517	Mag	Bio	Dino	For	For	For	-	Arc	Org	Diat	For	Arc
3405-1	864	-	-	-	-	-	-	-	-	-	-	-	-

GeoB No.	Water depth	large tubes (10cm diameter)								small tubes (6cm diameter)			
		1	2	3	4	5	6	7	8	1	2	3	4
3406-1	1957	Mag	Bio	Dino	For	For	For	-	Arc	Org	Diat	For	Arc
3407-2	2250	Sur	Sur	Sur	Sur	-	-	-	-	-	-	-	-
3408-1	1586	Sur	Sur	Sur	Sur	-	-	-	-	-	-	-	-
3409-2	2817	Sur	Sur	Sur	Sur	-	-	-	-	-	-	-	-
3410-1	1260	Sur	Sur	Sur	Sur	-	-	-	-	-	-	-	-
3411-1	1160	Sur	Sur	Sur	Sur	-	-	-	-	-	-	-	-
3414-3	3753	Mag	Bio	Dino	For	For	-	-	Arc	Org	Diat	-	Arc

Arc - Archive (GeoB)
Bio - Biomarker (Hebbeln, GeoB)
DD - Diatoms and Dinoflagellates (GeoB)
Dino - Cysts of Dinoflagellates (SO-101/3: Biebow, GEOMAR, SO-102/2: Hoek, GeoB))
Fau - Faunal composition (Spiegler, GEOMAR)
For - Foraminiferal assemblages and stable oxygen and carbon isotopes (Hebbeln, GEOB)
Mag - Magnetotactic bacteria (Petermann, GeoB)
MPI - Biogeochemical investigations (Glud, MPI)
Org - Organic geochemistry (Wagner, GeoB)
PP - Physical Properties (Biebow, GEOMAR)
Rad - Radiolaria, surface sample (GeoB)
Sur - unspecified surface sample (GeoB)
Sed - Sedimentology (Locker, GeoB)

- organic matter composition: the tubes have been cut in 1 cm slices, which have been frozen;
- diatom assemblages: the tubes have been cut in 1 cm slices, which were stored in methanol or ethanol at 4°C;
- dinoflagellate assemblages: the tubes have been cut in 1 cm slices, which were stored at 4°C;
- organic petrography: a small tube has been frozen;
- oxygen content: microprobe analysis of the whole sediment column;
- geochemical investigations;
- magnetotactic bacteria;
- at the most stations a sample of bottom water has been sucked of from one of the 10 cm diameter tubes in order to measure its stable oxygen and carbon isotope composition;
- one or two tubes have been frozen as archive material.

At stations were the benthic lander systems have been deployed an additional multicorer was taken for a different set of biogeochemical analyses. A detailed overview about the MUC-sampling is given in Tab. 2.

Gravity corer - In order to get long sediment cores, gravity corer with 6 m or 12 m tubes have been used. A total of 72 sediment cores have been retrieved with recoveries between 77 and 1025 cm. The total core recovery during SO101/3, SO-102/1 and SO-102/2 was 325 m, including 9.6 m for geochemical studies and 10 m for studies at Geomar in Kiel.

At the coring sites two main problems hampered the collection of longer sediment cores. Along the continental slope the sediments became quite stiffy and consolidated already a few meters below sediment surface. Due to the stiffness of the sediments at almost all continental slope stations the copper plates inside the core catcher have been partly or totally destroyed. Therefore, the mechanism to keep the sediments inside the tubes could not work perfectly. That is probably one reason resulting in core lengths of less than 10 m. The main reason for that, however, has been the strong consolidation of the sediments below ca. 5 m sediment depth. The consolidated sediments didnot allow a deeper penetration of the gravity corer. Due to this effect quite a number of 12 m tubes have been bent by trying to obtain longer sediment cores and there was no chance at all to try 18 m tubes.

At the oceanic sites comparable problems occured. Specially at the deeper sites (>2000 m) along the Nazca Ridge the cores stucked in 5 m to 6 m sediment depth. There, the sediments found in the core catcher consisted of an almost dry and very hard nannofossil ooze, which was not possible to penetrate with the gravity corer. On the shallower sites (<2000 m) the sediments were much coarser, consisting mainly of foraminifera sand, again hard to penetrate by a gravity corer. At these shallow sites the retrieved sediments cores were even shorter and at some stations the tubes even have been bent.

Originally it was planned to use a piston corer, which has been provided by the Geological Institute, University of Kiel. However, the provided equipment allowed only the use of an 18 m tube for the piston corer. The experience with the gravity corers showed, that the use of such a long tube would have been just a waste of material, because an 18 m tube will almost certainly bend if penetration is less 10 m. For that reason the piston corer has not ben used during this cruise.

Before preparing the gravity corer the plastic liners had been marked lengthwise with a straight line in order to retain the orientation of the core, even after it was cut into segments. Once on board, the sediment core was cut into 1 m pieces, closed with caps on both ends and inscribed

after standard scheme. Afterwards, the core segments have been cut into two halves. One half, the so-called archive half, was used for core description, core photography, smear slide sampling, measurements of backscattered light using a colour scanner and, only during leg 1, for measurements of the magnetic suszeptibility. The work half were sampled for paleomagnetic investigations in 10 cm intervals, with two series of syringes for geochemical and faunal studies, both at 5 cm intervals. For preliminray biostratigraphic studies, the cores from the Iquique Ridge and from the Nazca Ridge have been sampled also with syringes at 5 cm intervals in the uppermost 20 cm of the cores and at 20 cm intervals further downcore. The sampling holes were plugged with pieces of polystyrol and both halves of the cores were stored in core tubes. To avoid fungal infestation of the cores, a sponge soaked in a fungicide solution was put into each core tube before closing and storing at 4°C.

4.6. Core Description and Smear Slide Analysis

(F. Lamy, M. Marchant, H. Kinkel, G. Meinecke and D. Hebbeln)

Methods - The core description summarizes the most important results obtained by shipboard analysis of each sediment core following ODP convention. Core descriptions for all retrieved sediment cores are shown in Fig. 15 to 74. The lithological information indicated in the lithology column is based on visual analysis of the core. In the structure column the intensity of bioturbation (as well by visual analysis) together with individual or special features such as rock-/ or shell-.fragments and possible turbiditic layers is shown. The hue and chroma attributes of colour were determined by comparison with the MUNSELL soil colour charts and are given in the colour column in the MUNSELL notation. All descriptive informations from the cores were taken inmediately after splitting them.

On SO-102 a Minolta CM - 2002™ hand-held spectrophotometer was initially used to measure percent reflectance values of sediment color at 31 wavelength channels over the visible light range (400-700 nm). The digital reflectance data of the spectrophotometer readings were routinely obtained from the surfaces of all split cores recovered during the cruise to provide a continuous record of color variations from every core.

Most of the cores show no distinct variation in lithology and color. For these cores the observed reflectances were dominated by very high variability of individual measurements (noise)

that mostly results from burrowing, which left disseminated millimeter-sized black spots in the sediment. The presence of silt laminae also affected the reflectance values.

Trace components might affect the color spectrum significantly. The presence of strong color signals associated with minor amounts of oxyhydroxides or sulfides masks the underlying color changes in the major lithologic components (Mix et al., 1992). To isolate these effects the ratio of reflectance between particular wavelength bands can be used. According to Mix et al. (1992) the most prominent reflectance differences are between the red (650-700 nm) and the blue (450-500 nm) spectral bands. To add more information to the core description also the red/blue ratio (700 nm : 450 nm) for each core is displayed in Fig. 15 to 74.

In order to support the macroscopic core description a smear slide analysis was carried out. Smear slides were taken from every sediment core and mounted with Canada-Balsam (n=1.54). Smear slides were primarily taken from all representative lithologies, and from striking or unique layers of particular interest. Altogether 852 smear slides from 59 cores were examined on board using a light microscope at 25 to 100x magnification with cross polarized and transmitted light.

The smear slide analysis differentiates biogenic (foraminifera, coccolithophorids, radiolarians, diatoms etc) and non-biogenic components (clay minerals, quartz, feldspar etc). The sediment classification is based on ODP nomenclature following the terminology of DEAN et al. (1985) and is given in the following text, but not in the lithology column.

Shipboard results - Cores were examined from 4 transects of the continental slope at latitudes around 33°S (transect A), 41° to 43°S (transect B), 35°S (transect C) and 27° to 30°S (transect D). The cores consist mainly of hemipelagic sediments. Turbidites have been observed in some of them. In addition, some cores from deep-sea areas at ca. 43°S; 80°W (1 core) and 35°S; 83 to 88°W (2 cores) have been recovered. They consist of pelagic biogenous sediments. Additional cores were taken from pelagic regions in form of transects of the Iquique-Ridge (ca. 25°S; 75°W) and the Nazca-Ridge (ca. 21°S; 82°W). These cores consist exclusively of pelagic biogenous sediments. Finally 2 cores were recovered at the western end of the oceanographic transect at 28°S; 88°W. They are composed of deep sea clay and calcareous to siliceous biogenous sediments.

Transect A

Core GeoB 3301-3 (water depth 974 m; 33°08,8´S; 71°58,9´W, length 466 cm, Fig. 15)

This core is nearly exclusively composed of brown olive silty clay, except for the upper 10 cm which contain an olive gray sandy clay and the interval between 390 and 425 with dark brown clayey sandy silt. There are no turbidites encountered and the sediments are only in smaller intervals bioturbated. Some shell fragments have been observed. According to the smear slide analysis the sediment of the whole core is classified as a rock fragment volcanic glass bearing clay.

Core GeoB 3302-1 (water depth 1498 m; 33°13,1´S; 72°05,4´W; length 412 cm, Fig. 16)

Lithologically the upper 212 cm of the core consist of olive to olive gray sandy silty clay. The remaining part of the core is silty clayey, the colour is olive brown gray. The sediment is partly bioturbated and between 250 and 312 cm some shell fragments were observed. No turbidites are present. According to the smear slide analysis the sediments of the whole core are classified as a volcanic glass rock fragment bearing clay.

Core GeoB 3303-2 (water depth 1984 m; 33°12,4´S: 72°10,5´W; length 389 cm, Fig. 17)

The sediments of this core mainly consist of an olive gray silty clay, except for the uppermost 6 cm, where sand is present. The amount of bioturbation is variable and shell fragments are rarely present. No turbidites have been observed. The sediment rock name, according to the smear slide analysis, is volcanic glass rock fragment bearing clay and does not change throughout the core.

Core GeoB 3304-5 (water depth 2411 m; 32°53,4´S; 72°11,5´W; length 911 cm, Fig. 18)

Only the uppermost 200 cm of the core contain gray olive sandy silty clay, while the remaining part consists of an interbedding of the same sediment and dark gray sandy layers. Between a depth of 200 and 500 cm of depth the sandy layers are turbiditic. At a depth of 616 cm, a shell fragment was observed. The sediment is partly bioturbated. According to the smear slide analysis the sediment of the core is classified as a volcanic glass rock fragment bearing clay.

Core GeoB 3305-1 (water depth 3028 m; 32°51,1´S; 72°25,4´W; length 424 cm, Fig. 19)

This core can be clearly divided in two segments. The upper part (0 to 160 cm) is lithologically an olive gray silty clay which is partly bioturbated. The lower part (160 to the bottom of the

core) can be described as an interbedding of silty clay with sand layers which are only a few cm of thickness. One sand layer (280 to 283 cm) shows a turbiditic structure. The silty clay is often bioturbated and contains several sand lenses between 225 to 300 cm depth. The colour of the lower part is more variable and ranges from olive gray to brown, and in some parts green and purple colours are also present. The sediment rock name according to the smear slide analysis is rock fragments bearing clayey nannofossil ooze (0 to 40 cm) and volcanic glass rock fragment bearing clay (40 cm to end) except for one sample (110 cm) which is a volcanic glass rock fragment bearing clay nannofossil ooze.

Core GeoB 3306-4 (water depth 4080 m; 33°00,9´S; 72°29,5´W; lentgh 538 cm, Fig. 20)

This core consists nearly exclusively of silty clay. In the uppermost 300 cm there are some layers with a small sand content, but only one layer (285 cm) can be titled as sand. The colour changes between brown gray, olive gray and dark gray. Mixed and patchy colours are present. The grade of bioturbation of the uppermost 200 cm is small but increases in the lower part of the core. No turbidites have been observed. The sediment rock name according to the smear slide analysis is variable. In the upper half of the core radiolarian (Nassellaria group) oozes are dominating while the samples from the lower half mainly contain sponge spicules oozes.

Core GeoB3308-1 (water depth 3625 m; 33°07,9´S; 73°44,9´W; length 937 cm, Fig. 21)

This core is lithologically composed of silty clay with some sand patches (around 500 cm) or lenses (around 600 cm). At a depth of 525 cm a turbiditic layer is present. The colour of the sediment is variable and changes from olive gray, olive brown and brown to gray brown. The grade of bioturbation is high in the uppermost 300 cm of the core and again around 500 cm. The remaining sediments show only scarce bioturbation. The smear slide analysis shows variable sediment types. Some samples consist mainly of biogenous components (nannofossil oozes), while in others terrigenous components are dominating (clays).

GeoB 3311-1 (water depth 472 m; 33°36,4´S; 72°02,8´W; length 385 cm, Fig. 22)

This core is nearly exclusively composed of olive gray to brown gray silty clay. Only between 2 and 7 cm a sandy turbiditic layer occurs and at a depth of 220 cm a brown gray sandy silty clay is present. As a striking feature a complete bivalve was observed at a depth of 69 cm. The sediments are partially bioturbated. According to the smear slide analysis the sediment is classified as a quartz bearing rock fragment clay. The content of the components throughout the core is very homogeneous.

GeoB 3365-2 (water depth 2449 m; 32°17,1´S; 72°16,0´W; length 193 cm, Fig. 42)

The uppermost 90 cm consist of olive, dark olive and dark gray silty clay and clayey silt. Bioturbation is commonly observed. From 90 to 160 cm numerous sand layers and lenses (mostly turbiditic) of a dark olive silty clay are observed. The lowermost 15 cm of the core show a strongly bioturbated dark olive gray silty clay. The smear slide analysis allows to classify all samples as volcanic glass rock fragment bearing clay.

Transect B

GeoB 3312-5 (water depth 580 m; 41°00,5´S; 74°20,2´W; length 471 cm, Fig. 23)

This core is lithologically dominated by silty clay with colours ranging from dark gray olive to olive gray. The uppermost 9 cm are composed of olive gray sand which is turbiditic. Between 100 and 135 cm some shell fragments were observed and between 200 and 300 cm rock fragments occur with a diameter up to 0.5 cm. At 440 cm a gastropode shell was found. Bioturbation is common throughout the core but more intense in the upper 200 cm. According to the smear slide analysis the core is mainly dominated by clay with an increasing content towards the bottom of the core. In the uppermost 60 cm the sediments are classified as clayey foraminifera ooze and in the middle part (60 to 270 cm) as clayey nannofossil ooze. In the remaining part of the core biogenous components are only minor and the sediments are classified as calcite clay.

GeoB 3313-1 (water depth 850 m; 41°00,0´S; 74°27,0´W; length 807 cm, Fig. 24)

This core exclusively consists of silty clay. The colours are mostly olive to dark olive gray. In the lower half of the core the colours are partly patchy. The bioturbation is strong throughout the core increasing slightly towards the bottom. In some parts of the core a H_2S-smell can be noted. Shell fragments have been observed at a depth of 452 cm. Turbiditic layers are not present. According to the smear slide analysis the terrigenous components (mainly rock fragments and clay) are homogenous throughout the core and are the dominating components. The biogenic components are more variable and become more frequent at a depth of 154 cm. Down to this depth the sediment is classified as rock fragment bearing clay, from 154 to 355 cm as a clayey diatom ooze, from 406 to 666 cm as clayey nannofossil ooze and from 666 cm to the bottom as clayey nannofossil foraminifera ooze.

GeoB 3314-3 (water depth 1647 m; 41°36,2´S; 74°58,8´W; length 577 cm, Fig. 25)

The sediments of this core are mainly composed of silty clay. The colours are variable and change between olive, olive gray and dark gray. Between 70 and 170 cm 4 turbiditic layers were identified, which consist of dark gray to gray olive sand. Another turbidite occurs at 505 cm. In the lower half of the core a special feature was observed, namely mud pellets and rarely a H_2S smell. Shell fragments appear around 150 cm and 500 cm. Bioturbation is common thoughout the core and generally moderate. According to the smear slide analysis terrigenous particles (rock fragments and clay) are the dominant components while biogenous particles are minor and consist of nannofossils and foraminifera in changing abundances.The sediment rock types are clayey nannofossil and clayey foraminifera ooze.

GeoB 3315-1 (water depth 1999 m, 41°40,1´S; 75°02,7´W; length 616 cm, Fig. 26)

This core is exclusively composed of silty clay which is pedominantly olive gray. At a depth of 382 cm, the succession is disturbed by a 3 cm thick gray olive sandy turbiditic layer. The whole core is intensively bioturbated. A shell fragment was observed at 569 cm and in some parts of the core a H_2S smell was noted. According to the smear slide analysis rock fragment clays are predominant, however, some samples are clayey biogenous oozes.

GeoB 3316-4 (water depth 2575 m, 41°56,3´S; 75°12,8´W, length 554 cm, Fig. 27)

The whole core mainly consists of olive silty clay. Mollusc shell fragments were found at depths of 201 cm and 320 cm. Bioturbation is moderate throughout the core and only the lowermost part is strongly bioturbated. According to the smear slide analysis the sediments are nearly exclusively classified as clayey nannofossil oozes.

GeoB 3317-1 (water depth 2882 m, 42°00,8´S; 75°18,2´W, lenght 413 cm, Fig. 28)

The sediments of this core are composed of olive to olive gray silty clay with interbedded sand layers throughout the core. The sand layers are dark to dark gray and mostly turbiditic. The upper165 cm of the core are not bioturbated but deeper sediments show partly a slight to moderate bioturbation. According to the smear slide analysis rock fragment clays and clayey nannofossil oozes are dominating. Turbiditic layers show a high quartz content.

GeoB 3318-3 (water depth 3183 m, 42°02,3´S; 75°19,3´W, lenght 574 cm, Fig. 29)

The core consists of olive to olive gray silty clay, which sometimes has a certain sand content. Some of the sandy layers show a turbiditic structure especially in the upper 120 cm and around

400 cm. Real sand layers are rare. Shell fragments and clay concretions occur in some parts throughout the core. Bioturbation is rare in this core and has been observed only between 200 and 300 cm and in the lowermost 100 cm. According to the smear slide analysis all sediments were classified as volcanic glass rock fragment bearing clay.

GeoB 3323-9 (water depth 3703 m, 43°13,1´S; 75°57,0´W, length 299 cm, Fig. 30)

The uppermost 150 cm consist of olive to olive gray silty clay, which is slightly bioturbated between 100 and 150 cm. From 150 cm to the end of the core sand layers and lenses occur in increased frequency and thickness towards the buttom. The structure of these layers often is turbiditic. Bioturbation is nearly absent. The smear slide analysis of the uppermost 150 cm shows mainly rock fragment bearing clay. Deeper volcanic glass becomes abundant (volcanic glass clay). As a conspicuous feature a sponge spicule (45%) ooze was observed at a depth of 170 cm.

Transect C

GeoB 3349-3 (water depth 2466m; 35°15,2´S; 73°25,2´W; length 566 cm, Fig. 34)

Lithologically the uppermost 300 cm consist of a homogenous olive silty clay which is only partly sligthly bioturbated. From 300 cm to the bottom of the core the lithology remains almost constant, only between 360 and 430 cm some sand content was noted. The colours are more diverse. They change from olive green over green to black in the lowest 100 cm of the core, where a H_2S smell was observed. Bioturbation is variable but especially strong between 430 and 550 cm. According to the smear slide analysis all sediments were classified as volcanic glass rock fragment bearing clay.

GeoB 3350-2 (water depth 3750 m; 35°15,0S; 73°34,6W; length 582 cm, Fig. 35)

The uppermost 425 cm of the core is composed of silty clay with colours ranging from olive gray to dark oliv gray. Shell fragments were observed around 100 cm depth. At 150 cm a turbiditic layer is present. Bioturbation is nearly absent. From 425 cm down to the end of the core numerous sand layer occur, which are mostly turbiditic. Around 420 cm shell fragments occur frequently. Bioturbation is almost absent. The smear slide analysis shows variable sediment rock types. Predominantly volcanic glass rock fragment bearing clays occur. Two samples were classified as clayey sponge spicule ooze, one as a clayey nannofossil ooze and one, as a special feature, as quartz pyrite volcanic glass bearing rock fragment clay (537 cm).

GeoB 3352-1 (water depth 2104 m; 35°13,0´S; 73°19,0´W, length 391 cm, Fig. 36)

Between the top of this core and 190 cm mainly olive gray to dark olive silty clay with some sand lenses, which may be partly turbiditic, occurs. Bioturbation was noted around 180 cm. Shell fragments were observed in the uppermost cm of the core. From 190 cm up to the bottom of the core dark olive gray silty clay again predominates but frequently sand layers are present, which are mostly turbiditic. Around 350 cm the sediments are bioturbated. According to the smear slide analysis all the samples are classified as volcanic glass rock fragment bearing clay.

GeoB 3354-2 (water depth 3239 m; 35°13,0´S; 73°29,3´W; length 623 cm, Fig. 37)

From the top up to a depth of 270 cm the core is composed of olive gray silty clay, partly characterized by slight bioturbation. Shell fragments were observed at 117 cm. Beginning at a depth of 270 cm the silt content increases (clayey silt). Between 350 and 390 cm the sediment was disturbed and no description was possible. In the lowest part of the core again silty clay with colours ranging from olive gray to dark olive gray is dominating. From 440 to 500 cm a turbiditic sand layer and some sand lenses occur with the sediment partially bioturbated. Shell fragments are abundant in the lowermost meter of the core. The smear slide analyses shows dominating volcanic glass rock fragment bearing clay. From 100 cm to 200 cm nannofossil ooze occur and one sample of the lowermost meter of the core was classified as a sponge spicule ooze.

GeoB 3355-3 (water depth 1505 m; 35°13,0´S; 73°07,0´W; length 631 cm, Fig. 38)

The uppermost 380 cm of this core consist of homogenous dark olive to dark olive gray silty clay. Shell fragments were observed at a depth of 100 cm. Bioturbation occurs around 300 cm. The remaining part of the core is lithologically similar but turbidites are present at depths of 380 cm and between 550 and 570 cm. The lowermost 40 cm of the core is classified as a clayey silt. Bioturbation is nearly absent and was only observed around 560 cm depth. According to the smear slide analysis the sediments were classified as volcanic glass rock fragment bearing clay, except for one sample (605 cm) which is a clayey nannofossil ooze. In the lower part of the core the pyrite content of some samples exceeds 10%.

GeoB 3357-2 (water depth 2104 m: 35°17,0´S: 73°13,1´W; length 496 cm, Fig. 39)

From the top to a depth of 230 cm the lithology is a homogenous silty clay. The colour is olive gray. Occasionally a slight bioturbation occurs. Shell fragments were observed at a depth of 89

cm. Between 150 and 200 cm a H_2S smell was noted. The remaining part of the core consists of clayey silt, silty clay and rare turbiditic sand layers.The colour of the sediment is exclusively dark gray. A shell fragment is present at 307 cm. Bioturbation is nearly absent. The smear slide analysis allows to classify the sediments as a volcanic glass rock fragment bearing clay but one sample (60 cm) was named a clayey diatom ooze.

GeoB 3358-1 (water depth 797 m; 35°13,0´S; 72°56,1´W; length 122 cm, Fig. 40)

This very short core consists exclusively of olive to dark olive silty clay. Only the uppermost 10 cm show bioturbation. Shell fragments occur occasionally. No turbidites are present. According to the smear slide analysis all samples are volcanic glass rock fragment bearing clays.

GeoB 3359-3 (water depth 678 m; 35°13,0´S; 72°48,5´W; length 380 cm, Fig. 41)

Like the previous core the sediments are olive gray silty clays. Bioturbation was partly observed but is generally rare. Shell fragments are common throughout the core. Turbidites do not occur. The smear slide analysis shows exclusively volcanic glass rock fragment bearing clays.

Transect D

GeoB 3368-2 (water depth 3238 m: 30°21,6´S; 71°57,5´W; length 462 cm, Fig. 43)

This core is composed of olive gray silty clay with numerous sandy layers and lenses, which are often turbiditic. Bioturbation occurs in the upper 160 cm and again in the lowermost 100 cm of the core. Shell fragments were observed at a depth between 360 and 425 cm. According to the smear slide analysis the sediments are predominantly volcanic glass rock fragment bearing clays. One sample (227 cm) was classified as a clayey foraminifera ooze and another one (286 cm) as a clayey sponge spicule ooze.

GeoB 3369-1 (water depth 3457 m; 30°21,6´S; 72°01,0´W; length 552 cm, Fig. 44)

The lithology of this core can be characterized as an interbedding of a few cm thick sandy layers and lenses with olive to olive gray silty clay. The sand layers mostly show a turbiditic structure. Bioturbation is generally rare. Some shell fragments occur throughout the core. The smear slide analysis allows to classify the mayority of the samples as volcanic glass rock fragment bearing clay. Only between 120 cm 300 cm clayey nannofossil oozes are present.

GeoB 3373-2 (water depth 1581 m; 27°30,0´S; 71°12,5´W; length 426 cm, Fig. 45)

This core is mainly composed of silty clay, only between 115 cm to 135 cm clayey silt occurs. No turbidites are present. The colour range shows a cylic variation between olive gray and dark gray brown. Bioturbation is common throughout the core. Shell fragments were observed between 75 and 95 cm depth. The smear slide analysis shows rock fragment bearing clay as the main sediment type. In the uppermost and lowermost part of the core some clayey nannofossil oozes are present.

GeoB 3374-2 (water depth 1352 m; 27°28,4´S; 71°10,3´W; length 477 cm, Fig. 46)

The core consists exclusively of silty clay. The colours are variable and range from dark olive gray to olive, between 70 and 100 cm the colour of the sediment is dark gray green. The whole core is intensively bioturbated in some intervals. No turbidites were observed. According to the smear slide analysis the uppermost samples (0 to 66 cm) were classified as quartz volcanic glass rock fragment bearing clay. The remaining sediments are volcanic glass rock fragment bearing clays, except for one sample (152 cm) which was classified as a clayey sponge spicule ooze.

GeoB 3375-1 (water depth 1947 m; 27°28,0´S; 71°15,1´W; length 489 cm, Fig. 47)

The lithology is very similar to the previous core. Silty clays are again the only sediment type. The colours range from olive gray to green gray. Bioturbation is common throughout the core and is partly strong. No turbidites are present. The smear slide analysis allows to classify the sediments as volcanic glass rock fragment bearing clay in the upper part of the core, while in the lower part beginning at a depth of 223 cm volcanic glass rock fragment bearing clay nannofossil oozes were observed.

GeoB 3376-1 (water depth 2445 m, 27°28,0´S; 71°21,7´W; length 475 cm, Fig. 48)

The core is composed of a homogenous dark gray brown to olive gray silty clay. Bioturbation is rare throughout the core and occurs only in the uppermost 130 cm and in the lowermost 100 cm of the core. Shell fragments occasionally occur in the lower half of the core. According to the smear slide analysis the sediments were exclusively classified as volcanic glass rock fragment bearing clay. Only two samples show higher biogenous contents and are characterized as clayey nannofossil foraminifera ooze (283 cm) and clayey nannofossil ooze (424 cm).

GeoB 3377-2 (water depth 3584 m; 27°28,0´S; 71°31,6´W; length 510 cm, Fig. 49)

The lithology of this core is very homogenous and consists only of silty clay. The colours range from dark gray brown to olive gray. Bioturbation is common in the uppermost 100 cm and again between 200 and 300 cm. The lowermost 10 cm are also bioturbated. The smear slide analysis allows to classify the majority of the samples as volcanic glass rock fragment bearing clay, except some samples with abundant nannofossils (mostly volcanic glass rock fragment bearing clay nannofossil oozes).

GeoB 3378-1 (water depth 3288 m; 27°30,0´S; 71°30,0´W; length 559 cm, Fig. 50)

This core also exclusively consists of silty clay ranging in colour from dark gray brown to olive gray. Only the uppermost few cm are of a brown colour. The sediments show partly a slight to moderate bioturbation. Turbidites do not occur. The smear slide analysis shows rock fragment bearing clay as the predominant sediment type. In the lower part of the core biogenous components become more frequent (rock fragment bearing clay nannofossil ooze).

Oceanic area west of transects B and C

One additional core was recovered in an oceanic basin west of transect B and two cores west of transect C. The sediments consist mainly of deep sea clay with minor amounts of biogenous calcareous components.

GeoB 3327-5 (water depth 3534 m; 43°14,4´S; 79°59,4´W; length 900 cm, Fig. 31)

The sediments of this core consist mainly of gray, gray brown and brown clay with lower amounts of biogenous components, predominantly foraminifera and nannofossils. The sediments were classified as clayey foraminifera, clayey nannofossil or clayey foraminifera nannofossil ooze. In the lower part of the core some green ash layers were observed. The lowermost sample is a clay bearing nannofossil ooze (898 cm). Bioturbation is present throughout the core except for the interval from 420 to 620 cm.

GeoB 3336-2 (water depth 3967 m; 35°30,0´S; 87°59,9´W; length 540 cm, Fig. 32)

The core is composed exclusively of red brown clay with up to 15% nannofossils. These sediments were classified as clays or nannofossil bearing clay. Two samples (440 cm and 517 cm) contain predominatly nannofossils (70%) and are classified therefore as clayey nannofossil oozes. Bioturbation only ocassionally occurs in the uppermost 200 cm.

GeoB 3339-1 (water depth 3789 m; 35°15,0´S; 83°29,4´W; length 100 cm, Fig. 33)

The sediments of this short core change from the top towards the bottom. The colour of the silty clay ranges from dark brown in the upper part to brown yellow in the lower part of the core. A slight bioturbation is partly present. The clay content decreases from 40 to 10%, while the nannofossil content increases from 30 to 60%. Sponge spicules are present throughout the core and constribute ca. 30% of the whole content. The sediments were classified as clay nannofossil sponge spicule ooze and clay sponge spicules bearing nannofossil ooze.

Iquique Ridge

Three cores were recovered from this area. The sediments are very similar and consist mainly of nannofossil oozes.

GeoB 3387-1 (water depth 2631 m; 25°37,9´S; 75°31,5´W; length 569cm, Fig. 51)
GeoB 3387-4 (water depth 2632 m; 25°37,9´S; 75°31,5´W; length 543 cm, Fig. 52)

The two cores were recovered at the same position and are therefore described together. They consist exclusively of foraminifera nannofossil oozes, with little variations in the contents of foraminifera between 20 and 40%. The colour is always light brown. The bioturbation of the sediments is moderate to intense throughout each core.

GeoB 3388-1 (water depth 3558 cm; 25°13,2´S; 75°31,5´W; length 722 cm, Fig. 53)

In comparison to the two previous cores the lithology of this core is more variable. The main components are again nannofossils which range between 60 and 90%, followed by foraminifera ranging from 1 to 33%. A few samples contain clay up to 18%. The sediments are classified as foraminifera bearing nannofossil oozes which dominate over clay foraminifera bearing nannofossil ooze and clay nannofossil oozes. The distribution of the different sediment types is irregular. The colours of the sediments are white and light brown to brown. Bioturbation is common throughout the core and ranges between moderate and strong.

Nazca Ridge

In the area of the Nazca Ridge 19 cores have been recovered in 3 transects over the ridge. The sediments of the cores are mainly biogenous calcareous oozes with minor amounts of deep sea clay.

GeoB 3389-2 (water depth 4482 m; 21°43,5´S; 80°54,6´W; length 342 cm, Fig. 54)

The uppermost 180 cm of this core are mainly composed of dark brown clay (volcanic glass bearing clay). At a depth of 96 cm a volcanic ash layer occurs. The remaining part of the core consists of light brown nannofossil ooze with varying contents of foraminifera, sponge spicules and clay. Foraminifera become more abundant in the lowermost 50 cm of the core. Bioturbation does not occur throughout the core.

GeoB 3390-3 (water depth 3266 m; 21°37,1´S; 81°04,3´W; length 358 cm, Fig. 55)

The sediment of this core is very homogenous and is composed of light brown foraminifera bearing nannofossil ooze up to a depth of 250 cm and nannofossil ooze in the remaining part of the core. Bioturbation is moderate to strong throughout the core.

GeoB 3391-1 (water depth 2295 m; 21°32,3´S; 81°11,7´W; length 542 cm, Fig. 56)

The whole core is composed of light brown foraminifera bearing nannofossil ooze. The foraminifera content ranges from 18 to 40%. There are no other components present. The sediments are moderately to strongly bioturbated.

GeoB 3392-2 (water depth 1751 m; 21°26,6´S; 81°16,1´W; length 543 cm, Fig. 57)

The core consists of light gray to light brown foraminifera bearing nannofossil ooze. Foraminifera are more abundant in the uppermost half of the core (30%) and decrease downwards (down to 10%) except for the lowermost sample which contains 28%. Bioturbation is present throughout the core and varies from slight to moderate.

GeoB 3393-1 (water depth 1373 m; 21°19,2´S; 81°27,1´W; length 549 cm, Fig. 58)

The sediments of this core are very homogenous and consist always of foraminifera bearing nannofossil ooze. The colour ranges from light brown and light brown gray to white. Bioturbation is predominantly weak, however in some intervals moderate.

GeoB 3394-2 (water depth 1983 m; 21°13,6´S; 81°39,5´W; length 551 cm, Fig. 59)

The whole core is composed of foraminifera bearing nannofossil ooze except for the interval between 215 and 290 cm depth, where nannofossil oozes are predominant. The colours are very homogenous and change slightly between very light and light brown. Bioturbation is intense in the uppermost 100 cm of the core and only slight in the remaining part.

GeoB 3395-1 (water depth 2414 m; 21°04,9´S; 81°49,1´W; length 518 cm, Fig. 60)

The core is very similar to the previous one and also contains mainly foraminifera bearing nannofossil ooze. In the upper middle part of the core the foraminifera content decreases and the sediments were classified as nannofossil oozes. The colours range from white to light brown. Bioturbation is mostly moderate to strong and decreases in the lowermost 100 cm of the core.

GeoB 3396-1 (water depth 3102 m; 20°53,0´S; 82°07,3´W; length 545 cm, Fig. 61)

Nearly all sediments of this core were classified as foraminifera bearing nannofossil ooze. The foraminifera content mainly ranges between 10 and 20%. Some samples of the upper part of the core contain less than 10% foraminifera and are therefore nannofossil oozes. The colours are slightly lighter than in the previous core and range form white to very light brown. The whole core is bioturbated. The strength of bioturbation is mainly moderate.

GeoB 3397-1 (water depth 3453 m; 20°47,4´S; 82°15,7´W; length 467 cm, Fig. 62)

The sediments of this core consist mainly of nannofossil oozes, though in some parts of the lower half of the core the foraminifera content is slightly higher and exceeds 10% (foraminifera bearing nannofossil oozes). The colours range from ligth to very ligth brown. A mainly moderate bioturbation was observed throughout the core.

GeoB 3398-2 (water depth 3189 m; 21°24,2´S; 82°54,6´W; length 435 cm, Fig. 63)

The sediments were predominatly classified as foraminifera bearing nannofossil oozes. The foraminifera content ranges mainly between 30 and 35%. Primarily in the lower half of the core the foraminifera content is partly below 10% and nearly pure nannofossil oozes are present. The colours are principally very light brown. Bioturbation is strong in the uppermost 100 cm ot the core and only slight in the remaining part.

GeoB 3399-1 (water depth 2890 m; 21°34,9´S; 82°41,1´W; length 533 cm, Fig. 64)

The core consists exclusively of white to light brown foraminifera bearing nannofossil ooze. Foraminifera contents range from 14 to 34%. The sediments are nearly completely bioturbated only minor parts of the lower half of the core do not show bioturbation.

GeoB 3401-2 (water depth 2468 m; 21°49,4´S; 82°26,2´W; length 538 cm, Fig. 65)

The core consists exclusively of light brown to white nannofossil ooze. Bioturbation is rather strong in its upper part, decreasing towards the end of the core. For this core no smear slide data exists.

Geo B 3402-2 (water depth 2890 m; 22°03,1´S; 82°08,6´W; length 538 cm, Fig. 66)

This core consists exclusively of light to very light brown foraminifera bearing nannofossil ooze. The foraminifera content ranges from 16 to 38% throughout the core. Bioturbation is moderate to strong in the uppermost 200 cm of the core and mainly slight to absent in the remaining part.

GeoB 3403-2 (water depth 3529 m; 22°06,0´S; 82°04,8´W; length 77 cm, Fig. 67)

This very short core is composed of brown nannofossil ooze, one sample (5 cm) was classified as a foraminifera bearing nannofossil ooze with a foraminifera content of 10%. Bioturbation is nearly absent.

GeoB 3406-2 (water depth 1953 m; 22°55,8´S; 82°46,5´W; length 535 cm, Fig. 68)

Compared to the previous cores the foraminifera content of the sediments is generally higher and ranges between 18 and 45%. The sediments were classified as foraminifera bearing nannofossil oozes. The colour of the sediments is white to very light brown. Bioturbation is predominatly slight to moderate and only in minor parts absent.

GeoB 3407-1 (water depth 2250 m; 22°40,3´S; 82°36,7´W; length 554 cm, Fig. 69)

The lithology of this core is similar to that of the previous one. All sediments were classified as foraminifera bearing nannofossil ooze with foraminifera contents ranging from 12 and 40%. The colour varies between white and light brown. The lowermost 100 cm of the core show a rythmic variation of colours in a scale of 5 to 10 cm. Bioturbation is partly strong in the upper 150 cm of the core. The remaining part of the core is only subordinatly bioturbated.

GeoB 3408-2 (water depth 1583 m; 22°31,4´S; 82°31,1´W; length 122 cm, Fig. 70)

The uppermost 40 cm of this core contain 42 to 45% of foraminifera, while in the remaining part of this short core the foraminifera content is reduced to ca. 20%. All samples were classified as foraminifera bearing nannofossil ooze. The colour ranges from light to very light brown. In the uppermost half of the core a slight bioturbation occassionally occurs.

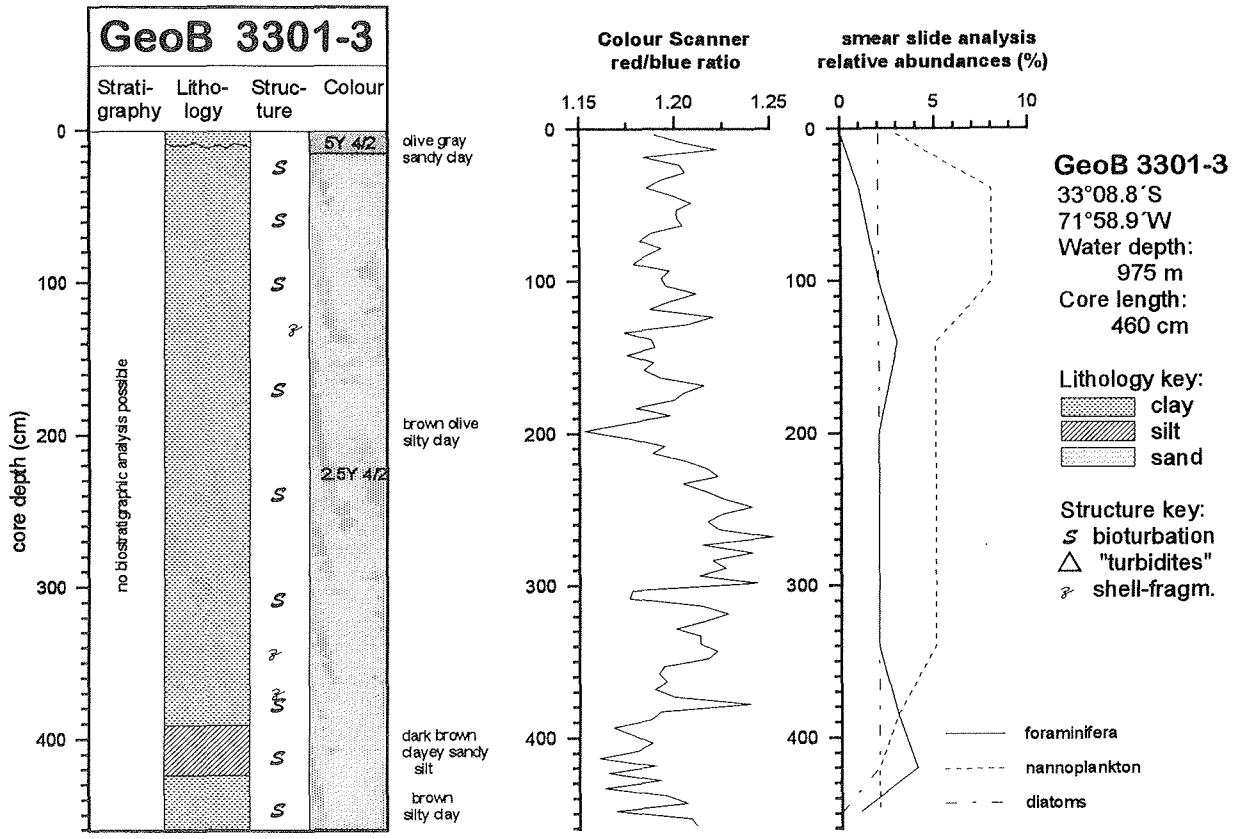

Fig. 15: Core desription, colour scanner and smear slide data for Core 3301-3

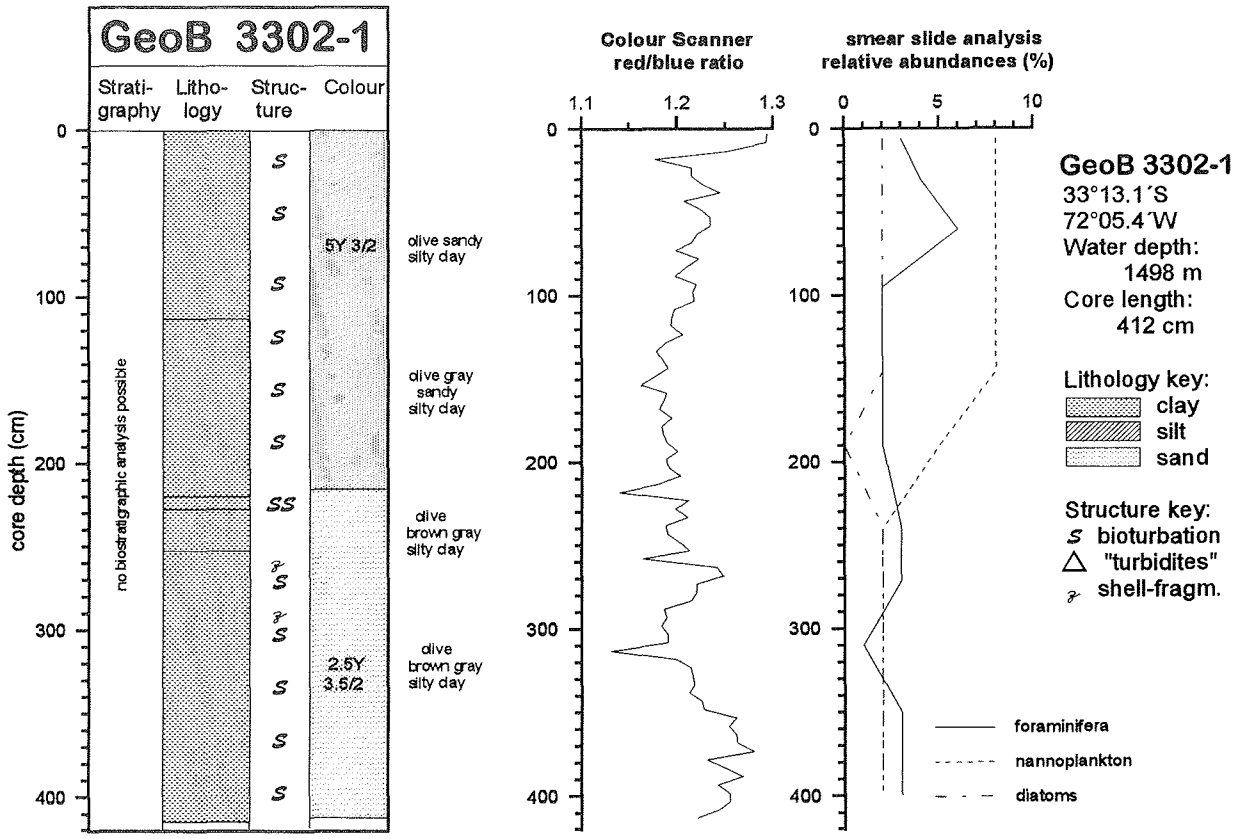

Fig. 16: Core desription, colour scanner and smear slide data for Core 3302-1

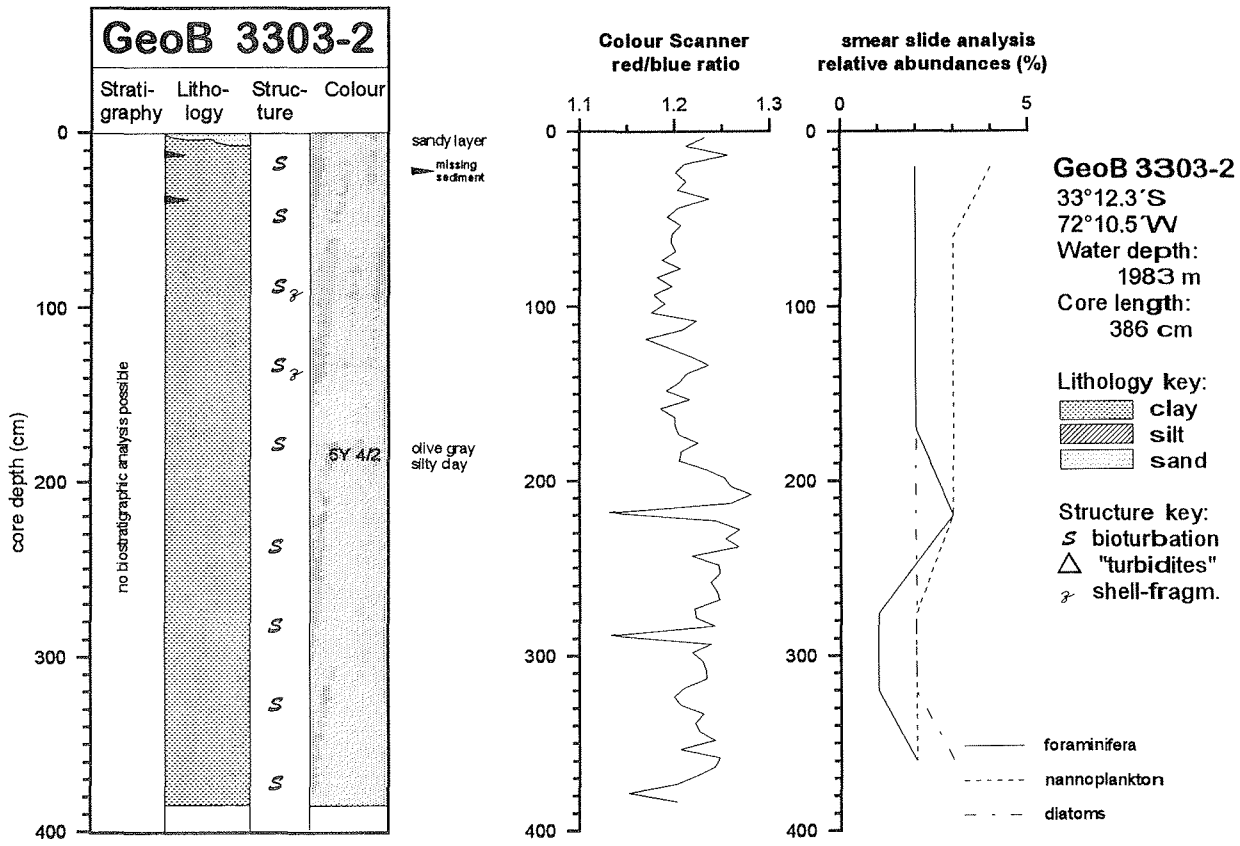

Fig. 17: Core desription, colour scanner and smear slide data for Core 3303-2

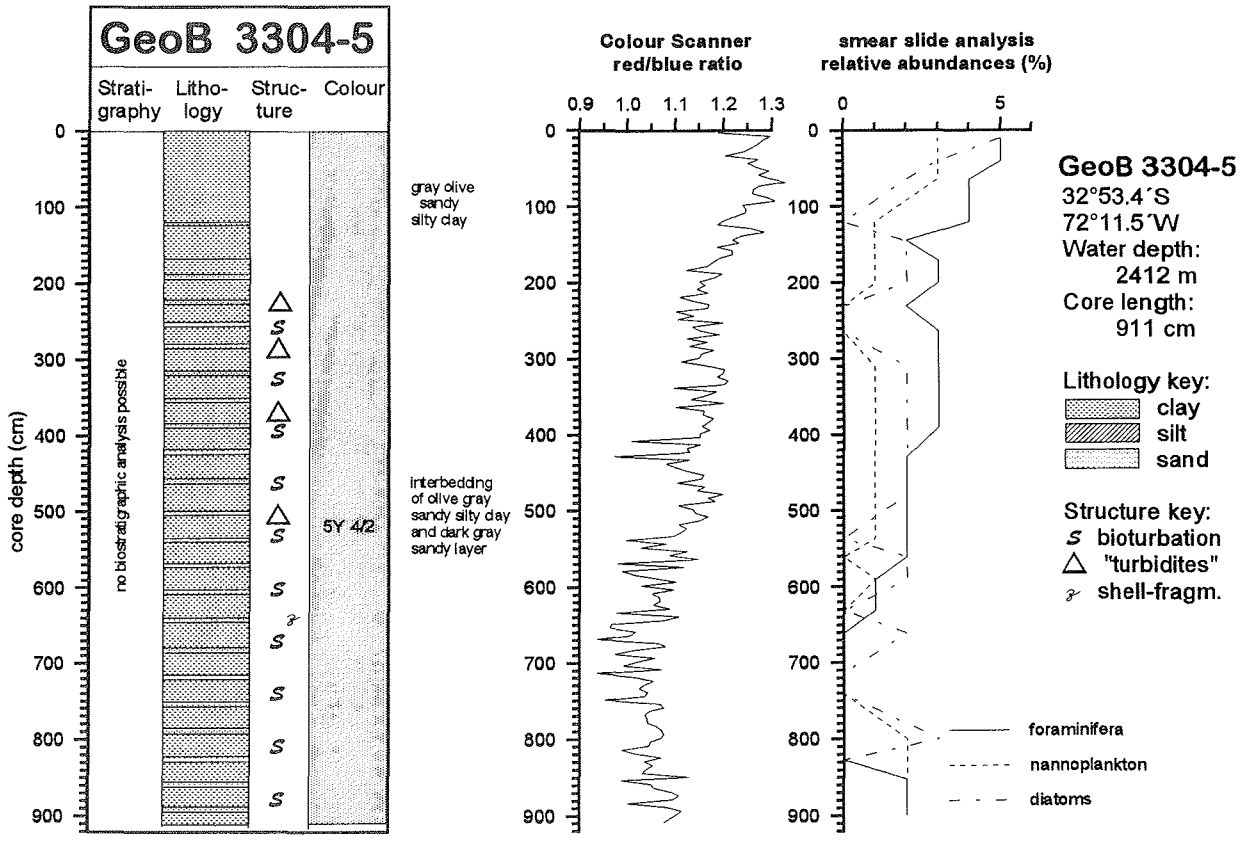

Fig. 18: Core desription, colour scanner and smear slide data for Core 3304-5

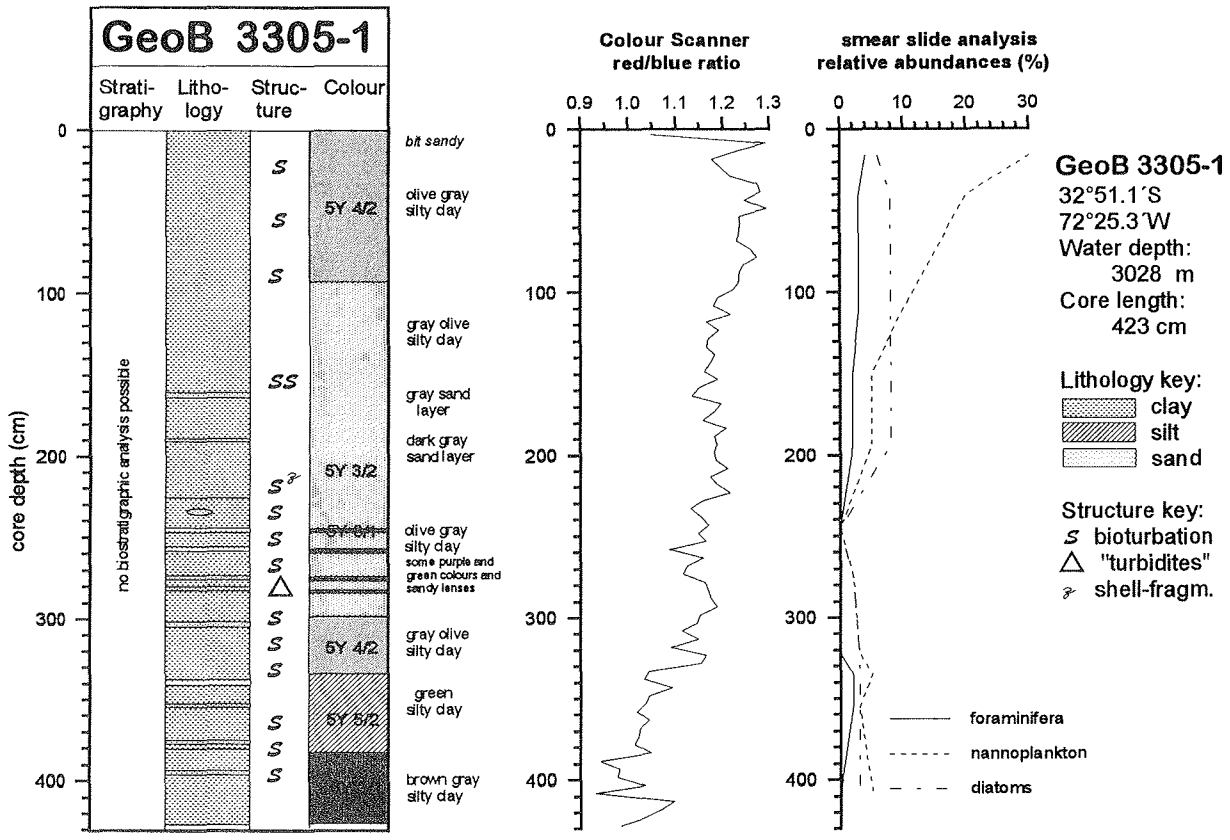

Fig. 19: Core desription, colour scanner and smear slide data for Core 3305-1

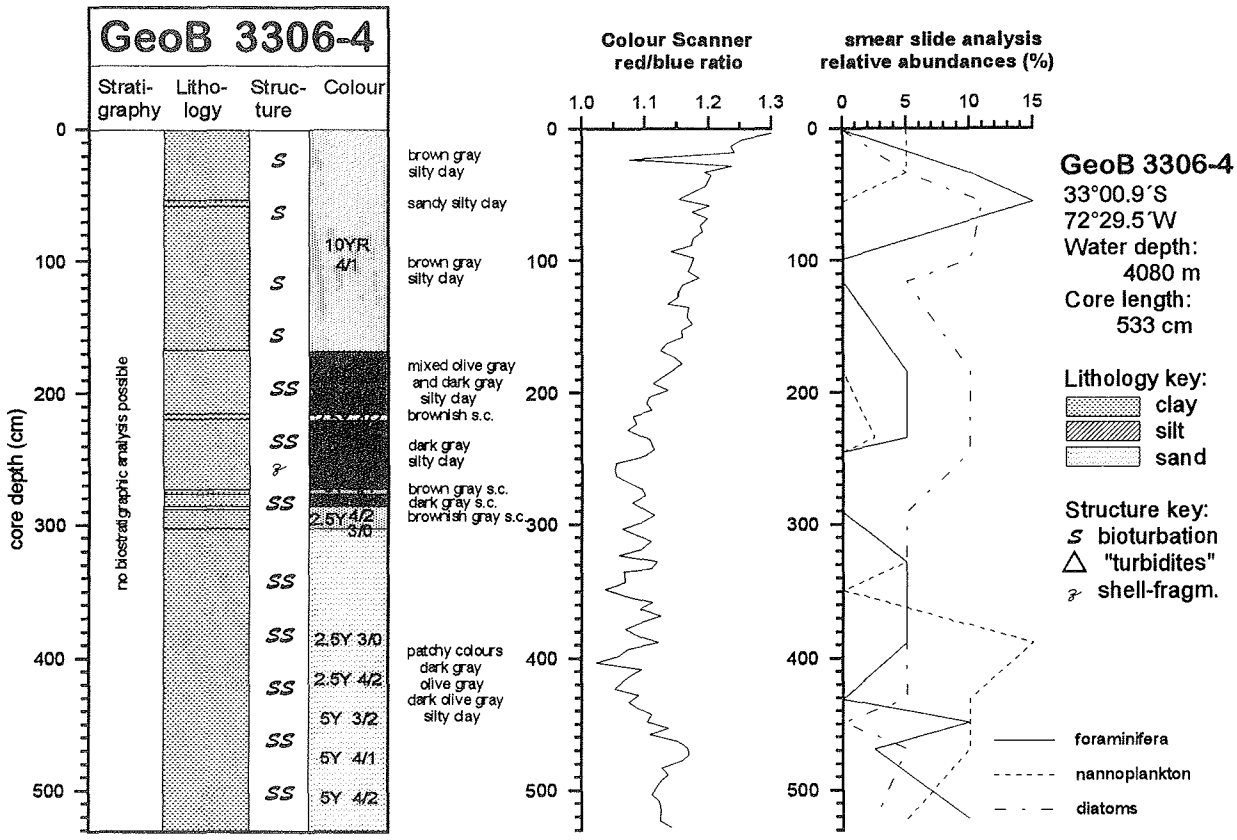

Fig. 20: Core desription, colour scanner and smear slide data for Core 3306-4

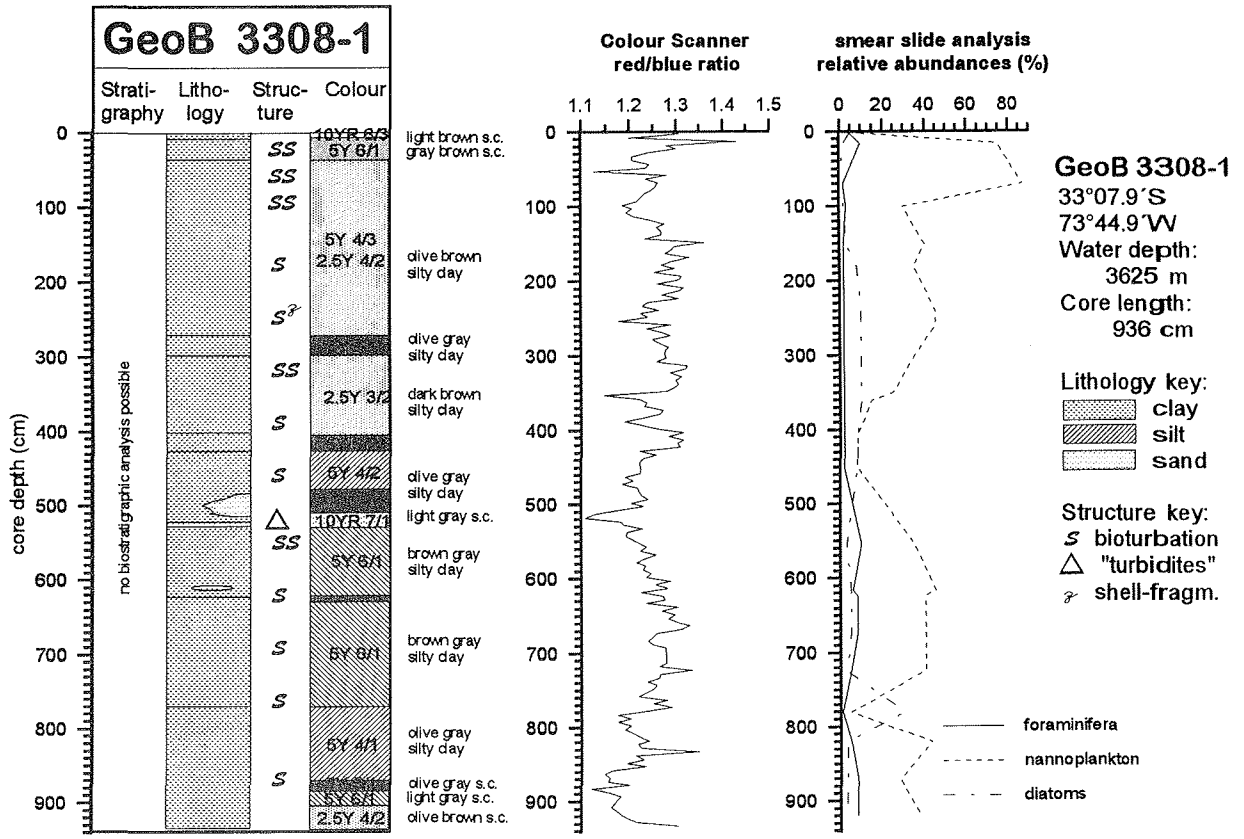

Fig. 21: Core desription, colour scanner and smear slide data for Core 3308-1

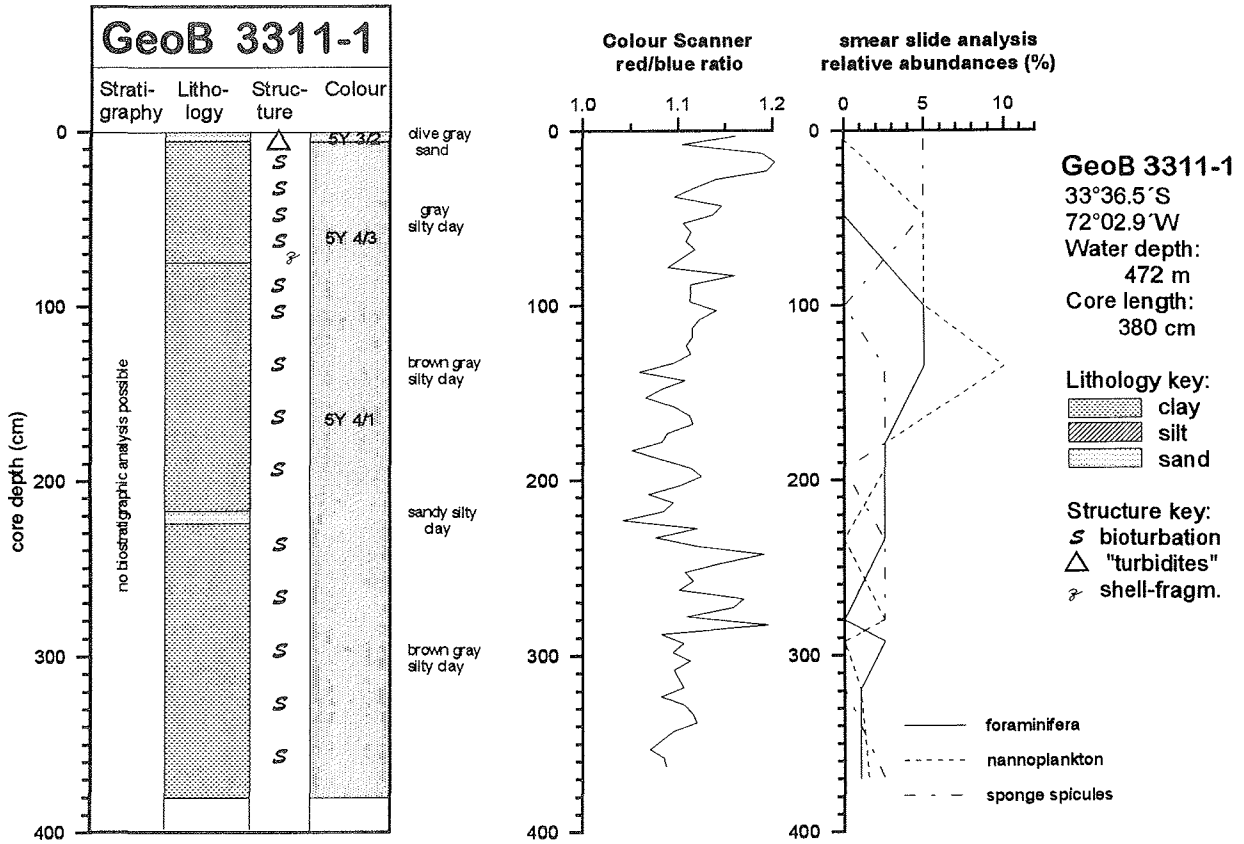

Fig. 22: Core desription, colour scanner and smear slide data for Core 3311-1

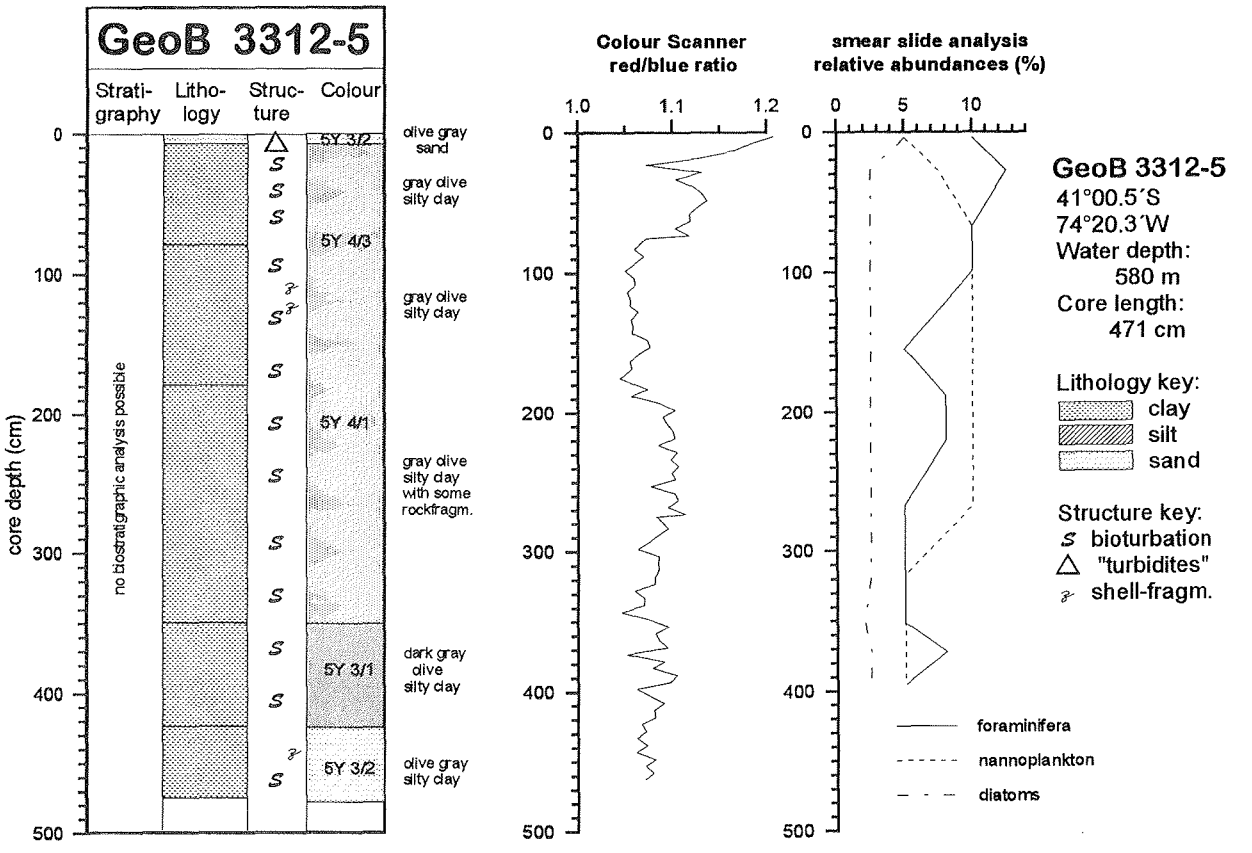

Fig. 23: Core desription, colour scanner and smear slide data for Core 3312-5

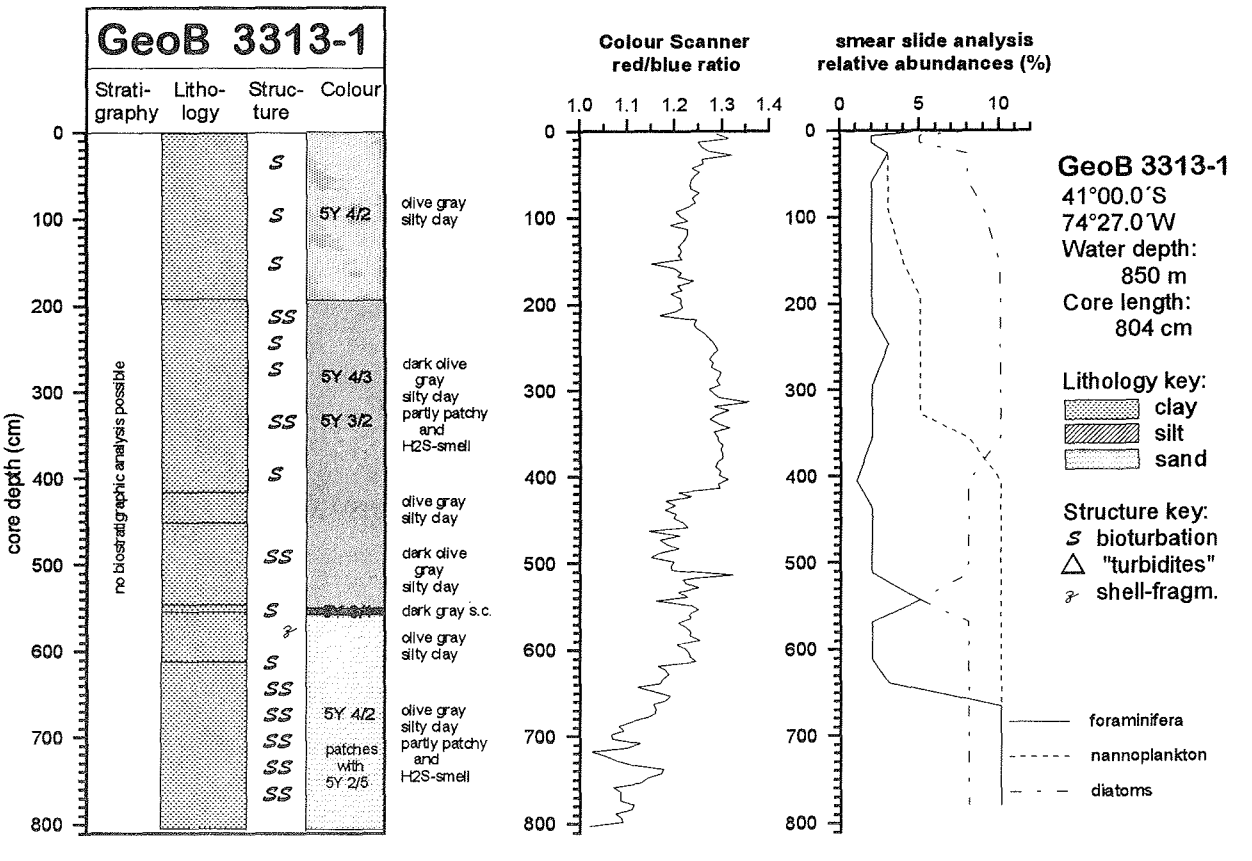

Fig. 24: Core desription, colour scanner and smear slide data for Core 3313-1

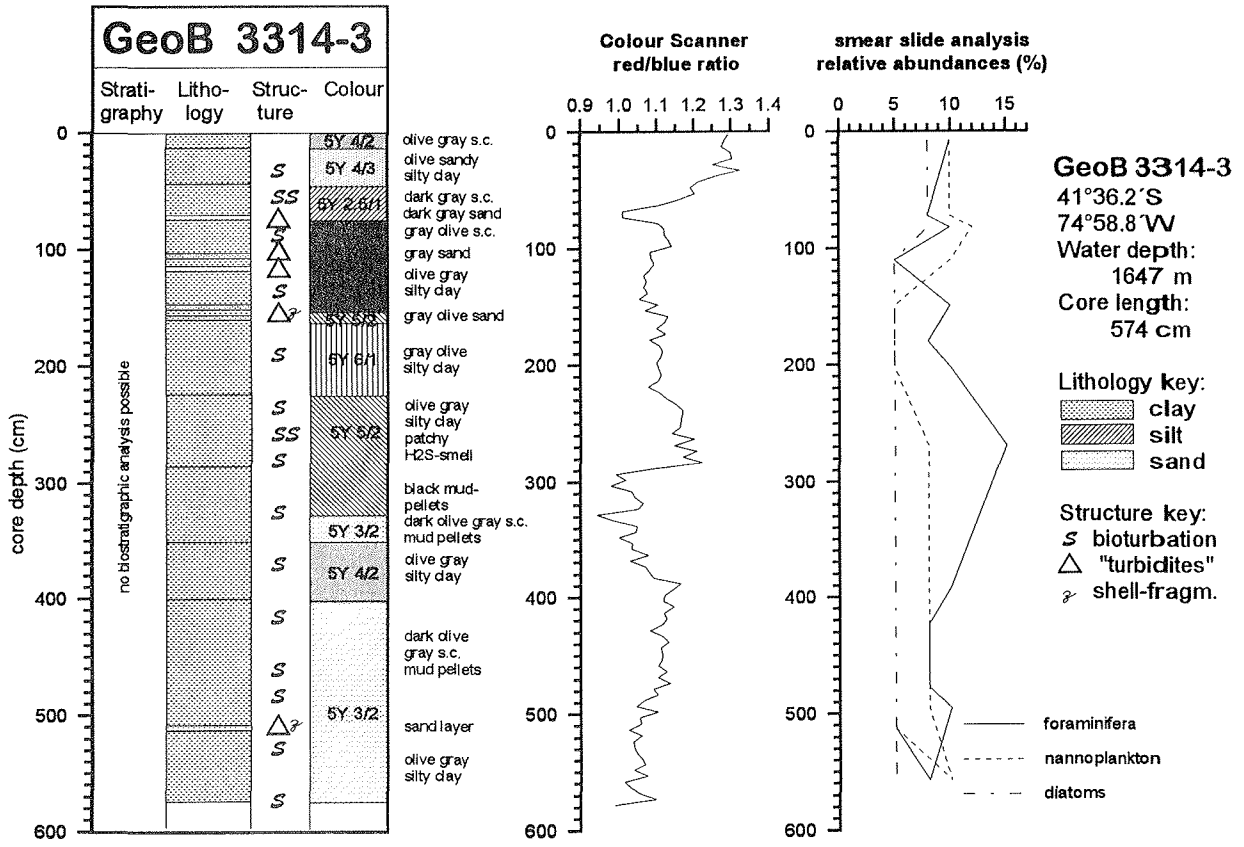

Fig. 25: Core desription, colour scanner and smear slide data for Core 3314-3

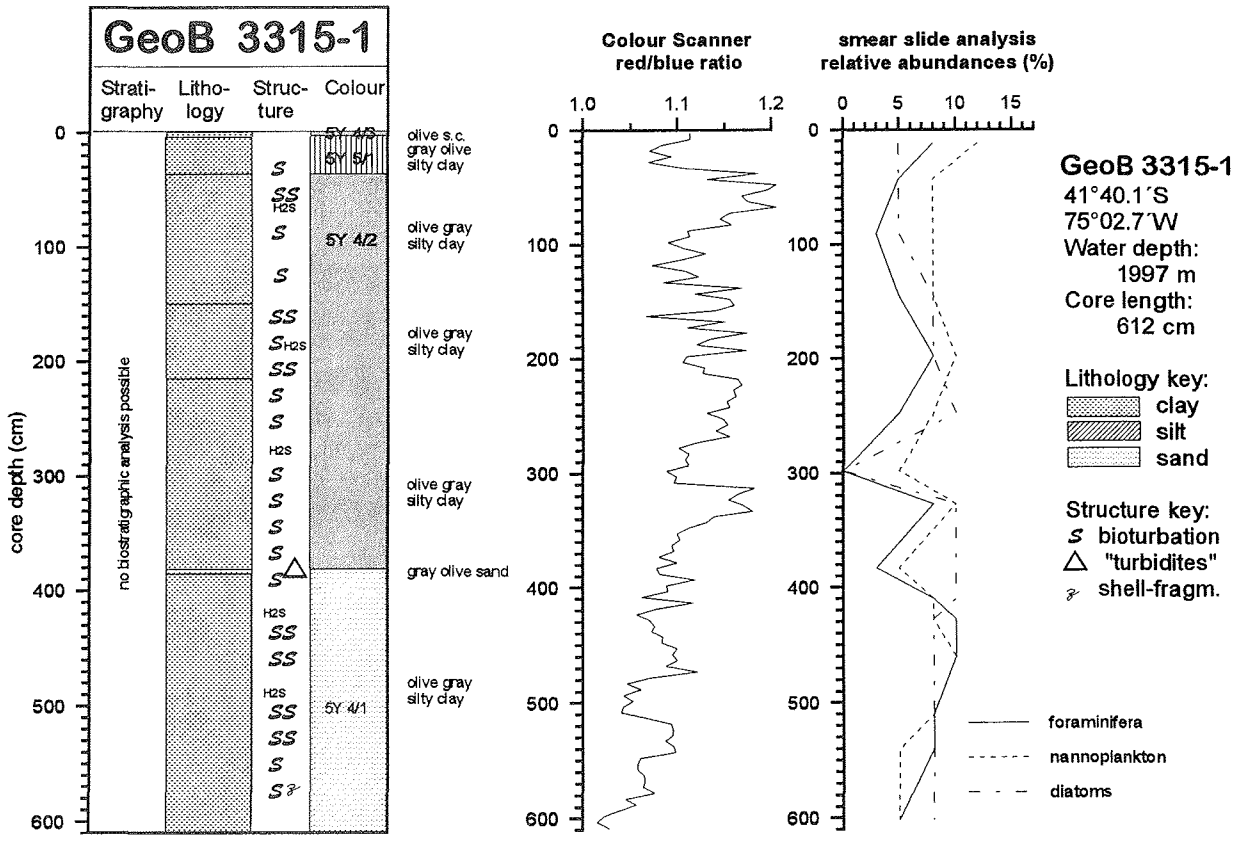

Fig. 26: Core desription, colour scanner and smear slide data for Core 3315-1

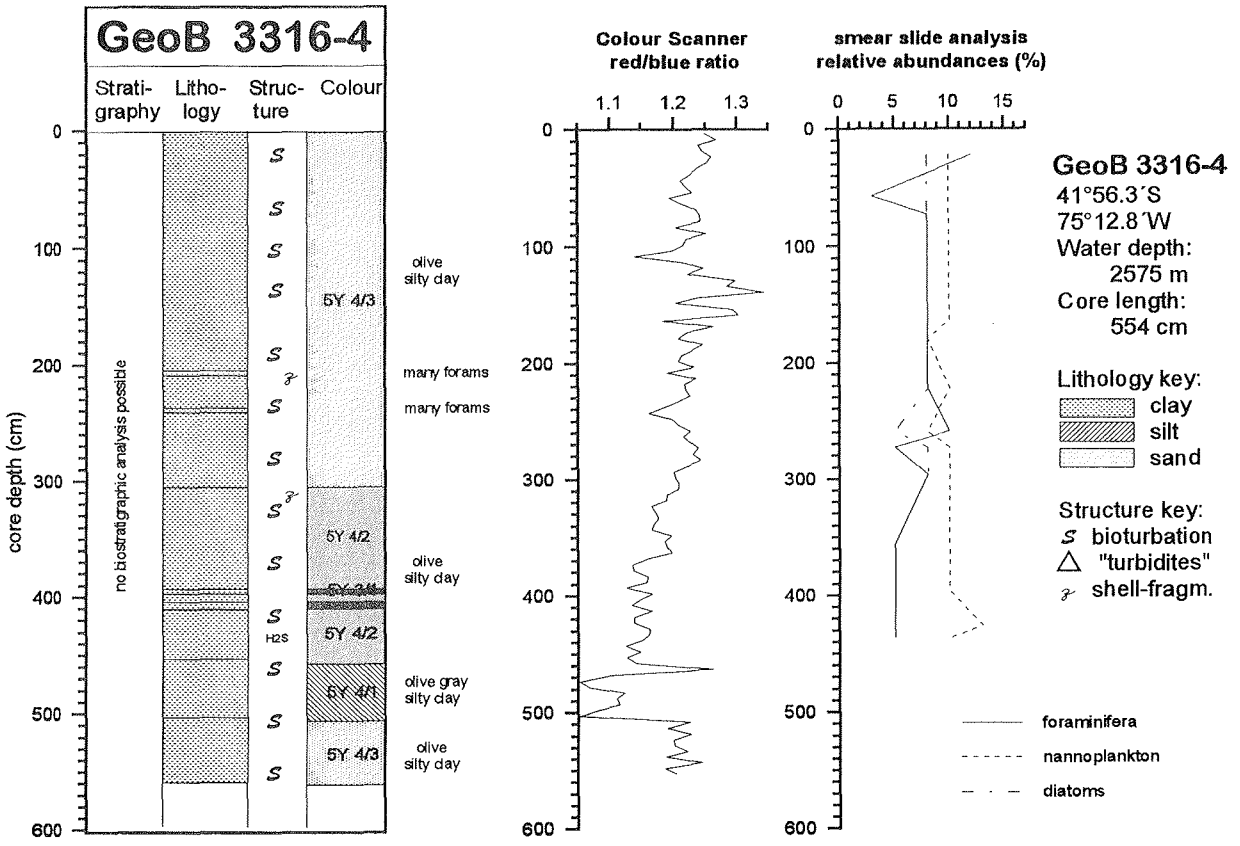

Fig. 27: Core desription, colour scanner and smear slide data for Core 3316-4

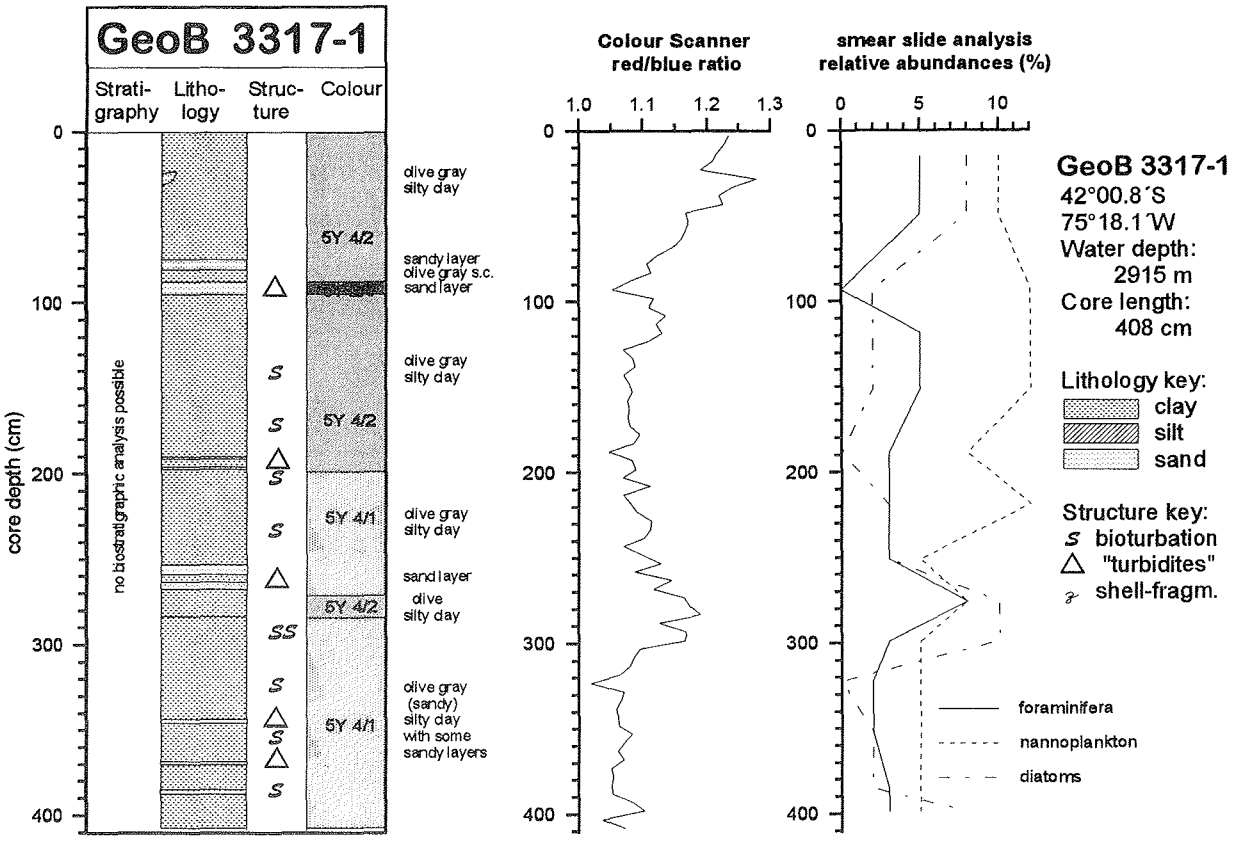

Fig. 28: Core desription, colour scanner and smear slide data for Core 3317-1

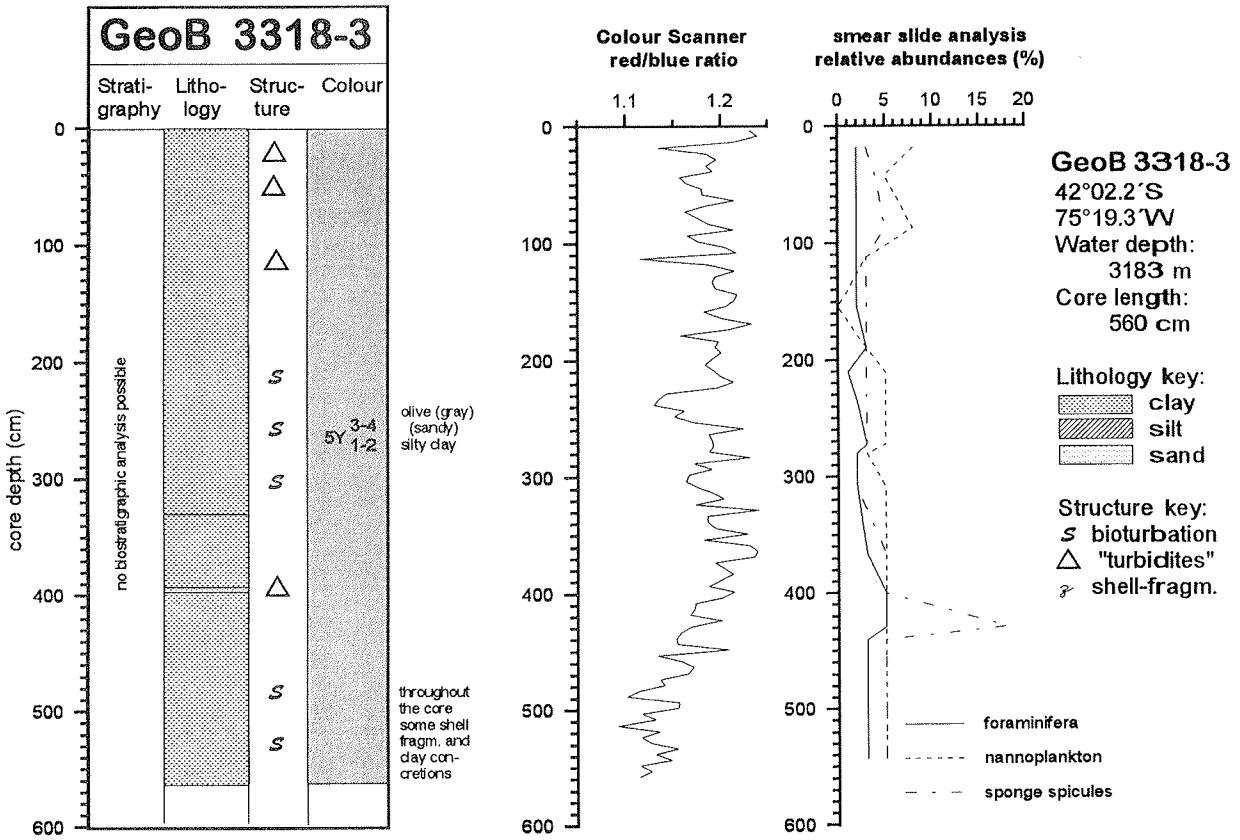

Fig. 29: Core desription, colour scanner and smear slide data for Core 3318-3

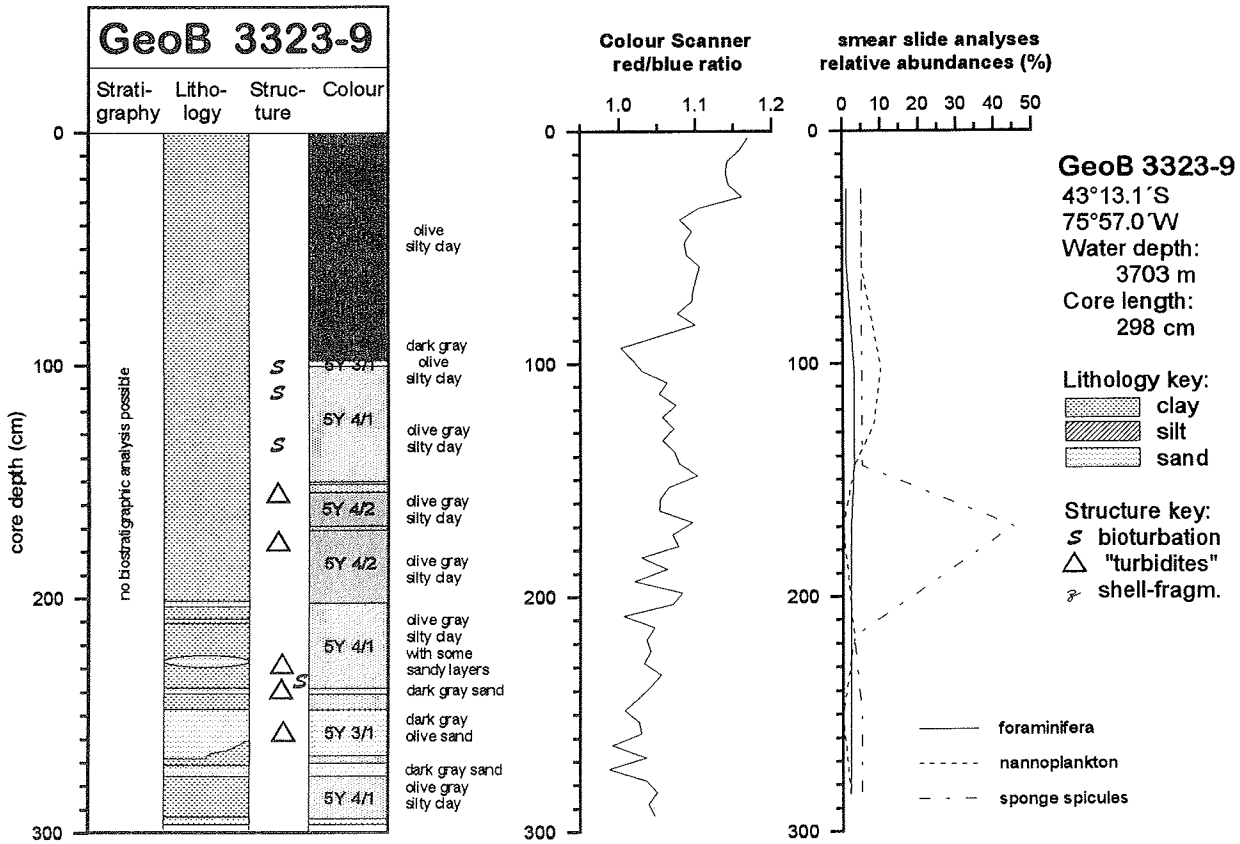

Fig. 30: Core desription, colour scanner and smear slide data for Core 3323-9

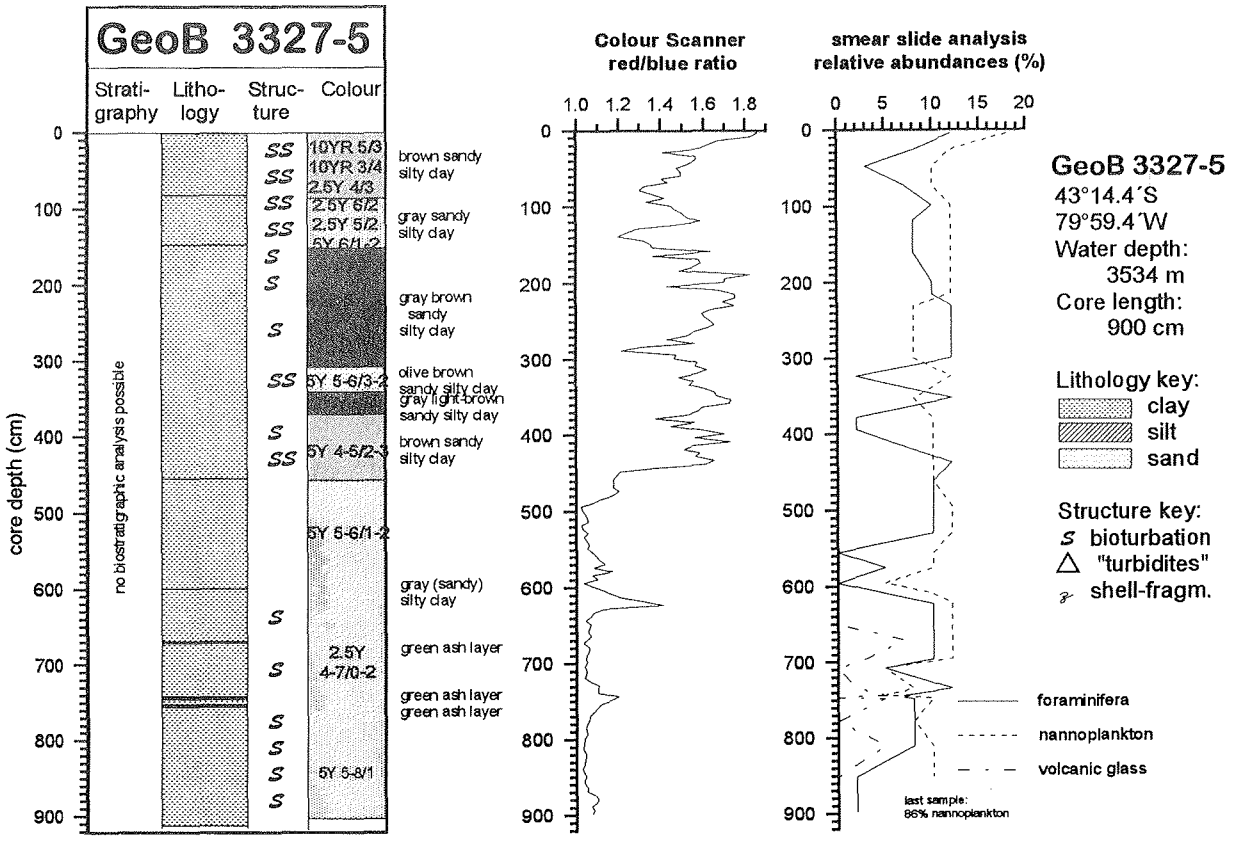

Fig. 31: Core desription, colour scanner and smear slide data for Core 3327-5

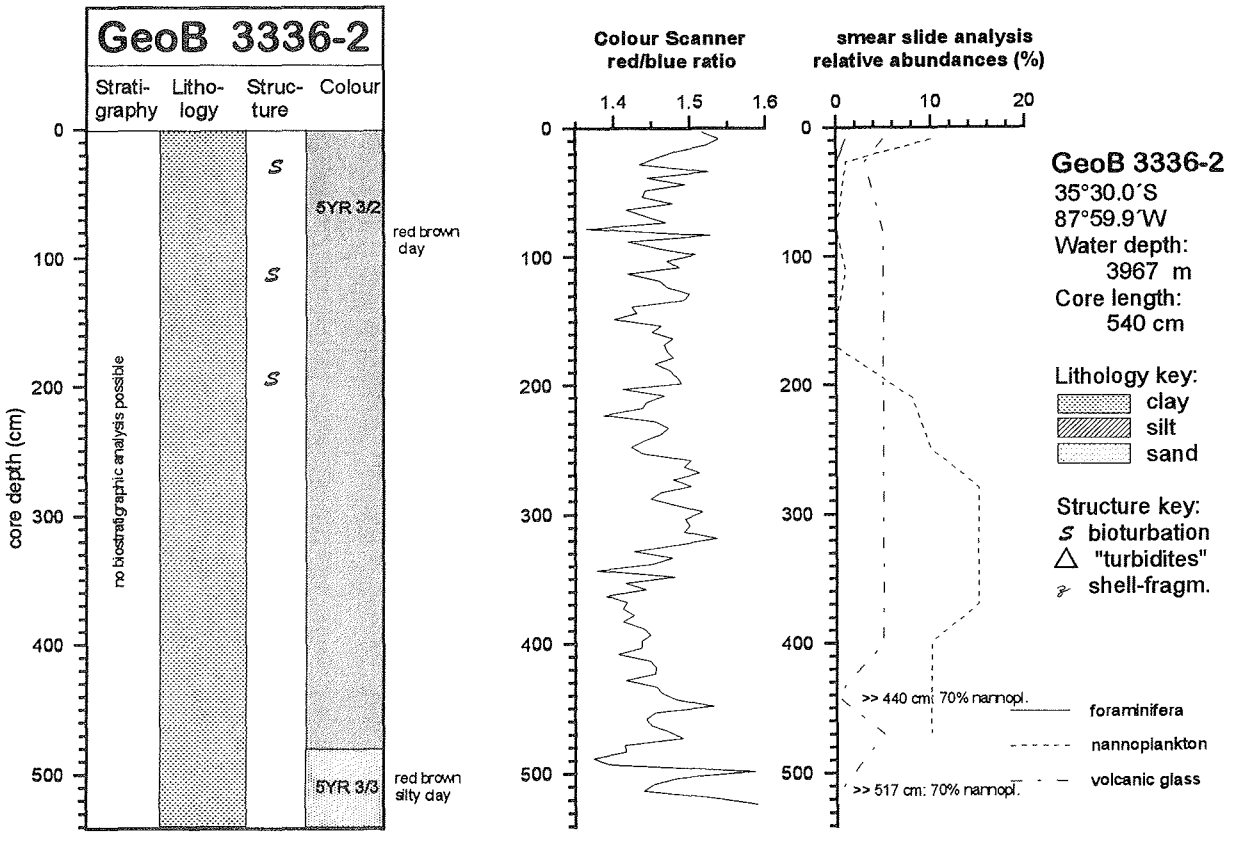

Fig. 32: Core desription, colour scanner and smear slide data for Core 3336-2

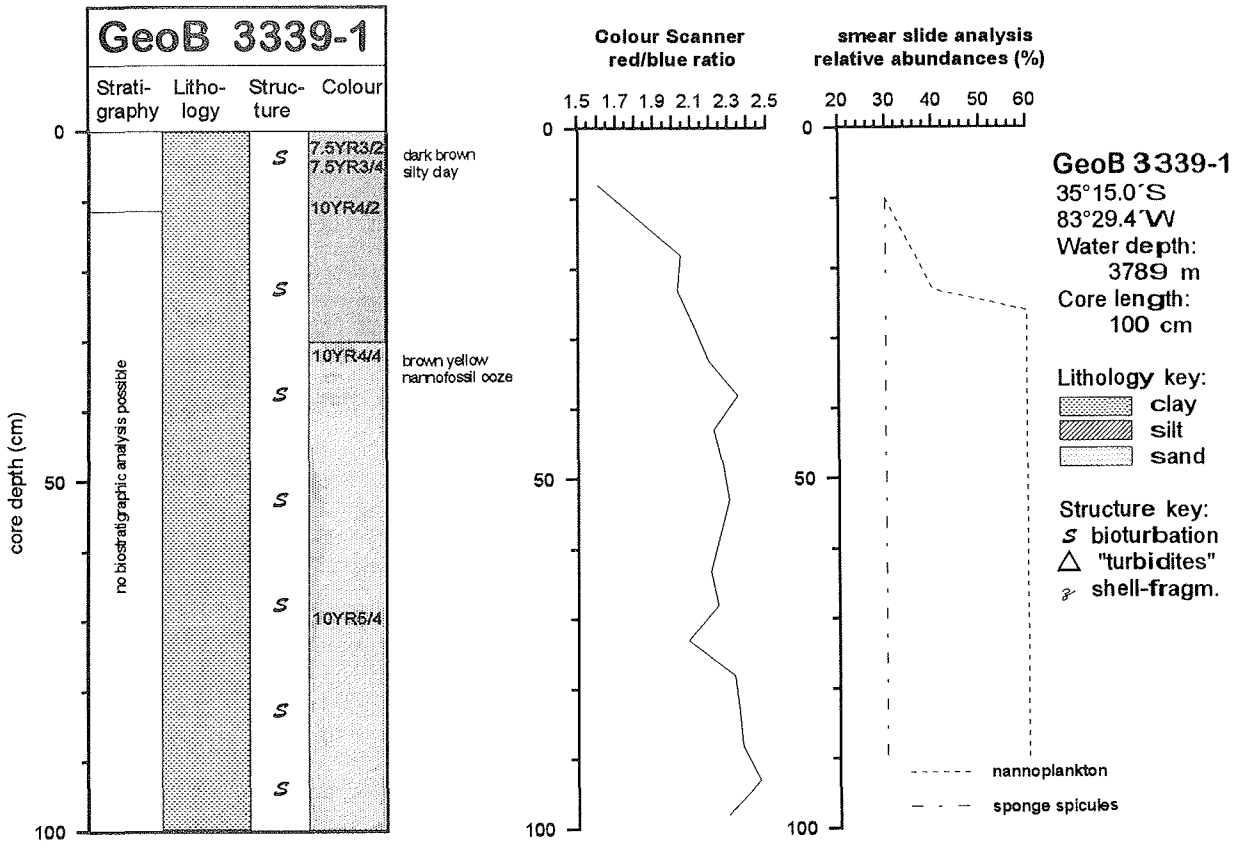

Fig. 33: Core desription, colour scanner and smear slide data for Core 3339-1

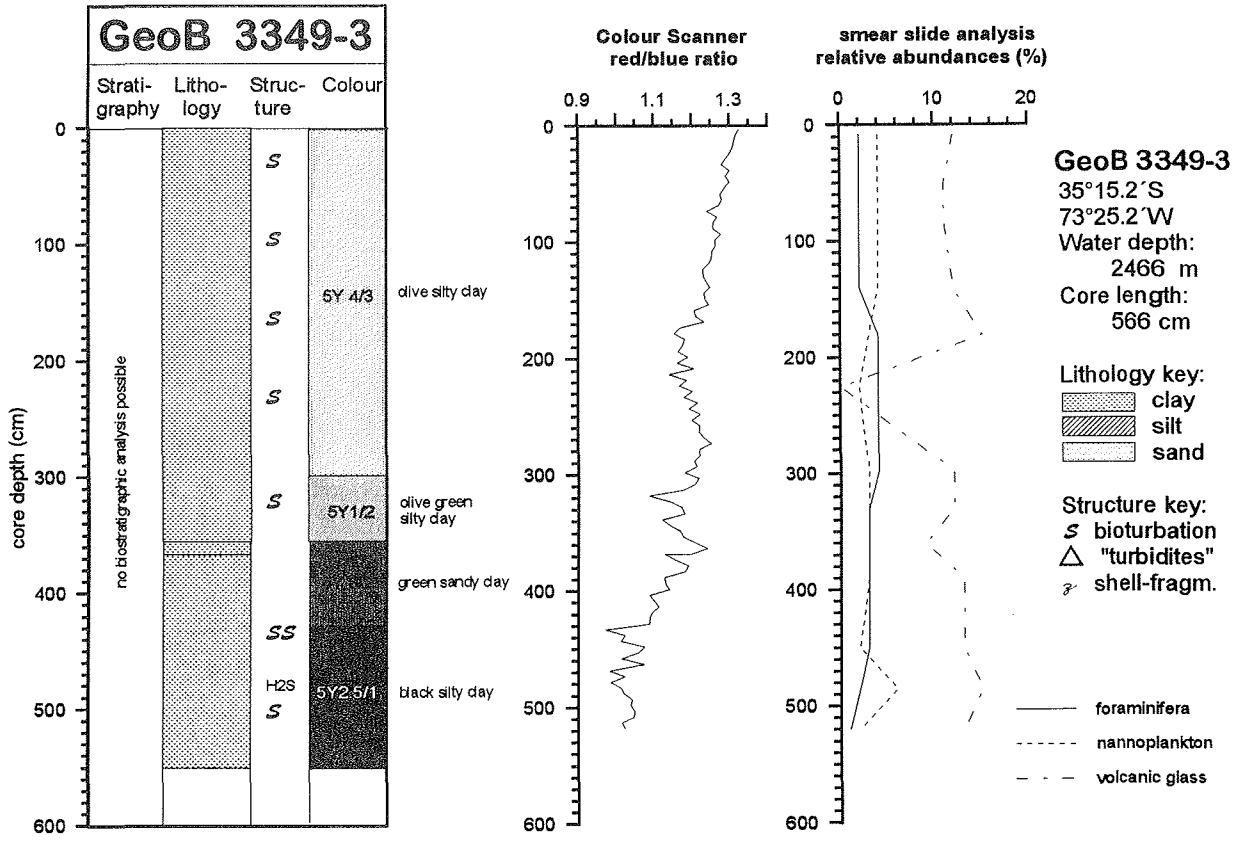

Fig. 34: Core desription, colour scanner and smear slide data for Core 3349-3

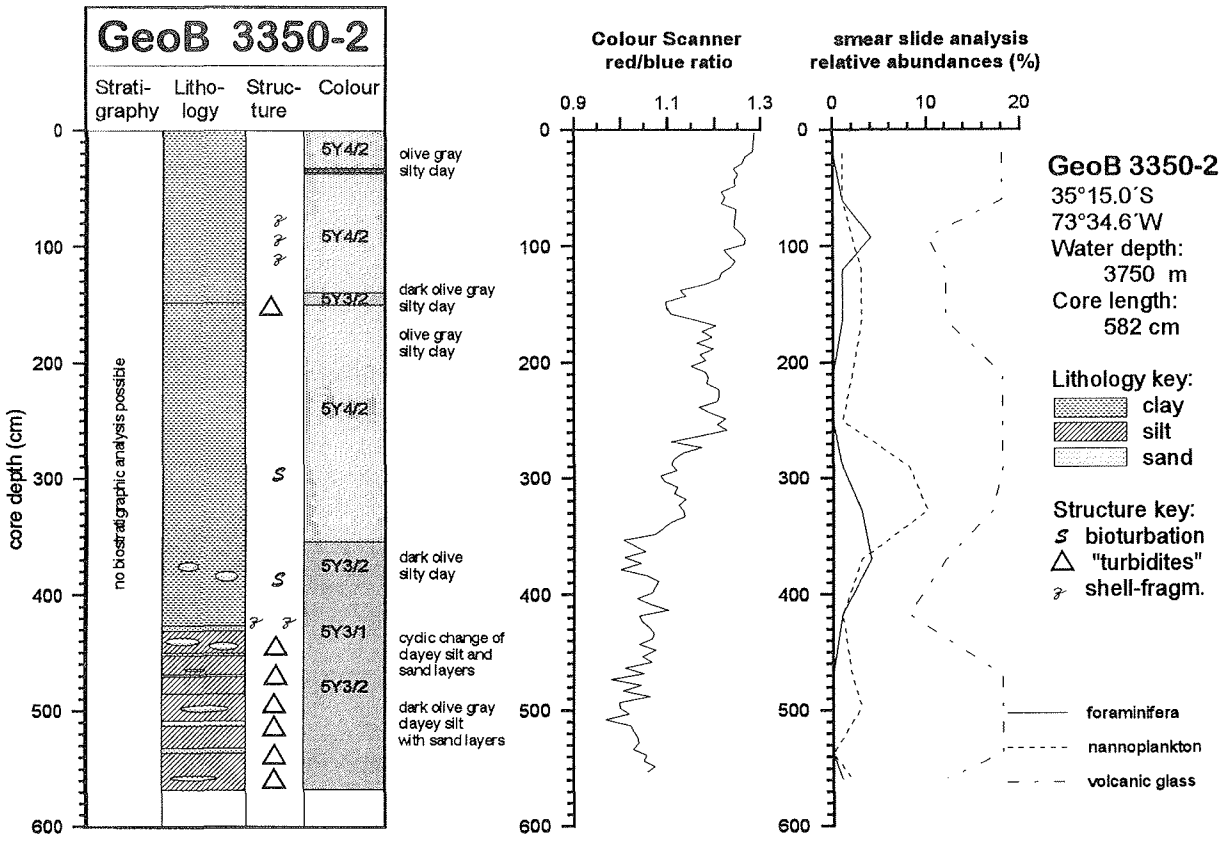

Fig. 35: Core desription, colour scanner and smear slide data for Core 3350-2

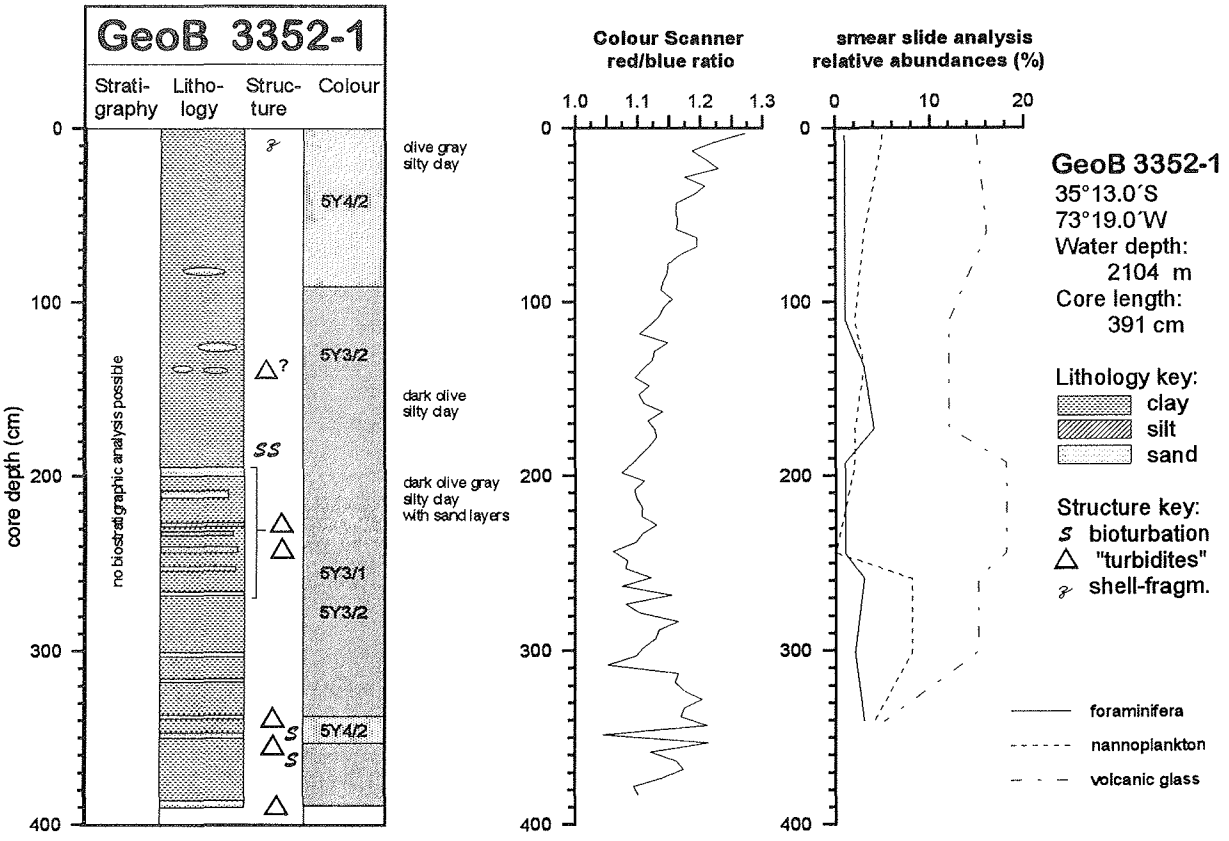

Fig. 36: Core desription, colour scanner and smear slide data for Core 3352-1

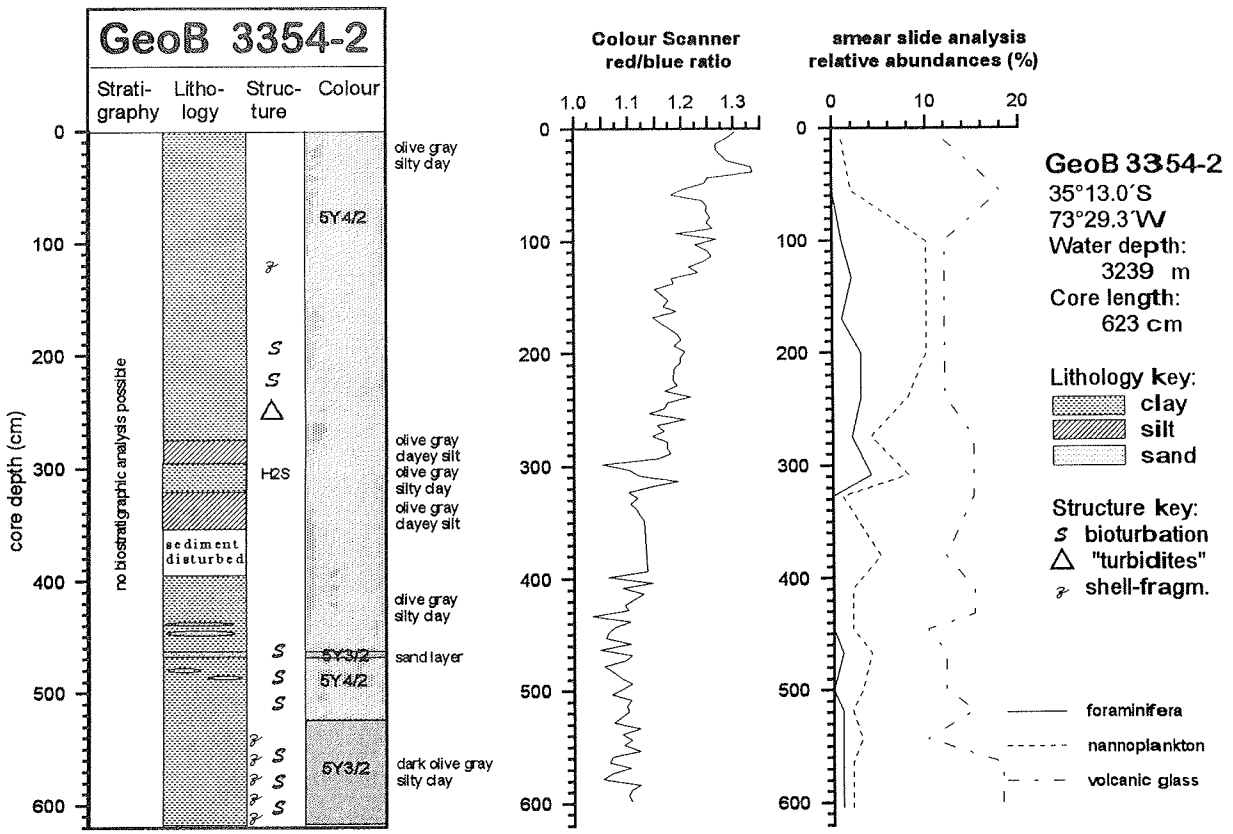

Fig. 37: Core desription, colour scanner and smear slide data for Core 3354-2

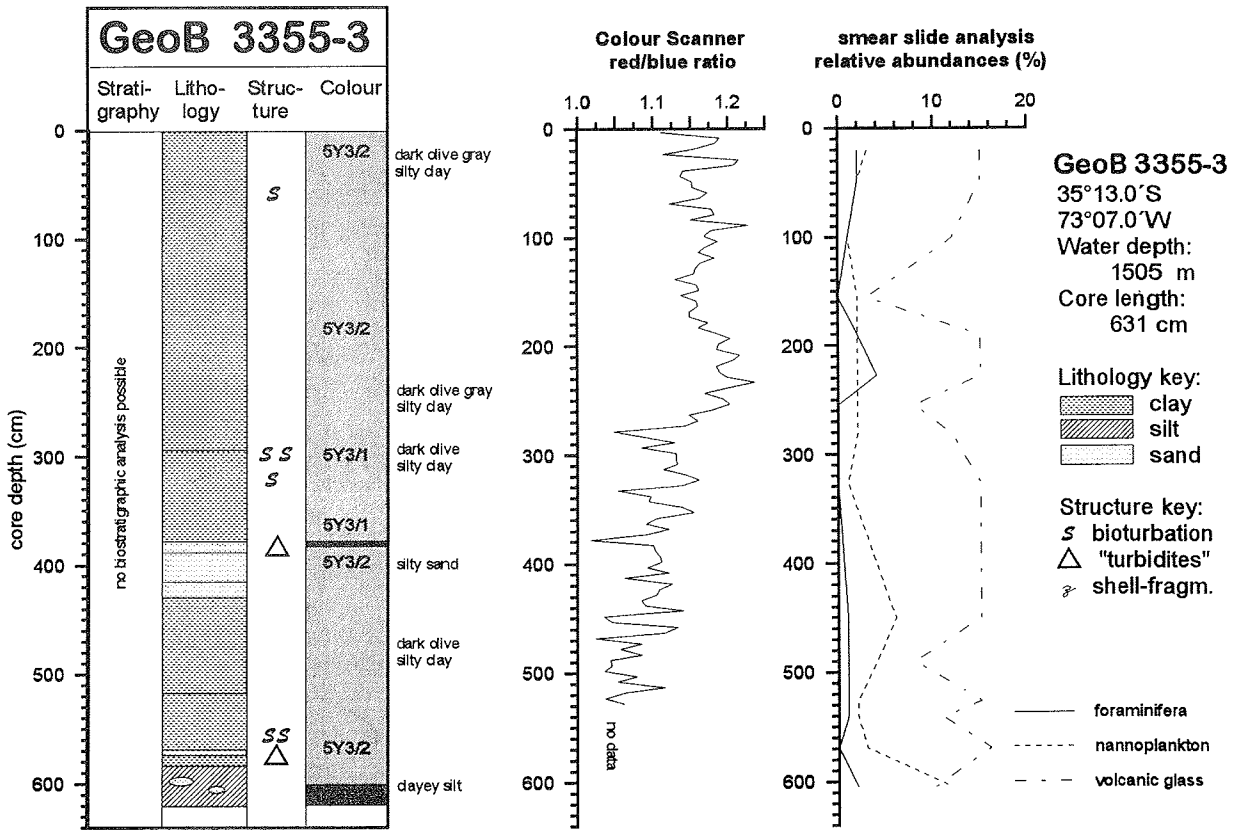

Fig. 38: Core desription, colour scanner and smear slide data for Core 3355-3

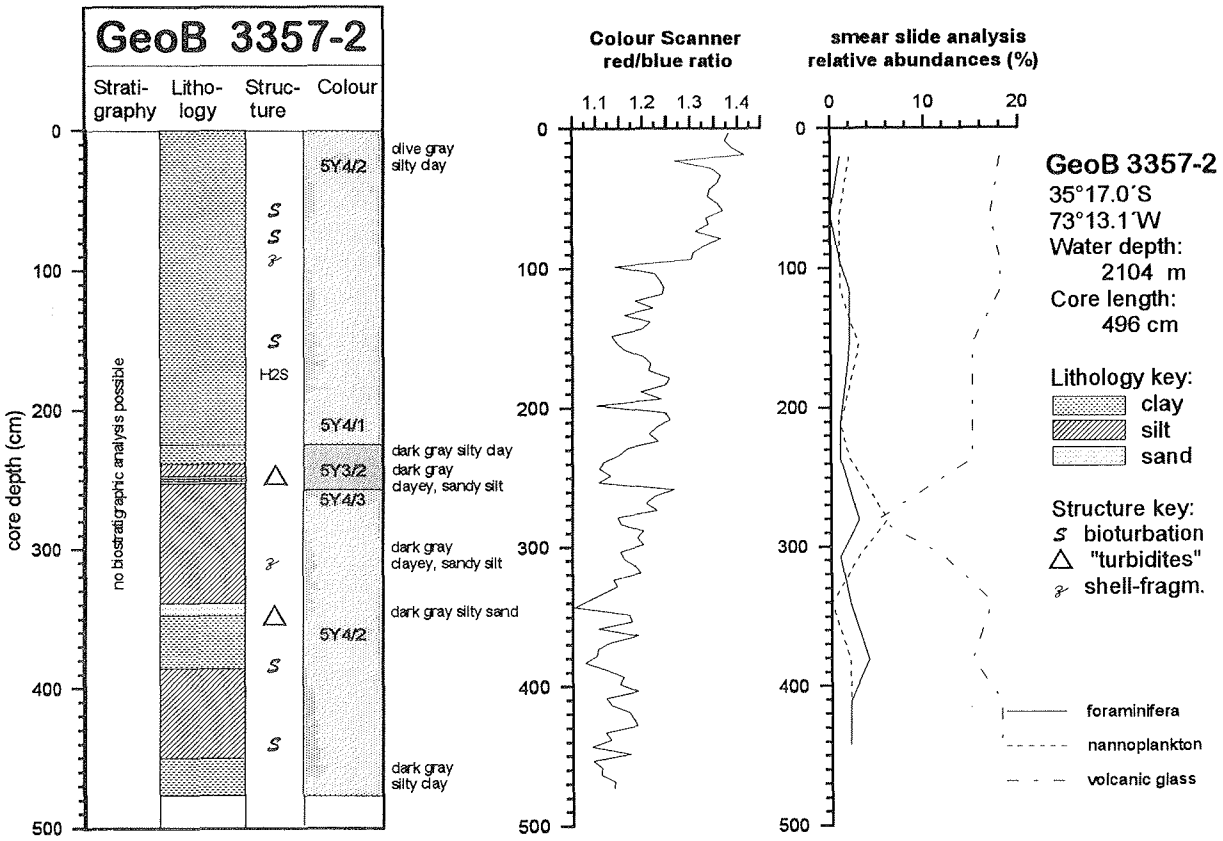

Fig. 39: Core desription, colour scanner and smear slide data for Core 3357-2

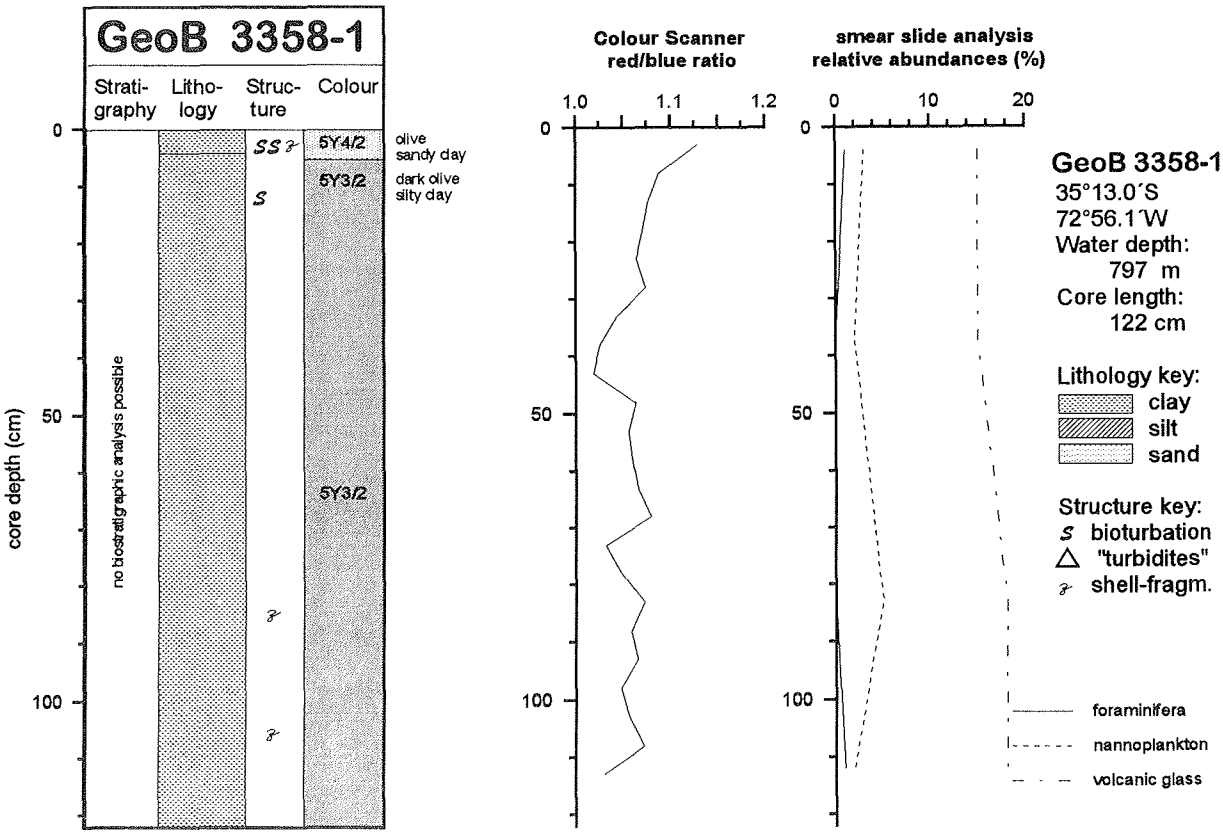

Fig. 40: Core desription, colour scanner and smear slide data for Core 3358-1

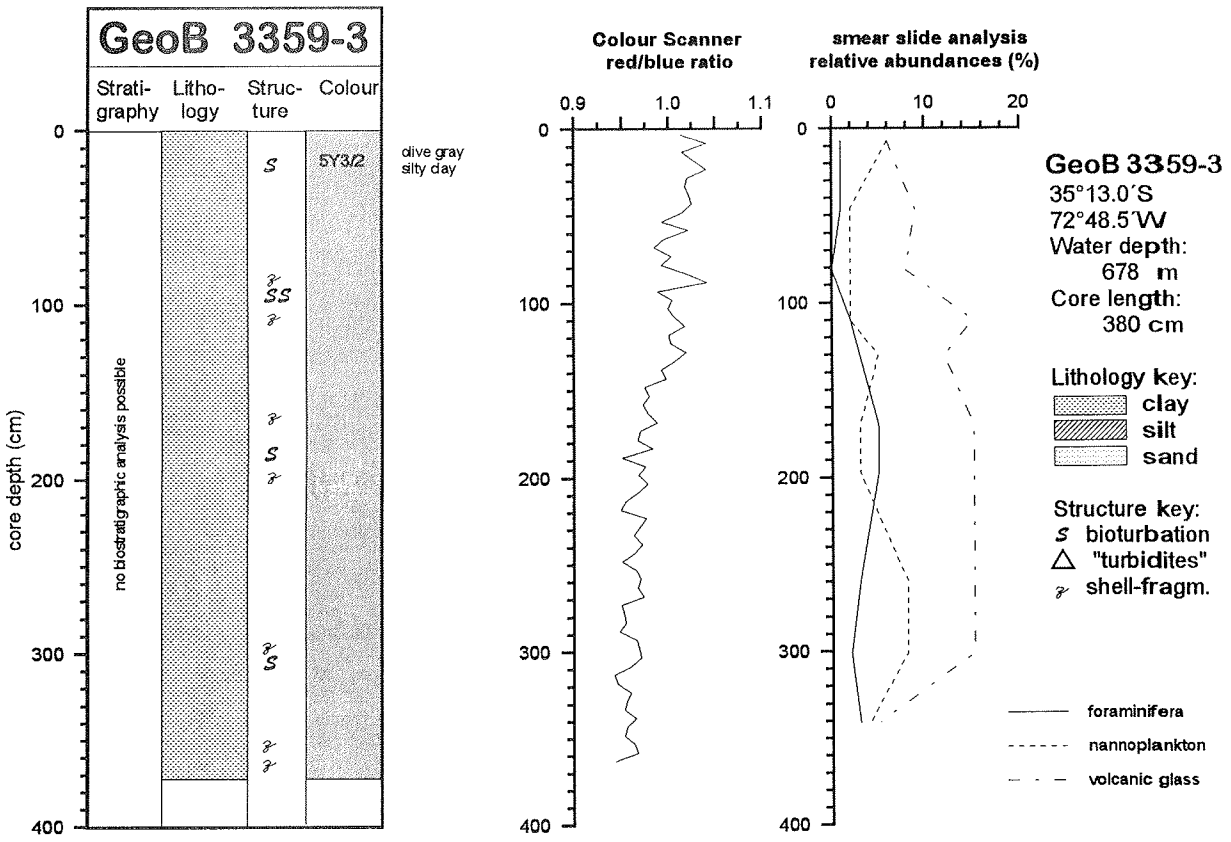

Fig. 41: Core desription, colour scanner and smear slide data for Core 3359-3

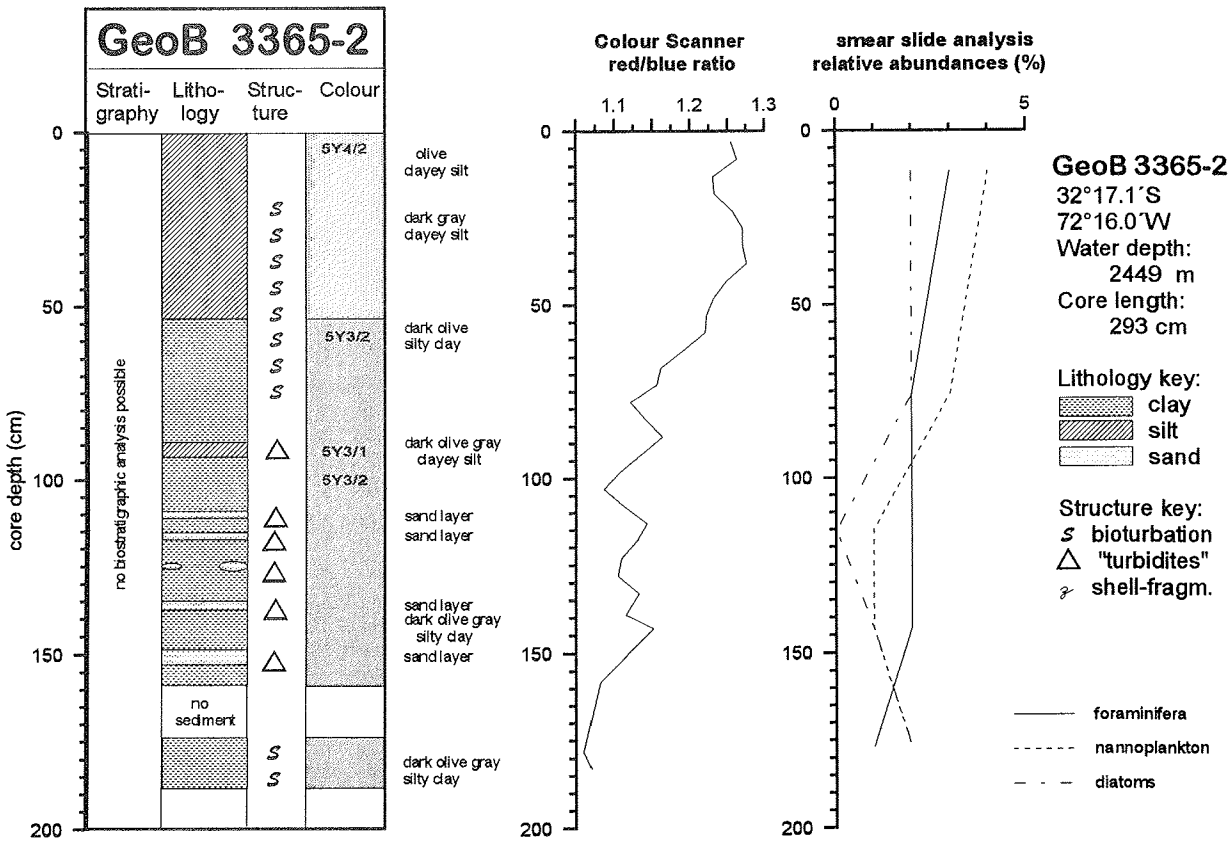

Fig. 42: Core desription, colour scanner and smear slide data for Core 3365-2

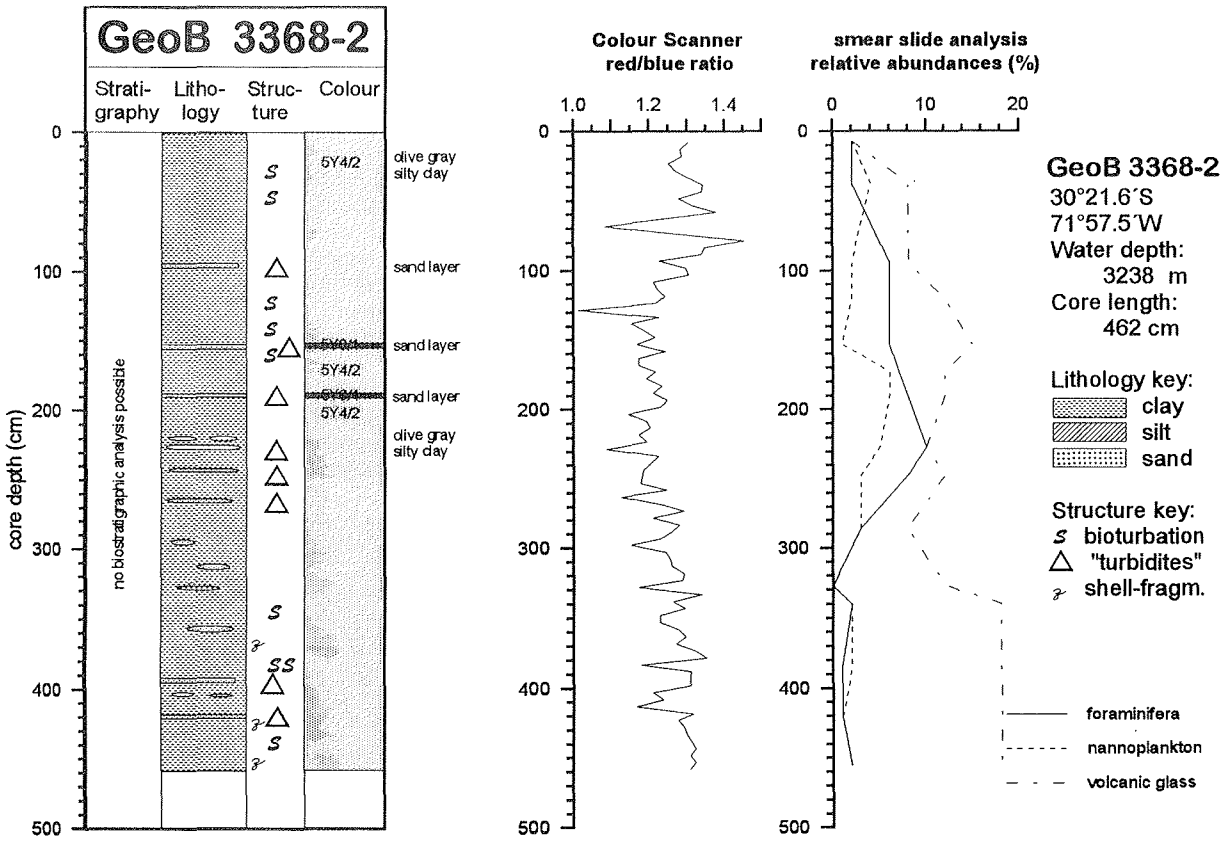

Fig. 43: Core desription, colour scanner and smear slide data for Core 3368-2

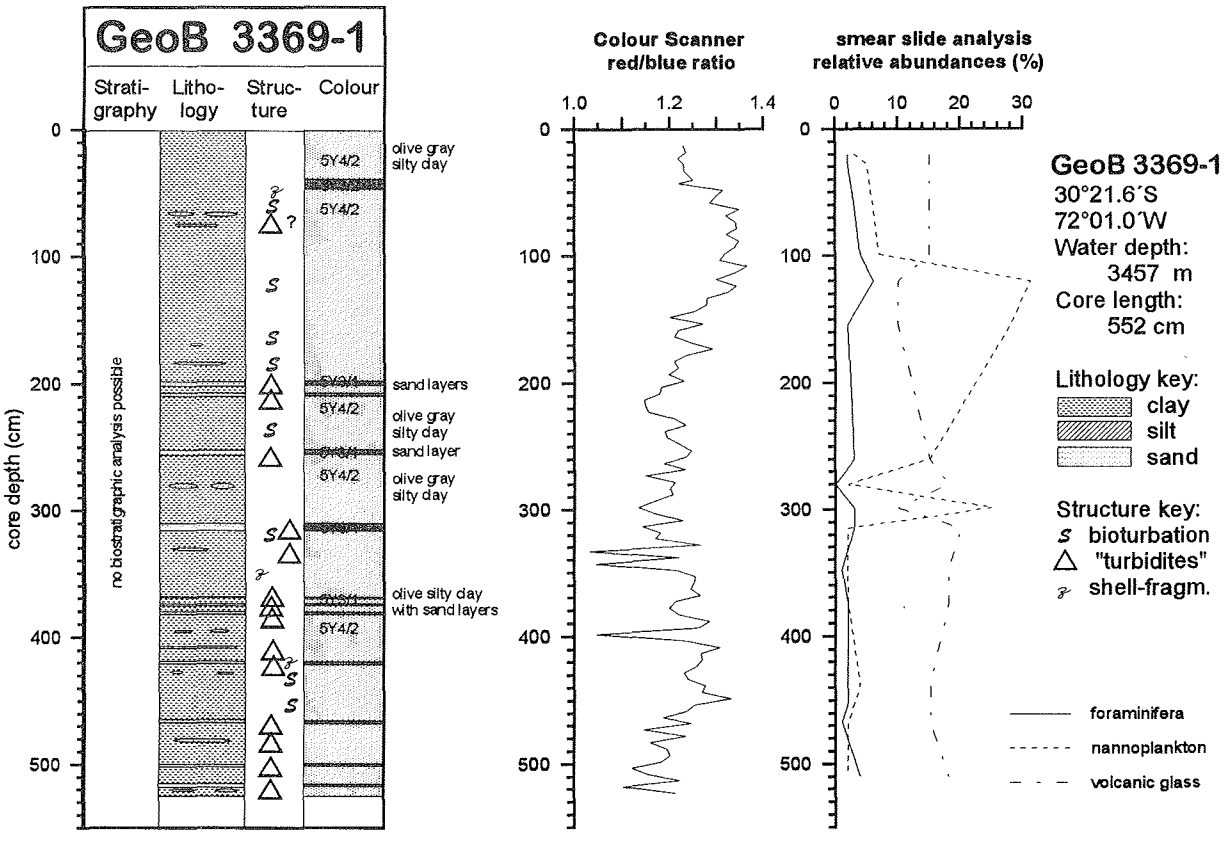

Fig. 44: Core desription, colour scanner and smear slide data for Core 3369-1

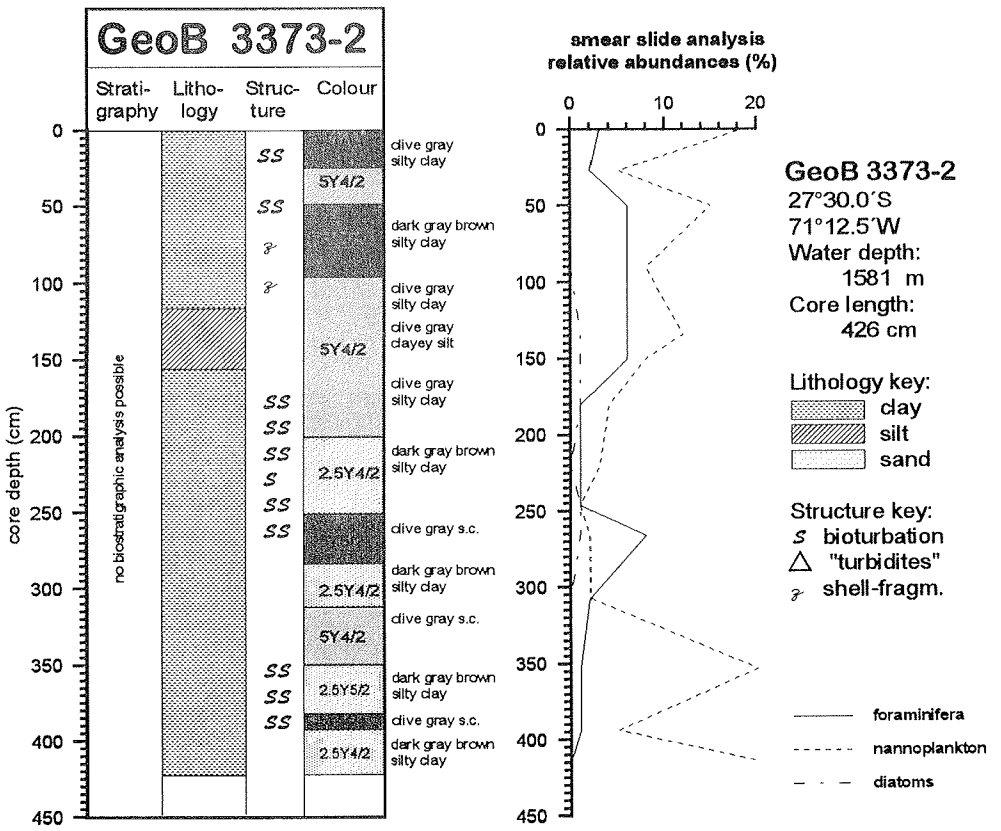

Fig. 45: Core desription and smear slide data for Core 3373-2

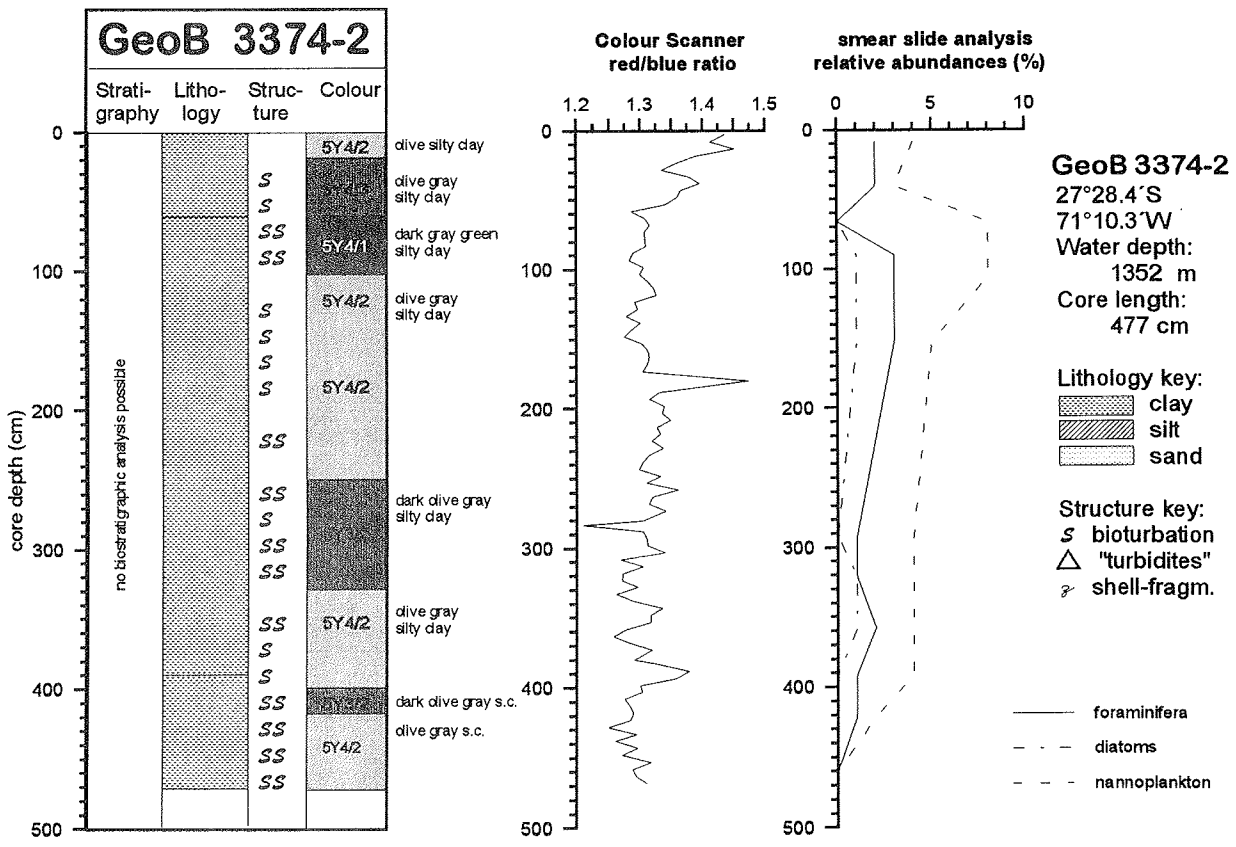

Fig. 46: Core desription, colour scanner and smear slide data for Core 3374-2

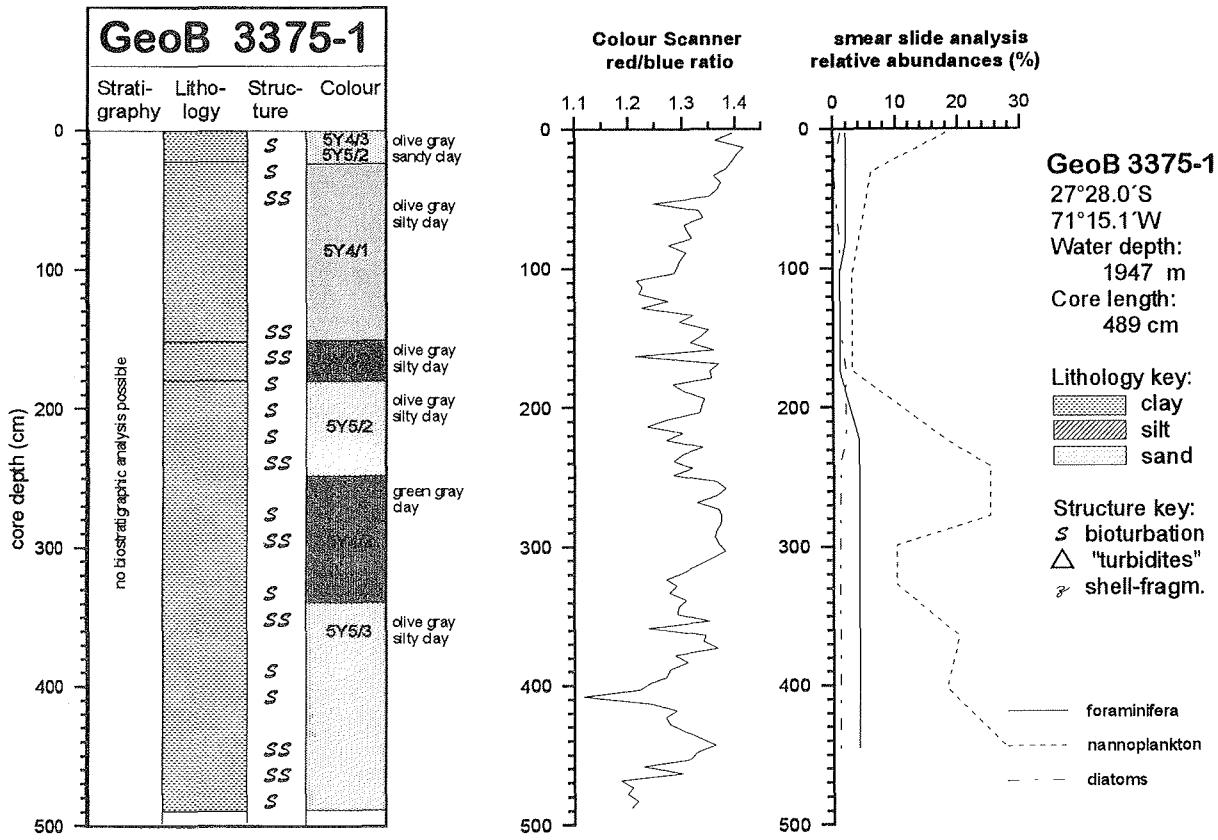

Fig. 47: Core desription, colour scanner and smear slide data for Core 3375-1

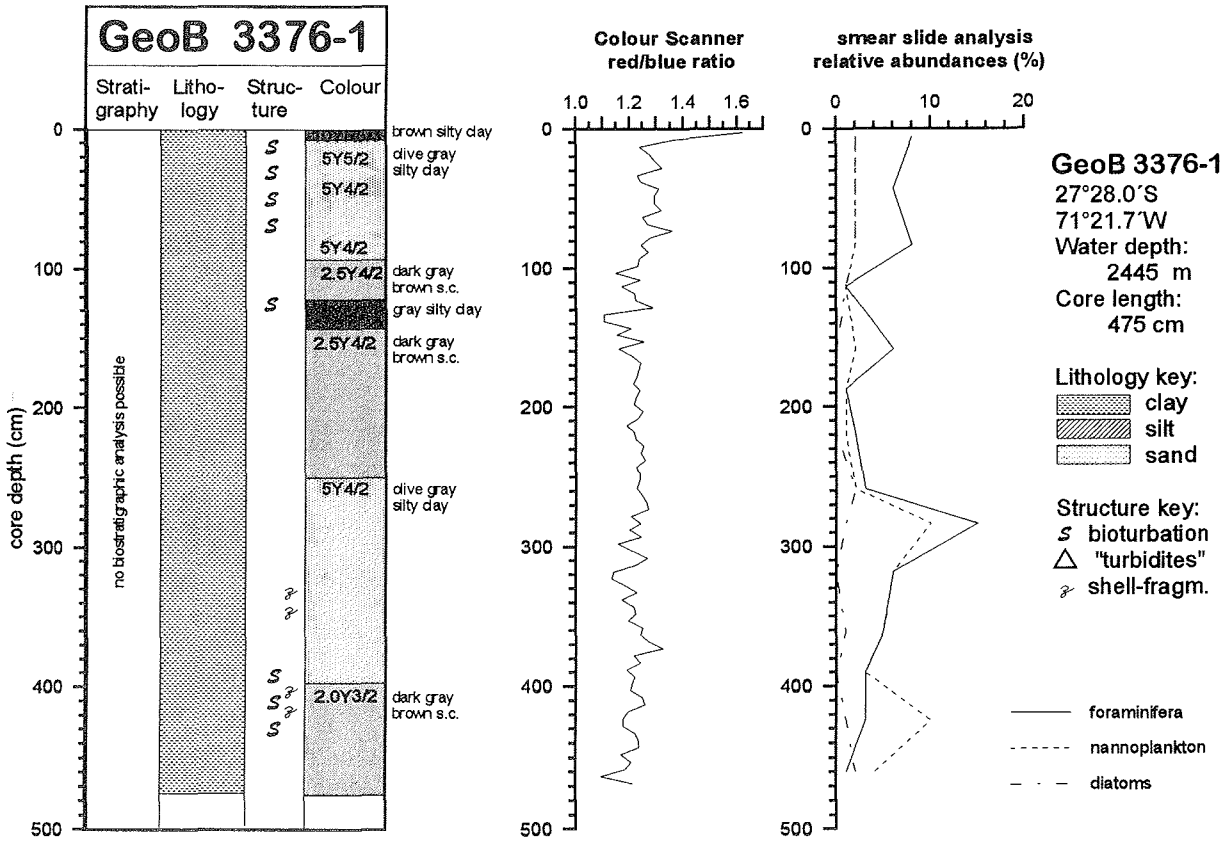

Fig. 48: Core desription, colour scanner and smear slide data for Core 3376-1

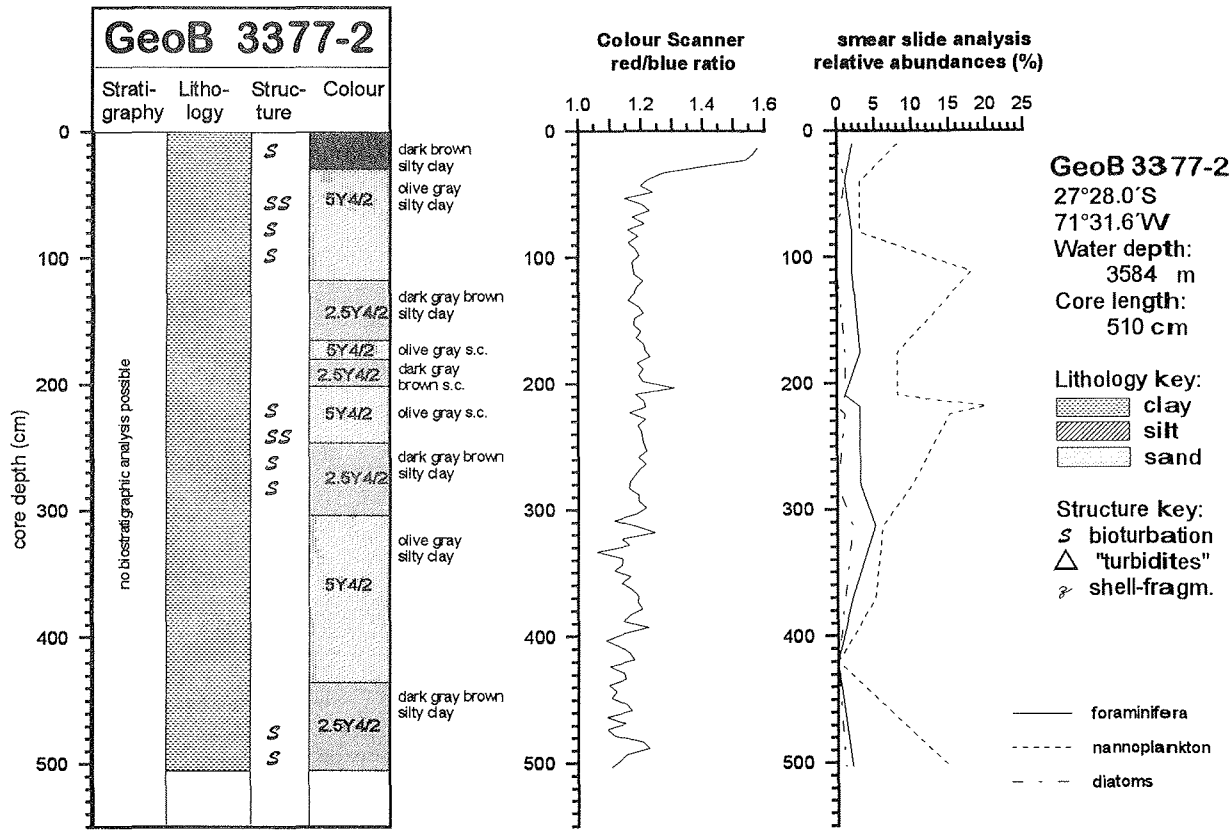

Fig. 49: Core desription, colour scanner and smear slide data for Core 3377-2

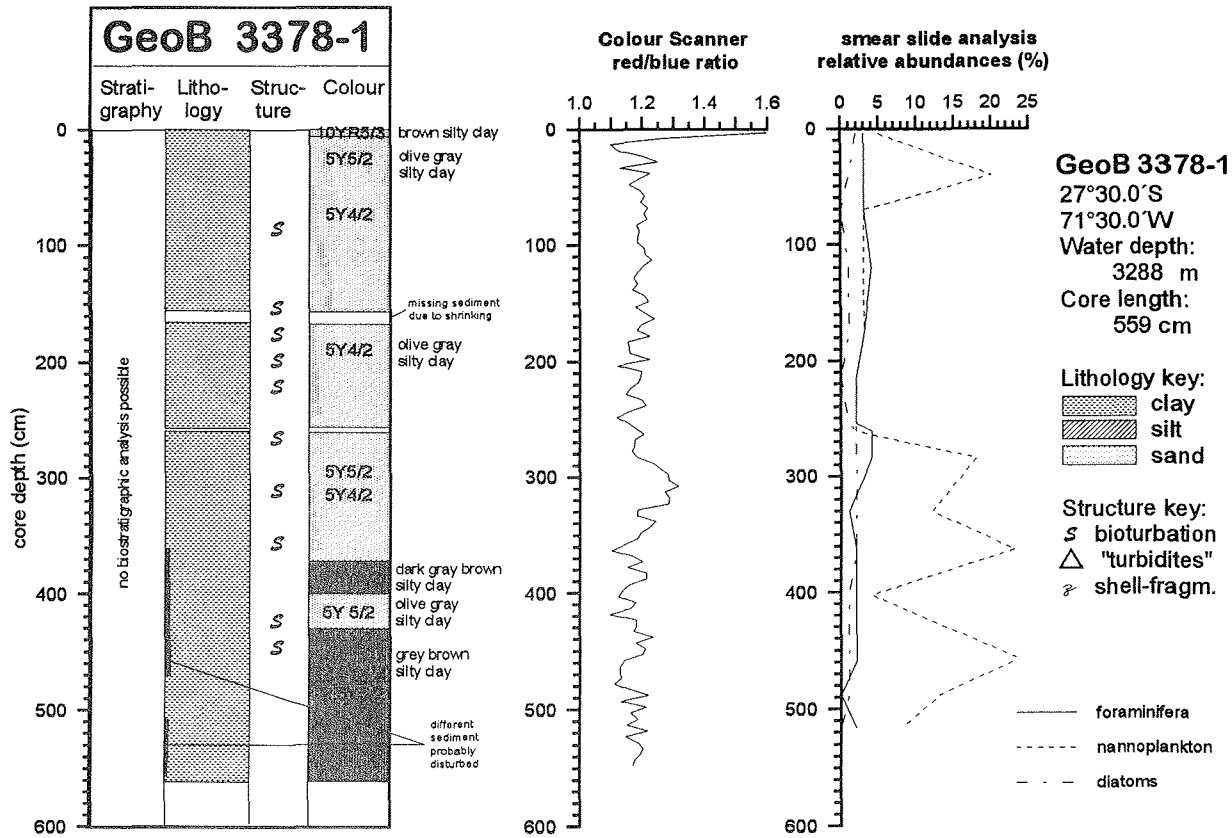

Fig. 50: Core desription, colour scanner and smear slide data for Core 3378-1

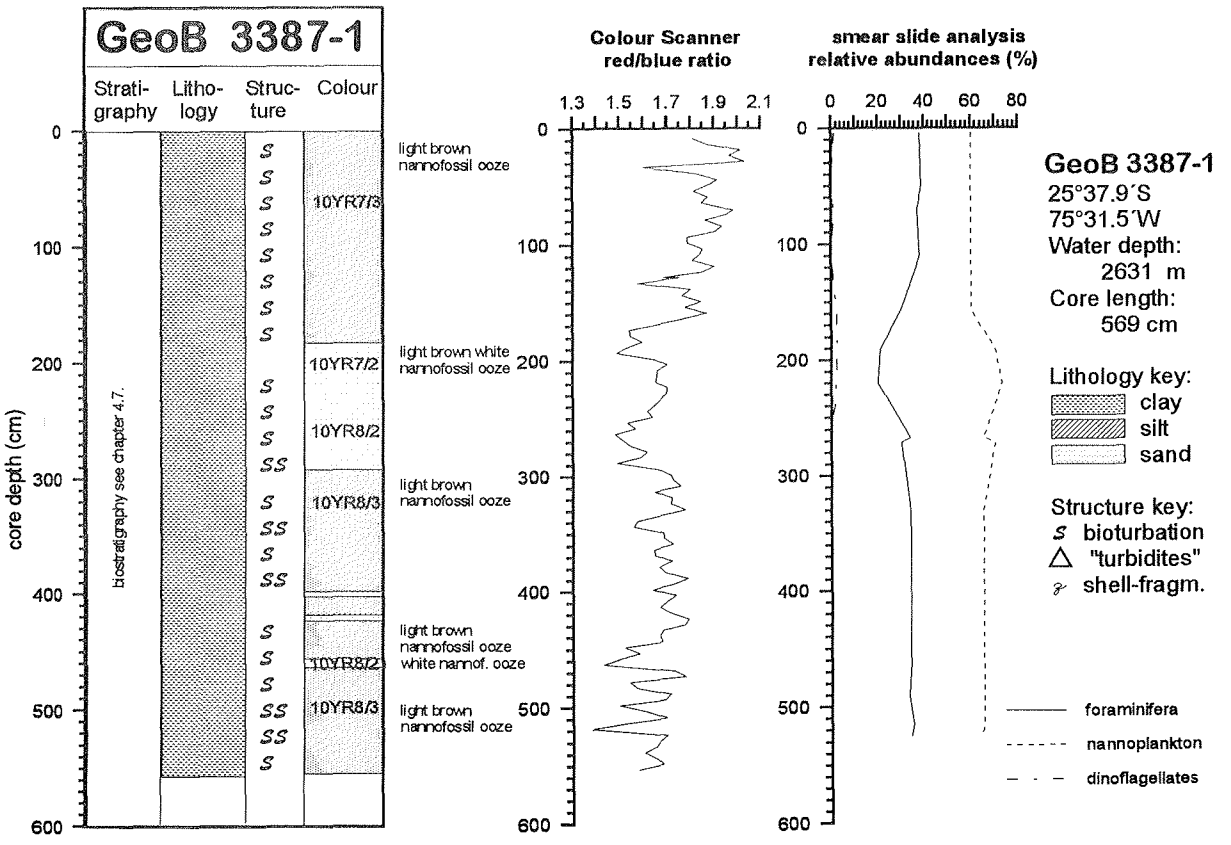

Fig. 51: Core desription, colour scanner and smear slide data for Core 3387-1

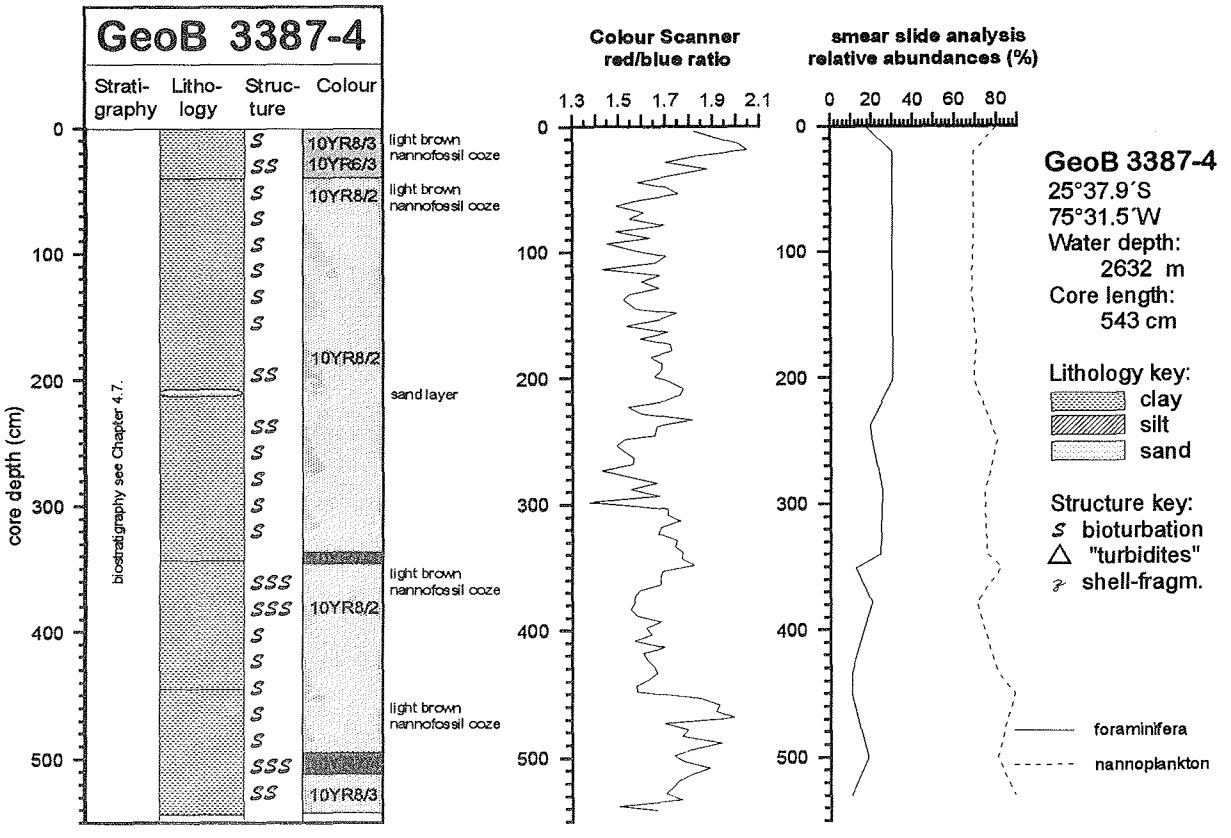

Fig. 52: Core desription, colour scanner and smear slide data for Core 3387-4

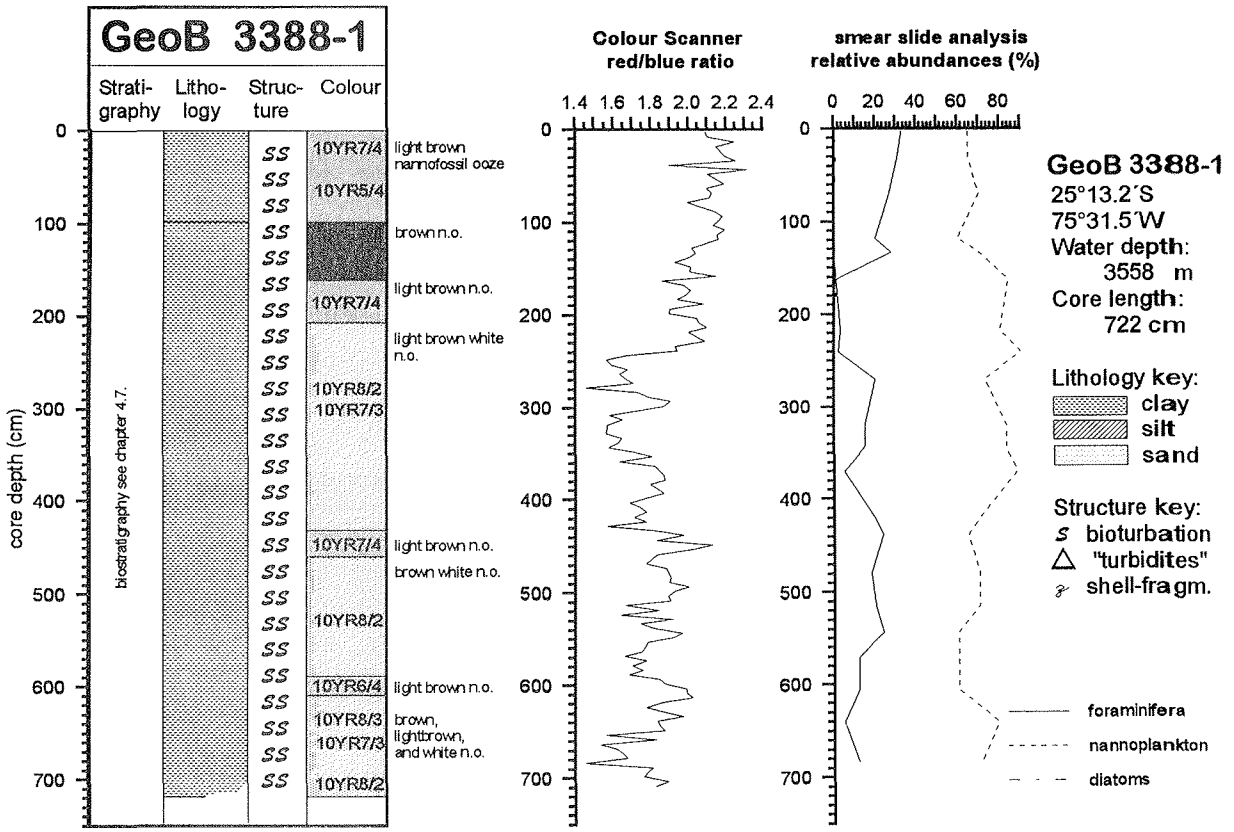

Fig. 53: Core desription, colour scanner and smear slide data for Core 3388-1

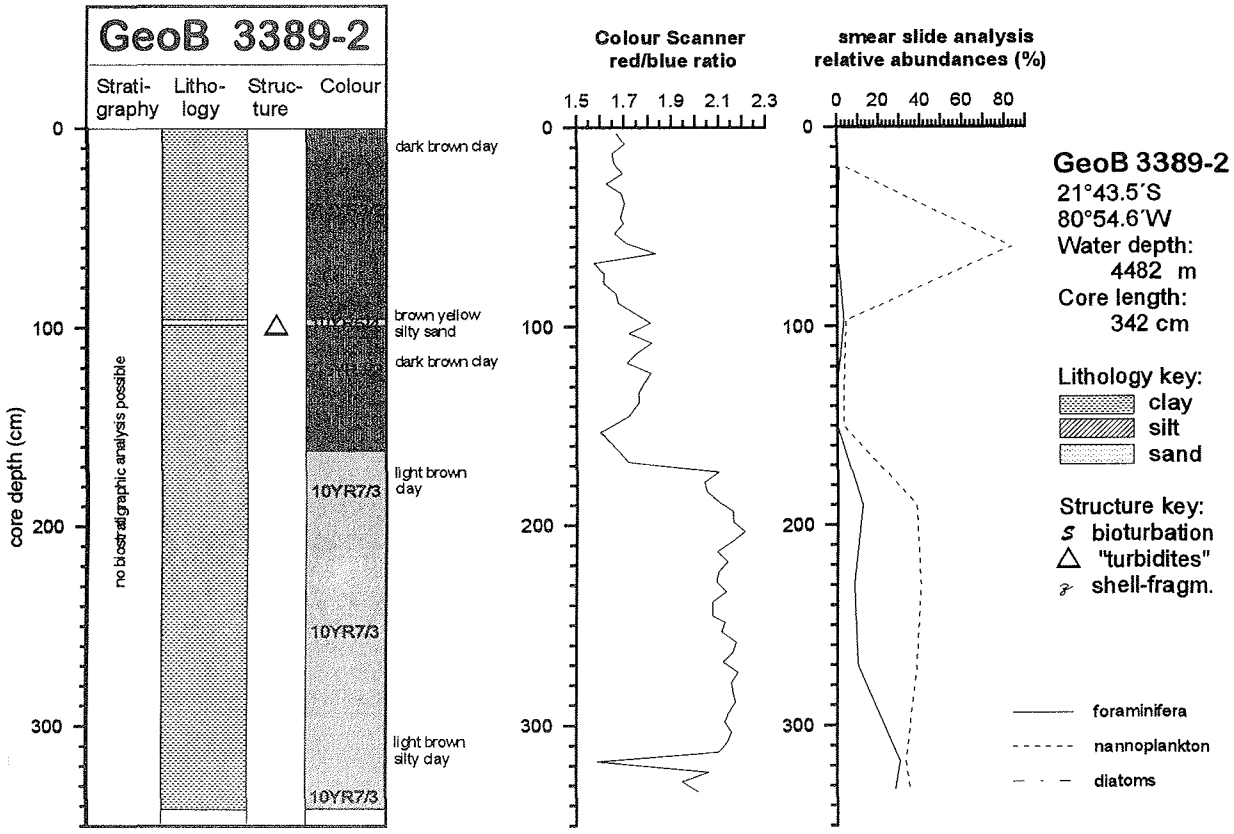

Fig. 54: Core desription, colour scanner and smear slide data for Core 3389-2

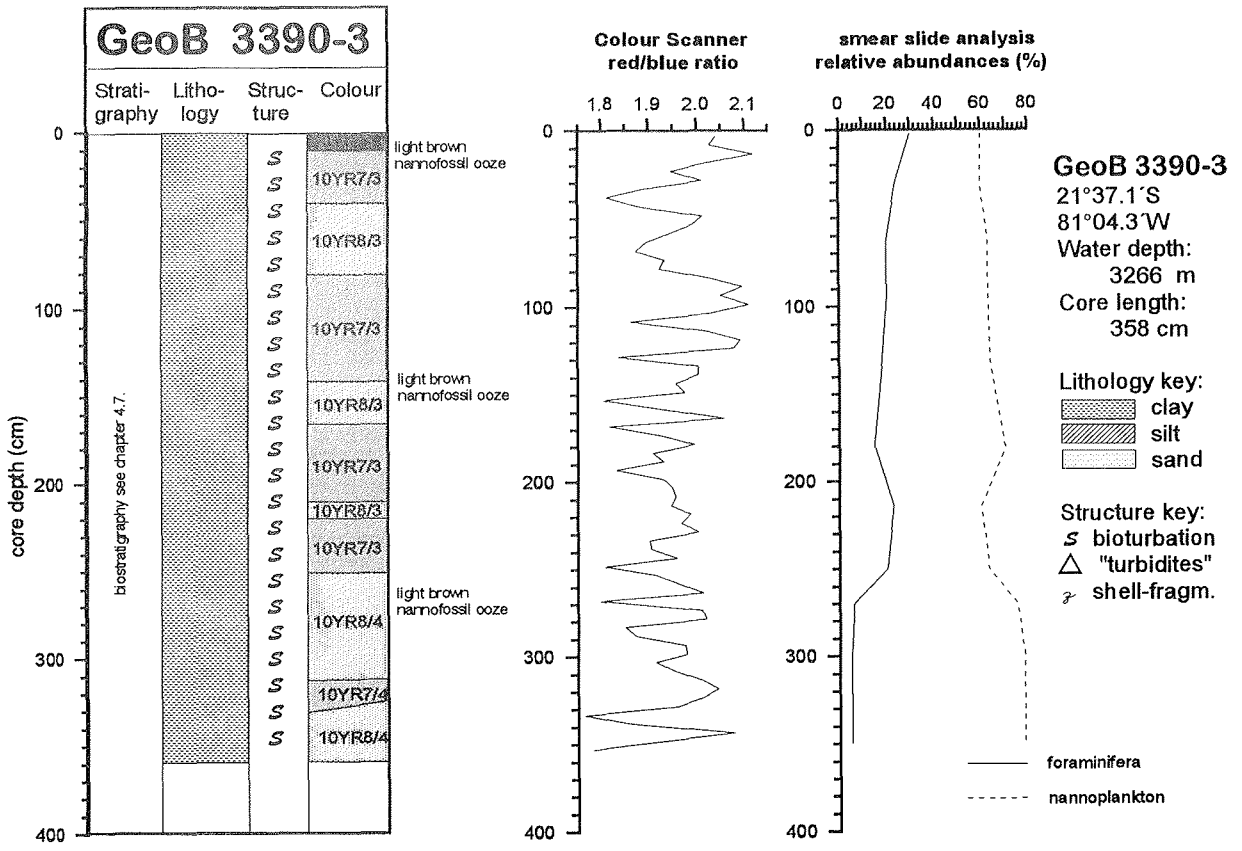

Fig. 55: Core desription, colour scanner and smear slide data for Core 3390-3

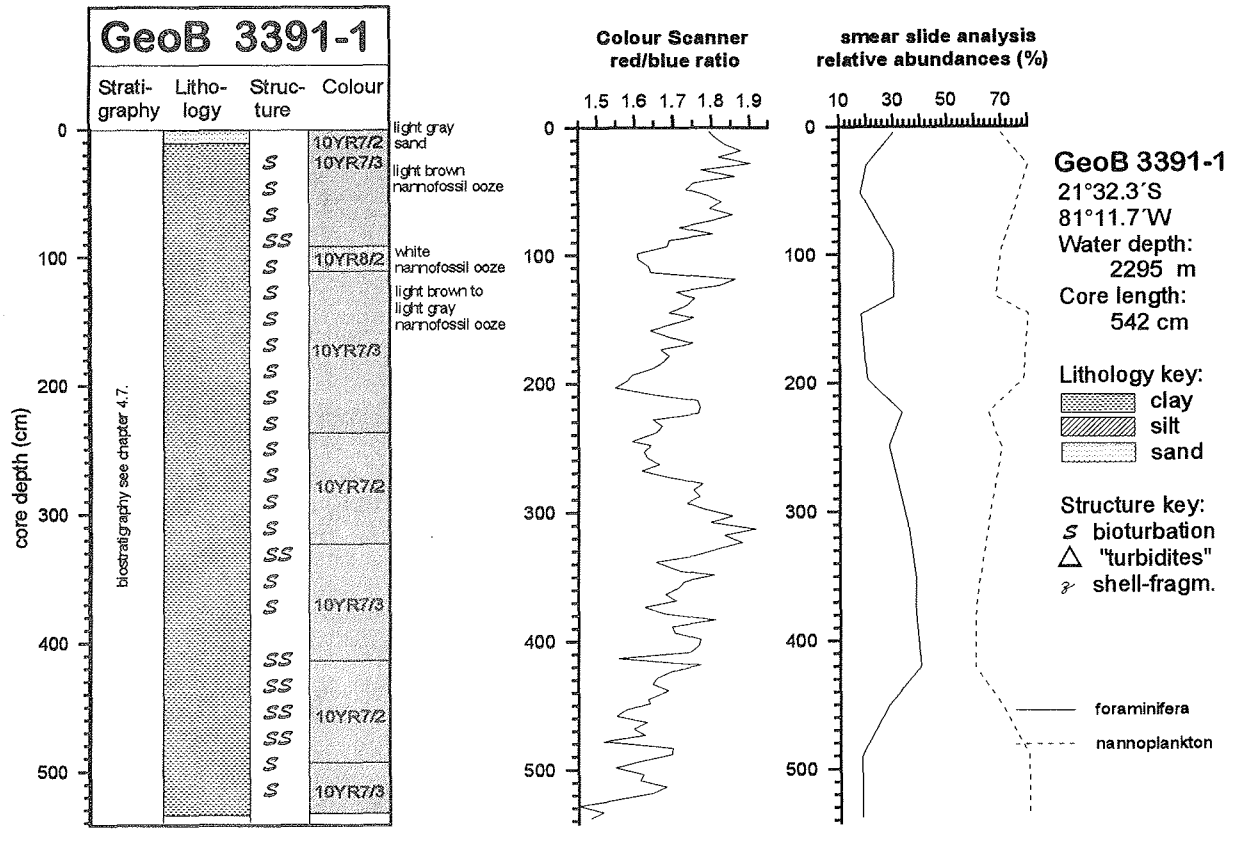

Fig. 56: Core desription, colour scanner and smear slide data for Core 3391-1

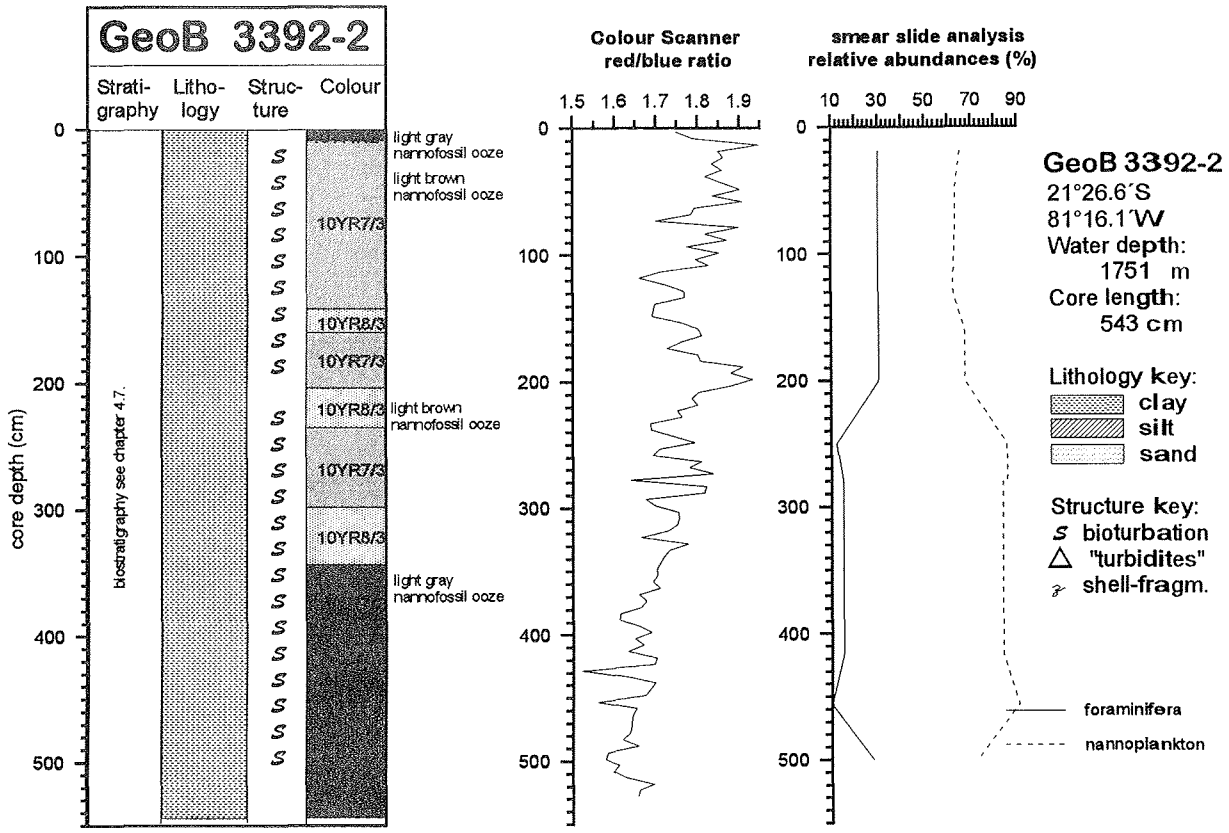

Fig. 57: Core desription, colour scanner and smear slide data for Core 3392-2

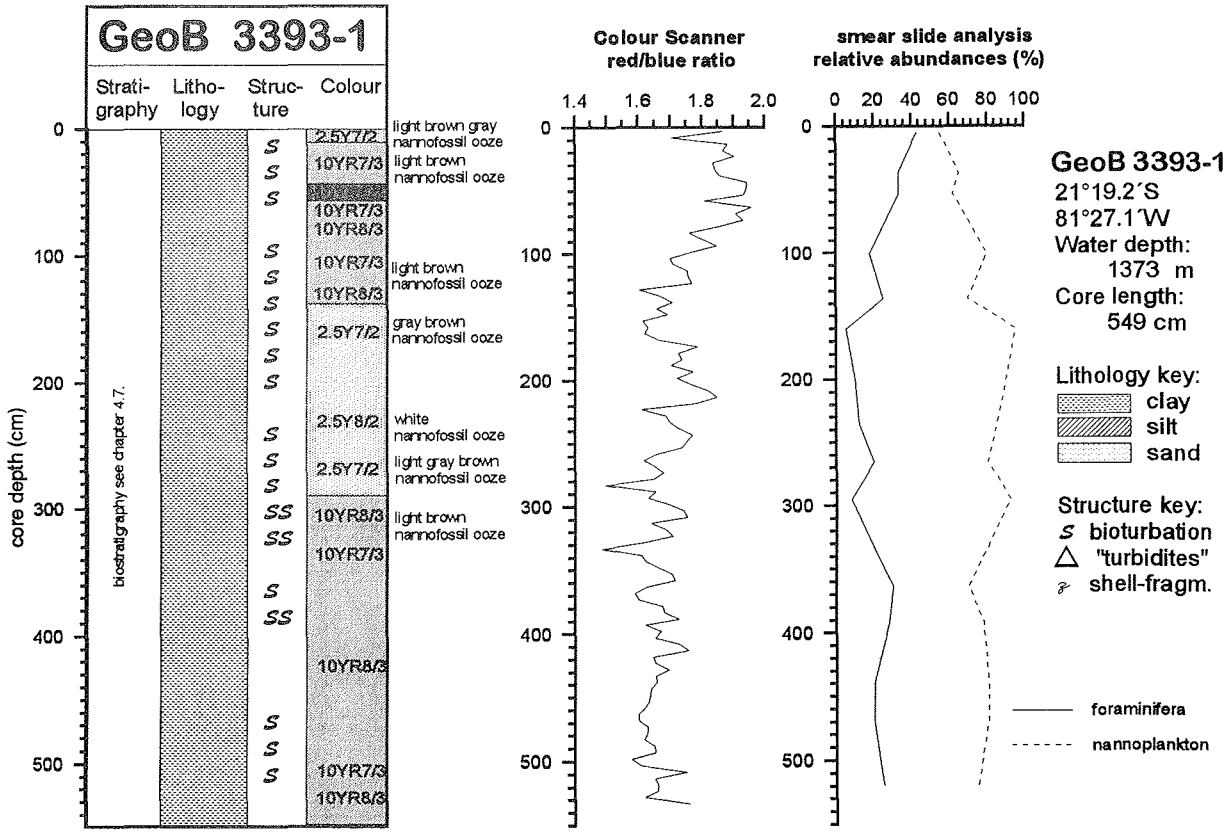

Fig. 58: Core desription, colour scanner and smear slide data for Core 3393-1

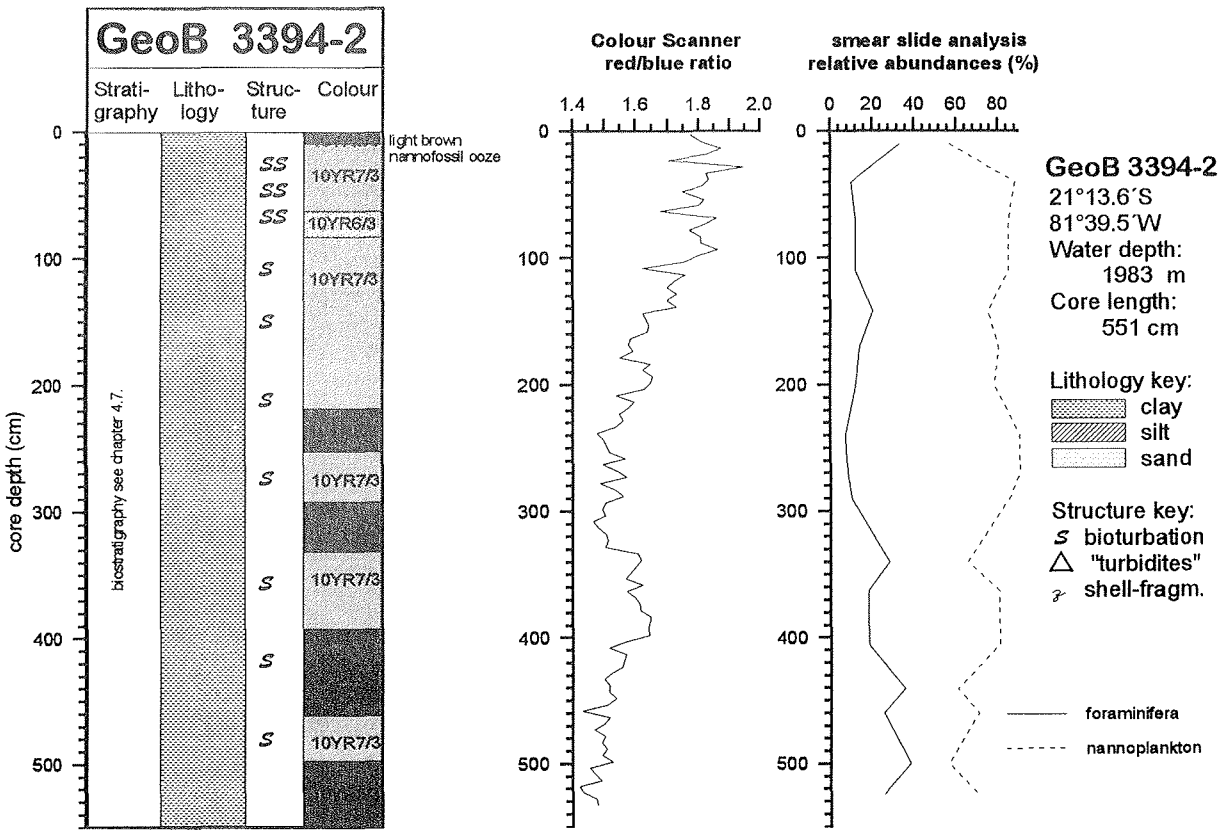

Fig. 59: Core desription, colour scanner and smear slide data for Core 3394-2

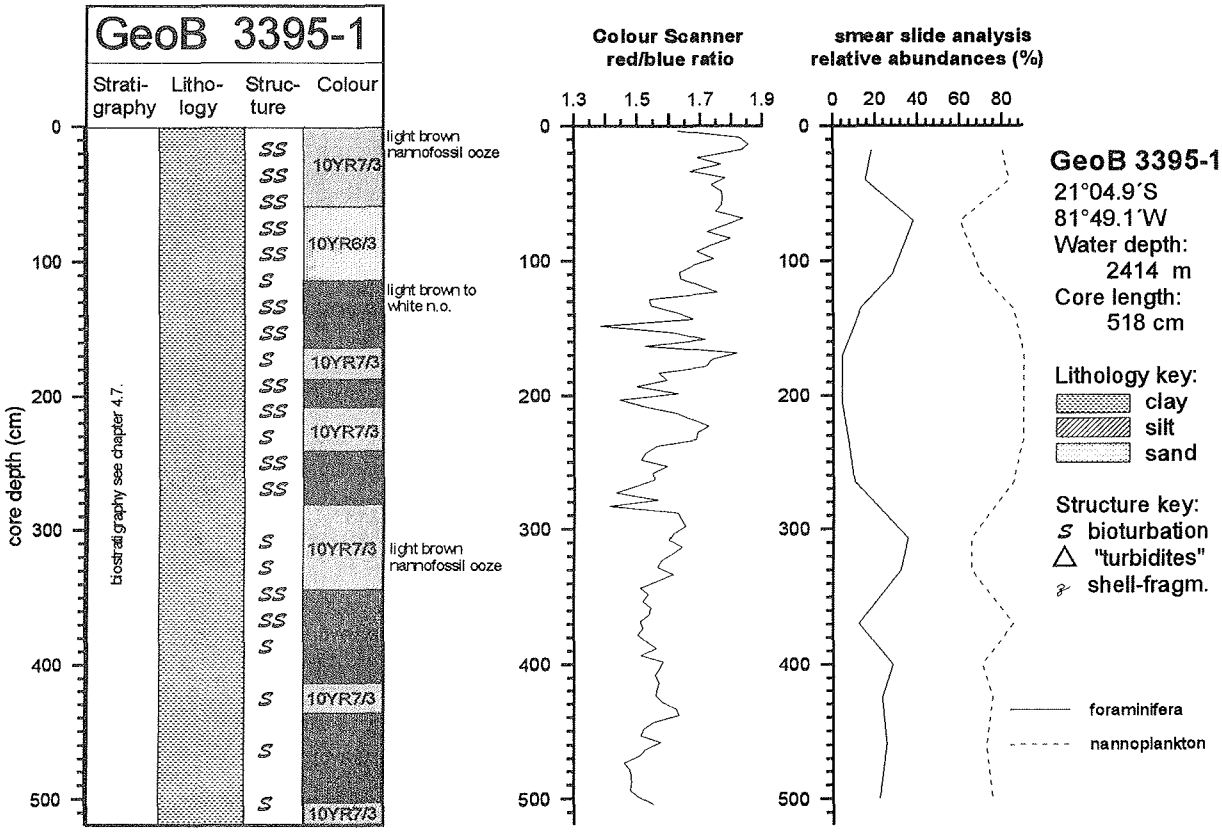

Fig. 60: Core desription, colour scanner and smear slide data for Core 3395-1

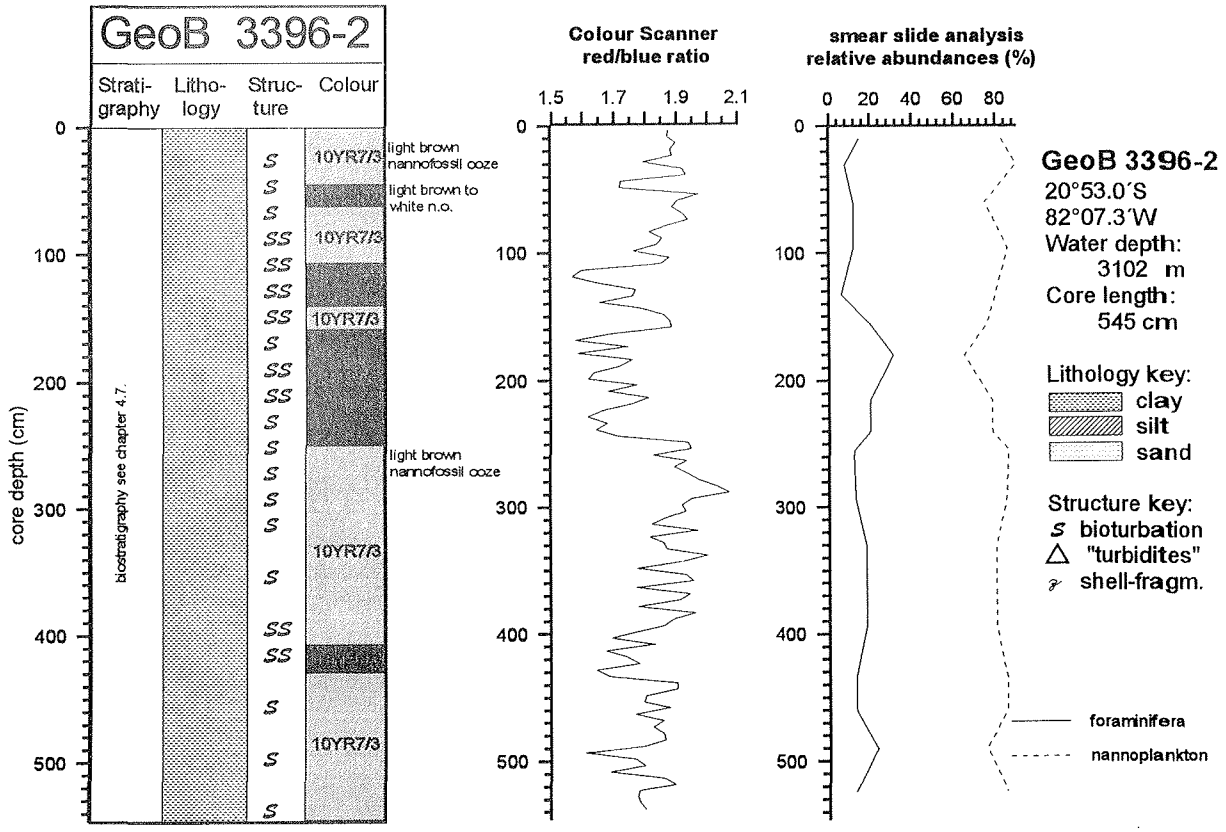

Fig. 61: Core desription, colour scanner and smear slide data for Core 3396-2

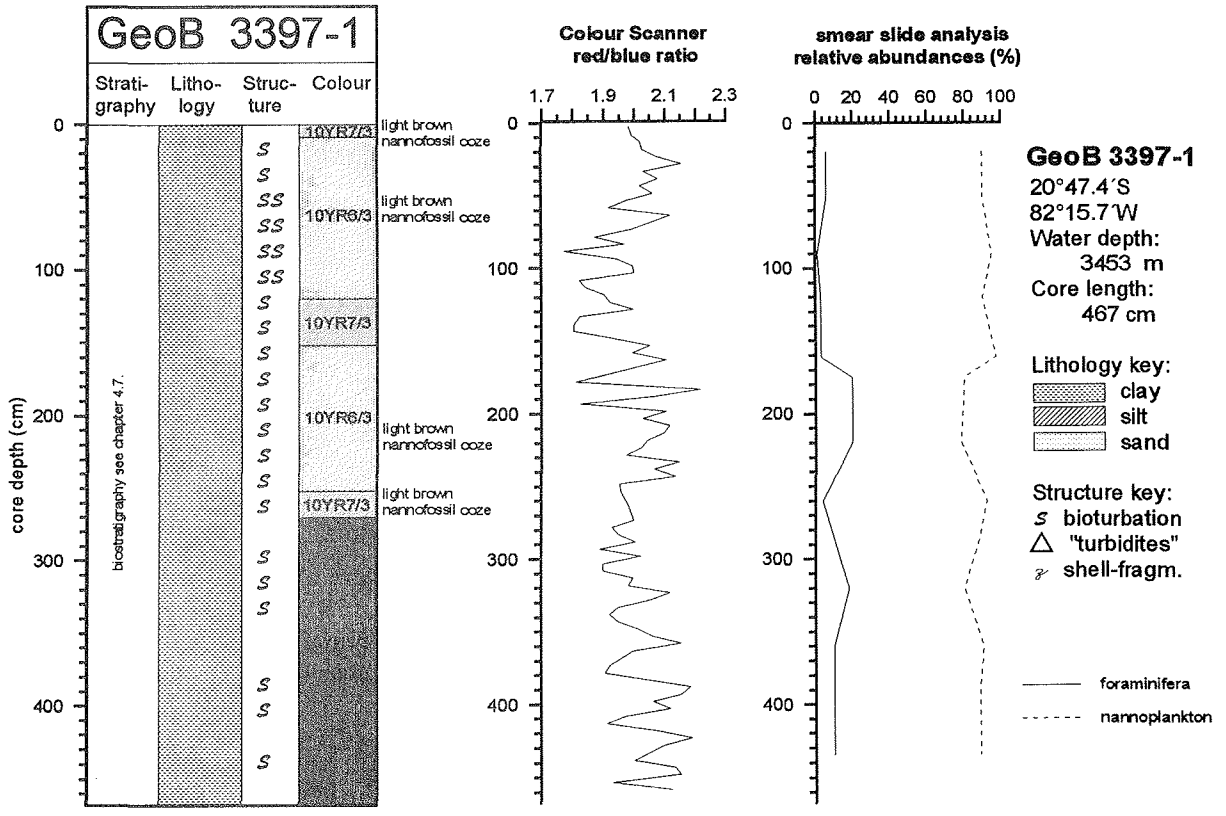

Fig. 62: Core desription, colour scanner and smear slide data for Core 3397-1

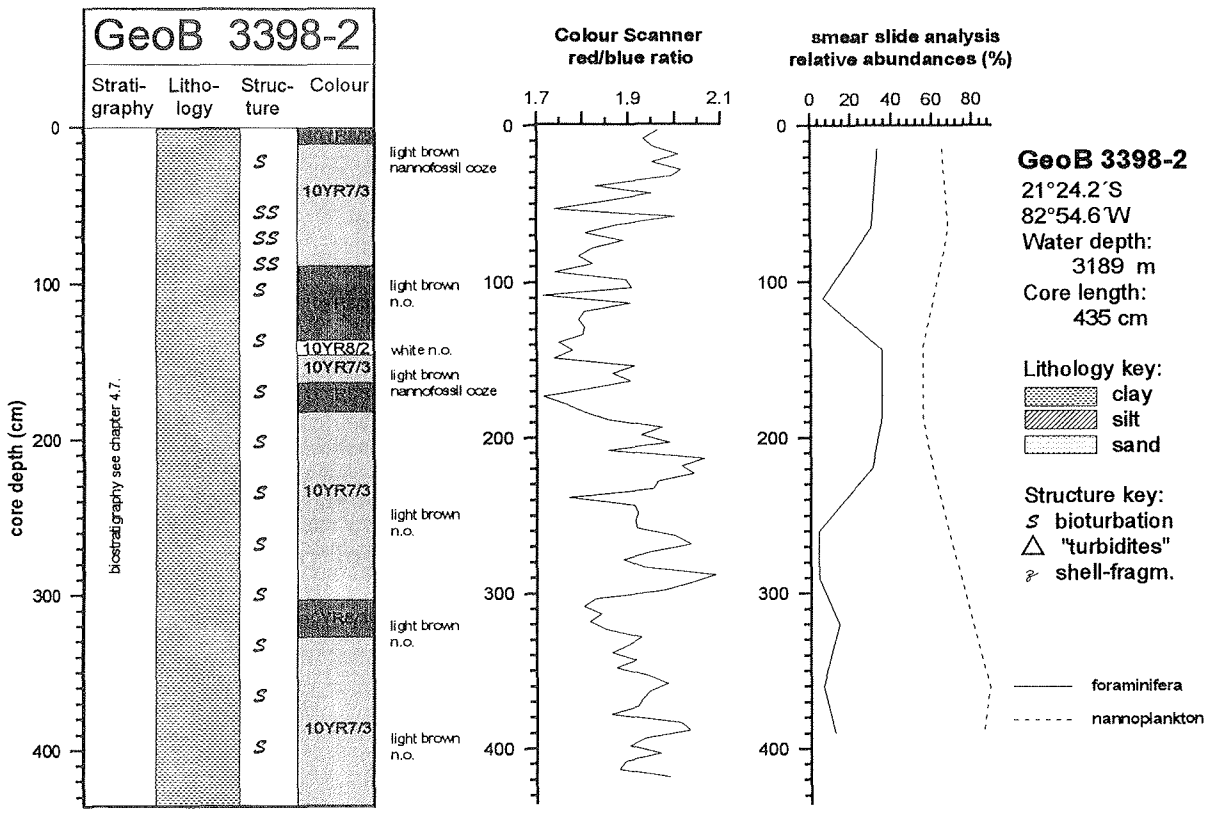

Fig. 63: Core desription, colour scanner and smear slide data for Core 3398-2

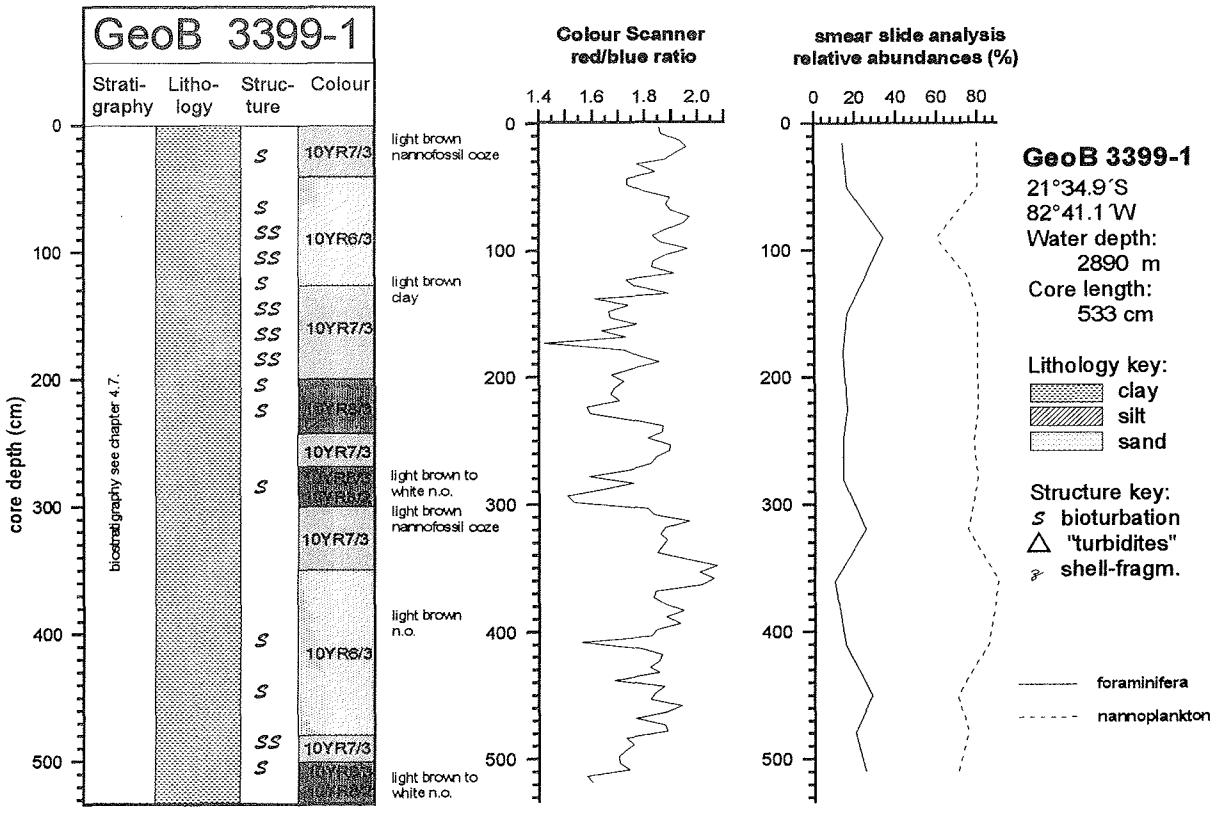

Fig. 64: Core desription, colour scanner and smear slide data for Core 3399-1

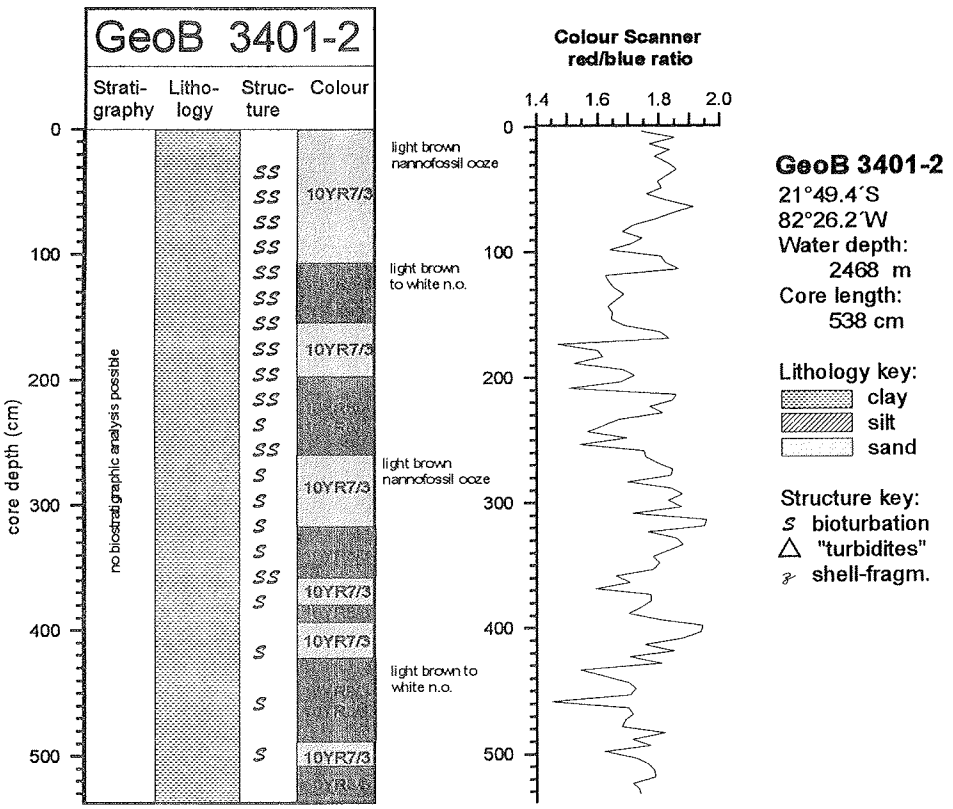

Fig. 65: Core description and colour scanner data for Core 3401-2

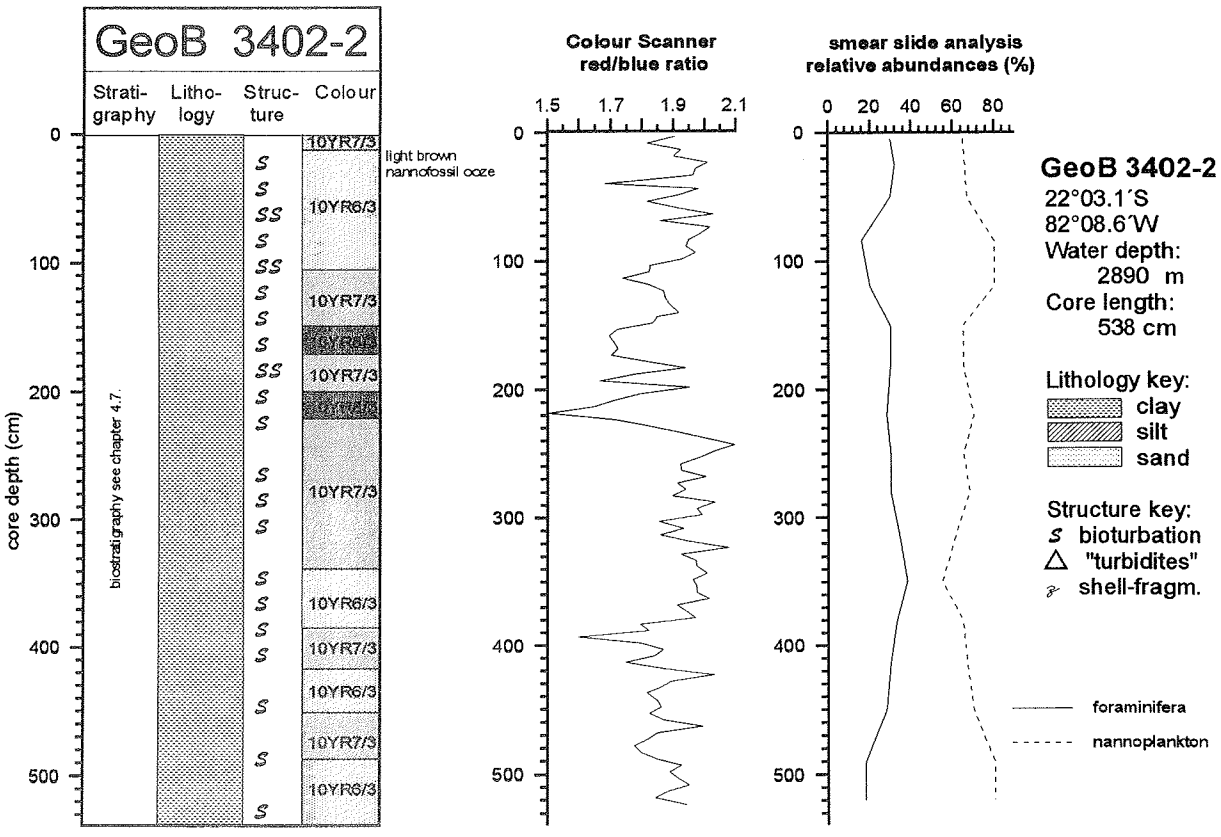

Fig. 66: Core description, colour scanner and smear slide data for Core 3402-2

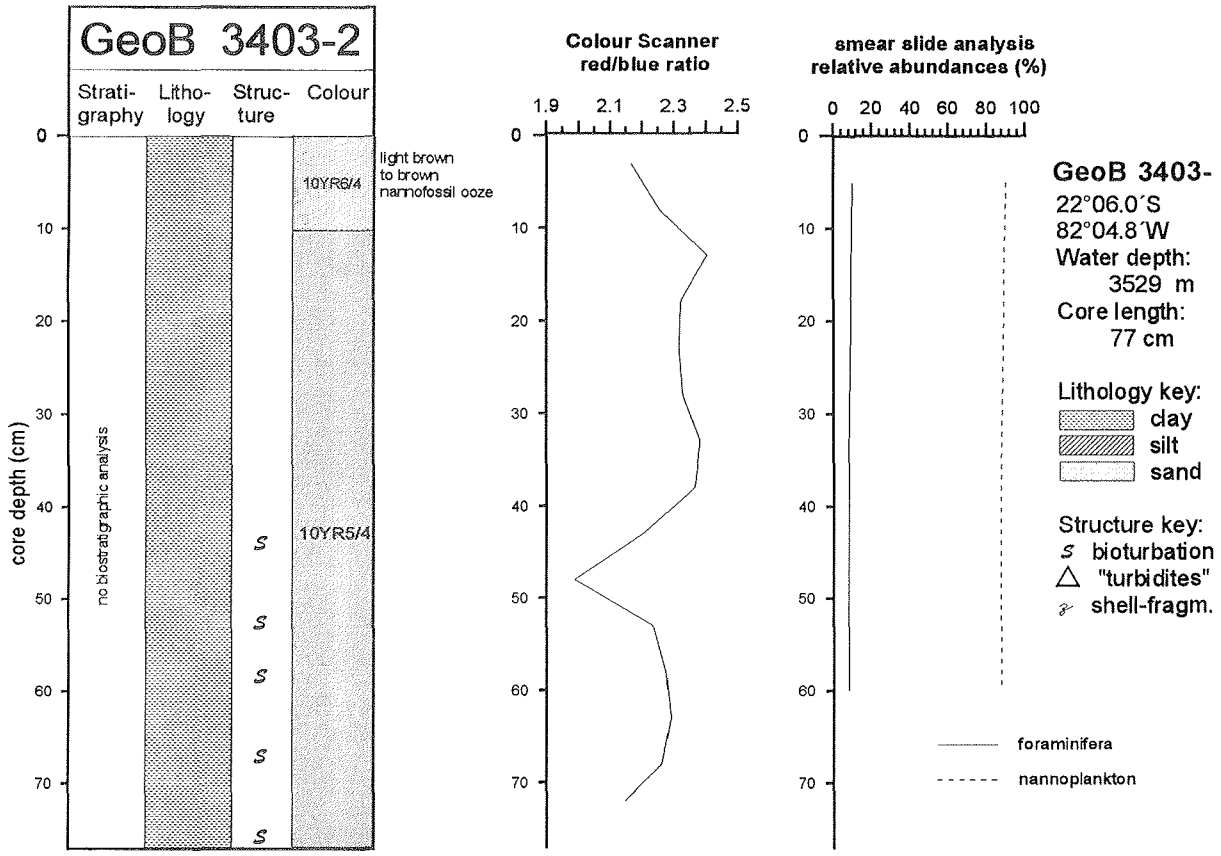

Fig. 67: Core desription, colour scanner and smear slide data for Core 3403-2

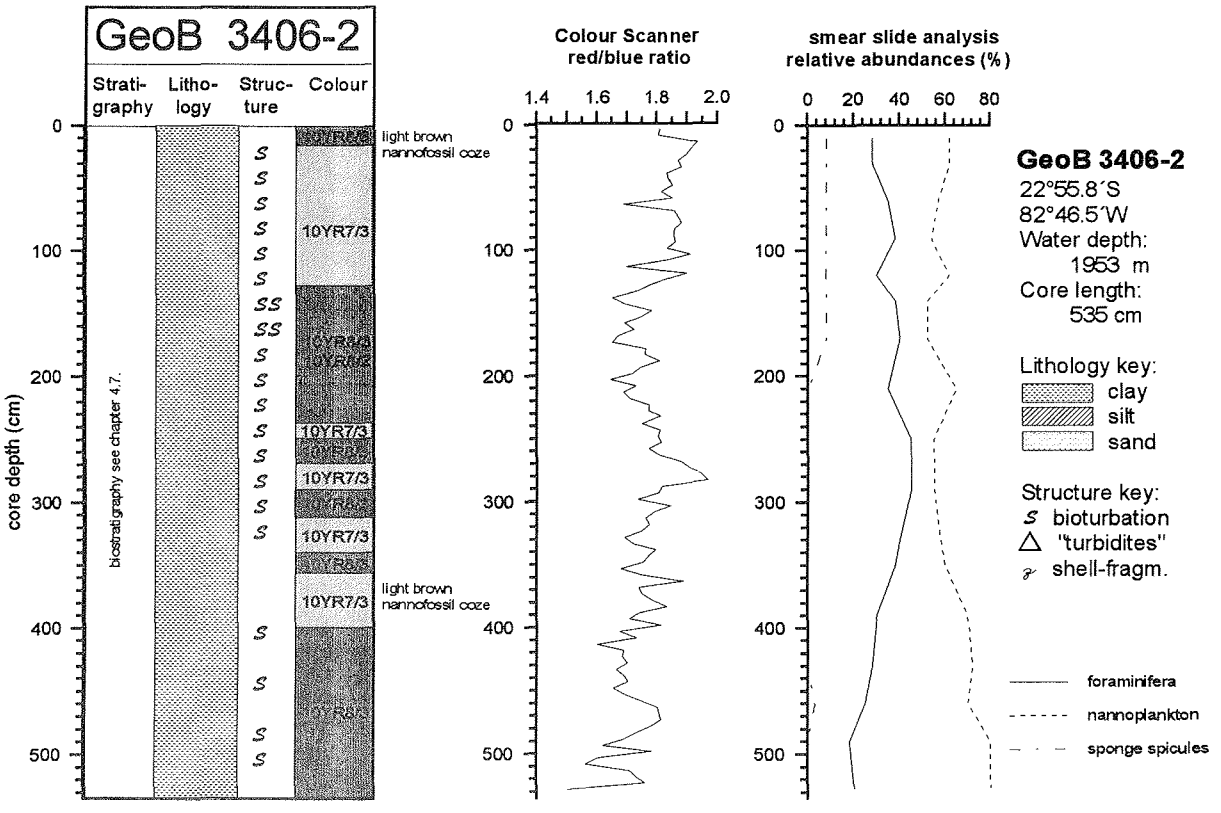

Fig. 68: Core desription, colour scanner and smear slide data for Core 3406-2

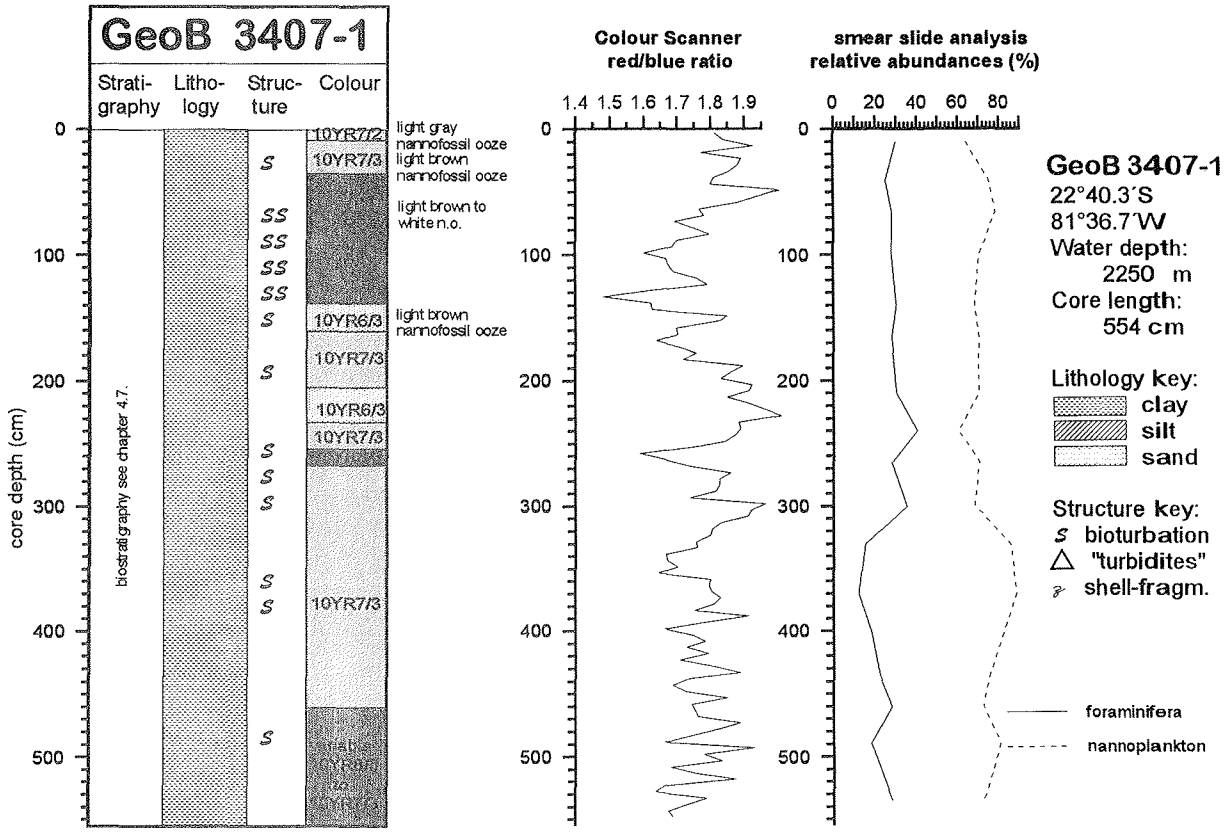

Fig. 69: Core desription, colour scanner and smear slide data for Core 3407-1

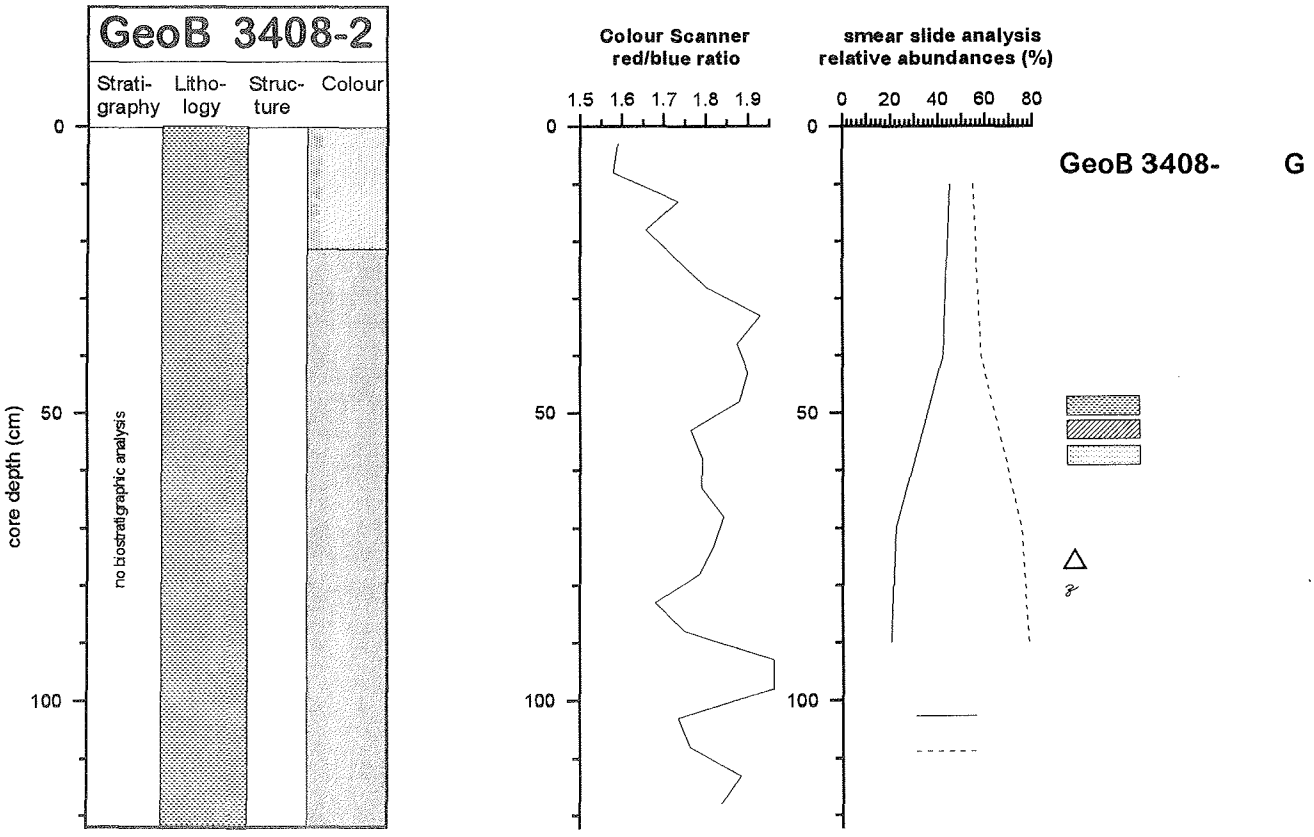

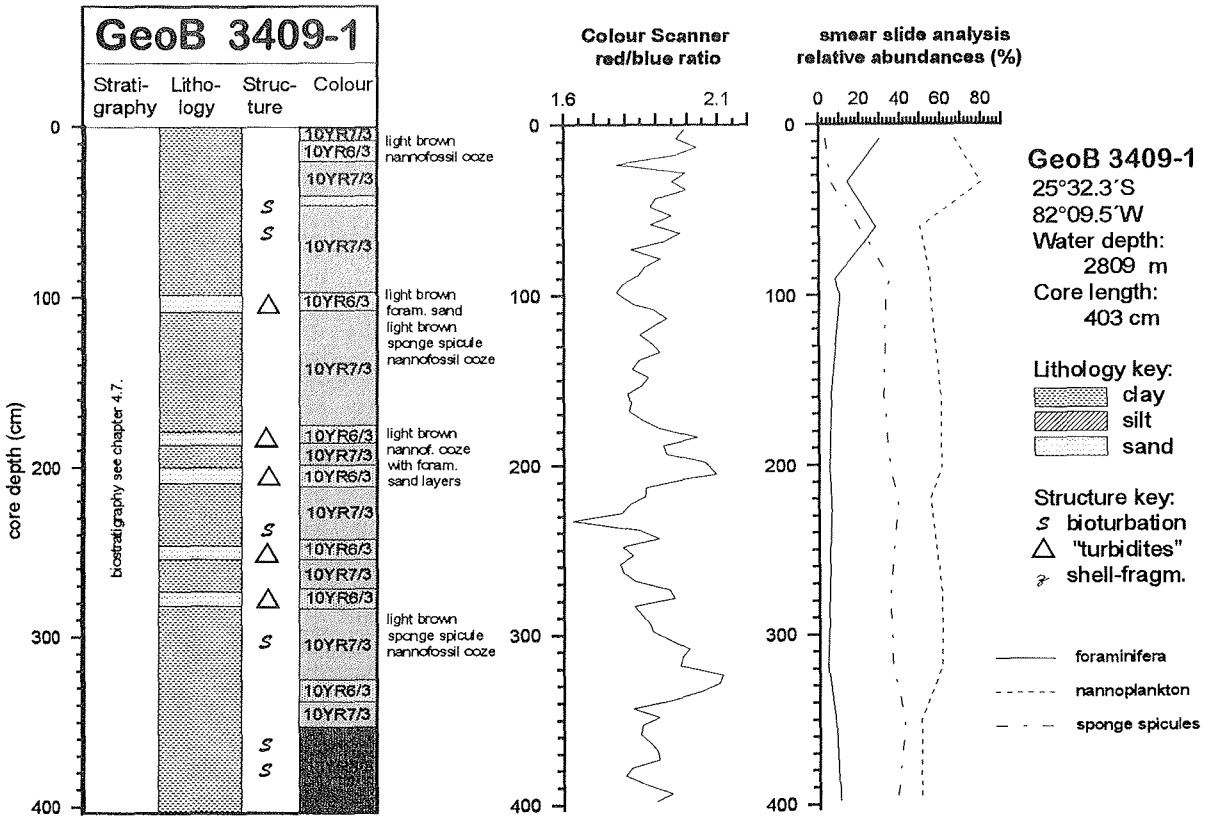

Fig. 71: Core desription, colour scanner and smear slide data for Core 3409-1

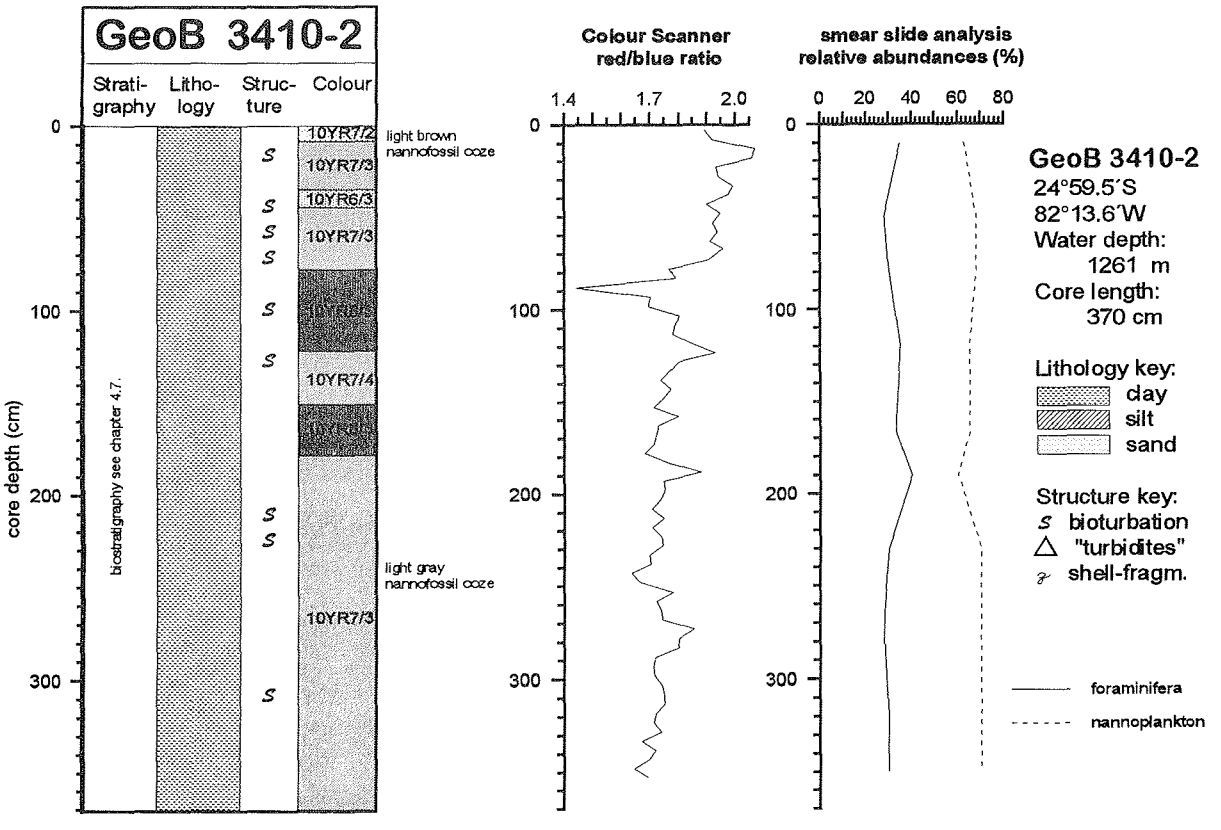

Fig. 72: Core desription, colour scanner and smear slide data for Core 3410-2

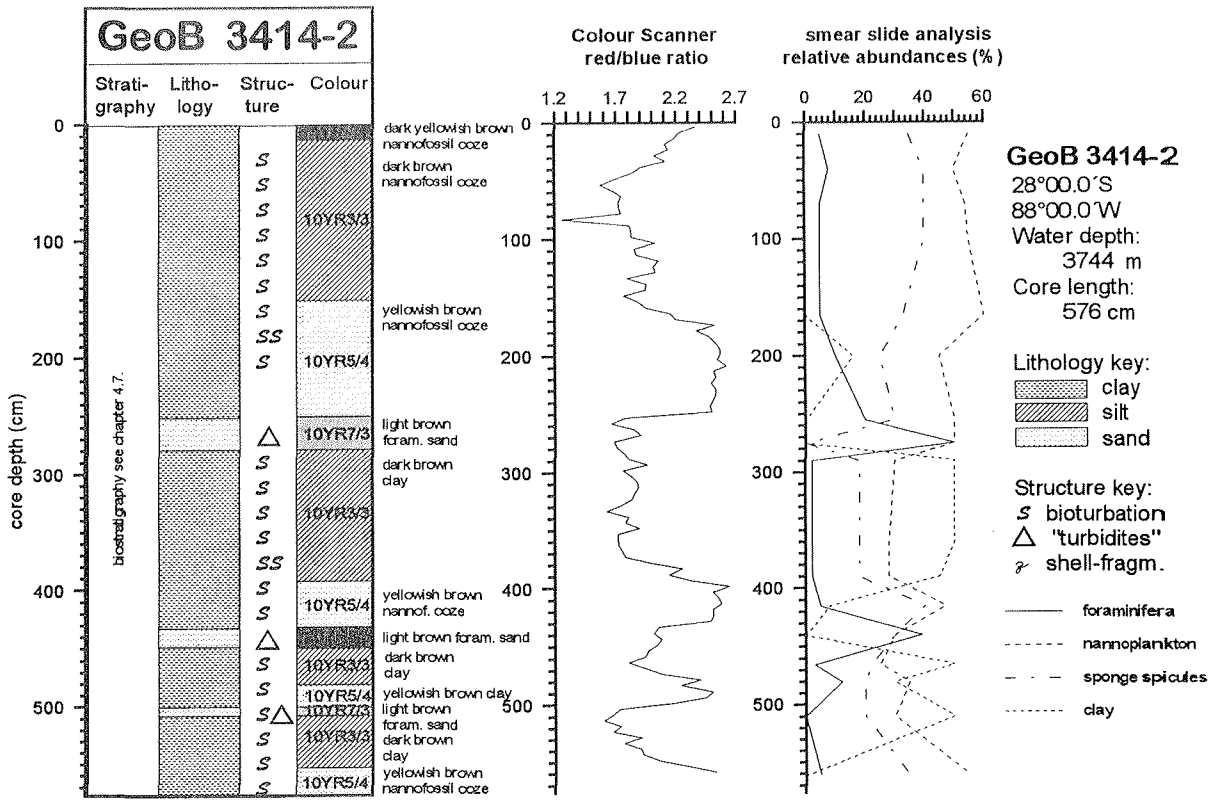

Fig. 73: Core desription, colour scanner and smear slide data for Core 3414-2

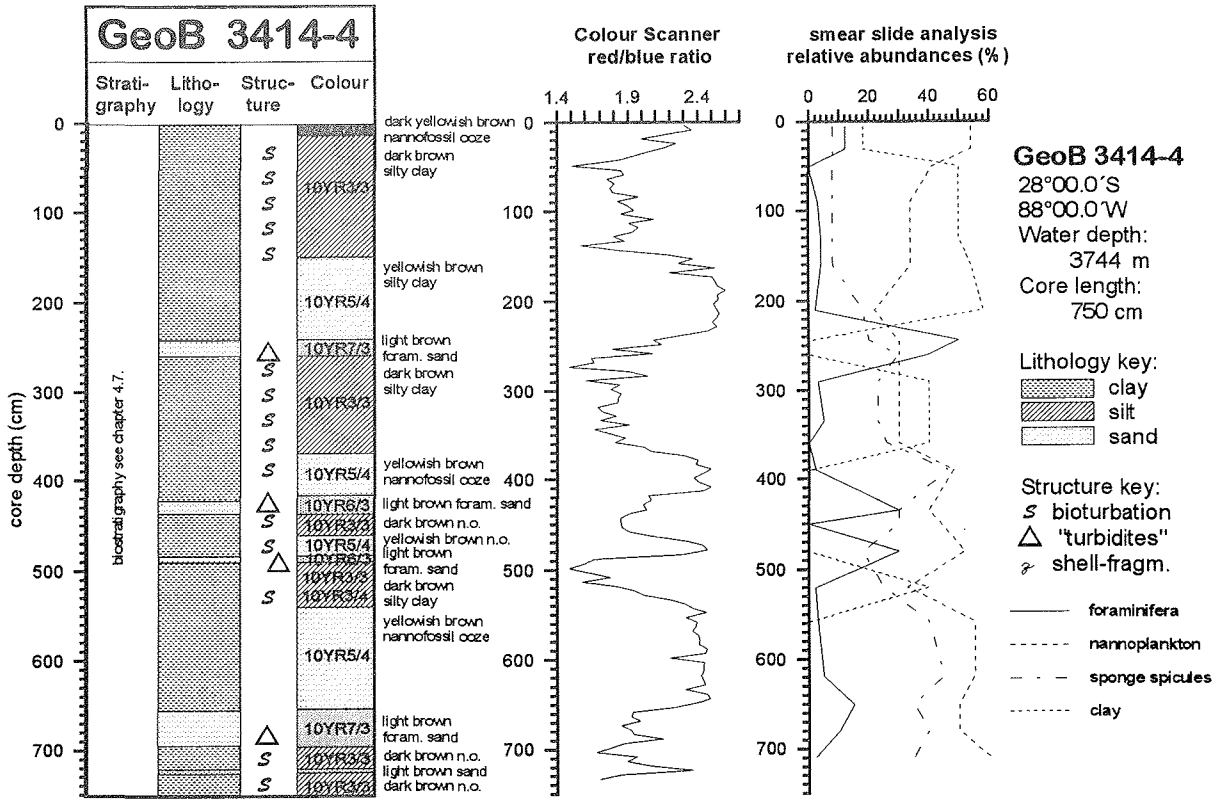

Fig. 74: Core desription, colour scanner and smear slide data for Core 3414-4

The cores GeoB 3409-1 and 3410-2 have been retrieved from a seamount 180 nm south of the Nazca Ridge.

GeoB 3409-1 (water depth 2809m; 25°32,3´S; 82°09,5´W; length 403 cm, Fig. 71)

The sediments of this core are more variable. Foraminifera are frequent (14 to 30%) in the uppermost 60 cm of the core and occur together with nannofossils which are dominating (foraminifera bearing nannofossil ooze). In the remaining part of the core sponge spicules become recurrent and reach up to 42%. Foraminifera are less frequent in this part and only occasionally reach 10%. The sediments are therefore predominatly sponge spicule bearing nannofossil oozes. The colour differs slightly between light and very light brown. Bioturbation is mostly absent. As a special feature slightly coarser layers occur which may be partly turbiditic.

Geo B 3410-2 (water depth 1261 m; 24°59,5´S; 82°13,6´W; length 370 cm, Fig. 72)

The lithology of this core is very homogenous and is composed of foraminifera bearing nannofossil ooze. The contents of foraminifera vary between 28 and 40%. Colours range from light brown to very light brown. In the uppermost 150 cm a frequent slight to moderate bioturbation occurs, while in the remaining part bioturbation is nearly absent.

Oceanic area at 28°S; 88°W

Two more cores were recovered from the oceanic basin at the western end of the oceanographic transect at 28°15´S. They show a cyclic intercalation of deep sea clay and calcareous to siliceous biogenous sediments in a m-scale.

GeoB 3414-2 (water depth 3744 m; 28°S; 88°W; length 576 cm, Fig. 73)
GeoB 3414-4 (water depth 3744 m; 28°S; 88°W; length 750 cm, Fig. 74)

In these cores three sediment types were observed which show cyclic distribution. In the longer core four cycles are present. Each sequence begins with a light brown turbiditic layer which consists of foraminifera, nannofossils and sponge spicules in changing proportions (sponge spicule nannofossil bearing foraminifera ooze and foraminifera sponge spicule bearing nannofossil ooze), followed by a yellowish brown sponge spicule bearing nannofossil ooze which finally changes gradually to dark brown clay nannofossil to clay sponge spicules bearing nannofossil ooze. The thickness of the sequences is variable. Except for the turbiditic parts a slight bioturbation is present throughout the core.

4.7. Preliminary Stratigraphy

(O. Romero and B. Donner)

Methods - The preliminary on-board biostratigraphic analysis was made on gravity cores by taking samples in 5 cm intervals in the upper 50 cm of each core and in 20 cm intervals from 50 cm to the bottom. Depending on the sediment composition, 2-8 ml of the sample material has been sieved over a 63 µm sieve, dried in an oven at 60°C and finally filled into 5 ml glass tubes. The amount of material in the glass tubes was used as an indicator for the relative sand content of the samples. It varies depending on the fertility of the surface water and can also be an indicator of carbonate dissolution.

The biostratigraphic classification is made by determinig the abundance of planktonic foraminifera of the *Globorotalia menardii* complex. This group of foraminifers consists of five closely related warm-water species and/or subspecies which thrive in tropical and subtropical waters, in temperatures of about 20-30°C. On the basis of a cyclical appearance and disappearance of these species during the Quaternary ERICSON & WOLLIN (1968) defined a biostratigraphic zonation scheme (below called E&W zones) using a letter notation from Z (= Holocene) to Q in order of increasing age. Because of a direct correlation of the zones Z to U with isotopic stages the following ages are assumed for the zone boundaries: Z/Y = 12 kyr, Y/X = 70 kyr, X/W = 130 kyr, W/V = 185 kyr and V/U = 370 kyr. Other useful stratigraphic markers that could be used to recognize older sediments (e.g. from Tertiary era) are the appearance of *Globorotalia truncatulinoides* and/or disappearance of *Globigerinoides sacculifer fistulosa* in Pleistocene in comparison to Pliocene sediments.

For example in the present-day Atlantic Ocean the distribution of the subspecies *Globorotalia menardii menardii* is mainly limited to the geographical area from 20°N to 10°S. According to BOLTOVSKOY (1975) South American Pacific Ocean foraminifera are poorly studied and he states that the maximal latitudinal penetration to the south of the *G. menardii* complex in surface waters adjacent to the South American continent is 20°S.

Pacific pelagic sediment cores show a „sandfraction" curve which - in contrast to Atlantic sediments - runs with its maxima slightly after the peaks of the „number of *G.menardii*". That means, maxima in sand content correlate with warmage/iceage boundaries (~Deglaciation/Inglaciation) and do not correlate with maxima in number of *G. menardii*.

The working area during SONNE cruises SO 102/1+2 in the southeastern Pacific ranges from 20°S to 43°S. A biostratigraphic classification was tried only in those 23 cores from the northernmost coring positions, which contained a sufficient content of foraminifera.

Results

IQUIQUE-RIDGE

GeoB 3387-1	length: 569 cm	WD: 2631 m	(Fig. 75)
GeoB 3387-4	length: 543 cm	WD: 2632 m	(Fig. 76)
GeoB 3388-1	length: 722 cm	WD: 3558 m	(Fig. 77)

At station GeoB 3387 two cores with comparable length were taken. In core GeoB 3387-1 the X/W boundary is reached (~ bottom sediments older than 130 kyr). The different zones proposed by the *G. menardii* distribution are supported by the results of the "sand content". The sedimentation rate is ~3.5 cm/kyr. In GeoB 3387-4 only boundary Z/Y can be detected. A comparison indicates that GeoB 3387-4 has a stratigraphical length similar to ~300 cm core depth in GeoB 3387-1 and, thus, has a much higher sedimentation rate. Core GeoB 3388-1 also reaches zone W (bottom sediment older than 130 kyr). However, the position of the X/W boundary cannot be defined exactly.

NAZCA-RIDGE

GeoB 3390-3	length: 358 cm	WD: 3266 m	(Fig. 78)
GeoB 3391-1	length: 542 cm	WD: 2295 m	(Fig. 79)
GeoB 3392-2	length: 543 cm	WD: 1751 m	(Fig. 80)
GeoB 3393-1	length: 549 cm	WD: 1373 m	(Fig. 81)
GeoB 3394-2	length: 551 cm	WD: 1983 m	(Fig. 82)
GeoB 3395-1	length: 530 cm	WD: 2414 m	(Fig. 83)
GeoB 3396-2	length: 545 cm	WD: 3102 m	(Fig. 84)
GeoB 3397-1	length: 467 cm	WD: 3453 m	(Fig. 85)
GeoB 3398-2	length: 435 cm	WD: 3189 m	(Fig. 86)
GeoB 3399-1	length: 433 cm	WD: 2890 m	(Fig. 87)
GeoB 3402-2	length: 538 cm	WD: 2890 m	(Fig. 88)
GeoB 3406-2	length: 535 cm	WD: 1953 m	(Fig. 89)
GeoB 3407-1	length: 554 cm	WD: 2250 m	(Fig. 90)

Cores GeoB 3390-3 to GeoB 3397-1 were taken on our northeastern transect crossing Nazca Ridge. In GeoB 3390-3 (Fig. 78) the Z/Y boundary is reached in ca. 45 cm core depth. Further downcore the interpretation is difficult, however, zone X has likely been reached. GeoB 3391-1, 3392-2, 3393-1 and 3394-2 (Fig. 79-82), all from shallower regions of the Nazca Ridge, show a strange double peak in „number of *G. menardii*" in the upper 100 cm, which makes a definition of the Z/Y boundary problematic. Normally, zone Y is characterized by very low

amounts of *G. menardii*. Nevertheless, only the upper of those two peaks corresponds probably to zone Z. If also the lower peak would be part of Z, the Z/Y boundary (12 kyr) would be very deep indicating unlikely high Holocene sedimentation rates. Because of these difficulties an exact correlation between peaks and E&W zones in these cores is not possible.

GeoB 3395-1, 3396-2, 3398-2, and 3399-1 (Fig. 83, 84, 86, 87) from the northwestern flank of the Nazca Ridge show a first peak in *G. menardii* distribution close to the core top (corresponding to zone Z). A second peak is clearly visable between 50 and 100 cm core depth, resembling GeoB 3391-1 to 3394-2. Concerning the sand content, in cores GeoB 3395-1 to 3399-1 the second *G. menardii* peak would more likely be part of zone Z, because the sand content decreases afterwards. But again, pelagic Holocene sedimentation rates at the order of 8 cm/kyr seem rather unlikely, although not impossible.

GeoB 3397-1 (Fig. 85), the core from the lower slope of the Nazca Ridge (3453 m), shows a quite good correlation between sand content and number of *G. menardii*. Here it cannot be differentiated exactly if the double peak in *G. menardii* number in ~180 cm core depth belongs already to zone X or if it is still part of isotopic stage 3 (zone Y). GeoB 3402-2 (Fig. 88) also shows two peaks in *G. menardii* distribution within the upper 100 cm. In Fig. 88 a suggestion for the zonation is given. According to this the core reaches zone V (older than 185 kyr).

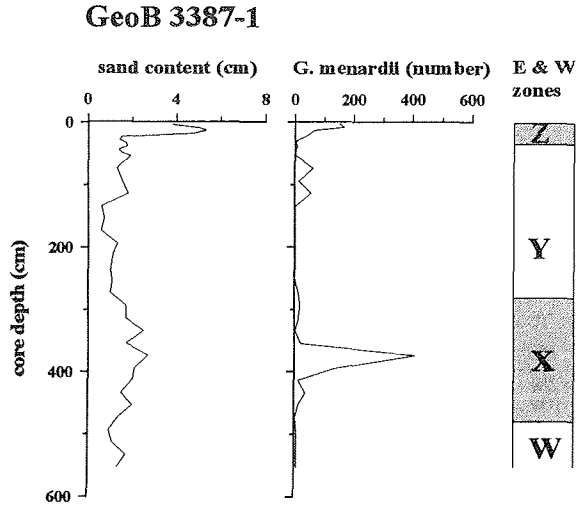

Abb. 75: Biostratigraphic analysis of Core GeoB 3387-1

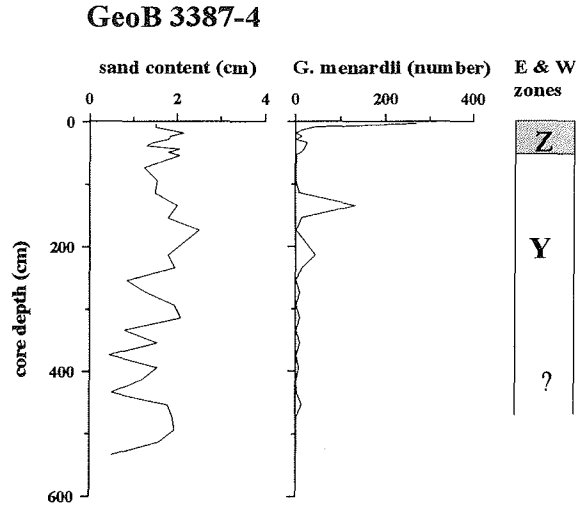

Abb. 76: Biostratigraphic analysis of Core GeoB 3387-4

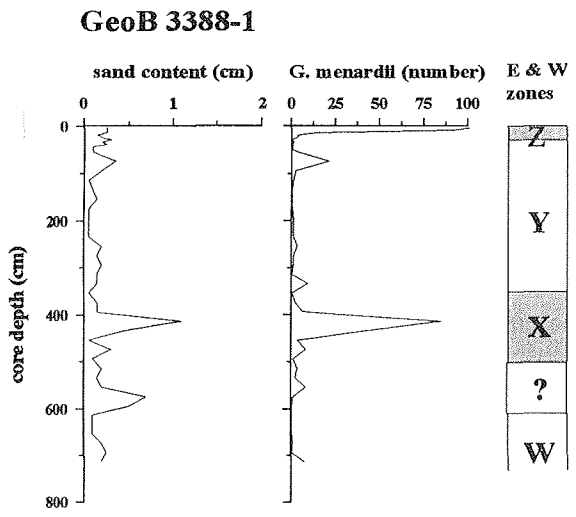

Abb. 77: Biostratigraphic analysis of Core GeoB 3388-1

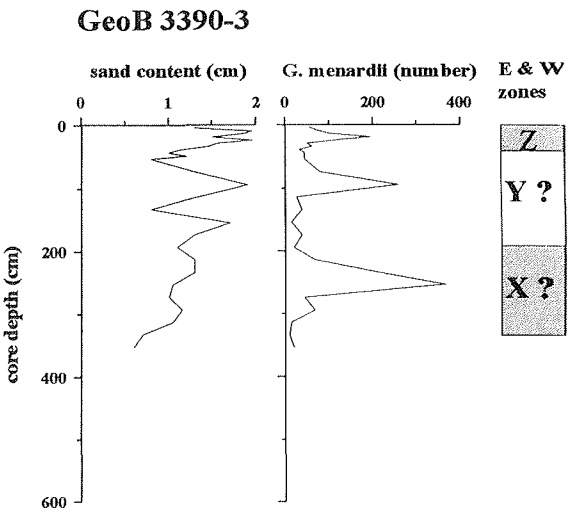

Abb. 78: Biostratigraphic analysis of Core GeoB 3390-3

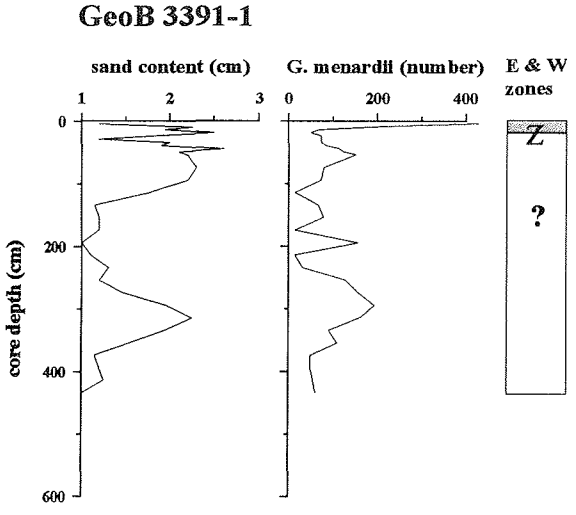

Abb. 79: Biostratigraphic analysis of Core GeoB 3391-1

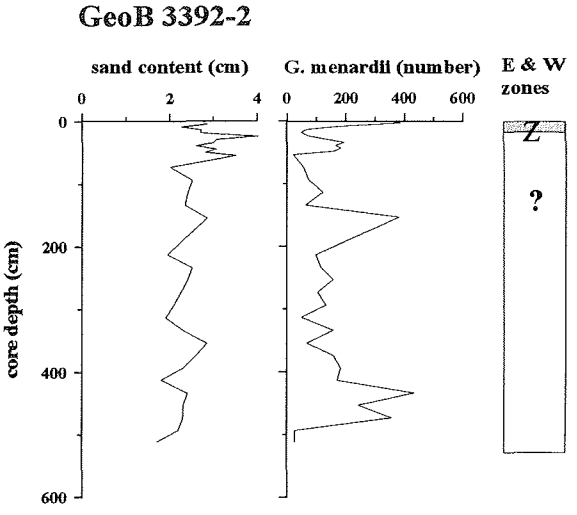

Abb. 80: Biostratigraphic analysis of Core GeoB 3392-2

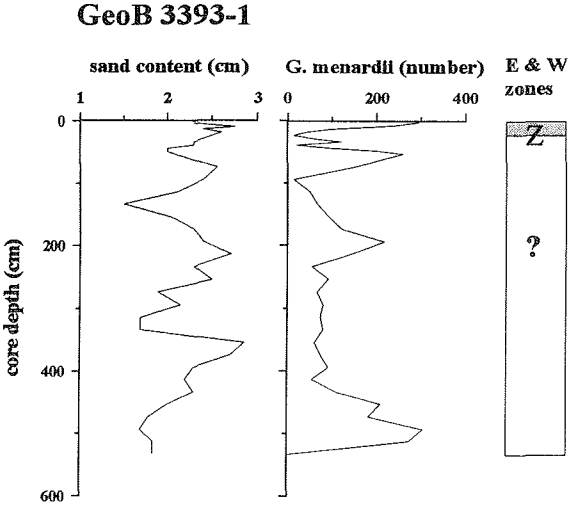

Abb. 81: Biostratigraphic analysis of Core GeoB 3393-1

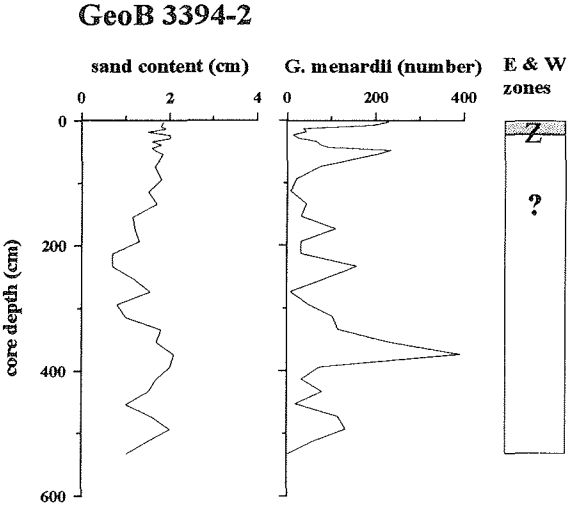

Abb. 82: Biostratigraphic analysis of Core GeoB 3394-2

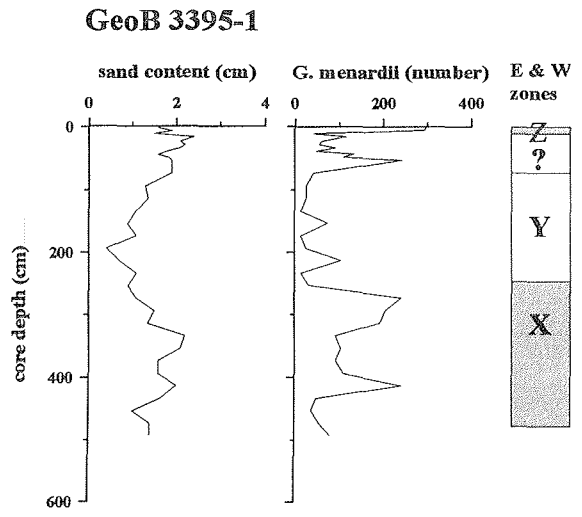

Abb. 83: Biostratigraphic analysis of Core GeoB 3395-1

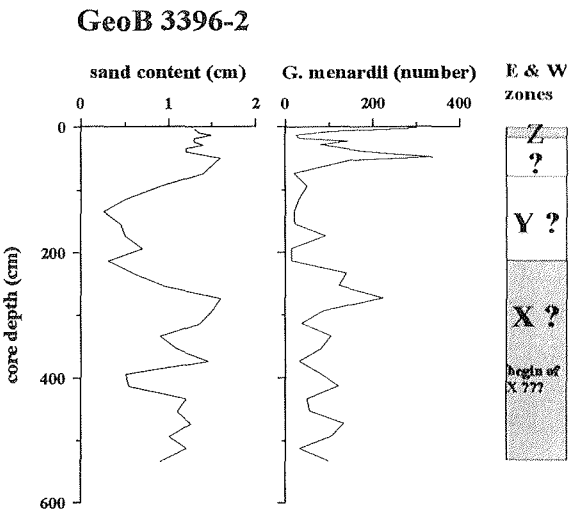

Abb. 84: Biostratigraphic analysis of Core GeoB 3396-2

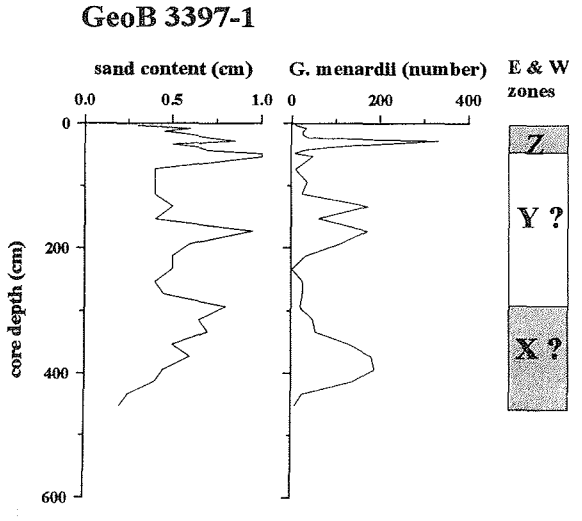

Abb. 85: Biostratigraphic analysis of Core GeoB 3397-1

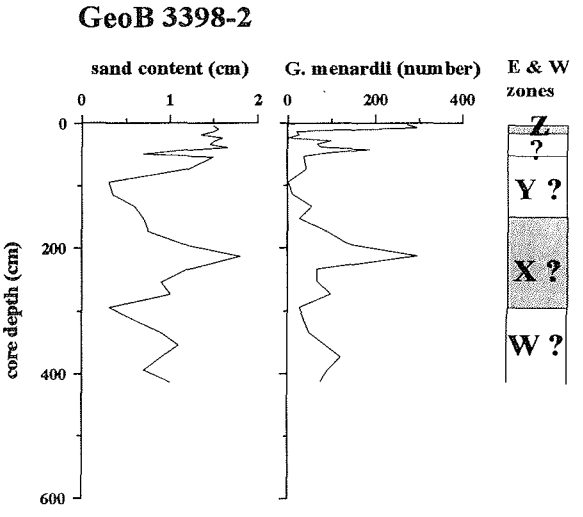

Abb. 86: Biostratigraphic analysis of Core GeoB 3398-2

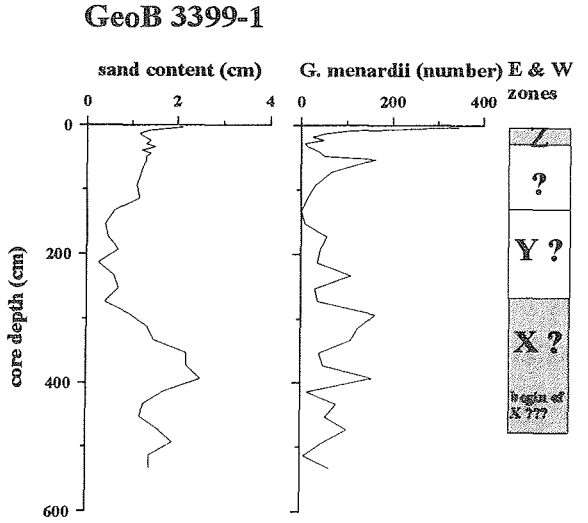

Abb. 87: Biostratigraphic analysis of Core GeoB 3399-1

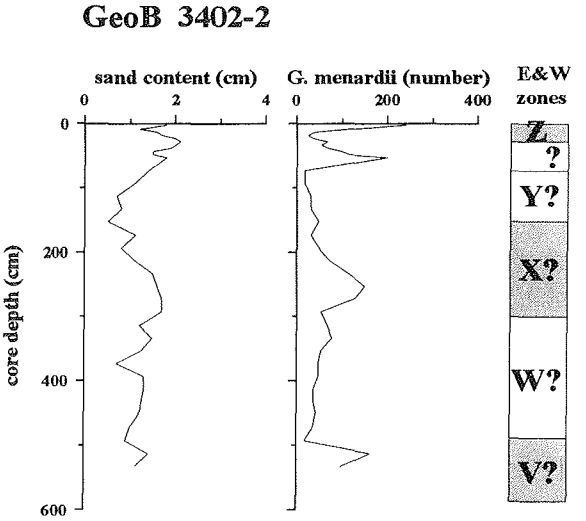

Abb. 88: Biostratigraphic analysis of Core GeoB 3402-2

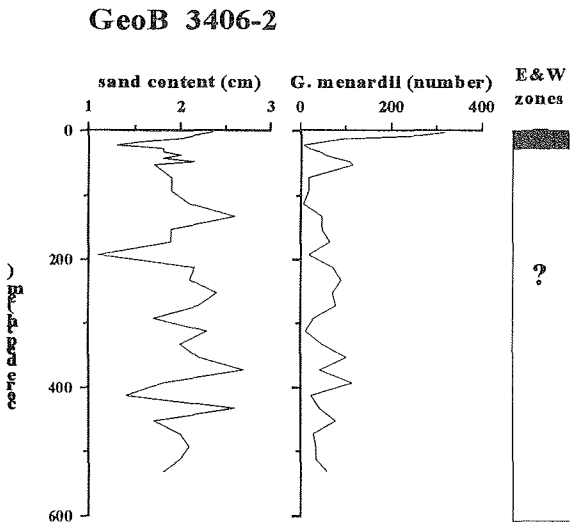

Abb. 89: Biostratigraphic analysis of Core GeoB 3406-2

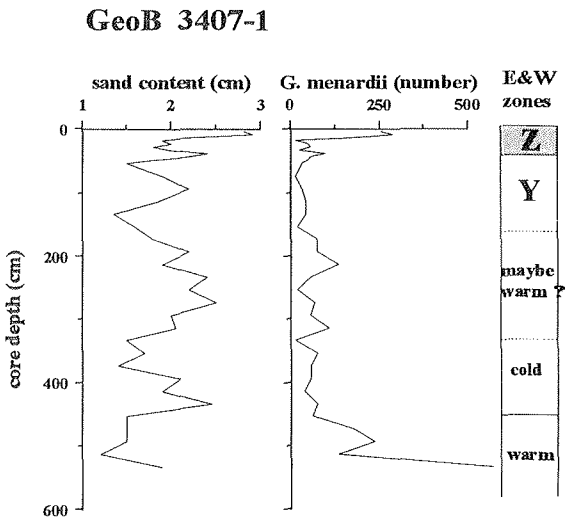

Abb. 90: Biostratigraphic analysis of Core GeoB 3407-1

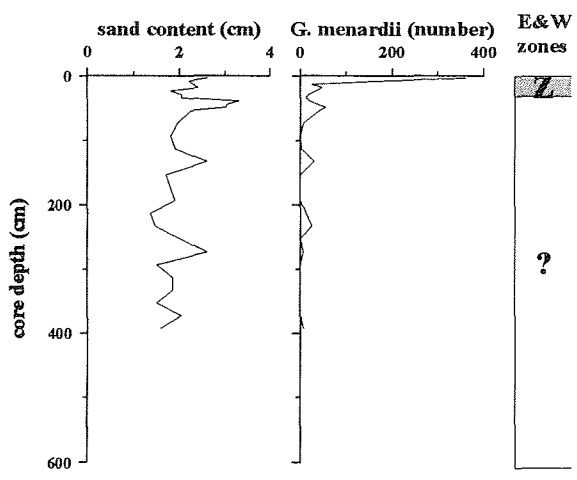

Abb. 91: Biostratigraphic analysis of Core GeoB 3409-1

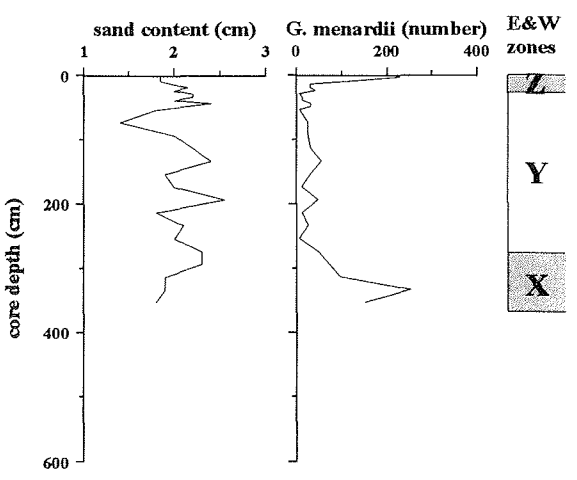

Abb. 92: Biostratigraphic analysis of Core GeoB 3410-2

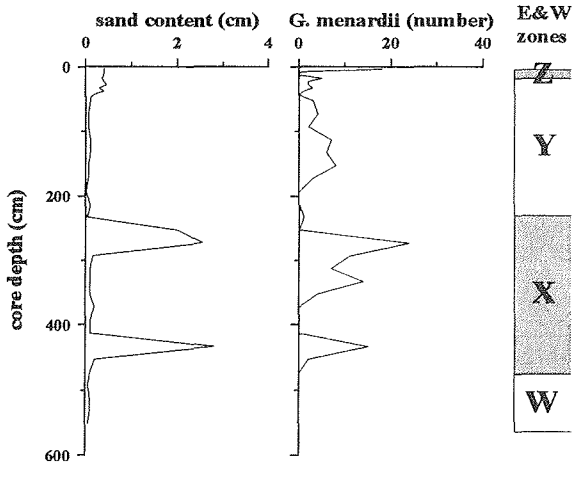

Abb. 93: Biostratigraphic analysis of Core GeoB 3414-2

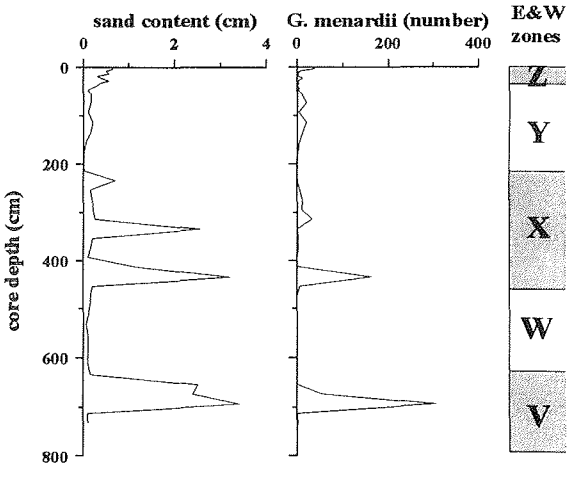

Abb. 94: Biostratigraphic analysis of Core GeoB 3414-4

Cores GeoB 3406-2 and 3407-1 (Fig. 89 and 90) are both located at the southwesternmost part of the Nazca Ridge at a water depth of ~2000 m. In both cores a second peak in the *G. menardii* distribution within the upper 100 cm is still to be seen but it is smaller in comparison to the above mentioned cores. In both cores only zone Z can clearly be distinguished.

In conclusion, it can be stated that all cores from Nazca Ridge do show problems in dating according to Ericson & Wollin. Striking is the nearly always appearing second peak (within the upper 100 core cm) in the *G. menardii* distribution which makes a clear zonation impossible. However, the *G. menardii* data seem to be a potential tool to correlate most of the cores to each other.

SEAMOUNT

GeoB 3409-1	length: 403 cm	WD: 2809 m	(Fig. 91)
GeoB 3410-2	length: 370 cm	WD: 1261 m	(Fig. 92)

GeoB 3409-1 and GeoB 3410-2, located at a seamount 150 nm south of the Nazca Ridge, do not show these difficulties. In GeoB 3409-1 (Fig. 91) from 2800 m water depth zone Z can clearly be picked. Further downcore the number of *G. menardii* is rather low indicating a zone Y age. In GeoB 3410-2 (Fig. 92) from 1260 m water depth it seems that zone X is reached (core bottom older than 70 kyr).

GeoB 3414-2	length: 576 cm	WD: 3744 m	(Fig. 93)
GeoB 3414-4	length: 750 cm	WD: 3744 m	(Fig. 94)

The cores GeoB 3414-2 and 3414-4 (Fig. 93 and 94) from 3744 m water depth are from the same site. Both cores show comparable results regarding the "sand content" and the amount of *G. menardii*. GeoB 3414-2 reaches zone W (older than 130 kyr), GeoB 3414-4 reaches probably zone V (older than 185 kyr). The sedimentation rate is ~3 cm/kyr.

4.8. Magnetic Susceptibility

(H. Petermann)

Magnetic volume susceptibility κ is defined by the equations:

$$B = \mu_0 \cdot \mu_r \cdot H = \mu_0 \cdot (1 + \kappa) \cdot H = \mu_0 \cdot H + \mu_0 \cdot \kappa \cdot H = B_0 + M$$

with the magnetic induction B, the absolute / relative permeability μ_0 / μ_r, the magnetizing field H, and the volume magnetization M. κ is a dimensionless quantity describing to what extend a material is magnetized by an external magnetic field.

In deep-sea sediments magnetic susceptibility values mainly reflects the concentration of the ferrimagnetic mineral fraction: (titano-) magnetites. Diamagnetic (calcite or opal) and paramagnetic contributions (mainly clay minerals) are of minor importance. In most cases susceptibility values in marine sediments may vary from $-15 \cdot 10^{-6}$ for sediments consisting of pure calcite or opal to a maximum of some $10.000 \cdot 10^{-6}$ for basaltic debris rich in (titano-) magnetite.

During this cruise magnetic susceptibility was measured on split cores using a commercial Bartington M.S.2 susceptibility meter with a spot sensor (F-sensor) positioned on the surface. Downcore logs were determined at centimeter intervals. therefore smoothing the core log slightly. Spatial resolution of the F-sensor is approximately 2 cm, far better than for the loop sensor M.S.2.C (8 cm) usually used on ship cruises. (Bleil et al., 1994). Changes in the sediment color correlated well with changes in the magnetic susceptibility. Color laminations thinner than 1 cm were not reproduced in the magnetic suceptibility record due to the restricted resolution of the F-sensor.

Values for the magnetic susceptibility were high on to the continental slope and continental rise off Chile (Cores 3313-1, 3315-1, 3316-4, 3317-1 and 3323-9) reaching several $1000 \cdot 10^{-6}$ SI (Fig. 95, 96). This might be attributed to the terrigeneous input from the Chilean coast. In core 3315-1 a rapid decrease in magnetic susceptibility with depth was measured, indicating reductive diagenesis of the ferrimagnetic mineral fraction in sulfidic environment. In the lower parts of this core H_2S could be smelled. Susceptibilities of the pelagic cores 3327-5 and 3336-2 are lower (still up to $1200 \cdot 10^{-6}$ SI), probably reflecting a reduced terrigenic input compared to the cores from the continental slope. The susceptibility log from cores 3313-1 and 3327-5 show similar variations with depth. As a first impression core 3313-1 covers the same time interval as the first 380-390 cm of core 3327-5.

Magnetic susceptibility and the spectral reflectance were compared for the core 3323-9 (Fig. 97). Both, susceptibility values and the reflectance ratio at different wave lengths were

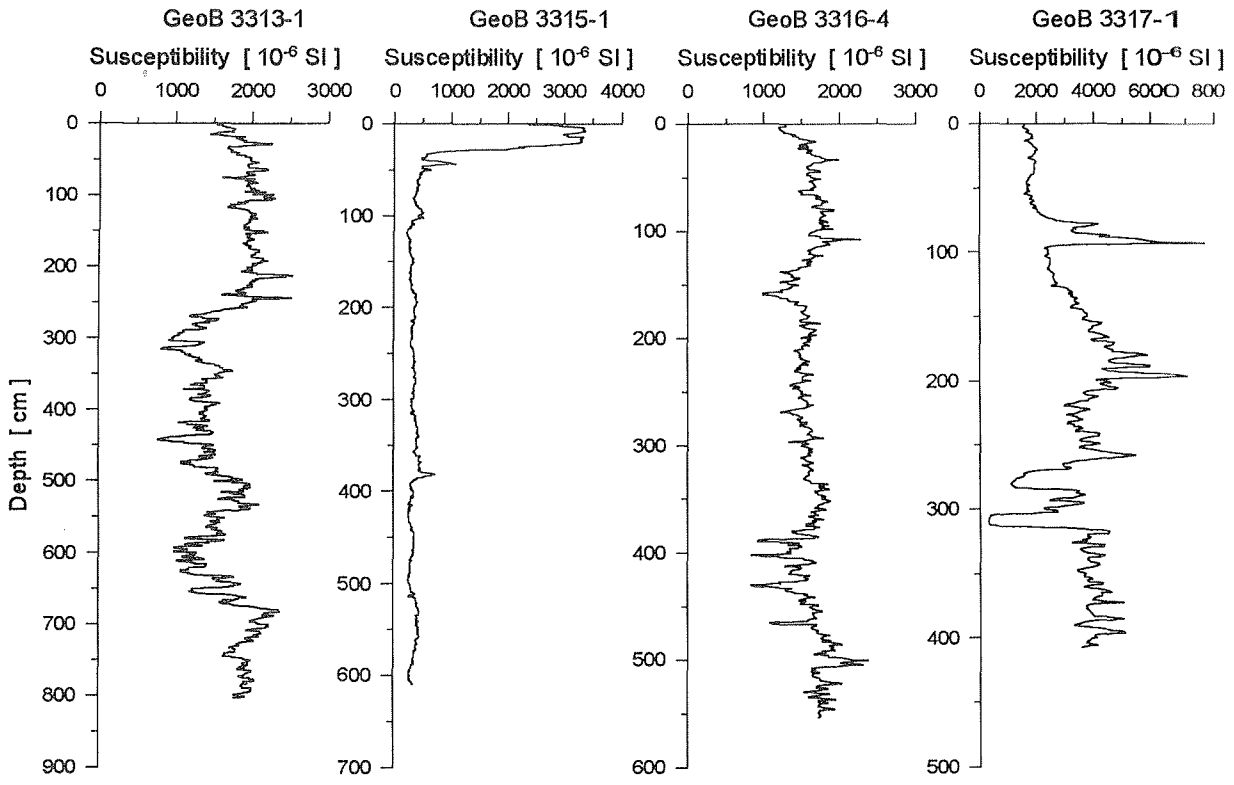

Fig. 95: Magnetic susceptibility logs for cores GeoB 3313-1, GeoB 3315-1, GeoB 3316-4 and GeoB 3317-1.

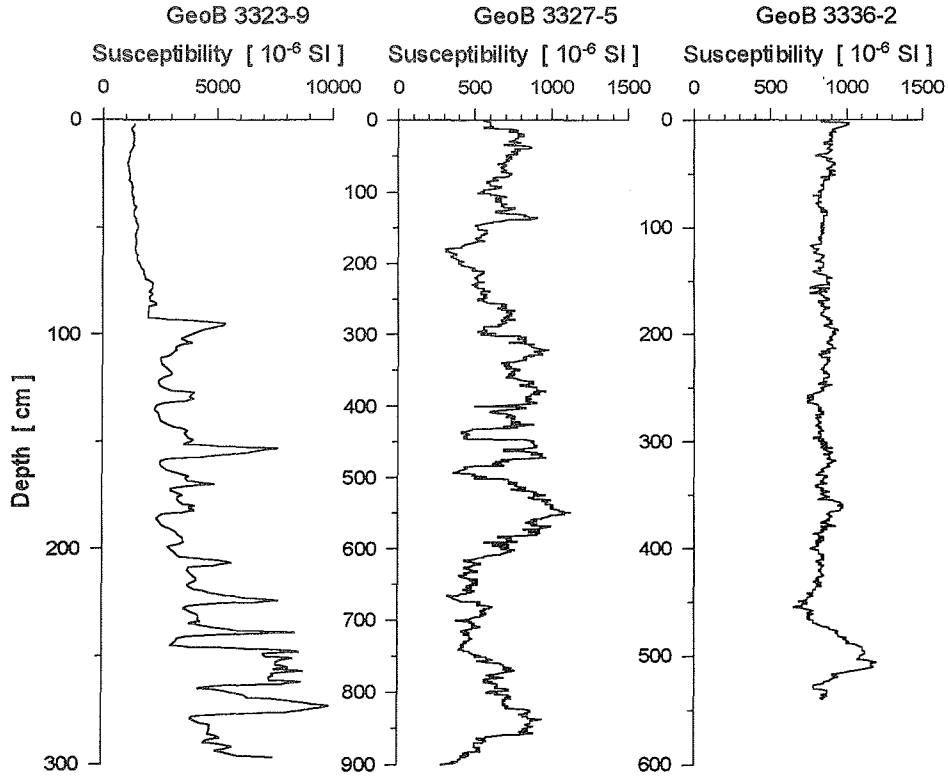

Fig. 96: Magnetic susceptibility logs for cores GeoB 3323-9, GeoB 3327-5 and GeoB 3336-2.

measured at centimeter intervals. Susceptibility was higher in sediments with a lower red/blue ratio. Susceptibility versus red/blue (700 nm/450 nm) ratio gave a correlation coefficient r = 0.8457. Using all 274 undisturbed measurements the correlation is significant on a significance level α of 0.0001.

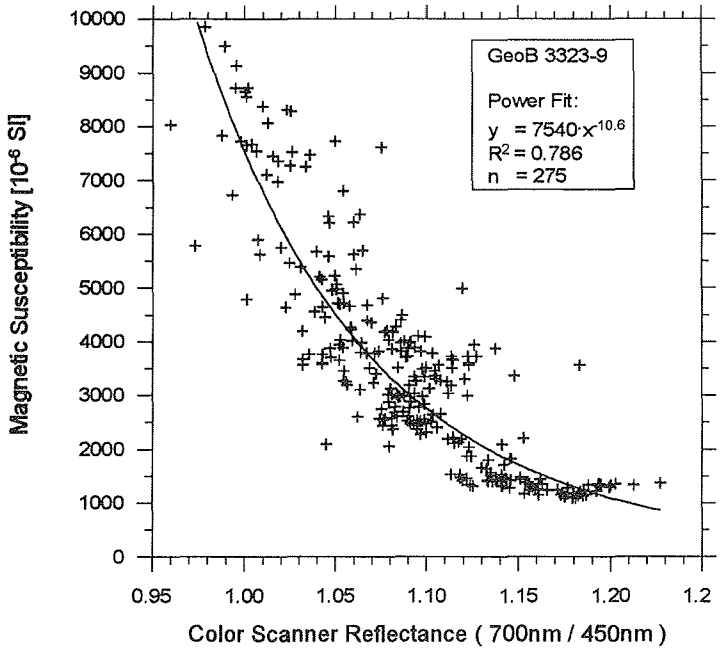

Fig. 97: Magnetic susceptibility as a function of the ratio of spectral reflectance (700 nm / 450 nm) measured with the colour scanner.

4.9. Porewater Chemistry

(R. Haese and C. Hensen)

The geochemical studies during the Sonne cruise SO 102 focus mainly on the

- Determination of diffusive fluxes and geochemical processes at the sediment/water interface in order to characterize and to quantify early diagenetic mineralization processes.
- Determination of pore water concentration profiles in the sedimentary sequence to study the influence of early diagenetic processes on the preservation or overprinting of paleoclimatic signals and geophysical properties.

Experimental Methods - To prevent a warming of the sediments all cores were immediately placed in a cooling room after recovery and maintained at a temperature of 4°C. The gravity cores were first cut into segments of 1 m length and processed in the course of the following days. All work carried out on opened cores were carried out in a glove box under argon atmosphere. The multicorers were processed within a few hours after recovery. The overlying bot-

tom water of the multicorers was carefully removed with help of a siphon to avoid destruction of the sediment surface. During the subsequent cutting of the core into slices for pressure filtration, pH and Eh measurements were performed at a resolution of 0.5 cm. On a second, parallel multicorer tube conductivity and temperature were measured to calculate sediment density and porosity.To get a better understanding of biogeochemical effects induced by warming and decompression parallel multicorer cores were kept under different conditions: Either the pH, oxygen concentration, temperature and water flow were kept constant according to bottom water (in situ) conditions or the multicorer core was stored in the cooling room while simulating a bottom water flow by a pump and tubing system.

The gravity cores were cut lengthwise. On the work-halves pH and Eh were determined and sediment samples were taken for pressure filtration. Conductivity and temperature were measured on the archive halves. Samples for sequential extractions of the solid phase were kept in glas bottles under argon atmosphere. For pressure filtration Teflon- and PE-squeezers were used. The squeezers were operated with argon at a pressure gradually increasing up to 5 bar. Depending on the porosity and compressibility of the sediments, up to 20 ml of pore water were recieved from each sample. The pore water was retrieved through 0.2 µm cellulose acetate membrane filters.

The following parameters were measured on board: pH, Eh, conductivity, temperature, NO_3^-, NH_4^+, PO_4^{3-} and alkalinity. pH and Eh values were determined with electrodes before the sediment structure was disturbed by sampling for pressure filtration. NO_3^-, NH_4^+ and PO_4^{3-}.were measured photometrically with help of an autoanalyser using standard methods. Alkalinity was calculated from a volumetric analysis by tritration of 1 ml sample with HCl down to a pH value of 3.6. For later analysis of Fe^{2+}-concentrations subsamples of 2 ml were taken in the glove box and immediately conserved with 25 µl H_2SO_4 (1:4). Samples for SO_4^{2-} and Cl^- were diluted and will be analysed by ion chromatography (HPLC) at Bremen University.The remaining pore water samples were acidified with HNO_3-(suprapure) down to a pH value of 2 for the subsequent determination of cations by ICP and/or AAS. All pore water samples are maintained at 4°C until further treatment in Bremen.

Shipboard Results - Along a transect down the continental slope off Chile at about 41°S six multicorers and two gravity corers were analysed geochemically. The results are displayed in Fig. 98-105. The multicorer cores were cut into 0.5 cm thick slices within the first 3 cm and 1

GeoB 3312-2 (MUC)

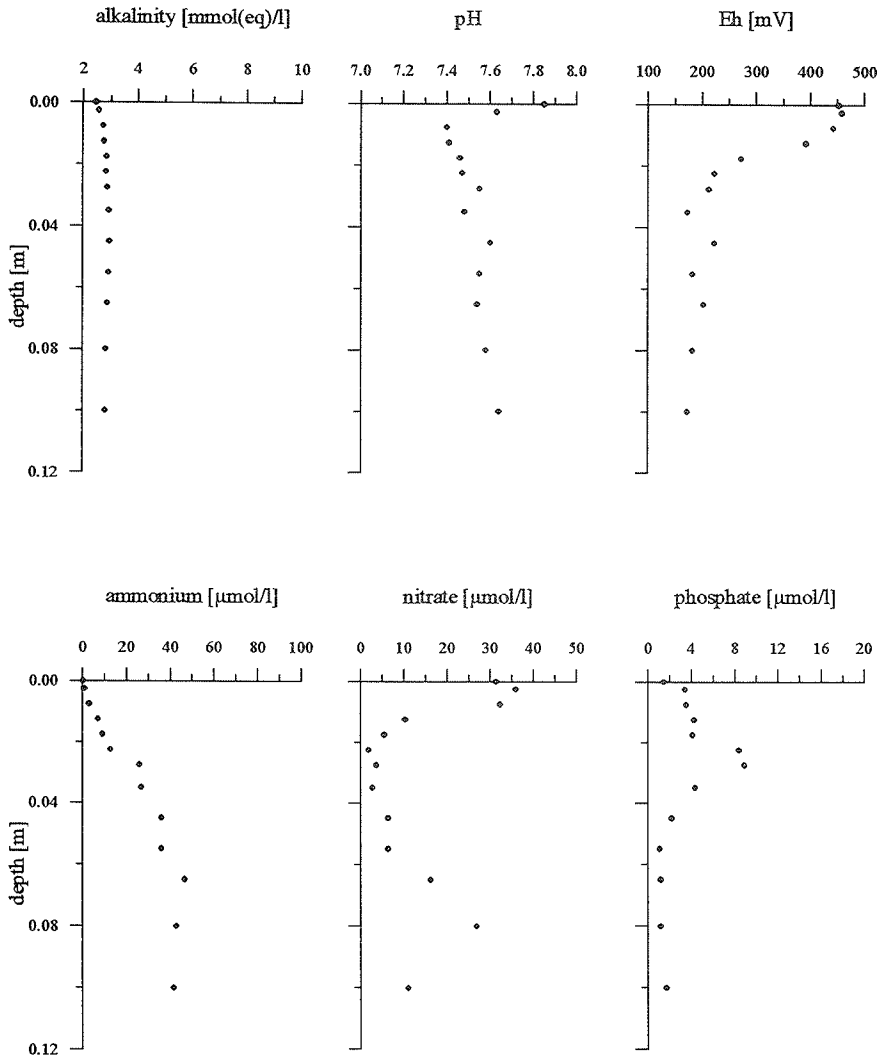

Fig. 98: Results of the porewater analyses of MUC-Core GeoB 3312-2

GeoB 3313-3 (MUC)

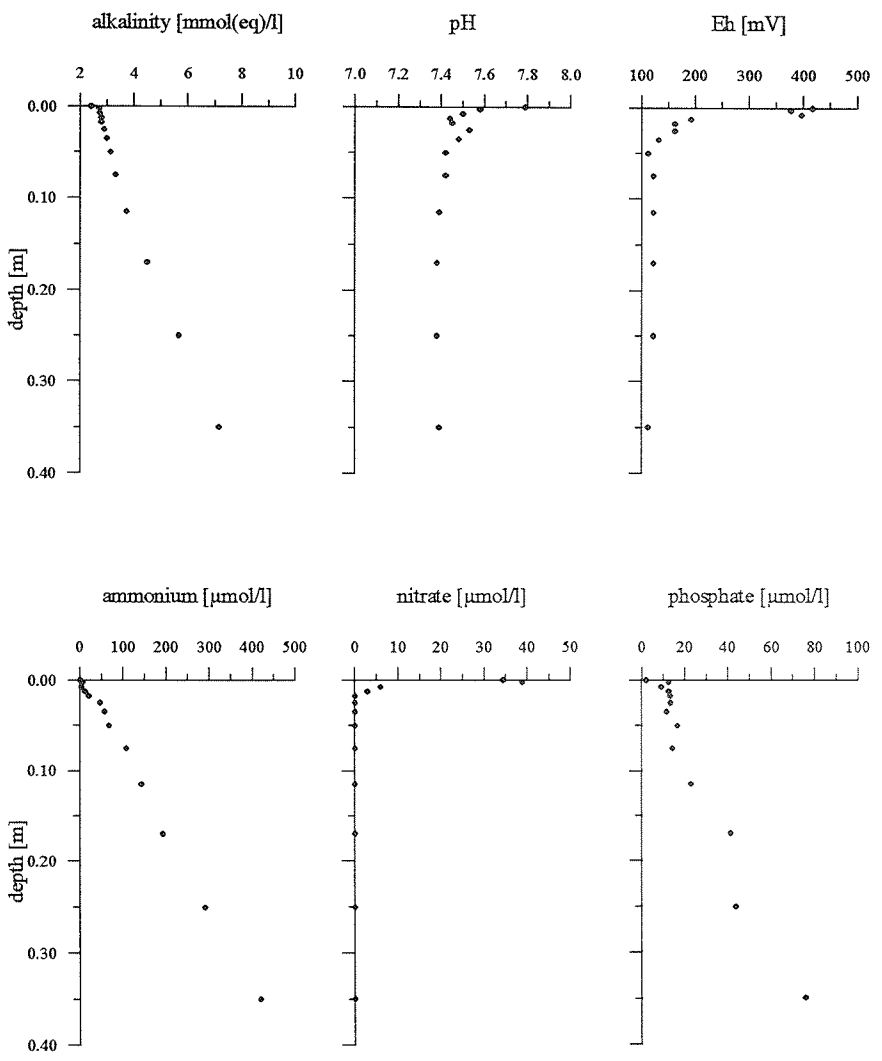

Fig. 99: Results of porewater analyses of MUC-Core GeoB 3313-3

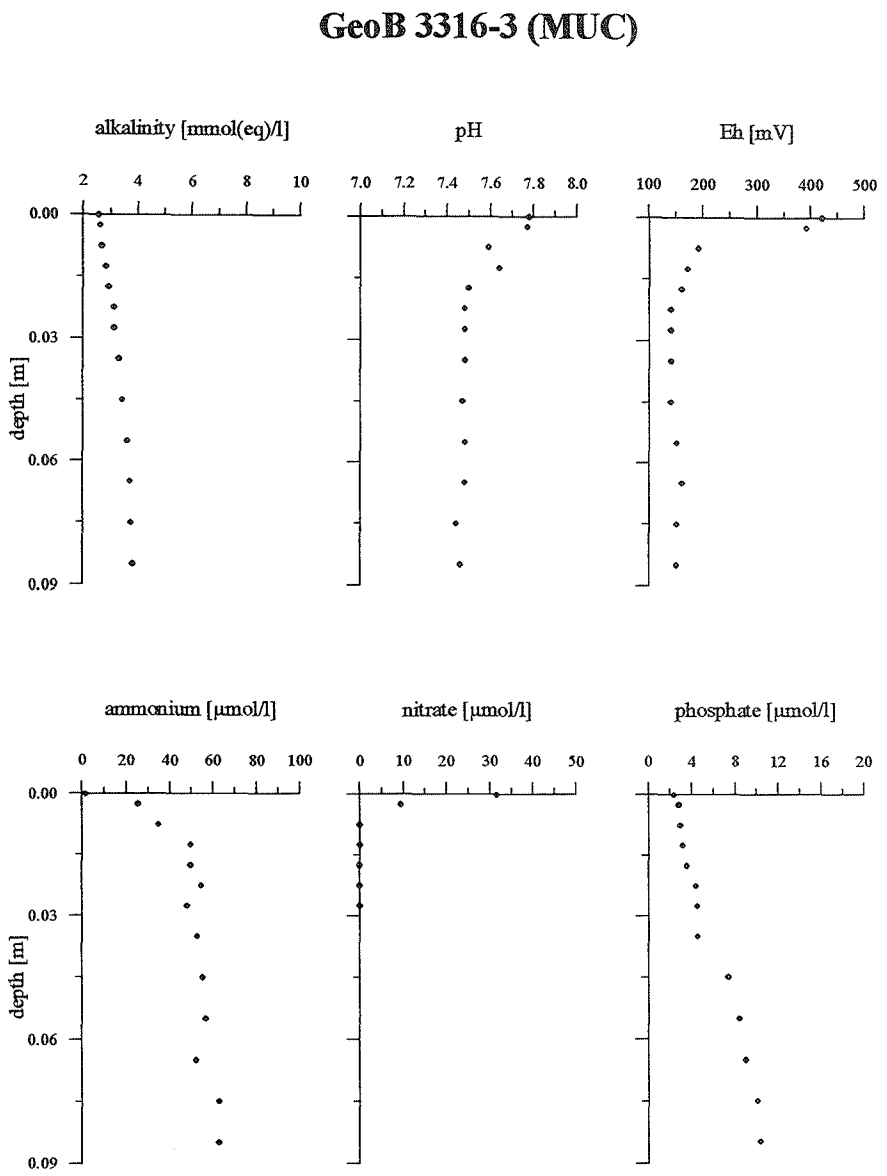

Fig. 100: Results of the porewater analyses of MUC-Core GeoB 3316-3

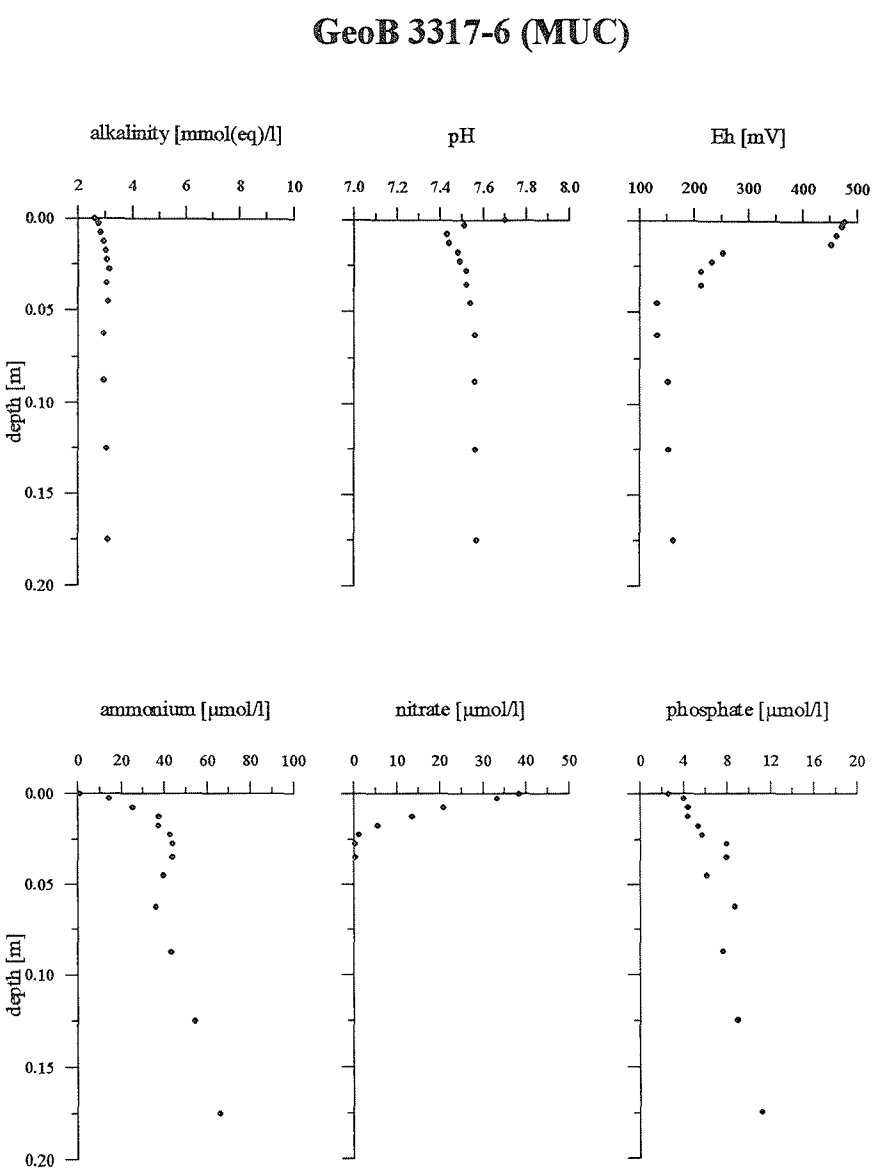

Fig. 101: Results of the porewater analyses of MUC-Core GeoB 3317-6

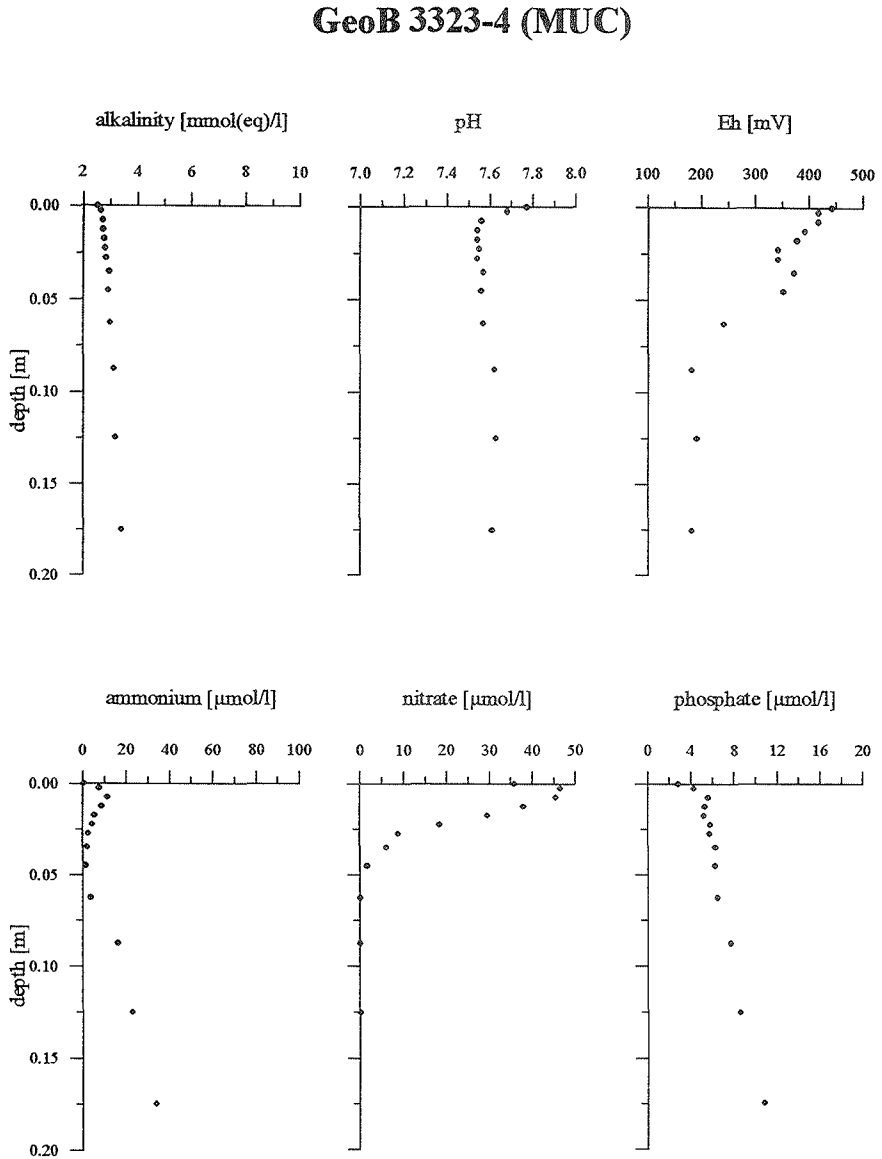

Fig. 102: Results of the porewater analyses of MUC-Core GeoB 3323-4

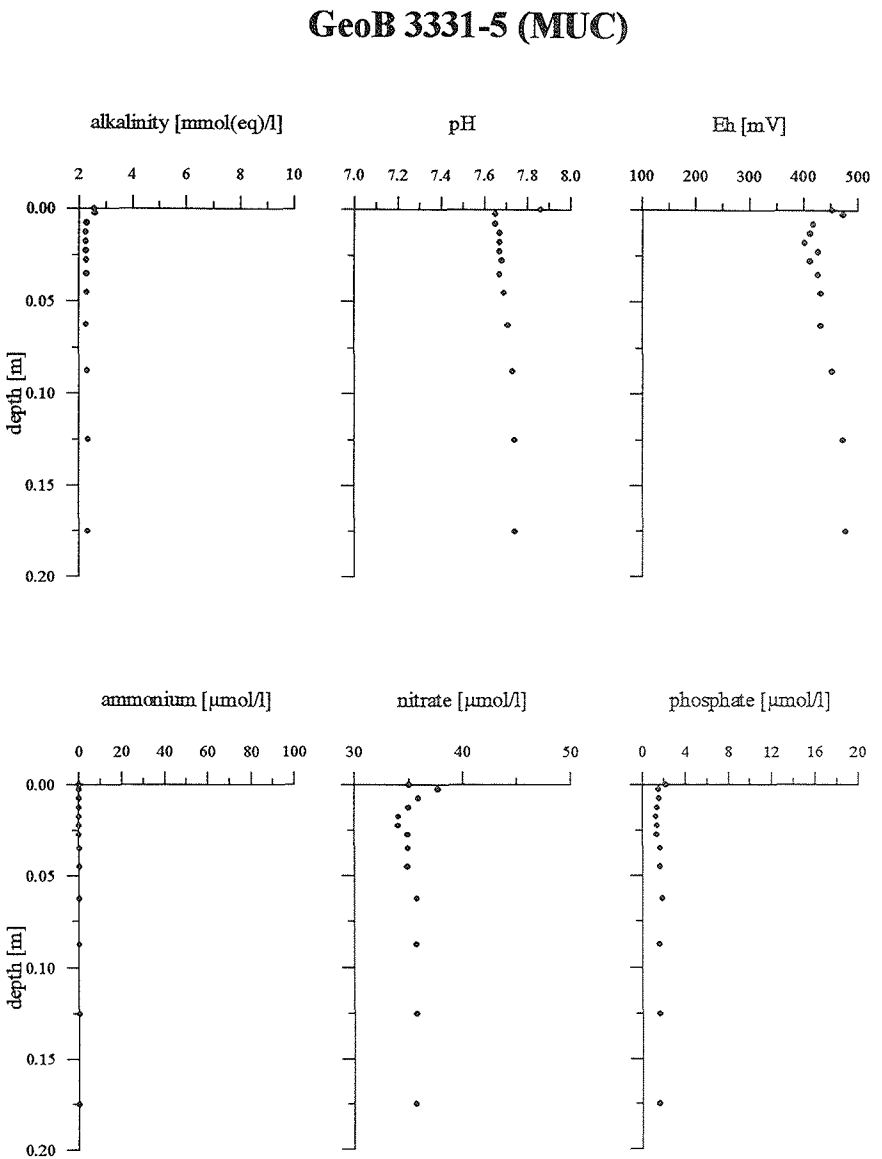

Fig. 103: Results of the porewater analyses of MUC-Core GeoB 3331-5

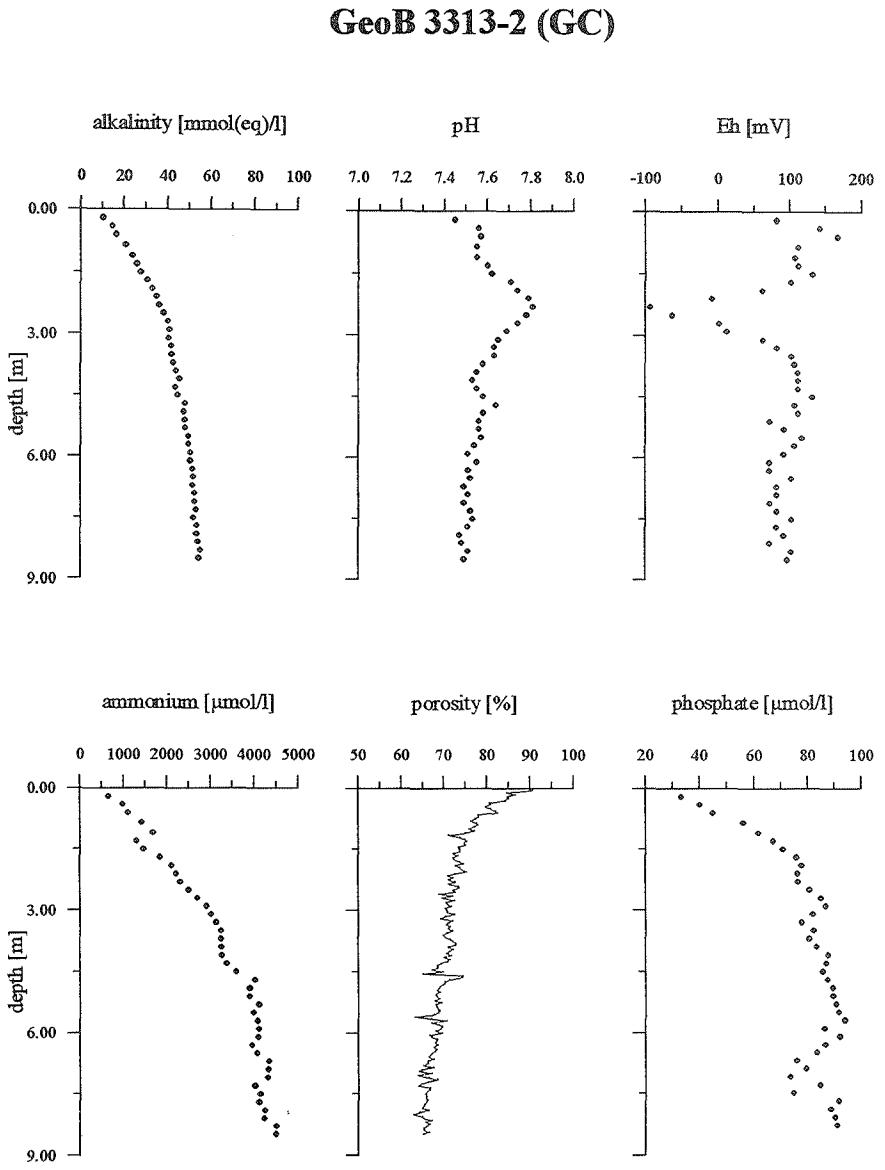

Fig. 104: Results of the porewater analyses of GC-Core GeoB 3313-2

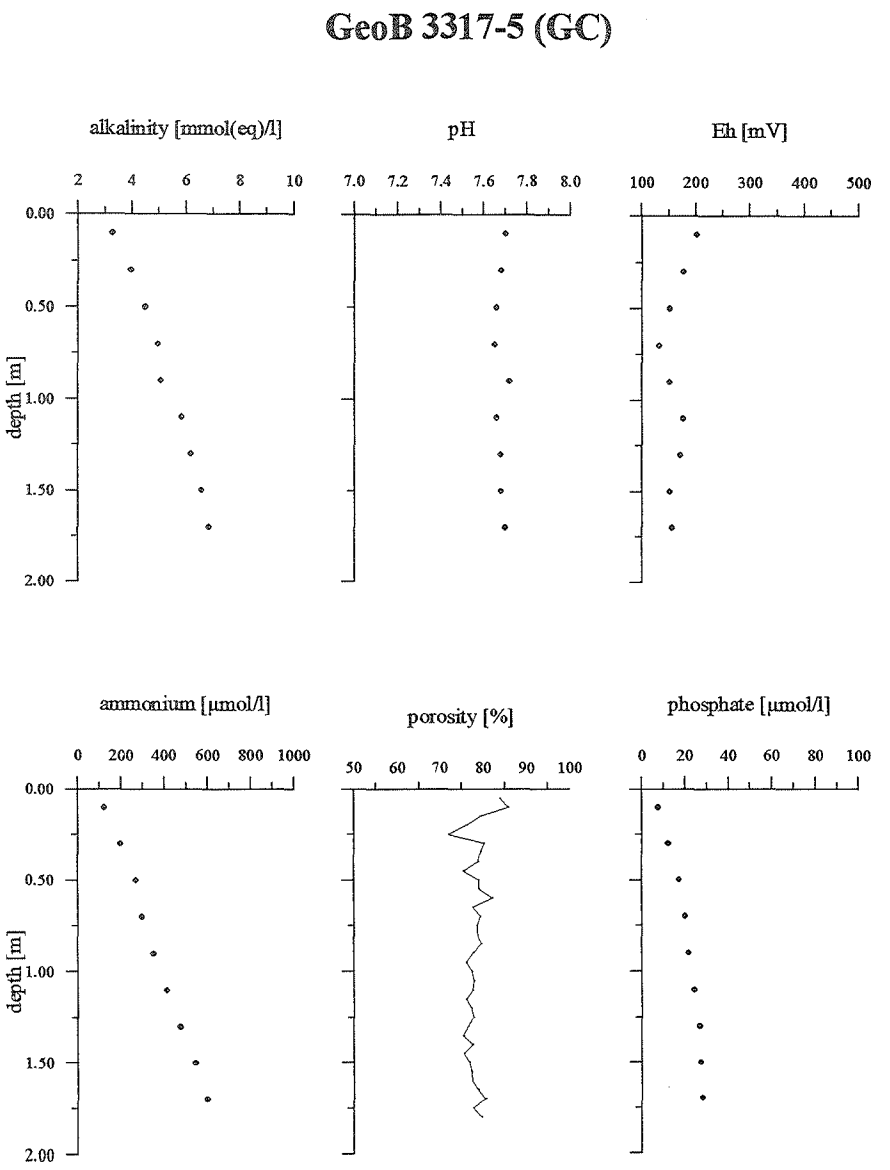

Fig. 105: Results of the porewater analyses of GC-Core GeoB 3317-5

to 5 cm thick slices with increasing depth for pore water squeezing. The gravity cores were sampled at 20 cm intervals for both pore water and solid phase analysis. The release of mineralization products within the upper centimeters generally increase with decreasing water depth (between 3700 and 850 m). At 580 m water depth (GeoB 3312-2) the activity again is strongly reduced.

Nitrate concentrations in the uppermost sediment layers and the overstanding bottom water range between 30-50 µmol/l at all stations. Nitrate build up by oxygen respiration and nitrate penetration depth turn out to be the most sensitive indicator for the intensity of near surface dissimilation processes next to oxygen. At station GeoB 3313-3 (850 m water depth) nitrate diminishes at 1 cm whereas at GeoB 3323-4 nitrate can be found to a depth of 7 cm. At stations where nitrate build up is well recorded one can observe a pH minimum. This is due to a release of protons (H^+) during oxygen respiration lowering the pH. At all stations a distinctive decrease of the redox potential (Eh) is appearened within the uppermost sediment. It correlates with the decrease of nitrate concentration. One can find that the higher the gradient of nitrate decrease the lower the Eh. Therefore, nitrate consumption drives the redox potential (Eh).

In non - sulfidic environments HCO_3^- is the master species (neglecting organic acids) and therefore it can be related to the amount of alkalinity. As organic matter mainly consits of C, N and P, products of early diagenesis are HCO_3^-, NH_4^+ and PO_4^{3-}. Concentration gradients of these components generally show a linear decrease towards the sediment surface. This indicates a release at greater depth and an upwards diffusive transport. As sulfate reduction is not indicated in these surface sediments by H_2S smell or black strikes or patches of FeS / pyrite, we assume sulfate reduction at greater depth deliberating HCO_3^-, NH_4^+ and PO_4^{3-}. Ammonium turns out to be the most sensitive product of early diagenetic products. At station GeoB 3317-7 a build up of ammonium reflects nitrate dissimilation and at station GeoB 3323-4 oxygen respiration.

Pore water chemistry of gravity cores (GC) reflect early diagenesic processes at greater depth. As could be deduced from multicorer results, station GeoB 3313 shows higher early diagenetic reactivity as GeoB 3317. This can also be seen by comparison of gravity core results. Alkalinity and ammonium are about 5 times higher and phosphate is about 3 times higher in concentration at station GeoB 3313-2 than at station Geo 3317-5. At station GeoB 3313-2 all parameters show a distinctive change at 2.5 meters. A source of early diagenetic products

(alkalinity, ammonium and phosphate) is indicated along with a minimum of Eh and a maximum of pH. These changes strongly indicate an intense sulfate reduction zone, especially as sulfide could be smelled and black patches of FeS / pyrite were observed below. It is striking that at this depth a strong decrease of magnetic susceptibility was measured which suggests a present day reduction of ironoxides such as magnetite by sulfide. Further solid phase investigations will be conducted at this core to estimate the availability of 'reactive' iron(hydr)oxides for microbial dissismilation in near surface sediments in contrast to the availablity towards reduction by sulfide at greater depth.

4.10. Magnetotactic and Extracellularly Magnetite Producing Bacteria

(H. Petermann)

Introduction - Magnetotactic bacteria synthesize intracellularly magnetite particles of distinct morphologies and in a narrow size distribution. These particles are called magnetosomes (Balkwill et al., 1980). Their formation is controlled by a membrane that surrounds the magnetosomes. Magnetotactic bacteria live in the sediment within a well defined near surface layer.

The biological advantage of intracellular magnetite formation is not yet satisfactorily understood. A possible explanation is that magnetotactic bacteria use their magnetosomes for orientation in the Earth's magnetic field. When displaced from their adequate environment in the sediment, they can swim back along a straight line parallel to the Earth's magnetic field. Magnetotactic bacteria from the northern hemisphere preferably swim towards the north, magnetotactic bacteria from the southern hemisphere swim to the south. In both cases they swim down to the sediment. After lysis of the organic parts of the bacteria, magnetosomes are preserved in many sediments and contribute to a variable degree to the remanent magnetization. Due to their specific magnetic properties, they are excellent recorders of the palaeomagnetic signal.

Sampling - Duing the cruise surface sediment samples recovered with the of multiple corer at 17 sites were investigated for living magnetotactic bacteria (Tab. 3). For each core depth profiles were taken with a piston pipette, that allows to sample individual layers. When the pipette is sticked through the sediment surface to a chosen depth, the piston prevents collecting particles from higher layers.

Investigation technique - During earlier expeditions it turned out, that magnetotactic bacteria from deep-sea sediments are rather sensitive to warming in the laboratory. In order to attain quantitative estimates of the number of magnetotactic bacteria, the samples were therefore kept cool during each step of investigation. After retrieval on board the cores were immediately stored in a refrigerator. Measurements indicated that temperature in the core never was higher than 8 - 10 °C, in most cases maximum temperature was below 8°C.

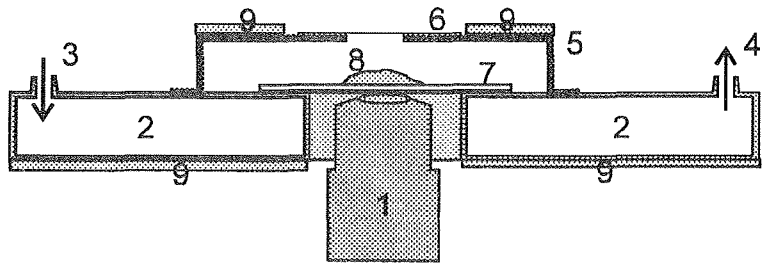

Fig. 106: Cooling device of the microscope: 1 Objective, 2 object-table with chambers for cooling water, 3 water inlet, 4 water outlet, 5 metalic lid, 6 glass slide, 7 microscope slide, 8 sediment suspension, 9 thermal insulation

Microscopic observations were done in a room kept at about 14.6-15.5°C. Additionally the specimen slide was cooled by pumping iced water through the microscope table. To prevent warming of the samples by advection of warmer air from the laboratory an insulated metal lid with a glass cover was installed over the microscope slide. Fig. 106 shows a sketch of the cooling device. Preliminary measurements suggest that the temperature in the speciman was never higher than 7°C during observation.

During the cruise living magnetotactic bacteria were investigated using a specially equipped inverse microscope. Three pairs of orthogonal coils cancel the Earth's magnetic field and provide a homogeneous magnetic field $< 3 \cdot 10^{-4}$ T of adjustable direction. Magnetotactic bacteria can be identified by their swimming behaviour parallel to the magnetic field. Bacteria that follow repeated changes of the field direction can definitely be distinguished from nonmagnetic bacteria. 50 µl of sediment suspension (from a defined depth) are placed to the microscope slide. Depending on the water content, a fringe of water of variable extend forms around the sediment. Magnetotactic bacteria swim parallel to the direction of the applied magnetic field until they reach the edge of the drop where they are counted. Important observations are recorded on videotape.

Results - Magnetotactic bacteria could be detected at 12 of 17 sampling sites. A summary of the results including geographical position, water depth, maximum number of magnetotactic bacteria in 50 µl and the depth of highest concentration is given in Tab. 3.

Highest concentrations of magnetotactic bacteria were found in sediments from the upper continental slope off Chile. Their actual numbers drastically decreased with increasing distance from the coast. No living magnetotactic bacteria could be observed in pelagic sediments West of 78°W. The geographic distribution of the samples with a classification of the respective numbers of magnetotactic bacteria is shown in Fig. 107.

From Fig. 107 and Tab. 3 it is obvious, that the number of counted magnetic bacteria decreases with increasing water depth at the sampling site. In Figure 3XX the maximum concentrations of magnetotactic bacteria at each site is plotted as a function of water depth. On the southern profile across the continental margin at 41°/43° S counted numbers are lower in sediments of similar water depths than on the northern profile at 35° S.

Depth profiles of magnetotactic bacteria - At every site the depth distribution of the magnetotactic bacteria in the sediment was determined. They live close to the sediment-surface, with

Table 3: Sampling sites, maximum numbers of magnetotactic bacteria in 50 µl of sediment and depth of maximum abundance of magnetotactic bacteria.

Station	Latitude	Longitude	Water depth [m]	Max. number of magnetotactic bacteria	Depth of max. abundance [cm]
GeoB 3312-2	41°00.5'S	74°20.2'W	584	500	2
GeoB 3313-3	41°00.0'S	74°27.0'W	851	150	2
GeoB 3314-2	41°36.2'S	74°58.8'W	1652	250	3
GeoB 3316-3	41°56.3'S	75°12.8'W	2575	1	1
GeoB 3317-6	42°00.8'S	75°18.1'W	2923	10	2
GeoB 3323-5	43°13.1'S	75°57.0'W	3702	2	0.2
GeoB 3327-6	43°14.4'S	79°59.5'W	3535	0	–
GeoB 3331-5	43°13.4'S	86°00.0'W	3741	0	–
GeoB 3336-3	35°30.0'S	88°00.0'W	3995	0	–
GeoB 3337-5	35°15.1'S	86°00.6'W	4073	0	–
GeoB 3339-2	35°15.0'S	83°29.3'W	3792	0	–
GeoB 3349-4	35°15.1'S	73°25.2'W	2471	1000	2
GeoB 3352-2	35°13.0'S	73°19.0'W	2108	600	1
GeoB 3353-1	35°15.0'S	73°34.6'W	3749	80	2
GeoB 3355-4	35°13.1'S	73°07.0'W	1511	1500	1
GeoB 3359-1	35°13.0'S	72°48.5'W	680	800	1
GeoB 3360-1	35°13.0'S	72°45.6'W	586	7000	1

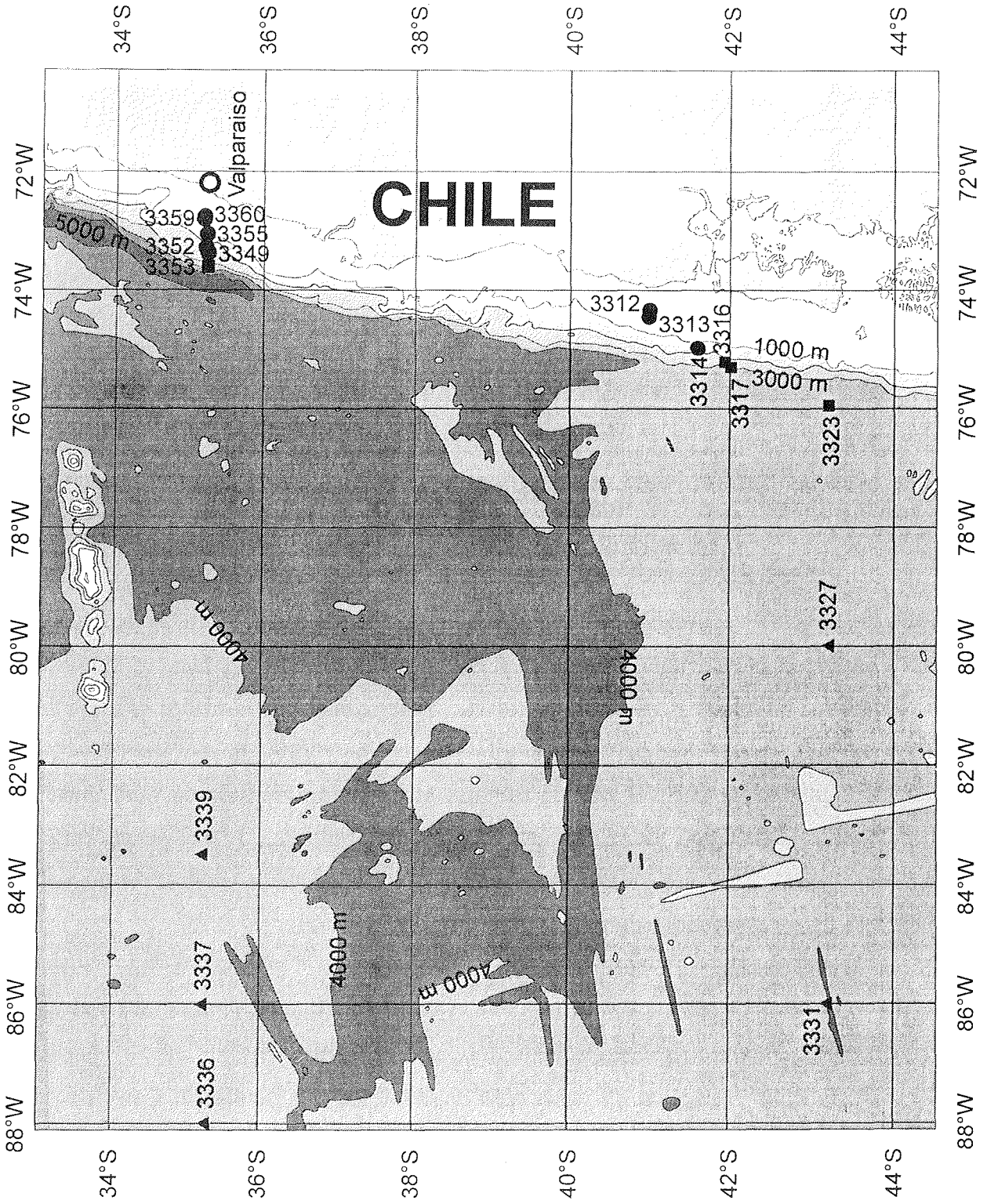

Fig. 107: Map of the sampling sites for magnetotactic bacteria. Dots denote sites with maximum concentrations of more than 100 magnetotactic bacteria, filled squares sites with maximum concentrations between 1 and 100 in a sample of 50 µl. Filled triangles mark sites where no actively swimming magnetotactic bacteria could be detected.

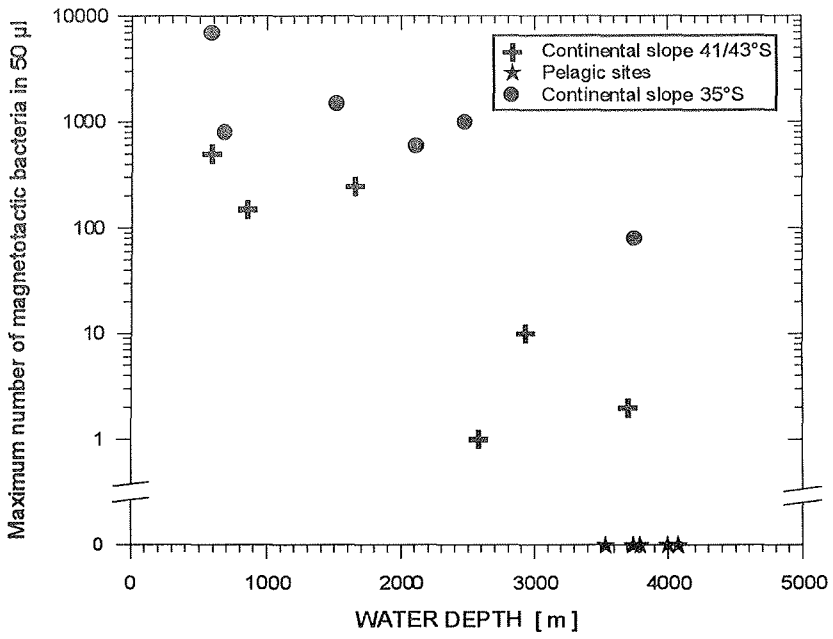

Fig. 108: Maximum concentrations of magnetotactic bacteria as a function of water depth at the sampling sites. Different symbols denote the southern continental slope at 41°/43°S (GeoB 3312 - 3323), the continental slope at 35°S (GeoB 3349 - 3360) and pelagic sites (GeoB 3327 - 3337).

the depth of the highest concentration varying between 0.1 and 3 cm (see Tab. 3). No actively swimming magnetotactic bacteria were found in layers deeper than 10 cm. Fig. 109 shows the depth profiles for six stations, where magnetotactic bacteria could be identified in more than one depth interval. Also plotted are the depth profiles of nitrate in the pore-water (data from Haese & Hensen, Chapter 4.9). Maximum numbers of magnetotactic bacteria were found in the denitrification zone below the maximum concentration of nitrate. Oxygen penetrates into the sediment to about the depth of maximum nitrate concentration. Thus, most of the magnetotactic bacteria live in anaerobic sediments.

Samples from the sites GeoB 3312 and GeoB 3313 were kept in the refrigerator for two weeks and the depth distribution of magnetotactic bacteria was controlled several times. It remained constant with time indicating that the majority of magnetic bacteria permanently dwells in the anoxic zone.

Morphologies of magnetotactic bacteria - Different morphologies of magnetotactic bacteria could be recognized in the light-microscope. Coccoid bacteria were found in highest numbers, but spirilla and rod-shaped bacteria were also identified.

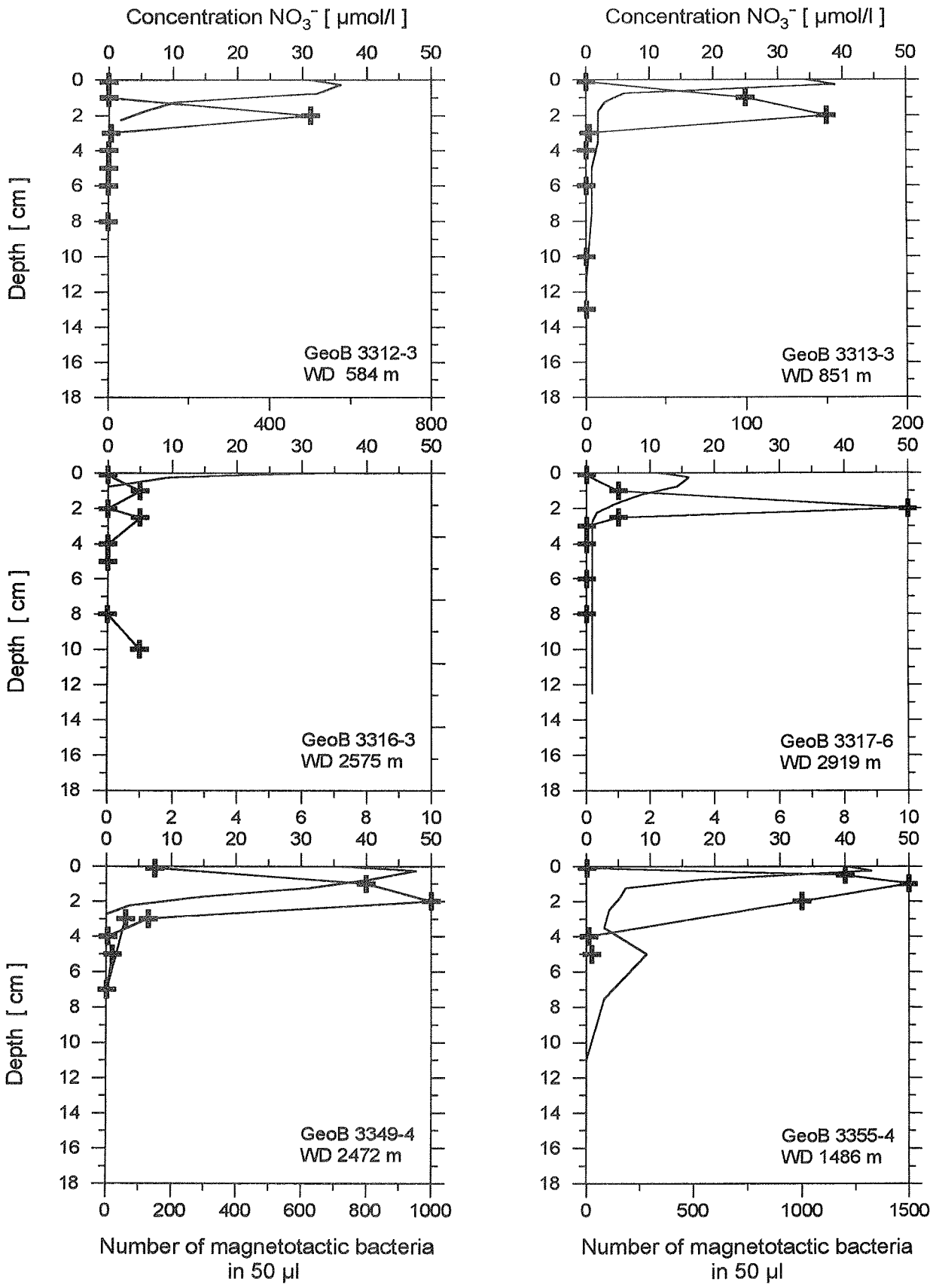

Fig. 109: Depth profiles of magnetotactic bacteria (solid line with symbols) and of nitrate (solid line) measured in the pore-water (data from Haese & Hensen, Chapter 4.9.) for six stations. The names of the stations and the respective water depths are noted in each plot.

In Core 3349-4 characteristic morphological forms occured in subsequent strata of the sediment column. At a depth of one centimeter a population of magnetic spirilla dominated. One centimeter below very rapid moving cocci (>100µm/s) that typically had three highly light-refracting dots occurred in greatest abundance. Between three and five centimeters depth a big coccus with two spots, similar to *Bilophococcus magnetotacticus* (Moench, 1988) predominated. A sketch of these morphologies in given in Fig. 110. A similar but less unequivocal distribution of different morphologies of magnetotactic bacteria with depth was observed at several other stations.

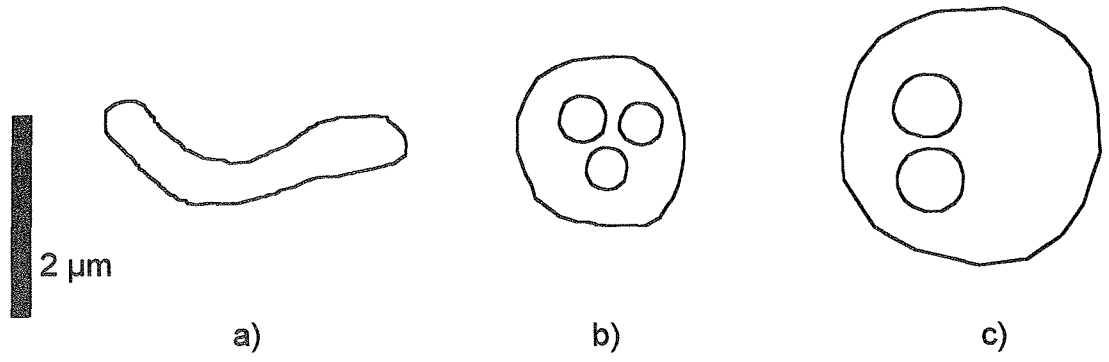

Fig. 110: Sketch of the morphological forms (average sizes) of magnetotactic bacteria dominating at different depths in core 3349-1. a) Spirillum (1 cm depth), b) coccus (2 cm depth), c) coccus (3-5 cm depth).

Bacteria that extracellularly produce magnetite - The first cultivation of bacteria that extracellularly produce magnetite particles of irregular shape and grain sizes between 6 and 25 nm was described by Lovely et al. (1987). Magnetite is a by-product of metabolism of these heterotrophic bacteria. They oxidize organic compounds by reducing Fe(III). Magnetite is formed in a biologically induced process, it presumably grows abiotically in the chemical environment regulated by these bacteria. The grown particles are superparamagnetic and have an extremely high magnetic susceptibility. Only clusters of these particles can carry a weak remanent magnetization, therefore they are not well suited for palaeomagnetic purposes.

It is not known whether these bacteria occur in pelagic sediments and if they contribute to the magnetic susceptibility signal. To test the occurence of these bacteria, 0.3 µl of sediment suspension from specified sediment depths was filled into bottles containing culturing media. Culturing media suitable for different strains of these bacteria were provided by R. Roselló-Mora (Technische Universität München). As the bacteria are strictly anaerobic, culture bottles had to be filled and sealed in argon atmosphere. Magnetic susceptibility of the bottles was

measured with a magnetic susceptibility meter *Kappabridge KLY-2* before and after filling with sediments and will be monitored in the laboratory in Bremen.

4.11. Moorings

(D. Hebbeln, G. Ruhland, D. Beese and S. Hormazabal)

As part of the international JGOFS-Eastern Boundary Current Study two deep-sea moorings are deployed at ~30°S off the chilean coast. Both moorings have been deployed five months earlier, in January 1995, with the chilean R/V ABATE MOLINA, which is also supposed to recover them in January 1996.

On June 4 the oceanographic mooring COSMOS #7 (30°21.4`S, 71°47´W) has been recovered. The mooring was equipped with 3 Aanderaa current meters (RCM 7) in 170 m, 400 m, and 700 m (Fig. 111), respectively, which all recorded the current, temperature and salinity data continuously throughout the period of deployment. Most of the time the currents went south with maximum velocities of 54 cm/sec in 170 m water depth in February 1995. After the mooring as been prepared for another six month period it has been redeployed as COSMOS #8 (Fig. 111) the same day.

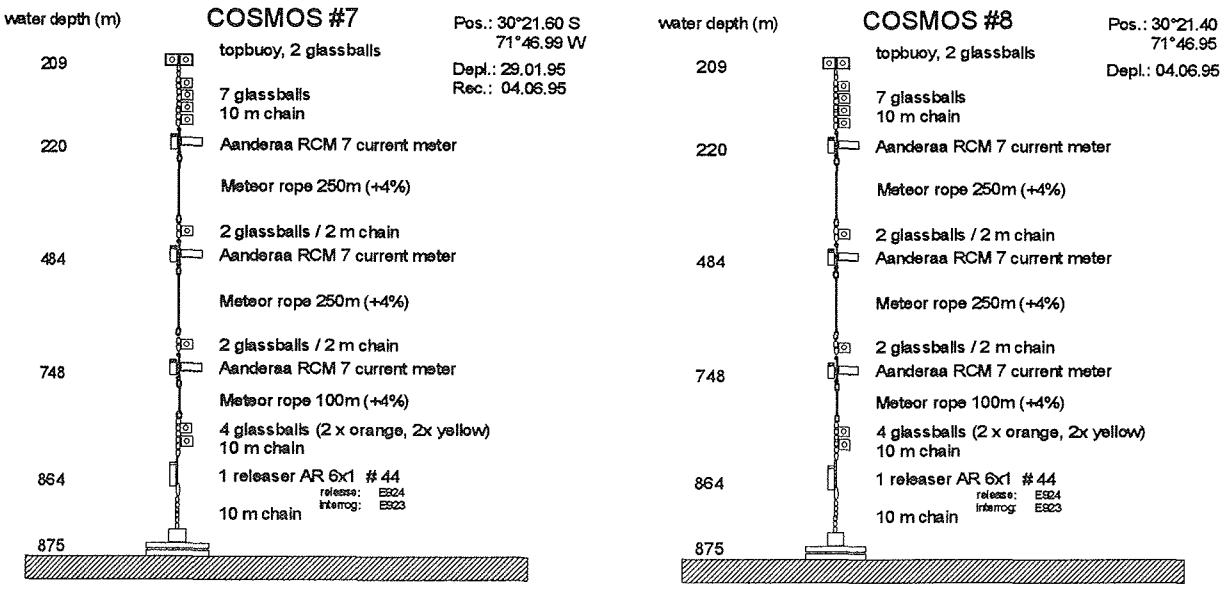

Fig. 111: Configuration of the moorings COSMOS #7 and COSMOS #8

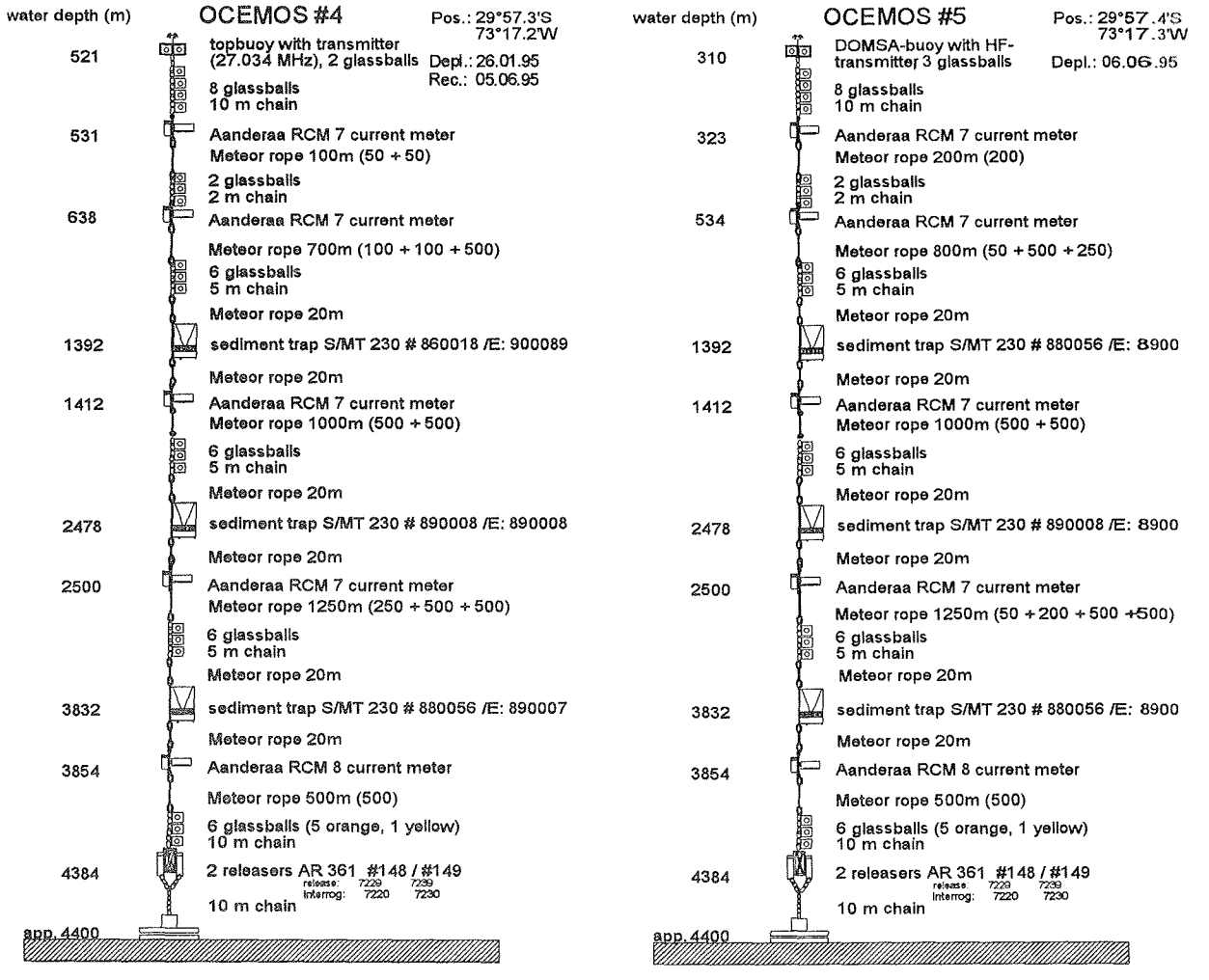

Fig. 112: Configuration of moorings OCEMOS #4 und OCEMOS #5

On the next day, June 5, the 4000 m long sediment trap mooring OCEMOS #4 (29°57′S, 73°17′W) has been taken up. This mooring consisted of 3 sediment traps (SMT 230) and 5 Aanderaa current meters (RCM 7) (Fig. 112). During the passed 5 months all 3 sediment traps, deployed in ~1000 m, ~2000 m and ~3500 m, respectively, collected the particle flux continuously in six day intervals. Throughout the 5 months there was only little variation in the amount of trapped material. In contrast to earlier deployments at the same site, a high number of large pteropods (up to 1 cm) could have been observed in the sample bottles. The samples have been poisened with $HgCl_2$ and stored at 4°C. It took several hours to fix up the whole array, thus, the redeployment as OCEMOS #5 (Fig. 112) has been carried out on June 6.

5. Acknowledgements

The scientific party onboard R/V SONNE during leg 1 and 2 of cruise SO-102 gratefully achknowledges the friendly cooperation and efficient technical assistance of Captain Bruns and his crew.

Thanks are also due to the German Ministery of Research (BMBF), which funded the cruise within the project "CHIPAL - Spätquartäre Variationen der Paläoproduktivität im östlichen Süd-Pazifik vor Chile".

6. Station list

The sediment cores taken during the third leg of R/V SONNE cruise 101 are part of the scientific program of cruise 102 and they have been openend and described during this cruise. For that reason a station list of those stations from SO-101 on which sediment cores have been taken is attached to the station list of SO-102.

GeoB No.	Ships No.	Date 1995	Equip-ment	Bottom contact (UTC)	Latitude	Longitude	Water depth [m]	Recovery [cm]	Remarks
CRUISE SO 101-3 SE-PACIFIC									
Transect A									
3301-1	001	25.04	MUC	20:25	33°08,8S	71°58,9W	969m	-	not released
3301-2		25.04.	MUC	21:37	33°08,8S	71°58,9W	970m	27 cm	core recovery 8/8, 2/4
3301-3		25.04.	RC					-	Releaser has to be changed
3301-4		26.04.	SL12	0:33	33°08,8S	71°58,9W	974m	466 cm	
3302-1	002	26.04	SL6	3:35	33°13,1S	72°05,4W	1498m	412 cm	
3302-2		26.04	MUC	5:45	33°13,1S	72°05,2W	1502m	24 cm	core recovery 7/8, 2/4
3303-1	003	26.04	MUC	8:15	33°12,4S	72°10,5W	1983m	27 cm	core recovery 8/8, 4/4
3303-2		26.04	SL6	10:14	33°12,4S	72°10,5W	1984m	389 cm	
3304-1	006	27.04	CTD/RO	0:24	32°53,3S	72°11,6W	2412m		max. depth 2372m
3304-2		27.04	CTD/RO	2:35	32°53,4S	72°11,6W	2412m		max. depth 500m
3304-3		27.04	MUC	4:13	32°53,4S	72°11,5W	2413m	25 cm	core recovery 4/8, 4/4
3304-4		27.04	RC	6:55	32°53,4S	72°11,5W	2412m	-	not released
3304-5		27.04	SL12	9:32	32°53,4S	72°11,5W	2411m	917 cm	
3305-1	007	27.04	SL12	13:09	32°51,1S	72°25,4W	3028m	424 cm	
3305-2		27.04	MUC	15:45	32°51,1S	72°25,4W	3029m	30 cm	core recovery 4/8, 4/4
3306-1	012	29.04	CTD/RO	1:04	33°00,9S	72°29,5W	4078m		max. depth 4041m
3306-2		29.04	MUC	7:10	33°00,9S	72°29,5W	4076m	12 cm	core recovery 0/8, 2/4
3306-3		29.04	MUC	10:50	33°00,9S	72°29,5W	4075m	-	no core recovery
3306-4		29.04	SL12	14:19	33°00,9S	72°29,5W	4077m	538 cm	
3307-1	015	30.04	SL6	13:35	32°54,2S	73°54,6W	435m	-	no core recovery
3307-2		30.04	SL6	14:28	32°53,9S	73°54,6W	432m	-	tube bended, no core recovery
3308-1	016	30.04	SL12	17:45	33°07,9S	73°44,9W	3625m	937 cm	
3308-2		30.04	SL12	21:32	33°07,9S	73°44,9W	3621m	1025 cm	GEOMAR (Spiegler)
3308-3		01.05	MUC	0:30	33°07,9S	73°44,9W	3620m	12 cm	core recovery 1/8, 4/4
3308-4	018	01.04	MUC	16:47	33°07,9S	73°44,9W	3631m	-	only surface sample
3309-1	021	03.05	SL6	10:30	33°09,4S	72°49,4W	5419m	-	no core recovery, tube bended
3310-1	023	04.05	RC	4:05	33°14,6S	72°50,3W	5412m	36 cm	
3311-1		06.05	SL6	11:02	33°36,4S	72°02,8W	472m	385 cm	
3311-2		06.05	MUC	11:53	33°36,4S	72°02,8W	471m	5 - 8cm	core recovery 0/8, 4/4

GeoB No.	Ships No.	Date 1995	Equip-ment	Bottom contact (UTC)	Latitude	Longitude	Water depth [m]	Recovery [cm]	Remarks
CRUISE SO 102-1 SE-PACIFIC									
Transect B									
3312-1	1	11.05	CTD/RO	15:04	41°00,5′S	74°20,2′W	582		max. depth
3312-2		11.05	MUC	16:12	41°00,5′S	74°20,2′W	584		
3312-3		11.05	Profilur	17:12	40°59,4′S	74°20,0′W	597		Lander deployed
		12.05		4:35	41°59,7′S	74°20,2′W			Lander recovered
3312-4		11.05	Elinor	17:00	40°59,5′S	74°20,1′W	606		Lander deployed
		12.05		7:55	40°59,6′S	74°19,9′W			Lander recovered
3312-5		11.05	SL6	18:52	41°00,5′S	74°20,2′W	580	478 cm	
3312-6		11.05	CTD/RO	15:21	41°00,5′S	74°20,2′W	585		max. depth
3312-7	3	12.05	MUC	5:25	41°00,6′S	74°20,3′W	582		
3312-8		12.05	MUC	6:05	41°00,5′S	74°20,2′W	579		core recovery 4/8, 2/4
3313-1	2	12.05	SL12	0:47	41°00,0′S	74°27,0′W	852	807 cm	
3313-2		12.05	SL12	2:28	41°00,0′S	74°27,0′W	853	874 cm	Geochemistry
3313-3		12.05	MUC	9:12	41°00,0′S	74°27,0′W	851	47 cm	core recovery 4/8, 2/4
3314-1	4	12.05	CTD/RO	18:56	41°36,3′S	74°58,8′W	1649		max. depth 100m
3314-2		12.05	MUC	20:03	41°36,2′S	74°58,8′W	1652		core recovery 4/8, 4/4
3314-3		12.05	SL12	21:38	41°36,2′S	74°58,8′W	1647	577 cm	
3315-1	5	13.05	SL12	1:05	41°40,1′S	75°02,7′W	1999	616 cm	
3315-2		13.05	MUC	3:05	41°40,1′S	75°02,7′W	2001		no core recovery
3315-3		13.05	MUC	4:35	41°40,1′S	75°02,8′W	2001		no core recovery
3316-1	6	13.05	MUC	10:20	41°56,2′S	75°12,8′W	2574		core recovery 0/8, 4/4
3316-2		13.05	CTD/RO	11:32	41°56,3′S	75°12,8′W	2574		max. depth 100m
3316-3		13.05	MUC	12:47	41°56,3′S	75°12,8′W	2575		core recovery 3/8, 2/4
3316-4		13.05	SL12	14:53	41°56,3′S	75°12,8′W	2575	554 cm	
3316-5		13.05	CTD/RO	16:08	41°56,2′S	75°12,8′W	2574		max. depth 100m
3317-1	7	13.05	SL12	19:55	42°00,8′S	75°18,2′W	2882	413 cm	
3317-2		13.05	Elinor	21:30	42°01,9′S	75°18,1′W	3012		Lander deployed
		14.05		23:25	42°02,1′S	75°18,2′W			Lander recovered
3317-3		13.05	Profilur	21:35	42°01,9′S	75°18,1′W	3018		Lander deployed
		14.05		23:50	42°02,0′S	75°17,9′W			Lander recovered
3317-4		13.05	SL12	22:57	42°00,8′S	75°18,1′W	2922		tube bended, no core recovery
3317-5		14.05	SL6	1:13	42°00,8′S	75°18,1′W	2923	195 cm	
3317-6		14.05	MUC	3:35	42°00,8′S	75°18,1′W	2923		core recovery 3/8, 4/4
3317-7		14.05	MUC	4:57	42°00,8′S	75°18,1′W	2919		core recovery 6/8, 4/4
3318-1	8	14.05	CTD/RO	10:24	42°02,8′S	75°29,9′W	3176		max. depth 100m
3318-2		14.05	MUC	12:12	42°02,3′S	75°19,3′W	3207	52	core recovery 6/8, 3/4
3318-3		14.05	SL6	14:25	42°02,3′S	75°19,3′W	3183	574 cm	
3318-4		15.05	CTD/RO	0:02	42°02,0′S	75°17,9′W	3208		max. depth 100m
Oceanographic Profile #1									
3319-1	9	15.05	CTD/RO	6:55	43°15,0′S	74°45,0′W	143		max. depth 125m
3319-2		15.05	MUC	7:26	43°15,0′S	74°45,0′W	143		no core recovery, some coarse sand

GeoB No.	Ships No.	Date 1995	Equip-ment	Bottom contact (UTC)	Latitude	Longitude	Water depth [m]	Recovery [cm]	Remarks
3319-3		15.05	MUC	7:45	43°15,0′S	74°45,0′W			no core recovery
3320-1	10	15.05	CTD/RO	9:16	43°15,0′S	75°00,0′W	185		max. depth 175m
3321-1	11	15.05	CTD/RO	11:12	43°15,0′S	75°15,0′W	595		max. depth 500m
3321-2		15.05	MUC	12:10	43°15,0′S	75°15,0′W	593		no core recovery
3322-1	12	15.05	CTD/RO	14:00	43°15,0′S	75°15,0′W	3481		max. depth 494m
3322-2		15.05	CTD/RO	15:23	43°13,9′S	75°29,7′W	3459		max. depth 3455
3323-1	13	15.05	Elinor	20:07	43°13,0′S	76°00,0′W			Lander deployed
		16.05		17:41	43°13,0′S	76°00,0′W			Lander recovered
3323-2		15.05	Profilur	20:15	43°13,0′S	76°00,0′W			Lander deployed
		16.05		21:14	43°12,9′S	76°00,0′W			Lander recovered
3323-3		15.05	CTD/RO	21:57	43°14,0′S	76°00,0′W	3678		max. depth 3643
3323-4		16.05	MUC	1:55	43°13,1′S	75°57,0′W	3697		core recovery 1/8, 4/4
3323-5		16.05	MUC	4:43	43°13,1′S	75°57,0′W	3702		core recovery 3/8, 2/4
3323-6		16.05	MUC	7:25	43°13,1′S	75°57,0′W	3700		core recovery 1/8, 3/4
3323-7		16.05	MN	9:30	43°13,0′S	75°57,0′W	3701		max. depth 500m
3323-8		16.05	CTD/RO	11:03	43°14,0′S	76°00,0′W	3677		max. depth 404m, 1 sampler destroyed
3323-9		16.05	SL6	13:45	43°13,1′S	75°57,0′W	3703	299 cm	
3323-10		16.05	CTD/RO	15:50	43°12,5′S	75°59,6′W	3679		max. depth 101m
3324-1	14	17.05	CTD/RO MIC	3:40	43°13,9′S	76°59,7′W	3548		MIC not released
3325-1	15	17.05	CTD/RO	10:17	43°14,0′S	78°00,0′W	3628		max. depth 507m
3325-2		17.05	MN	11:18	43°14,1′S	77°59,9′W	3621		max. depth 500m
3325-3		17.05	CTD/RO	13:55	43°14,1′S	78°00,0′W	3619		max. depth 3585m
3326-1	16	17.05	CTD/RO MIC	21:12	43°14,0′S	79°00,0′W	3635		core recovery 2/4
3327-1	17	18.05	Elinor	3:25	43°14,0′S	80°00,0′W	3533		Lander deployed
		18.05		18:02	43°14,3′S	80°00,1′W			Lander recovered
3327-2		18.05	Profilur	4:05	43°14,0′S	80°00,1′W	3533		Lander deployed
		18.05		8:20	43°14,3′S	80°00,0′W			Lander recovered (uncontrolled release)
3327-3		18.05	CTD/RO	5:36	43°14,0′S	80°00,0′W	3498		max. depth 3481m
3327-4		18.05	CTD/RO	9:44	43°14,0′S	80°00,0′W	3505		max. depth 399m
3327-5		18.05	SL12	11:48	43°14,4′S	79°59,5′W	3531	900 cm	
3327-6		18.05	MUC	14:15	43°14,4′S	79°59,5′W	3535		core recovery 0/8, 4/4
3327-7		18.05	MN	15:50	43°14,4′S	79°59,5′W	3531		max. depth 500m
3327-8		18.05	CTD/RO	16:35	43°14,4′S	79°59,5′W	3523		max. depth 149m
3328-1	18	19.05	CTD/RO MIC	0:30	43°14,0′S	81°00,0′W	3693		core recovery 3/4
3329-1	19	19.05	CTD/RO	8:10	43°14,1′S	82°00,0′W	3252		max. depth 3190m
3329-2		19.05	MN	10:13	43°14,0′S	82°00,0′W	3270		max. depth 500m
3329-3		19.05	CTD/RO	12:11	43°14,0′S	82°00,0′W	3261		max. depth 504m
3330-1	20	19.05	CTD/RO	21:10	43°14,0′S	83°59,9′W	2490		max. depth 505m
3330-2		19.05	MN	22:08	43°14,0′S	84°00,0′W	2556		max. depth 500m
3330-3		20.05	CTD/RO	0:19	43°14,0′S	84°00,0′W	2583		max. depth 2494m

GeoB No.	Ships No.	Date 1995	Equip-ment	Bottom contact (UTC)	Latitude	Longitude	Water depth [m]	Recovery [cm]	Remarks
3331-1	21	20.05	Profilur	10:07	43°14,0'S	86°00,0'W	3795		Lander deployed
		21.05		0:11	43°14,1'S	85°59,4'W	3939		Lander recovered
3331-2		20.05	Lander S4	10:14	43°14,0'S	86°00,0'W	3795		Lander deployed
		20.05		23:12					Lander released
		21.05		4:00					Lander not recovered
3331-3		20.05	CTD/RO	10:32	43°14,0'S	86°00,0'W	3820		max. depth 404m
3331-4		20.05	MUC	12:53	43°13,4'S	86°00,0'W	3763		MPI-MUC, not released
3331-5		20.05	MUC	15:25	43°13,4'S	86°00,0'W	3741		MPI-MUC, core recovery 8/8, 4/4
3331-6		20.05	CTD/RO	16:57	43°13,4'S	86°00,0'W	3737		max. depth 203m
3331-7		20.05	SL12	18:43	43°13,4'S	86°00,0'W	3776		no core recovery
3331-8		20.05	CTD/RO	21:50	43°14,8'S	85°59,9'W	3927		max. depth 3822
3331-9		21.05	MN	0:48	43°14,1'S	85°59,4'W	3939		max. depth 500m
3332-1	22	21.05	CTD/RO	11:07	41°53,1'S	86°20,9'W	3338		max. depth 204m
3333-1	23	21.05	CTD/RO	17:15	40°47,6'S	86°38,9'W	3514		max. depth 505m
Oceanographic Profile #2/1									
3334-1	24	22.05	CTD/RO	11:07	37°32,0'S	87°29,5'W	3996		max. depth 201m
3335-1	25	22.05	CTD/RO	17:10	36°33,5'S	87°44,3'W	3881		max. depth 199m
3336-1	26	23.05	CTD/RO	1:25	35°30,0'S	88°00,0'W	3978		max. depth 3800
3336-2		23.05	SL12	4:55	35°30,0'S	88°00,0'W	4032	540 cm	
3336-3		23.05	MUC	7:45	35°30,0'S	88°00,0'W	3995		core recovery 3/8, 4/4
3337-1	27	23.05	Profilur	18:33	35°15,0'S	86°00,0'W	4079		Lander deployed
		24.05		9:32	35°15,4'S	86°00,0'W			Lander recovered
3337-2		23.05	CTD/RO	18:57	35°15,0'S	86°00,1'W	4069		max. depth 407m
3337-3		23.05	SL12	22:14	35°17,1'S	86°16,8'W	3815		no core recovery, tube bended
3337-4		24.05	MN	1:15	35°15,1'S	86°00,6'W	4074		max. depth 500m
3337-5		24.05	MUC	3:26	35°15,1'S	86°00,6'W	4073		core recovery 4/8, 4/4
3337-6		24.05	CTD/RO	6:35	35°15,1'S	86°00,6'W	4081		max depth 4046
3338-1	28	24.05	CTD/RO	18:58	35°15,0'S	84°00,0'W	3984		max. depth 405m
3338-2		24.05	MN	20:00	35°15,0'S	84°00,0'W	3986		max. depth 500m
3338-3		24.05	CTD/RO	22:25	35°15,0'S	84°00,0'W	3987		max. depth 3914m
3339-1	29	25.05	SL6	4:51	35°15,0'S	83°29,4'W	3789	100 cm	
3339-2		25.05	MUC	7:40	35°15,0'S	83°29,3'W	3792		core recovery 4/8, 2/4
3339-3		25.05	SL12	10:18	35°15,0'S	83°29,4'W	3792		no core recovery, tube bended
3339-4		25.05	CTD/RO	11:44	35°15,0'S	83°29,4'W	3799		max. depth 196m
3340-1	30	25.05	CTD/RO	18:48	35°15,0'S	82°00,0'W	3924		max. depth 405m
3340-2		25.05	MN	19:52	35°15,0'S	82°00,0'W	3935		max. depth 500m
3340-3		25.05	CTD/RO	22:40	35°15,0'S	82°00,0'W	3930		max. depth 3939m
3341-1	31	26.05	CTD/RO	6:35	35°15,0'S	81°00,0'W	3994		max. depth 3939m
3342-1	32	26.05	CTD/RO	13:45	35°15,0'S	80°00,0'W	3893		max. depth 409m
3342-2		26.05	MN	14:46	35°15,0'S	80°00,1'W	3902		max. depth 500m

GeoB No.	Ships No.	Date 1995	Equip-ment	Bottom contact (UTC)	Latitude	Longitude	Water depth [m]	Recovery [cm]	Remarks
3342-3	32	26.05	CTD/RO	17:08	35°15,0'S	80°00,0'W	3916		max. depth 3874m
3343-1	33	27.05	CTD/RO	1:23	35°15,0'S	79°00,0'W	3998		max. depth 3958m
3344-1	34	27.05	CTD/RO	8:03	35°15,0'S	77°59,8'W	4083		max. depth 404m
3344-2		27.05	MN	9:14	35°15,0'S	78°00,0'W	4087		max. depth 500m
3344-3		27.05	CTD/RO	12:22	35°15,0'S	78°00,0'W	4085		max. depth 4064 m
3345-1	35	27.05	CTD/RO MIC	20:28	35°15,0'S	77°00,0'W	4023		MIC has not released
3346-1	36	28.05	CTD/RO	04:35	35°15,0'S	76°00,0'W	4301		max. depth 4297 m
3346-2		28.05	MN	07:49	35°15,0'S	76°00,0'W	4306		max. depth 500 m
3346-3		28.05	CTD/RO	10:07	35°15,0'S	76°00,0'W	4301		max. depth 402 m
3347-1	37	28.05	CTD/RO MIC	16:35	35°15,0'S	75°00,0'W	4182	25 cm	max. depth 4171 m, core recovery 4/4
3348-1	38	28.05	CTD/RO	23:37	35°15,0'S	74°00,0'W	5019		max. depth 408 m
3348-2		29.05	MN	00:35	35°15,0'S	74°00,0'W	5017		max. depth 500 m
3348-3		29.05	CTD/RO	03:08	35°15,0'S	74°00,0'W	5021		max. depth 5018 m
Transect C									
3349-1	39	29.05	Profilur	09:16	35°15,3'S	73°25,2'W	2460		Lander deployed
			Profilur	23:10	35°15,5'S	73°25,3'W			Lander recovered
3349-2		29.05	Elinor	09:32	35°15,1'S	73°25,1'W	2460		Lander deployed
		30.05	Elinor	00:37	35°15,5'S	73°25,0'W			Lander recovered
3349-3		29.05	SL12	10:36	35°15,2'S	73°25,2'W	2466	566 cm	
3349-4		29.05	MUC	12:18	35°15,1'S	73°25,2'W	2471		core recovery 8/8, 4/4
3350-1	40	29.05	MUC	15:10	35°15,0'S	73°34,6'W	3750		MUC has not released
3350-2		29.05	SL12	18:30	35°15,0'S	73°34,6'W	3750	582 cm	**vgl. GeoB 3353-1**
3351-1	41	29.05	MN	23:40	35°15,5'S	73°25,4'W	2472		max. depth 500 m
3352-1	42	30.05	SL12	01:58	35°13,0'S	73°19,0'W	2104	391 cm	
3352-2		30.05	MUC	03:26	35°13,0'S	73°19,0'W	2108		core recovery 8/8, 4/4
3353-1	43	30.05	MUC	09:56	35°15,0'S	73°34,6'W	3749		core recovery 3/8, 4/4 **vgl. GeoB 3350-2**
3354-1	44	30.05	MUC	13:02	35°13,0'S	73°29,3'W	3233		core recovery 2/8, 4/4
3354-2		30.05	SL12	15:30	35°13,0'S	73^29,3'W	3239	623 cm	
3355-1	45	30.05	Profilur	06:13	35°13,0'S	73°06,6'W			Lander deployed
		30.05	Profilur	19:08	35°13,0'S	73°06,9'W			Lander recovered
3355-2		30.05	Elinor	06:25	35°13,0'S	73°06,5'W			Lander deployed
		30.05	Elinor	19:17	35°13,0'S	73°06,8'W			Lander recovered
3355-3		30.05	SL12	20:03	35°13,0'S	73°07,0'W	1505	?	
3355-4		30.05	MUC	21:15	35°13,1'S	73°07,0'W	1511	25 cm	core recovery 8/8, 4/4
3356-1	45	31.05	Profilur	00:25	35°13,1'S	73°13,2'W			Lander deployed
		31.05	Profilur	12:25	35°13,1'S	72°45,6'W			Lander recovered
3356-2		31.05	Profilur	00:25	35°13,1'S	73°13,2'W			Lander deployed
		31.05	Profilur	12:57	35°13,1'S	72°45,6'W			Lander recovered
3357-1	46	31.05	MUC	03:24	35°17,0'S	73°13,2'W	2103	44 cm	core recovery 6/8, 4/4
3357-2		31.05	SL12	05:00	35°17,0'S	73°13,1'S	2104 m	496 cm	

GeoB No.	Ships No.	Date 1995	Equip-ment	Bottom contact (UTC)	Latitude	Longitude	Water depth [m]	Recovery [cm]	Remarks
3358-1	47	31.05	SL12	07:30	35°13,0′S	72°56,1′S	797	122 cm	core bent, but o.k.
3358-2		31.05	MUC	08:20	35°13,0′S	72°56,1′W	800	1 cm	1 surface sample
3359-1	48	31.05	MUC	09:45	35°13,0′S	72°48,5′W	680	?	core recovery 4/8, 4/4
3359-2		31.05	CTD/RO	10:12	35°13,0′S	72°48,5′W	680		max. depth 100 m
3359-3		31.05	SL6	10:57	35°13,0′S	72°48,5′W	678	380 cm	
3360-1	49	31.05	MUC	13:21	35°13,0′S	73°45,6′W	586		MUC has not released
Oceanographic Profile #2/2									
3361-1	50	31.05	CTD/RO	14:32	35°15,0′S	72°45,0′W	442		max. depth 416 m
3362-1	51	31.05	CTD/RO	16:43	35°15,0′S	73°00,0′W	920		max. depth 892 m
3363-1	52	31.05	CTD/RO	21:29	35°15,0′S	73°30,0′W	3261		max. depth 3128 m
3364-1	53	1.06	CTD/RO	01:05	35°15,0′S	73°15,0′W	2073		max. depth 1818 m
Cruise	**SO 102-2**			**SE-Pacific**					
3365-1	1	3.06	MUC	19:18	32°17,1′S	72°16,0′W	2450	26 cm	core recovery 4/8, 4/4
3365-2		3.06	SL12	21:11	32°17,1′S	72°16,0′W	2449	193 cm	
JGOFS-Transect									
3366-1	2	4.06	CTD/RO	10:18	30°21,6′S	71°56,5′W	3195	-	max. depth 208 m
3367-1	3	4.06	Chc-7	13:18	30°21,8′S	71°47,2′W	-	-	recovery of mooring COSMOS #7
3367-2		4.06	Chc-8	18:08	30°21,6′S	71°46,0′W	-	-	deployment of mooring COSMOS #8
3368-1	5	4.06	CTD/RO	19:19	30°21,6′S	71°57,5′W	3237	-	max. depth 206 m
3368-2		4.06	SL6	20:55	30°21,6′S	71°57,5′W	3238	462 cm	
3368-3		4.06	CTD/RO	22:32	30°21,6′S	71°57,5′W	3234	-	max. depth 813
3368-4		5.06	MUC	00:02	30°21,6′S	71°57,5′W	3240	28 cm	core recovery 6/8, 4/4
3369-1	6	5.06	SL6	02:46	30°21,6′S	72°01,0′W	3457	552 cm	
3370-1	7	5.06	CTD/RO	10:20	29°57,5′S	73°16,5′W	4390	-	CTD has not released
3370-2		5.06	CTD/RO	11:01	29°57,5′S	73°16,5′W	4387	-	max. depth 324 m
3370-3		5.06	Cht-6	15:29	29°56,2′S	73°16,5′W	-	-	recovery of the mooring OCEMOS #4
3370-4		5.06	CTD/RO	18:02	29°57,3′S	73°17,2′W	4421	-	max. depth 4421 m
3371-1	8	6.06	MUC	03:25	30°21,6′S	72°01,1′W	3458	37 cm	core recovery 7/8, 4/4
3372-1	9	6.06	CTD/RO	10:46	29°57,3′S	73°17,2′W	4418	-	max. depth 202 m
3372-2		6.06	Cht7	15:09	29°16,3	73°17,2′W	-	-	deployment of the mooring OCEMOS #5
3372-3		6.06	CTD/RO	15:30	29°56,3′S	73°17,1′W	4416	-	max. depth 100 m
3372-4		6.06	MUC	17:22	29°56,3′S	73°17,2′W	4409	23 cm	core recovery 6/8, 4/4
3372-5		6.06	MN	19:16	29°56,3′S	73°17,2′W	4406	-	max. depth 500 m
Transect D									
3373-1	10	7.06	MUC	17:48	27°30,1′S	71°12,4′W	1580	20 cm	core recovery 3/8, 4/4
3373-2		7.06	SL6	19:05	27°30,0′S	71°12,5′W	1581	426 cm	

GeoB No.	Ships No.	Date 1995	Equip-ment	Bottom contact (UTC)	Latitude	Longitude	Water depth [m]	Recovery [cm]	Remarks
3374-1	11	7.06	MUC	20:47	27°28,4′S	71°10,3′W	1352	29 cm	core recovery 7/8, 3/4
3374-2		7.06	SL6	21:50	27°28,4′S	71°10,3′W	1352	477 cm	
3375-1	12	7.06	SL6	23:45	27°28,0′S	71°15,1′W	1947	489 cm	
3375-2		8.06	MUC	01:05	27°28,0′S	71°15,1′W	1948	26	core recovery 4/8, 4/4
3376-1	13	8.06	SL12	03:47	27°28,0′S	71°21,7′W	2445	475 cm	
3376-2		8.06	MUC	05:08	27°28,0′S	71°21,7′W	2437	23 cm	core recovery 6/8, 4/4
3377-1	14	8.06	MUC	08:08	27°28,0′S	71°31,5′W	3576	21 cm	core recovery 5/8, 4/4
3377-2		8.06	SL6	10:13	27°28,0`S	71°31,6′W	3584	510 cm	
3377-3		8.06	CTD/RO	11:30	27°28,0	71°31,5′W	3593	-	max. depth 200 m
3378-1	15	8.06	SL6	13:20	27°30,0′S	71°30,0′W	3288	559 cm	
3378-2		8.06	MUC	16:00	27°30,0′S	71°30,0′W	3286	38 cm	core recovery 7/8, 3/4
3378-3		8.06	CTD/RO	17:22	27°30,0′S	71°30,0′W	3288	-	max. depth 200 m
3378-4		8.06	TRAMP	19:38	27°30,0′S	71°30,0′W	3288	-	TRAMP lost due to broken rope
Oceanographic Profile # 3/1									
3379-1	16	9.06	CTD/RO	01:13	28°15,0′S	71°30,0′W	2108	-	max. depth 98 m
3379-2		9.06	CTD/RO	02:43	28°15,0′S	71°28,9′W	2092	-	max. depth 2074 m
3380-1	17	9.06	CTD/RO	07:07	28°15,0′S	71°45,0′S	3912	-	max. depth 3885m
3380-2		9.06	MN	09:34	28°15,0′S	71°45,0′W	3918	-	max. depth 500 m
3380-3		9.06	CTD/RO	11:36	28°15,0′S	71°45,0′W	3918	-	max. depth 304
3381-1	18	9.06	CTD/MIC	16:07	28°15,0′S	72°00,0′W	5256	< 2 cm	filled in bags
3382-1	19	9.06	CTD/RO	23:42	28°15,1′S	72°30,0′W	4520	-	max. depth 4521 m
3382-2		10.06	MN	02:43	28°15,0′S	72°29,9′W	4515	-	max. depth 500 m
3382-3		10.06	CTD/RO	04:47	28°15,0′S	72°29,7′W	4504	-	max. depth 349 m
3383-1	20	10.06	CTD/MIC	10:25	28°15,0′S	73°00,0′W	4207	22 cm	core recovery 4/4
3384-1	21	10.06	CTD/RO	17:51	28°15,1′S	74°00,0′W	4029	-	max. depth 300 m
3384-2		10.06	MN	19:00	28°15,0′S	74°00,0′W	4067	-	max. depth 500
3384-3		10.06	CTD/RO	21:51	28°15,0′S	74°00,0′W	4031	-	max. depth 3999 m
3385-1	22	11.06	CTD/RO	10:20	28°14,9′S	76°15,1′W	4150	-	max. depth 305 m
3385-2		11.06	MN	11:20	28°15,0′S	76°00,0′W	4163	-	max. depth 500 m
3385-3		11.06	CTD/RO	14:13	28°15,0′S	76°00,0′W	4190	-	max. depth 4139 m
Iquique-Ridge									
3386-1	23	12.06	SL6	08:09	25°43,5′S	75°32,5′W	1198	0 cm	no core recovery
3387-1	24	12.06	SL6	10:10	25°37,9′S	75°31,5′W	2631	569 cm	
3387-2		12.06	CTD/RO	11:15	25°37,9′S	75°31,5′W	2631	-	max. depth 279 m
3387-3		12.06	MUC	12:45	25°37,9′S	75°31,5′W	2629	25 cm	core recovery 4/8, 4/4
3387-4		12.06	SL12	14:15	25°37,9′S	75°31,5′W	2632	543 cm	
3388-1	25	12.06	SL12	19:14	25°13,2′S	75°31,5′W	3558	722 cm	
3388-2		12.06	MUC	21:21	25°13,2′S	75°31,5′W	3557	18 cm	core recovery 6/8, 4/4

GeoB No.	Ships No.	Date 1995	Equip-ment	Bottom contact (UTC)	Latitude	Longitude	Water depth [m]	Recovery [cm]	Remarks
Nazca-Ridge									
3389-1	26	14.06	CTD/RO	11:10	21°43,5′S	80°54,6′W	4485	-	max. depth 206 m
3389-2		14.06	SL12	12:55	21°43,5′S	80°54,6′W	4482	342 cm	
3389-3		14.06	MUC	15:26	21°43,5′S	80°54,6′W	4482	38 cm	core recovery 7/8, 3/4
3390-1	27	14.06	CTD/RO	18:02	21°37,1′S	81°04,3′W	3263	-	max. depth 203 m
3390-2		14.06	MUC	19:42	21°37,1′S	81°04,3′W	3243	22 cm	core recovery 7/8, 3/4
3390-3		14.06	SL12	21:35	21°37,1′S	81°04,3′W	3266	358 cm	core tube bend, core o.k.
3391-1	28	15.06	SL6	00:15	21°32,3′S	81°11,7′W	2295	542 cm	
3391-2		15.06	MUC	01:40	21°32,3′S	81°11,7′W	2296	0 cm	no core recovery
3391-3		15.06	MUC	03:19	21°32,3′S	81°11,7′W	2296	0 cm	no core recovery
3392-1	29	15.06	MUC	05:42	21°26,6′S	81°16,1′W	1723	0 cm	no core recovery
3392-2		15.06	SL6	06:50	21°26,6′S	81°16,1′W	1751	543 cm	
3393-1	30	15.06	SL6	16:10	21°19,2′S	81°27,1′W	1373	549 cm	
3393-2		15.06	CTD/RO	16:58	21°19,2′S	81°27,1′W	1373	-	max. depth 403 m
3393-3		15.06	MUC	18:17	21°19,2′S	81°27,1′W	1371	0 cm	MUC has not released
3393-4		15.06	MUC	19:42	21°19,2′S	81°27,1′W	1360	25 cm	core recovery 4/8, 4/4
3394-1	31	15.06	MUC	22:03	21°13,6′S	81°39,5′W	1982	25 cm	
3394-2		15.06	SL6	23:15	21°13,6′S	81°39,5′W	1983	551 cm	
3395-1	32	16.06	SL6	09:57	21°04,9′S	81°49,1′W	2414	530 cm	
3395-2		16.06	CTD/RO	10:48	21°04,9′S	81°49,1′W	2412	-	max. depth 205 m
3395-3		16.06	MUC	12.06	21°04,9′S	81°49,1′W	2413	12 cm	core recovery 3/8, 4/4
3396-1	33	16.06	MUC	15:47	20°53,0′S	82°07,3′W	3092	30 cm	core recovery 4/8, 4/4
3396-2		16.06	SL6	17:33	20°53,0′S	82°07,3′W	3102	545 cm	
3397-1	34	16.06	SL6	20:12	20°47,4′S	82°15,7′W	3453	467 cm	core tube bend, core o.k.
3397-2		16.06	MUC	22:16	20°47,4′S	82°15,7′W	3452	30 cm	core recovery 4/8, 4/4
3398-1	35	17.06	MUC	13:25	21°24,2′S	82°54,6′W	3191	30 cm	core recovery 4/8, 4/4
3398-2		17.06	SL12	15:14	21°24,2′S	82°54,6′W	3189	30 cm	
3398-3		17.06	CTD/RO	16:24	21°24,2′S	82°54,6′W	3193	-	max. depth 219 m
3399-1	36	17.06	SL6	19:18	21°34,9′S	82°41,1′W	2890	433 cm	
3399-2		17.06	MUC	21:06	21°34,9′S	82°41,1′W	2890	18 cm	core recovery 3/8, 4/4
3400-1	37	18.06	MUC	00:26	21°44,8′S	82°28,4′W	2541	14 cm	core recovery 4/8, 3/4
3400-2		18.06	SL6	01:54	21°44,8′S	82°28,4′W	2540	0 cm	no core recovery
3401-1	38	18.06	CTD/RO	11:47	21°49,3′S	82°26,2′W	2463	-	max. depth 204 m
3401-2		18.06	SL6	13:01	21°49,4′S	82°26,2′W	2468	538 cm	
3401-3		18.06.	MUC	14:36	21°49,4′S	82°26,2′W	2470	12 cm	
3402-1	39	18.06	MUC	18:27	22°03,1′S	82°08,6′W	2887	20 cm	core recovery 7/8, 4/4
3402-2		18.06	SL6	20:02	22°03,1′S	82°08,6′W	2890	538 cm	
3403-1	40	18.06	MUC	22:28	22°06,0′S	82°04,8′W	3517	26 cm	core recovery 7/8, 4/4
3403-2		19.06	SL6	00:18	22°06,0′S	82°04,8′W	3529	77 cm	core tube bend, core o.k.
3404-1	41	19.06	CTD/RO	12:23	23°09,6′S	82°52,4′W	1340	-	max. depth 204 m
3404-2		19.06	SL6	13:19	23°09,6′S	82°52,4′W	1444	0 cm	no core recovery

GeoB No.	Ships No.	Date 1995	Equip-ment	Bottom contact (UTC)	Latitude	Longitude	Water depth [m]	Recovery [cm]	Remarks
3405-1	42	19.06	MUC	14:47	23°07,9'S	82°54,1'W	864	0 cm	no core recovery
3406-1	43	19.06	MUC	17:07	22°55,8'S	82°46,5'W	1957	6 cm	core recovery 7/8, 4/4
3406-2		19.06	SL6	18:19	22°55,8'S	82°46,5'W	1953	535 cm	
3407-1	44	19.06	SL6	21:10	22°40,3'S	82°36,7'W	2250	554 cm	
3407-2		19.06	MUC	22:37	22°40,3'S	82°36,7'W	2250	< 2 cm	filled in bags
3408-1	45	20.06	MUC	00:43	22°31,4'S	82°31,1'W	1586	< 2cm	filled in bags
3408-2		20.06	SL6	01:46	22°31,4'S	82°31,1'W	1583	122 cm	
3409-1	47	20.06	SL6	23:24	25°32,3'S	82°09,5'W	2809	403 cm	
3409-2		21.06	MUC	01:00	25°32,3'S	82°09,5'W	2817	< 2 cm	filled in bags
3410-1	48	21.06	MUC	05:15	24°59,5'S	82°13,3'W	1260	< 2 cm	filled in bags
3410-2		21.06	SL6	06:06	24°59,5'S	82°13,6'W	1261	370 cm	
3411-1	49	21.06	MUC	07:30	24°56,9'S	82°13,7'W	1160	< 2 cm	filled in bags
3411-2		21.06	SL6	08:24	24°56,9'S	82°13,7'W	1261	0 cm	core tube bend at 210 cm, no core recovery
3412-1	50	21.06	CTD/RO	10:17	25°03,3'S	82°24,8'W	1552	-	max. depth 199 m
3413-1	51	22.06	CTD/RO	10:20	27°19,7'S	86°38,3'W	3878	-	max. depth 206 m
Oceanographic Profile # 3/2									
3414-1	52	22.06	CTD/RO	20:07	28°00,0'S	88°00,0'W	3743	-	max. depth 3652 m
3414-2		22.06	SL6	23:18	28°00,0'S	88°00,0'W	3744	576 cm	
3414-3		23.06	MUC	01:30	28°00,0'S	88°00,0'W	3753	30 cm	core recovery 6/8, 3/4
3414-4		23.06	SL12	03:36	28°00,0'S	88°00,0'W	3744	750 cm	
3415-1	53	23.06	CTD/RO	13:47	28°15,0'S	86°00,0'W	3925	-	max. depth 405 m
3415-2		23.06	MN	14:58	28°15,0'S	86°00,0'W	3941	-	max. depth 500 m
3415-3		23.06	CTD/RO	17:56	28°15,0'S	86°00,0'W	3934	-	max. depth 3912 m
3416-1	54	24.06	CTD/RO	07:50	28°15,0'S	84°00,0'W	3805	-	max. depth 3781 m
3416-2		24.06	CTD/RO	12:26	28°15,0'S	84°00,0'W	3805	-	max. depth 316 m
3417-1	55	24.06	CTD/RO	23:58	28°15,0'S	82°00,0'W	4150	-	max. depth 358 m
3417-2		25.06	MN	01:02	28°15,0'S	82°00,0'W	4150	-	max. depth 500 m
3417-3		25.06	CTD/RO	03:54	28°15,0'S	82°00,0'W	4147	-	max. depth 4121 m
3418-1	56	25.06	CTD/RO	16:35	28°15,0'S	80°00,0'W	4171	-	max. depth 335 m
3418-2		25.06	MN	17:44	28°15,0'S	80°00,0'W	4167	-	max. depth 500 m
3418-3		25.06	CTD/RO	20:26	28°15,0'S	80°00,0'W	4168	-	max. depth 4144 m
3419-1	57	26.06	CTD/RO	09:06	28°15,0'S	78°00,0'W	4215	-	max. depth 354 m
3419-2		26.06	MN	10:17	28°15,0'S	78°00,0'W	4211	-	max. depth 500 m
3419-3		26.06	CTD/RO	11:11	28°15,0'S	78°00,0'W	4214	-	max. depth 4176 m
3420-1	58	26.06	CTD/RO	22:28	28°15,0'S	77°00,0'W	4015	-	max. depth 3936 m
3421-1	46	20.06	CTD/RO	10:18	23°51,5'S	82°21,5'W	2091	-	max. depth 202 m (ex GeoB 3408a !!)

SL6,12 -Gravity corer, 6 or 12m long
CTD/RO - CTD with Rosette water sampler
MN - Multiple closing Planktonnet
TRAMP - autonomous profiler
MUC - Multicorer
RC - Reineck corer (small box corer)
MIC - Minicorer

Publications of this series:

No. 1 Wefer, G., E. Suess und Fahrtteilnehmer
Bericht über die POLARSTERN-Fahrt ANT IV/2, Rio de Janeiro - Punta Arenas, 6.11. - 1.12.1985.
60 pages, Bremen, 1986.

No. 2 Hoffmann, G.
Holozänstratigraphie und Küstenlinienverlagerung an der andalusischen Mittelmeerküste.
173 pages, Bremen, 1988.

No. 3 Wefer, G., U. Bleil, P.J. Müller, H.D. Schulz, W.H. Berger, U. Brathauer, L. Brück, A. Dahmke, K. Dehning, M.L. Duarte-Morais, F. Fürsich, S. Hinrichs, K. Klockgeter, A. Kölling, C. Kothe, J.F. Makaya, H. Oberhänsli, W. Oschmann, J. Posny, F. Rostek, H. Schmidt, R. Schneider, M. Segl, M. Sobiesiak, T. Soltwedel, V. Spieß
Bericht über die METEOR-Fahrt M 6/6, Libreville - Las Palmas, 18.2. - 23.3.1988.
97 pages, Bremen, 1988.

No. 4 Wefer, G., G.F. Lutze, T.J. Müller, O. Pfannkuche, W. Schenke, G. Siedler, W. Zenk
Kurzbericht über die METEOR-Expedition Nr. 6, Hamburg - Hamburg, 28.10.1987 - 19.5.1988.
29 pages, Bremen, 1988.

No. 5 Fischer, G.
Stabile Kohlenstoff-Isotope in partikulärer organischer Substanz aus dem Südpolarmeer (Atlantischer Sektor).
161 pages, Bremen, 1989.

No. 6 Berger, W.H. und G. Wefer
Partikelfluß und Kohlenstoffkreislauf im Ozean.
Bericht und Kurzfassungen über den Workshop vom 3.-4. Juli 1989 in Bremen.
57 pages, Bremen, 1989.

No. 7 Wefer, G., U. Bleil, H.D. Schulz, W.H. Berger, T. Bickert, L. Brück, U. Claussen, A. Dahmke, K. Dehning, Y.H. Djigo, S. Hinrichs, C. Kothe, M. Krämer, A. Lücke, S. Matthias, G. Meinecke, H. Oberhänsli, J. Pätzold, U. Pflaumann, U. Probst, A. Reimann, F. Rostek, H. Schmidt, R. Schneider, T. Soltwedel, V. Spieß
Bericht über die METEOR - Fahrt M 9/4, Dakar - Santa Cruz, 19.2. - 16.3.1989.
103 pages, Bremen, 1989.

No. 8 Kölling, M.
Modellierung geochemischer Prozesse im Sickerwasser und Grundwasser.
135 pages, Bremen, 1990.

No. 9 Heinze, P.-M.
Das Auftriebsgeschehen vor Peru im Spätquartär.
204 pages, Bremen, 1990.

No. 10 Willems, H., G. Wefer, M. Rinski, B. Donner, H.-J. Bellmann, L. Eißmann, A. Müller, B.W. Flemming, H.-C. Höfle, J. Merkt, H. Streif, G. Hertweck, H. Kuntze, J. Schwaar, W. Schäfer, M.-G. Schulz, F. Grube, B. Menke
Beiträge zur Geologie und Paläontologie Norddeutschlands: Exkursionsführer.
202 pages, Bremen, 1990.

No. 11 Wefer, G., N. Andersen, U. Bleil, M. Breitzke, K. Dehning, G. Fischer, C. Kothe, G. Meinecke, P.J. Müller, F. Rostek, J. Sagemann, M. Scholz, M. Segl, W. Thiessen
Bericht über die METEOR-Fahrt M 12/1, Kapstadt - Funchal, 13.3.1990 - 14.4.1990.
66 pages, Bremen, 1990.

No. 12 Dahmke, A., H.D. Schulz, A. Kölling, F. Kracht, A. Lücke
Schwermetallspuren und geochemische Gleichgewichte zwischen Porenlösung und Sediment im Wesermündungsgebiet.
BMFT-Projekt MFU 0562, Abschlußbericht.
121 pages, Bremen, 1991.

No. 13 Rostek, F.
Physikalische Strukturen von Tiefseesedimenten des Südatlantiks und ihre Erfassung in Echolotregistrierungen.
209 pages, Bremen, 1991.

No. 14 Baumann, M.
Die Ablagerung von Tschernobyl-Radiocäsium in der Norwegischen See und in der Nordsee.
133 pages, Bremen, 1991.

No. 15 Kölling, A.
Frühdiagenetische Prozesse und Stoff-Flüsse in marinen und ästuarinen Sedimenten.
140 pages, Bremen, 1991.

No. 16 SFB 261 (Hrsg.)
1. Kolloquium des Sonderforschungsbereichs 261 der Universität Bremen (14.Juni 1991): Der Südatlantik im Spätquartär: Rekonstruktion von Stoffhaushalt und Stromsystemen.
Kurzfassungen der Vorträge und Poster.
66 pages, Bremen, 1991.

No. 17 Pätzold, J., T. Bickert, L. Brück, C. Gaedicke, K. Heidland, G. Meinecke, S. Mulitza
Bericht und erste Ergebnisse über die METEOR-Fahrt M 15/2, Rio de Janeiro - Vitoria, 18.1. - 7.2.1991.
46 pages, Bremen, 1993.

No. 18 Wefer, G., N. Andersen, W. Balzer, U. Bleil, L. Brück, D. Burda, A. Dahmke, B. Donner, T. Felis, G. Fischer, H. Gerlach, L. Gerullis, M. Hauf, R. Henning, S. Kemle, C. Kothe, R. Melyooni, F. Pototzki, H. Rode, J. Sagemann, M. Schlüter, M. Scholz, V. Spieß, U. Treppke
Bericht und erste Ergebnisse über die METEOR-Fahrt M 16/1, Pointe Noire - Recife, 27.3. - 25.4.1991.
120 pages, Bremen, 1991.

No. 19 Schulz, H.D., N. Andersen, M. Breitzke, D. Burda, K. Dehning, V. Diekamp, T. Felis, H. Gerlach, R. Gumprecht, S. Hinrichs, H. Petermann, F. Pototzki, U. Probst, H. Rode, J. Sagemann, U. Schinzel, H. Schmidt, R. Schneider, M. Segl, B. Showers, M. Tegeler, W. Thiessen, U. Treppke
Bericht und erste Ergebnisse über die METEOR-Fahrt M 16/2, Recife - Belem, 28.4. - 20.5.1991.
149 pages, Bremen, 1991.

No. 20 Berner, H.
Mechanismen der Sedimentbildung in der Fram-Straße, im Arktischen Ozean und in der Norwegischen See.
167 pages, Bremen, 1991.

No. 21 Schneider, R.
Spätquartäre Produktivitätsänderungen im östlichen Angola-Becken: Reaktion auf Variationen im Passat-Monsun-Windsystem und in der Advektion des Benguela-Küstenstroms.
198 pages, Bremen, 1991.

No. 22 Hebbeln, D.
Spätquartäre Stratigraphie und Paläozeanographie in der Fram-Straße.
174 pages, Bremen, 1991.

No. 23 Lücke, A.
Umsetzungsprozesse organischer Substanz während der Frühdiagenese in ästuarinen Sedimenten.
137 pages, Bremen, 1991.

No. 24 Wefer, G., D. Beese, W.H. Berger, U. Bleil, H. Buschhoff, G. Fischer, M. Kalberer, S. Kemle von Mücke, B. Kerntopf, C. Kothe, D. Lutter, B. Pioch, F. Pototzki, V. Ratmeyer, U. Rosiak, W. Schmidt, V. Spieß, D. Völker
Bericht und erste Ergebnisse der METEOR-Fahrt M 20/1, Bremen - Abidjan, 18.11.1991- 22.12.1991.
74 pages, Bremen, 1992.

No. 25 Schulz, H.D., D. Beese, M. Breitzke, L. Brück, B. Brügger, A. Dahmke, K. Dehning, V. Diekamp, B. Donner, I. Ehrhardt, H. Gerlach, M. Giese, R. Glud, R. Gumprecht, J. Gundersen, R. Henning, H. Petermann, M. Richter, J. Sagemann, W. Schmidt, R. Schneider, M. Segl, U. Werner, M. Zabel
Bericht und erste Ergebnisse der METEOR-Fahrt M 20/2, Abidjan - Dakar, 27.12.1991 - 3.2.1992.
173 pages, Bremen, 1992.

No. 26 Gingele, F.
Zur klimaabhängigen Bildung biogener und terrigener Sedimente und ihrer Veränderung durch die Frühdiagenese im zentralen und östlichen Südatlantik.
202 pages, Bremen, 1992.

No. 27 Bickert, T.
Rekonstruktion der spätquartären Bodenwasserzirkulation im östlichen Südatlantik über stabile Isotope benthischer Foraminiferen.
205 pages, Bremen, 1992.

No. 28 Schmidt, H.
Der Benguela-Strom im Bereich des Walfisch-Rückens im Spätquartär.
172 pages, Bremen, 1992.

No. 29 Meinecke, G.
Spätquartäre Oberflächenwassertemperaturen im östlichen äquatorialen Atlantik.
181 pages, Bremen, 1992.

No. 30 Bathmann, U., U. Bleil, A. Dahmke, P. Müller, A. Nehrkorn, E.-M. Nöthig, M. Olesch, J. Pätzold, H.D. Schulz, V. Smetacek, V. Spieß, G. Wefer, H. Willems
Bericht des Graduierten Kollegs. Stoff-Flüsse in marinen Geosystemen.
Berichtszeitraum Oktober 1990 - Dezember 1992.
396 pages, Bremen, 1992.

No. 31 Damm, E.
Frühdiagenetische Verteilung von Schwermetallen in Schlicksedimenten der westlichen Ostsee.
115 pages, Bremen, 1992.

No. 32 Antia, E.E.
Sedimentology, Morphodynamics and Facies Association of a mesotidal Barrier Island Shoreface (Spiekeroog, Southern North Sea).
370 pages, Bremen, 1993.

No. 33 Duinker, J. und G. Wefer (Hrsg.)
Bericht über den 1. JGOFS-Workshop. 1./2. Dezember 1992 in Bremen.
83 pages, Bremen, 1993.

No. 34 Kasten, S.
Die Verteilung von Schwermetallen in den Sedimenten eines stadtbremischen Hafenbeckens.
103 pages, Bremen, 1993.

No. 35 Spieß, V.
Digitale Sedimentographie. Neue Wege zu einer hochauflösenden Akustostratigraphie.
199 pages, Bremen, 1993.

No. 36 Schinzel, U.
Laborversuche zu frühdiagenetischen Reaktionen von Eisen (III) - Oxidhydraten in marinen Sedimenten.
189 pages, Bremen, 1993.

No. 37 Sieger, R.
CoTAM - ein Modell zur Modellierung des Schwermetalltransports in Grundwasserleitern.
56 pages, Bremen, 1993.

No. 38 Willems, H. (Ed.)
Geoscientific Investigations in the Tethyan Himalayas.
183 pages, Bremen, 1993.

No. 39 Hamer, K.
Entwicklung von Laborversuchen als Grundlage für die Modellierung des Transportverhaltens von Arsenat, Blei, Cadmium und Kupfer in wassergesättigten Säulen.
147 pages, Bremen, 1993.

No. 40 Sieger, R.
Modellierung des Stofftransports in porösen Medien unter Ankopplung kinetisch gesteuerter Sorptions- und Redoxprozesse sowie thermischer Gleichgewichte.
158 pages, Bremen, 1993.

No. 41 Thießen, W.
Magnetische Eigenschaften von Sedimenten des östlichen Südatlantiks und ihre paläozeanographische Relevanz.
170 pages, Bremen, 1993.

No. 42 Spieß, V., A. Abelmann, T. Bickert, I. Brehme, R. Cordes, A.P. Cavalcanti de C. Laier, K. Dehning, T. v.Dobeneck, B. Donner, I. Ehrhardt, M. Giese, J. Grigel, R. Haese, W. Hale, S. Hinrichs, S. Kasten, C. Knaack, W.-T. Ochsenhirt, H. Petermann, R. Rapp, M. Richter, J. Rogers, A. Schmidt, M. Scholz, F. Skowronek, M. Teixeira de Oliveira, M. Zabel
Report and preliminary results of METEOR-Cruise M 23/1, Capetown - Rio de Janeiro, 4.2.1993 - 25.2.1993.
139 pages, Bremen, 1994.

No. 43 Bleil, U., A. Ayres Neto, D. Beese, M. Breitzke, K. Dehning, V. Diekamp, T. v.Dobeneck, A. Figueiredo, M. Pimentel Esteves, M. Giese, R. Glud, J. Grigel, J. Gundersen, R. Haese, S. Hinrichs, S. Kasten, G. Meinecke, S. Mulitza, H. Petermann, R. Petschik, R. Rapp, M. Richter, C. Rühlemann, M. Scholz, K. Wallmann, M. Zabel
Report and preliminary results of METEOR-Cruise M 23/2, Rio de Janeiro - Recife, 27.2.1993 - 19.3.1993
133 pages, Bremen, 1994.

No. 44 Wefer, G., D. Beese, W.H. Berger, K. Buhlmann, H. Buschhoff, M. Cepek, V. Diekamp, G. Fischer, E. Holmes, S. Kemle-von Mücke, B. Kerntopf, C.B. Lange, S. Mulitza, W.-T. Ochsenhirt, R. Plugge, V. Ratmeyer, C. Rühlemann, W. Schmidt, M. Schwarze, C. Wallmann, M. Zabel
Report and preliminary results of METEOR-Cruise M 23/3, Recife - Las Palmas, 21.3.1993 - 12.4.1993
71 pages, Bremen, 1994.

No. 45 Giese, M. und G. Wefer (eds.)
Bericht über den 2. JGOFS-Workshop. 18../19. November 1993 in Bremen.
93 pages, Bremen, 1994.

No. 46 Balzer, W., M. Bleckwehl, H. Buschhoff, G. Fischer, F.G. Palma, M. Kalberer, U. Kuller, V. Ratmeyer, U. Rosiak, D. Schneider, A. Zimmermann
Report and preliminary results of METEOR-Cruise M 22/1, Hamburg - Recife, 22.9. - 21.10.1992.
24 pages, Bremen, 1994.

No. 47 Stax, R.
Zyklische Sedimentation von organischem Kohlenstoff in der Japan See: Anzeiger für Änderungen von Paläoozeanographie und Paläoklima im Spätkänozoikum.
150 pages, Bremen, 1994.

No. 48 Skowronek, F.
Frühdiagenetische Stoff-Flüsse gelöster Schwermetalle an der Oberfläche von Sedimenten des Weser Ästuares.
107 pages, Bremen, 1994.

No. 49 Dersch-Hansmann, M.
Zur Klimaentwicklung in Ostasien während der letzten 5 Millionen Jahre: Terrigener Sedimenteintrag in die Japan See (ODP Ausfahrt 128).
149 pages, Bremen, 1994.

No. 50 Zabel, M.
Frühdiagenetische Stoff-Flüsse in Oberflächen-Sedimenten des äquatorialen und östlichen Südatlantik.
129 pages, Bremen, 1994.

No. 51 Bleil, U., M. Breitzke, K. Däumler, L. Dittert, J. Ewert, G. Kohl, B. Heesemann, W.-D. Heinitz, P. Helmke, H. Keil, T. Merkel, B. Pioch, F. Pototzki, U. Rosiak, R. Schneider, T. Schwenk, V. Spieß, G. Uenzelmann-Neben
Report and preliminary results of SONNE-Cruise SO 86, Buenod Aires - Capetown 22.4.1993 - 31.5.93
116 pages, Bremen, 1994.

No. 52 Symposium
The South Atlantic: Present and Past Circulation.
Bremen, Germany, 15 - 19 August 1994.
Abstracts
167 pages, Bremen, 1994.

No. 53 Kretzmann, U.B.
^{57}Fe-Mössbauer-Spektroskopie an Sedimenten - Möglichkeiten und Grenzen.
183 pages, Bremen, 1994.

No. 54 Bachmann, M.
Die Karbonatrampe von Organyà im oberen Oberapt und unteren Unteralb (NE-Spanien, Prov. Lerida): Fazies, Zyklo- und Sequenzstratigraphie.
147 pages, Bremen, 1994.

No. 55 Kemle-von Mücke, S.
Oberflächenwasserstruktur und -zirkulation des Südostatlantiks im Spätquartär.
151 pages, Bremen, 1994.

No. 56 Petermann, H.
Magnetotaktische Bakterien und ihre Magnetosome in Oberflächensedimenten des Südatlantiks.
134 pages, Bremen, 1994.

No. 57 Mulitza, S.
Spätquartäre Variationen der oberflächennahen Hydrographie im westlichen äquatorialen Atlantik.
97 pages, Bremen, 1994.

No. 58 Segl, M. and Cruise Participants
Report and preliminary results of METEOR-Cruise M 29/1, Buenos-Aires - Montevideo, 17.6.1994 - 13.7.1994
94 pages, Bremen, 1994.

No. 59 Bleil, U. and Cruise Participants
Report and preliminary results of METEOR-Cruise M 29/2, Montevideo - Rio de Janiero 15.7.1994 - 8.8.1994
153 pages, Bremen, 1994.

No. 60 Henrich, R. and Cruise Participants
Report and preliminary results of METEOR-Cruise M 29/3, Rio de Janeiro - Las Palmas 11.8.1994 - 5.9.1994
Bremen, 1994 (in preparation).

No. 61 Sagemann, J.
Saisonale Variationen von Porenwasserprofilen, Nährstoff-Flüssen und Reaktionen in intertidalen Sedimenten des Weser-Ästuars.
110 pages, Bremen, 1994.

No. 62 Giese, M. and G. Wefer
Bericht über den 3. JGOFS-Workshop. 5./6. Dezember 1994 in Bremen.
84 pages, Bremen, 1995.

No. 63 Mann, U.
Genese kretazischer Schwarzschiefer in Kolumbien: Globale vs. regionale/lokale Prozesse.
153 pages, Bremen, 1995.

No. 64 Willems, H., Wan X., Yin J., Dongdui L., Liu G., S. Dürr, K.-U. Gräfe
The Mesozoic development of the N-Indian passive margin and of the Xigaze Forearc Basin in southern Tibet, China. – Excursion Guide to IGCP 362 Working-Group Meeting "Integrated Stratigraphy".
113 pages, Bremen, 1995 (in press).

No. 65 Hünken, U.
Liefergebiets - Charakterisierung proterozoischer Goldseifen in Ghana anhand von Fluideinschluß - Untersuchungen.
270 pages, Bremen, 1995 (in press).

No. 66 Nyandwi, N.
The Nature of the Sediment Distribution Patterns in ther Spiekeroog Backbarrier Area, the East Frisian Islands.
162 pages, Bremen, 1995 (in press).